Dissertation

submitted to the
Combined Faculties for the Natural Sciences and for Mathematics
of the Ruperto-Carola University of Heidelberg, Germany
for the degree of
Doctor of Natural Sciences

presented by

Verena Siebert, M.Sc.
born in Lüneburg, Germany

Date of oral examination: 28.06.2022

Substrate recognition and cleavage by the mitochondrial rhomboid protease PARL

Referees:

Prof. Dr. Michael Brunner
Prof. Dr. Marius K. Lemberg

“Experience is like a lantern in the back, it only illuminates the part of the path that we already have behind us.”

Confucius

Manuscripts and publications derived from this work

Siebert V., Silber M., Heuten E., Muhle-Goll C., Lemberg M.K. Cleavage of PGAM5 by the intramembrane protease PARL is governed by transmembrane helix dynamics and oligomeric state. *bioRxiv preprint*, doi: https://doi.org/10.1101/2021.11.19.469224 (currently under revision at *J Biol Chem*)

Lysyk L., Brassard R., Arutyunova E., **Siebert V.**, Jiang Z., Takyi E., Morrison M., Young H.S., Lemberg M.K., O'Donoghue A.J., Lemieux M.J. (2021). Insights into the catalytic properties of the mitochondrial rhomboid protease PARL. *J Biol Chem*, doi: 10.1016/j.jbc.2021.100383

Engberg O.*, **Siebert V.*,** Ulbricht D.*, Döbel V., Penk A., Cichos F., Lemberg M.K., Huster D. The lipid distortion effect of the rhomboid GlpG. (Manuscript in preparation)

* equal contribution

Summary

Proteases have evolved in all kingdoms of life with the capability to catalyze irreversible and highly regulated hydrolysis of peptide bonds. Intramembrane proteases share common features as such enzymes are polytopic membrane proteins with their active sites buried several Ångstrom deep within the lipid bilayer. Although the list of physiological substrates is steadily growing, an important remaining question is whether these proteases have a conserved substrate recognition mechanism.

In the present thesis, I focused on the human mitochondrial rhomboid protease PARL and its substrate recognition and cleavage mechanism on the example of PGAM5. Dysfunctional mitochondrial quality control disturbs cellular energy metabolism and programmed cell death, triggering disruptive diseases such like neurodegeneration. Genetic deficiency of PGAM5 causes a Parkinson's-like movement disorder in mice. PARL serves as a safeguard of mitochondrial homeostasis and is processing PGAM5 when the mitochondrial membrane potential is disrupted. Until today, PGAM5 substrate determinants have not been rigorously investigated. Here, I characterize for the first time several cleavage determinants in PGAM5 on basis of mutational studies in human tissue culture, *in vitro* proteolytic assays with purified recombinant proteins and in a collaborative project using CD spectroscopy and liquid-state NMR. I can show that the N-terminal portion of the PGAM5 TM domain plays a special role and is a critical determinant for PARL-catalyzed processing. Interestingly, besides cleavage resistant forms, I obtained PGAM5 mutants with highly increased cleavage by PARL uncoupling it from its native regulation. NMR analysis revealed that the PGAM5 TM domain harbors two split helices zoned by a hinge-like loop and mutations within the N- or C-terminal helix suggest an altered interaction with PARL or bending into the PARL active site with subsequent modified intramembrane cleavage. Moreover, I found that a balanced net charge in the C-terminal juxtamembrane region prevents premature PGAM5 from PARL-catalyzed cleavage so that cleavage-resistant PGAM5 oligomers can assemble upon mitochondrial import. Under mitochondrial stress after disruption of the membrane potential with CCCP, I propose a model in which PGAM5 oligomers at the inner mitochondrial membrane disassemble into monomers by an unknown mechanism leading to efficient cleavage by PARL in order to trigger PGAM5's downstream activities. Taken together, my findings indicate that the substrate recognition mechanism of PARL relies on a membrane-potential-dependent oligomeric switch and different substrate features with hierarchical importance.

Zusammenfassung

Proteasen haben in allen Lebenswesen die Fähigkeit entwickelt, Peptidbindungen durch irreversible und stark regulierte Hydrolyse zu spalten. Intramembranproteasen haben einige gemeinsame Merkmale, wie ihre polytopische Struktur, in welcher die katalytischen Zentren mehrere Ångstrom tief in der Lipiddoppelschicht verborgen sind. Obwohl die Liste der physiologischen Substrate stetig wächst, bleibt die Frage, ob diese Proteasen einen konservierten Substraterkennungsmechanismus aufweisen.

In der vorliegenden Arbeit habe ich mich auf die Substraterkennung und -spaltung der menschlichen mitochondrialen Rhomboidprotease PARL am Beispiel des Substrats PGAM5 konzentriert. Eine dysfunktionale mitochondriale Qualitätskontrolle stört nicht nur den Energiestoffwechsel der Zellen, sondern auch die Aktivierung des programmierten Zelltods und kann folglich Krankheiten wie Neurodegeneration auslösen. Ein genetischer Mangel an PGAM5 führt bei Mäusen zu einer Parkinson-ähnlichen Bewegungsstörung. Die Rhomboidprotease PARL schützt das mitochondriale Gleichgewicht und prozessiert PGAM5, wenn das innere Membranpotential gestört ist. Bis heute wurden die genauen PGAM5-Substraterkennungsmuster nicht untersucht. Hier charakterisiere ich zum ersten Mal mehrere Spaltungsdeterminanten in PGAM5 auf Basis von Mutationsstudien in humaner Zellkultur, *in vitro* Proteolyse-Assays mit aufgereinigten rekombinanten Proteinen und in einem kollaborativen Projekt durch CD-Spektroskopie und Flüssigzustands-NMR. Ich kann zeigen, dass der N-terminale Teil der PGAM5 TM-Domäne eine besondere Rolle spielt und eine kritische Determinante für die PARL-katalysierte Prozessierung ist. Interessanterweise erhielt ich neben spaltungsresistenten Formen PGAM5-Mutanten mit stark erhöhter Spaltung, in welcher sie von ihrer nativen Regulation entkoppelt waren. NMR-Analyse zeigte, dass die PGAM5 TM-Domäne zwei geteilte Helices beherbergt, die durch eine gelenkartige Schleife zoniert sind. Mutationen innerhalb der N- oder C-terminalen Helix deuten auf eine veränderte Interaktion mit PARL oder Biegung in das aktive Zentrum von PARL mit anschließender modifizierter Intramembranspaltung hin. Außerdem fand ich heraus, dass eine ausgewogene Nettoladung in der C-terminalen Juxtamembran-Region eine vorzeitige Spaltung von PGAM5 durch PARL verhindert, so dass sich spaltungsresistente PGAM5-Oligomere beim mitochondrialen Import bilden können. Unter mitochondrialem Stress durch Entkopplung des Membranpotentials mit CCCP schlage ich ein Modell vor, in dem PGAM5-Oligomere in der inneren mitochondrialen Membran durch einen unbekannten Mechanismus in Monomere zerfallen, was in einer effizienten Spaltung durch PARL resultiert, um die nachgeschalteten Aktivitäten von PGAM5 auszulösen. Zusammenfassend zeigen meine Ergebnisse, dass der Substraterkennungsmechanismus von PARL auf einem membranpotentialabhängigen, oligomeren Schalter und verschiedenen Substratmerkmalen mit hierarchischer Bedeutung beruht.

Table of Contents

List of Figures

List of Tables

List of Abbreviations

Δ	Delta, deficient, change
$\Delta\Psi_{mito}$	magnitude of the inner mitochondrial membrane potential
AD	Alzheimer's disease
AAA	ATPase associated with diverse cellular activities
ADP	adenosine diphosphate
AIF	apoptosis-inducing factor
ATP	adenosine triphosphate
CCCP	carbonyl-cyanide m-chlorophenyl hydrazone
Ccp1	cytochrome c peroxidase
CFP	cyan fluorescent protein
CHX	cycloheximide
CJ	cristae junctions
CL	cardiolipin
DLPC	dilauroylphosphocholine
DMPC	dimyristoylphosphocoline
DMEM	Dulbeccos's modified eagle Medium
DPPC	dipalmitoylphosphocholine
Drp1	dynamin-related protein 1
EGF	epidermal growth factor
ER	Endoplasmic Reticulum
ERAD	endoplasmic reticulum-associated degradation
ETC	electron transport chain
FBS	fetal bovine serum
GFP	green fluorescent protein
IBM	inner boundary membrane
IF	immonuflourescence
IMM	inner mitochondrial membrane
IMP	inner membrane peptidase
IMS	intermembrane space
iRhom	inactive rhomboid
LacYTM2	second TM helix of *E. coli* LacY protein
LC3	microtubule-associated protein 1 light chain 3
MAM	mitochondria-associated ER-membrane
MBP	maltose-binding protein
Mfn1/2	mitofusin 1/mitofusin 2

Mgm1	mitochondrial genome maintenance 1
MIA	mitochondrial intermembrane space import and assembly machinery
MIM	mitochondrial import
MIP	mitochondrial intermediate peptidase
Miro	mitochondrial Rho GTPase
MPP	mitochondrial processing peptidase
MS	mass spectrometry
MTS	matrix targeting sequence
OMM	outer mitochondrial membrane
OMA1	overlapping with the M-AAA protease 1 homolog
OPA1	optic atrophy 1, dynamin-like 120 kDa protein
OXA	oxidase assembly machinery
PAGE	polyacrylamide gel electrophoresis
PAM	presequence translocase-associated motor
PARL	PINK1/PGAM5-associated rhomboid-like
Pcp1/Rbd1	processing of cytochrome c peroxidase 1/Rhomboid 1
PCR	polymerase chain reaction
PD	Parkinson’s disease
PE	phosphatidylethanolamine
PG	phosphatidylglycerol
PGAM5	PGAM family member 5
PINK1	PTEN-induced kinase 1
PHB1/2	prohibitin 1/prohibitin 2
POPC	palmitoyloleoylphosphocholine
PSEN1/2	presenilin 1/presenilin 2
RCC	respiratory chain complex
RHBDL	rhomboid-like protein
RIP	regulated intramembrane proteolysis
rpm	rounds per minute
RT	room temperature
SAM	sorting and assembly machinery
SDS	sodium dodecyl sulfate
SILAC	stable isotope labeling of amino acids in cell culture
SLP2	stomatin-like protein 2
SPP	signal peptide peptidase
SPPL	SPP-like protease
shRNA	small hairpin RNA

siRNA	small interfering RNA
TA	tail-anchored
TCA	trichloroacetic acid
TIM	translocase of the inner membrane
TM	transmembrane
TOM	translocase of the outer membrane
TrxA	thioredoxin 1
UPR	unfolded protein response
VDAC	voltage-dependent anion-selective channel protein
wt	wild type
ZMPSTE24	zinc metalloprotease STE24 homolog

1. Introduction

1.1. Proteolysis and quality control

Proteases, also termed peptidases, have evolved in all kingdoms of life with the capability to catalyze the breakdown of peptide bonds. This mechanism is called proteolysis, requires water and is in biological systems an irreversible post-translational reaction (Puente *et al.*, 2003). Interestingly, about two percent of the human and mouse genome encode for proteases highlighting their biological importance (Puente *et al.*, 2003; Rawlings *et al.*, 2004; Turk, 2006). Since accumulation of proteins, intact or damaged, can be cytotoxic in every compartment of the cell, their proteolytic degradation needs to be tightly controlled to maintain proper cellular function. The indispensable role of proteases in the maintenance of cellular protein homeostasis, referred to as proteostasis, underlies various biological processes including cell cycle progression, cell proliferation and apoptosis. Deregulation of proteases can be observed in the pathology of a variety of diseases (Puente *et al.*, 2003; Turk, 2006). Mostly, point mutations occur resulting in loss-of protease function as it has been shown in Papillon-Lefèvre syndrome (PLS) (Toomes *et al.*, 1999), limb-girdle muscular dystrophy type 2A (Huang and Wang, 2001), and nonsyndromic deafness (Guipponi *et al.*, 2002). But also, less frequent gain of-protease function mutations are observed, as shown in the presenilin-1 and -2 gene (*PSEN1* and *PSEN2*) which are linked to early-onset familial Alzheimer's disease (Citron *et al.*, 1997; Esler and Wolfe, 2001). Thus, pathological deregulations of proteases aroused interest in them as drug targets (Drag and Salvesen, 2010).

For the clearance of proteins, the eukaryotic cell operates with two major systems, in particular lysosomes and the ubiquitin-proteasome system (UPS). Lysosomes budding off from the trans-Golgi network are membrane-enclosed organelles of the endocytic system that harbor different enzymes with no strong substrate specificity in an acidic interior to break down endocytosed proteins, but also lipids and carbohydrates that are too large for the proteasome. Besides plasma membrane proteins and extracellular material that are taken up by endocytosis, also cytosolic proteins and whole organelles can be absorbed utilizing the autophagy pathway. Even macrophages that have engulfed bacteria can be cleared by lysosomes after fusion (Huotari and Helenius, 2011; Morishita and Mizushima, 2019). The UPS is based on the attachment of polyubiquitin as a marker that targets cytosolic and nuclear proteins for rapid degradation by the proteasome. The ubiquitin label can either be attached to the free N-terminus or to an internal lysine residue (Pickart and Eddins, 2004), threonine, serine or cysteine (Husnjak and Dikic, 2012). In this multistep process, ubiquitin is activated in an ATP-dependent manner by a ubiquitin-activating enzyme (E1), gets transferred to a ubiquitin-conjugating enzyme (E2) and is eventually bound to the substrate destined to be degraded by a ubiquitin-protein ligase (E3). Such polyubiquitinated substrates finally undergo

ATP-dependent proteasomal degradation, which releases the ubiquitin-tags to be recycled (Weissman *et al.*, 2011).

1.1.1. Mechanisms of peptide bond hydrolysis

Different classes of proteases exist, which are distinguished by their catalytic mechanism and residues. Generally, enzymes cleaving a protein from either its N- or C-terminus build the group of exopeptidases and differentiated as aminopeptidases or carboxypeptidases, respectively. Proteases that cleave proteins within the polypeptide chain are named endopeptidases (Turk, 2006). In total, seven distinct classes of proteases are known: metalloproteases, cysteine, aspartic acid, asparagine, glutamic acid, threonine and serine proteases (Puente *et al.*, 2003; Rawlings, 2017; Rawlings *et al.*, 2004). Catalytic activity of all of these protease classes underlies the same mechanism of nucleophilic attack on the peptide's carbonyl group by a pair of electrons which initiates proteolysis (Hollands and Fruton, 1969). However, the stabilization of the tetrahedral intermediate differs among the protease classes. Metalloproteases, aspartic acid, and glutamic acid proteases use only one activated water molecule as nucleophile attacking the carbonyl carbon of the substrate's peptide bond to generate the tetrahedral oxyanion intermediate in a single-step acid-base catalytic reaction. Subsequently the substrate is separated into two fragments after protonation of the scissile bond and rearrangement of the intermediate (James *et al.*, 1977; Suguna *et al.*, 1987). For cysteine, threonine and serine proteases the nucleophile is part of the enzyme itself. The active site of serine proteases for instance harbors a catalytic triad consisting of serine, histidine and aspartic acid to perform peptide bond hydrolysis (Blow *et al.*, 1969; James *et al.*, 1977). Here, the hydroxyl group of the serine residue acts as the nucleophile, that attacks the substrate's carbonyl group resulting in the formation of the tetrahedral oxyanion intermediate. This is followed by formation of an acyl-enzyme intermediate and liberation of the N-terminal fragment. A final hydrolysis step of the acyl-enzyme intermediate eventually results in generation and ejection of the C-terminal fragment from the enzyme's catalytic site (Hedstrom, 2002; Turk, 2006).

1.1.2. Regulation of proteolysis and specificity of proteases

Since hydrolysis of peptide bonds is irreversible in cells, proteolysis serves as an important type of cellular regulation and is tightly controlled on different levels. Besides regulation by endogenous or exogenous inhibitors (López-Otín and Bond, 2008), eukaryotic cells utilize classic control checkpoints along the stages of transcription, translation and post-translational modifications (Turk, 2006). Depending on the specific function or abundance, some proteases are ubiquitously expressed, like the lysosomal protease cathepsin, whereas others can be found only in certain cell types, or are expressed during certain developmental stages and cellular conditions, like the cytotoxic serine protease granzyme M (GrM) (de Koning *et al.*,

2010; Turk, 2006; Turk *et al.*, 2012). Some proteases are synthesized as inactive precursors that need to be activated by proteolytic cleavage to mature into the biologically active form. Alternatively, the enzyme's active site can undergo conformational rearrangement to become active (Ehrmann and Clausen, 2004). Interestingly, also epigenetic modifications are possible. Certain matrix metalloproteases (MMPs) could be shown to be regulated by stability, translation and degradation of mRNAs via RNA-binding proteins and microRNAs, spatial and temporal compartmentalization, oligomerization into functional complexes, or autolysis (López-Otín and Bond, 2008; López-Otín and Overall, 2002).

The substrate spectrum of proteases can either be narrow and highly specific, or overlapping with only loose specificity towards the substrates. Specificity first of all relies on the proteases' endo- or exopeptidase function (Taylor, 1993; Turk, 2006) and compartmentalization, since protease and substrate need to colocalize for a proper reaction (Ehrmann and Clausen, 2004). Furthermore, specificity is achieved by the structural properties of the protease's active site and by the consensus site of the substrate. Although usually not all consensus sites are recognized by a protease, a nomenclature was proposed by (Schechter and Berger, 1967) in order to systematically describe peptidase cleavage at the substrate scissile bond. Surrounding substrate residues are known as P1 and P1'. Subsequent residues towards the substrate N-terminus are numbered ascending P2, P3 and so on. Accordingly, residues towards the C-terminus are numbered P2', P3' and so forth. The substrate binding pocket, also known as subsite, in the enzyme is named with "S". Hence, respectively the S1 binding pocket accommodates the P1 residue, and so on. The reason why only a limited number of substrate consensus sites can be recognized and proteolytically processed is explained by the appearance of fully folded proteins. Conformations in which interaction partners can shield the scissile bond or where the cleavage site is buried deep in the protein fold, thereby preventing proteolysis, are very common (Ellison *et al.*, 1995; Reed *et al.*, 1975; Turk *et al.*, 2012). These restrictions on substrate consensus site availability are resumed in the term 'limited proteolysis'. Limited proteolysis is a frequent regulation mechanism in the cell and is deployed in various biological processes. For instance, thrombin activates platelets by limited proteolysis of protease-activated receptors (Kulman and Davie, 2013). Moreover, enteropeptidases in the mammalian digestive tract use limited proteolysis in the activation of precursor proteins, the so-called zymogens. Two well-studied examples are the activation of the zymogen plasminogen into its active form plasmin or trypsinogen into its active form trypsin (Kunitz, 1939; Swaisgood, 1995). Additionally, also transcription and growth factors can be liberated from their inactive membrane-bound precursors by limited proteolysis in cellular signaling (De Strooper *et al.*, 1999; Rawson *et al.*, 1997), which is commonly catalyzed by intramembrane proteases. For a detailed discussion of intramembrane proteolysis, see (**chapter 1.5**).

As an interesting remark, I want to mention that so far, no human protease is known to cleave after the amino acid residue glutamine, bringing viral protease inhibitors into the research focus

as just dealing with the Coronavirus SARS-CoV-2 pandemic. It could be shown that the SARS-CoV-2 main protease M^{pro}, as of many other coronaviruses (Kiemer *et al.*, 2004), exclusively processes polypeptide sequences after a glutamine residue, vaulting the main protease as an ideal drug target to fight COVID-19 (Hilgenfeld, 2014; Zhang *et al.*, 2020a; Zhang *et al.*, 2020b).

1.2. A correct mitochondrial architecture maintains cell homeostasis

Mitochondria are double-membrane-bound cell organelles that can be found in most eukaryotic organisms. Following the 'endosymbiosis theory', numerous lines of evidence are given that mitochondria developed over 1.5 billion years ago through the invasion of an aerobic α-proteobacterium that was integrated into a large anaerobic bacterium (Dyall *et al.*, 2004; Gray *et al.*, 1999). The mitochondrial genome is thought to be regulated dynamically (Zhang *et al.*, 2008), shares substantial similarities to bacterial genomes and is encrypted in a 16.5 kbp (kilo base pair) long ring-like DNA molecule (mtDNA). Due to the functional diversity of mitochondria, varying shapes and alterations in the mitochondrial proteome can be observed between different cells and tissues (Alberts *et al.*, 2015). The two structurally and functionally distinct mitochondrial membranes form smaller compartments, creating an 'outside' and an 'inside' of the membrane (Schatz and Dobberstein, 1996; van der Laan *et al.*, 2012). The outer mitochondrial membrane (OMM) represents a barrier to the cytosol on the one side and the intermembrane space (IMS) on the other side. The inner mitochondrial membrane (IMM) demarcates the IMS from the mitochondrial matrix, while forming cristae, loop-like invaginations protruding into the matrix (**Figure 1**) to enlarge the IMM surface up to five times. Further, in the IMM two topologically different domains can be divided: the inner boundary membrane (IBM), which underlies directly the OMM and second, the cristae membrane enclosing the intracristae space, which is connected to the IBM by tubular-shaped cristae junctions. These junctions were described to limit molecule diffusion between the IMS and the intracristae space, as well as between the IMM domains (Davies *et al.*, 2011; Strauss *et al.*, 2008; Vogel *et al.*, 2006; Wurm and Jakobs, 2006). Whereas the OMM harbors mainly porins for molecule diffusion as well as different translocase systems (Mannella, 1992), the IMM lacks porins and is impermeable to molecules. On the contrary, the IMM is considered as the protein-richest cellular membrane, comprising the oxidative phosphorylation complexes (OXPHOS) and F_1F_0-ATP synthase units (Stuart, 2002). The protein composition of the IBM and cristae membranes build by the IMM vary depending on its different functions (Vogel *et al.*, 2006; Werner and Neupert, 1972; Wurm and Jakobs, 2006). Whereas proteins involved in membrane remodeling and preprotein import are mainly found in the IBM (Suppanz *et al.*, 2009), respiration complexes and ATP synthetases are localized exclusively to cristae membranes (Gilkerson *et al.*, 2003). Without the correct mitochondrial architecture protein import into mitochondria would be hampered, since the translocase complexes of the outer and inner mitochondrial membrane have to be aligned (Chacinska *et al.*, 2009). Moreover, the OMM is

known to be physically linked with the Endoplasmic Reticulum (ER) to provide communication between the two organelles and metabolic exchange via mitochondria-associated ER-membranes (MAMs) (Hoppins *et al.*, 2011; Kornmann *et al.*, 2009; von der Malsburg *et al.*, 2011), highlighting the importance of a correct architecture of the mitochondrial membranes for mitochondrial function and thereby homeostasis of the entire cell.

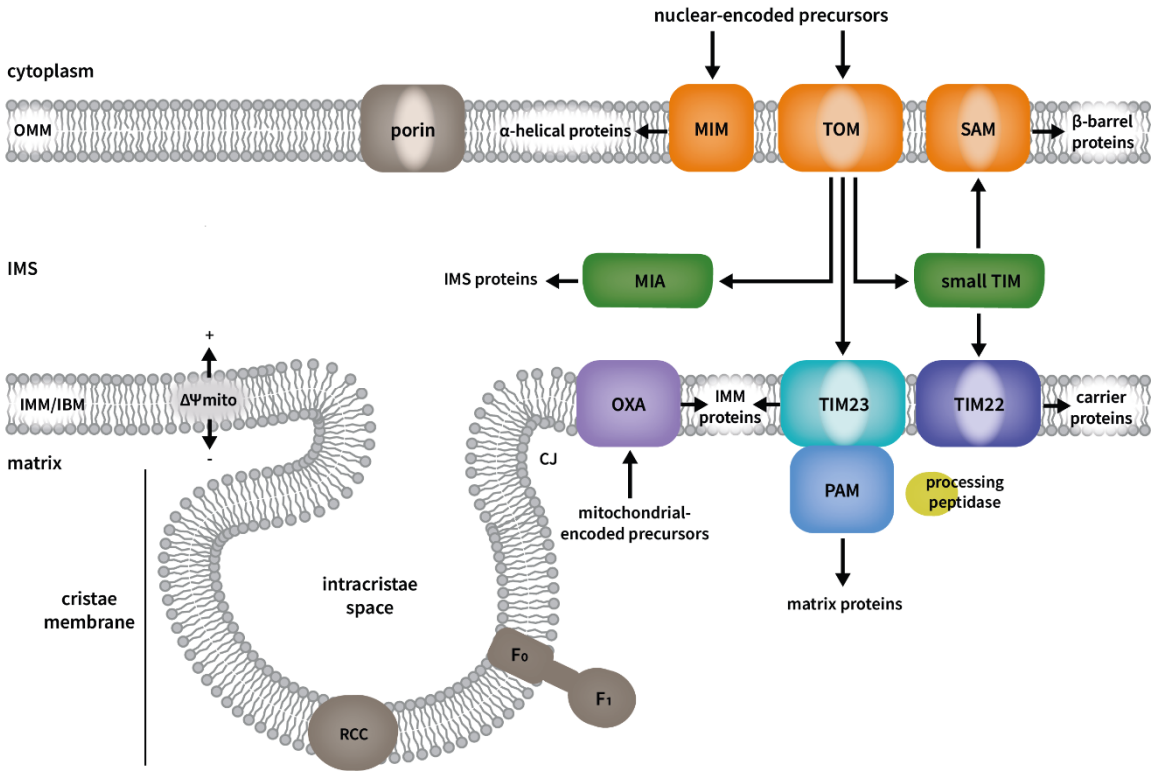

Figure 1 | Schematic representation of mitochondrial architecture and protein import pathways.
Preproteins carrying a presequence are imported by TOM and the presequence translocase TIM23. Hydrophilic proteins are imported into the matrix via PAM, whereas proteins with a hydrophobic sorting signal can be released into the IMM. Mitochondrial processing peptidases remove the presequences. Cysteine-rich IMS proteins are imported by TOM and MIA, inserting disulfide bonds into the imported proteins. Precursors of β-barrel proteins are imported via TOM to the small TIM chaperones and are inserted into the OMM by SAM. Precursors of IMM metabolite carriers are imported via TOM, small TIM chaperones, and the carrier translocase TIM22. Precursors of α-helical OMM proteins are imported by the MIM complex. The inner mitochondrial membrane potential ($\Delta\Psi_{mito}$) is necessary for correct protein translocation by the TIM23 and TIM22 complexes. Mitochondrial-encoded IMM precursors are exported from the matrix into the IMM via OXA. CJ: cristae junctions, F_1F_0: F_1F_0 ATP synthetase, RCC: respiratory chain complexes. Simplified from (Wiedemann and Pfanner, 2017).

1.2.1. Mitochondria function as 'powerhouses' of the cell

Mitochondria are the cell organelles that provide most of the cellular energy by generation of adenosine triphosphate (ATP) from adenosine diphosphate (ADP) out of saved energy from glucose or fatty acids under oxygen consumption by so-called oxidative phosphorylation. After import of pyruvate, which is the result of glycolysis into the mitochondrial matrix, bound energy from the covalent bonds of pyruvate is converted into high-energy electrons and stored in the reduced coenzymes NADH and $FADH_2$ as a result of the citric acid cycle. Such electrons are required to drive the electron transport chain in the respiration complexes within the cristae membranes. The resulting electron flow transports protons across the IMM into the IMS, which in turn generates potential energy in form of a pH gradient and an electrical potential across the membrane. As soon as protons flow back across the IMM down the potential energy gradient into the matrix and through F_1F_0-ATP synthase complexes, the energy is used to transform ADP to ATP in a phosphorylation reaction (Dimroth *et al.*, 2000; Mitchell and Moyle, 1967; Schultz and Chan, 2001). Moreover, mitochondria produce heat through proton leaking, (Vafai and Mootha, 2012). Although oxidative phosphorylation is an essential process of the metabolism, it produces dangerous reactive oxygen species (ROS) such as hydrogen peroxide and superoxide, resulting in the propagation of free radicals that damage cells, increase aging and senescence and in general can contribute to a range of pathologies (Murphy, 2009).

1.2.2. Mitochondria store calcium during physiological signaling

The main storage organelle for calcium (Ca^{2+}) in the eukaryotic cell is the ER. Nevertheless, also mitochondria can transiently save calcium in order to maintain cellular calcium homeostasis in a variety of cell types (Duchen, 2000; Rizzuto *et al.*, 1993). Calcium is associated with fertilization, functions as second messenger in cells and has an impact on the release of neurotransmitters, which are important for muscle contraction (Carafoli, 2004; Qi *et al.*, 2007). Due to close proximity of the ER and mitochondria via the MAMs, Ca^{2+}-funneling from the ER to mitochondria is driven by a calcium uniporter (Miller, 1998). This Ca^{2+} uniporter was described to function as the primary uptake mechanism and is dependent on the electrochemical potential gradient, which is maintained by functional respiration and the inner mitochondrial membrane potential ($\Delta\Psi_{mito}$) (Gunter *et al.*, 1998; Rizzuto *et al.*, 2000). Additional to the uniporter, a pathway for rapid Ca^{2+} uptake at physiological concentrations was described (Sparagna *et al.*, 1995), whereas export and re-equilibration of mitochondrial Ca^{2+} is mainly achieved through the activity of the mitochondrial Na^{+}-Ca^{2+} exchanger in the IMM (Cox *et al.*, 1993; Griffiths *et al.*, 1998; Miller, 1991). Mitochondrial Ca^{2+} uptake has a major impact on mitochondrial function as it mainly targets the citric acid cycle, since the rate-limiting enzymes are upregulated by Ca^{2+}-dependent processes (Maechler and Wollheim, 2000; Rizzuto *et al.*, 2000). Moreover, mitochondrial calcium levels control different cell-type specific functions,

including intracellular Ca^{2+} signaling (Dolmetsch *et al.*, 1998), cell metabolism (Hansford, 1994; McCormack and Denton, 1979; McCormack *et al.*, 1990) and cell survival (Cribbs and Strack, 2007; Orrenius *et al.*, 2003; Scorrano *et al.*, 2002).

1.2.3. Biosynthesis pathways rely on mitochondrial function

As variable the Ca^{2+}-dependent functions of mitochondria are, as variable is the influence of mitochondrial functions on different biosynthesis pathways. For instance, mitochondria cooperate with the ER via MAMs in the production of certain lipids (Vance and Shiao, 1996). Whereas phosphatidylglycerol, phosphatidylethanolamine and cardiolipin are synthesized in mitochondria, the ER generates lipids like phosphatidylserine, phosphatidylcholine and phosphatidylinositol that in turn are imported into mitochondria (Osman *et al.*, 2011). Besides lipid synthesis, mitochondria are also involved in the biogenesis of iron-sulfur clusters, steroids and heme. Iron-sulfur clusters function as ubiquitous cofactors of proteins with a role in electron transport, catalysis and environmental sensing (Lill, 2009). In steroid biogenesis, mitochondria comprise the rate-limiting and Ca^{2+}-dependent step of converting cholesterol to pregnenolone (Capponi *et al.*, 1988; Cherradi *et al.*, 1996; Python *et al.*, 1995; Rossier, 2006). Additionally, some essential reactions of eight enzymatic steps of the heme biosynthesis take place in mitochondria (Severance and Hamza, 2009). Heme functions as the prosthetic group in proteins of various cellular functions, for instance in respiratory proteins (York *et al.*, 1967).

1.2.4. Mitochondria and its multifaceted role in cell death pathways

Although mitochondria power life through their various metabolic functions, on the contrary they play a central role in apoptotic cell death as result of metabolic insults, stress or genotoxic reagents. Typically, the OMM is permeable to molecules smaller than 5 kDa but upon the induction of mitochondrial apoptosis the OMM forms pores as part of mitochondrial outer membrane permeabilization (MOMP) that allows it to accommodate proteins larger than 100 kDa (Kalkavan and Green, 2018). Further, MOMP leads to the release of various IMS proteins, including cytochrome c, Smac/DIABLO and Omi/HtrA2 that function as apoptogenic factors and commit a cell to die (Chipuk *et al.*, 2006; Green and Kroemer, 2004). In vertebrates two main pathways are known for apoptosis, often termed the extrinsic and intrinsic pathways, depending on the initiating signal (Strasser *et al.*, 1995). Whereas the extrinsic pathway is initiated via death receptors at the cell membrane, the intrinsic pathway involves mitochondria and is controlled by the BCL-2 protein family resulting in MOMP. Both pathways lead to the activation of caspases and formation of the apoptosome (Kroemer *et al.*, 2007; Li *et al.*, 1997; Vaux, 2011), leading to rapid apoptosis typically within a few minutes (Albeck *et al.*, 2008; Goldstein *et al.*, 2000). Activated caspases, which are cysteine-aspartic proteases, selectively cleave hundreds of different cellular key signaling factors (Salvesen and Ashkenazi, 2011)

leading to chromatin condensation, nuclear fragmentation, cell shrinkage, the generation of apoptotic bodies and finally removal by phagocytic cells (Ballard and Holt, 1968). In more detail, the BCL-2 protein family comprises anti-apoptotic proteins, pro-apoptotic effectors and pro-apoptotic BH3-only proteins (Youle and Strasser, 2008). When experiencing apoptotic stress, BH3-only proteins like BIK, BID, BIM and PUMA are activated via diverse ways, inhibit anti-apoptotic proteins or directly bind to other pro-apoptotic proteins in order to stimulate their activity, like BAX and BAK that eventually oligomerize and cause MOMP (Letai *et al.*, 2002; Willis *et al.*, 2007; Youle, 2007). On the contrary in healthy unstressed cells, anti-apoptotic BCL-2 proteins prevent MOMP by binding activated BAX and BAK effectors and BH3-only proteins (Llambi *et al.*, 2011). Whereas BAX was shown to travel between the cytosol and mitochondria in healthy unstressed cells, BAK has a transmembrane (TM) domain and is constitutively inserted into the OMM where it becomes retro-translocated by the anti-apoptotic BCL-X_L protein (Edlich *et al.*, 2011). Incomplete MOMP (iMOMP) or minority MOMP (miniMOMP) was observed in response to various stimuli often as the result of sublethal stress and can contribute to cellular recovery when caspase activity is blocked (Tait *et al.*, 2010). Such an incomplete execution with blocked caspase activity is also observed in cancer cells and as part of neurodegenerative disorders, highlighting again the important role of mitochondria in controlled elimination of cells (Bock and Tait, 2020; Carneiro and El-Deiry, 2020; Thompson, 1995).

1.3. Mitochondrial protein synthesis and targeting is highly regulated

Whereas the vast majority of approximately 1500 mitochondrial proteins in human are encoded in the nucleus and are synthesized on cytosolic ribosomes, in humans only 13 mitochondrial proteins are exclusively produced in the mitochondrial matrix. These proteins are mostly components of the multi-subunit electron transport chain (ETC) and OXPHOS (Calvo *et al.*, 2016; Mossmann *et al.*, 2012). In order to maintain mitochondrial protein homeostasis (proteostasis), a balanced interplay between protein expression, import/export and degradation is mandatory. Disturbances in this complex protein-equilibrium are related to a multitude of neurodegenerative diseases (Powers *et al.*, 2009). Whereas mitochondrial-encoded proteins are inserted co-translationally into the IMM (Ott and Herrmann, 2010), most of the nuclear-encoded mitochondrial proteins are post-translationally imported to become sorted to the respective sub-compartment. However, also co-translational import reactions are known to be mandatory for some mitochondrial proteins (den Brave *et al.*, 2021; Verner, 1993). Incorrect stoichiometric compositions of functional subunits, imbalances in their expression or proteins with impaired function due to modifications and folding immediately activate an independent proteolytic system, which allows the complete degradation of such proteins to amino acids (Quirós *et al.*, 2015; Stadtman and Berlett, 1998). Mitochondria are highly dynamic organelles, which are capable of changing their morphology in order to replace damaged

proteins or exchange mitochondrial contents as a form of complementation by undergoing fusion reactions. On the contrary, mitochondrial fission represents a way to eliminate impaired organelles by activation of the autophagy pathway (mitophagy) and facilitates apoptosis during high levels of cellular stress (Youle and van der Bliek, 2012). The correct interplay between protein import/export, degradation, fusion and fission is mandatory to maintain proper function of mitochondria-dependent energy production, signaling, biosynthesis and therefore cell survival.

1.3.1. Mitochondria strictly depend on import of precursor proteins from the cytosol

Nuclear-encoded proteins are imported into mitochondria post- and co-translationally to eventually being sorted to the correct destination via certain targeting signals, which can be found exposed at the protein N-terminus or internally integrated into the protein fold (Horwich *et al.*, 1985; Hurt *et al.*, 1984a, b; Pfanner *et al.*, 1987a). Therefore, three main classes can be distinguished: signal-anchored proteins, tail-anchored proteins, and polytopic (multispanning) outer-membrane proteins. Up to now, five different transport pathways are known, which are characterized by a different type of targeting signal, each (Wiedemann and Pfanner, 2017) (**Figure 1**). The vast majority of matrix proteins and many IMM proteins are synthesized with N-terminal targeting signals and are imported via the classical presequence pathway (Abe *et al.*, 2000; Roise *et al.*, 1986; Vögtle *et al.*, 2009). In this pathway, as outlined in the following paragraph, almost all precursors enter mitochondria by the translocase complexes of the outer membrane (TOM) and of the inner membrane (TIM), usually followed by removal of the N-terminal presequences upon completion of import (Hawlitschek *et al.*, 1988; Mossmann *et al.*, 2012). Contrary to that, precursor proteins with internal presequences utilize one of the four other major protein import pathways, that will be described in the following paragraphs, as they are not cleaved and the internal targeting signal remains part of the mature protein. Also here, the TOM complex functions as the main mitochondrial entry gate. Precursors of multispanning hydrophobic carrier proteins targeted to the IMM are imported via the carrier pathway, proteins targeted to the IMS use the oxidative folding pathway via the mitochondrial import and assembly (MIA) machinery, precursors of β-barrel proteins targeted to the OMM are imported via the β-barrel pathway and OMM proteins with α-helical TM segments utilize the mitochondrial import (MIM) complex. However, recent publications also describe import routes with combined elements of different import and processing pathways (Wiedemann and Pfanner, 2017). Depending on the maturation process also dual targeting of mitochondrial proteins was observed, for review see (Yogev and Pines, 2011). For instance, the mitochondrial PTEN-induced kinase 1 (PINK1) was found to be not fully imported into the IMM during its maturation, thereby spanning the OMM, IMS and IMM as import intermediate, losing

its membrane anchor by proteolytic cleavage and being released into the cytoplasm (Lin and Kang, 2010; Meissner *et al.*, 2011).

1.3.1.1. The presequence pathway: import of matrix and IMM proteins

About 60% of all nuclear-encoded mitochondrial proteins are synthesized in the cytosol with a cleavable presequence of variable length between <10 amino acid residues to even up to 100 residues at their N-termini, often termed mitochondrial targeting peptide or matrix-targeting signal (MTS). The presequences form positively charged amphipathic α-helices harboring a hydrophobic face (Roise *et al.*, 1986). Receptors and other import components specifically recognize the elements of the amphipathic helix during preprotein translocation involving TOM, the presequence translocase of the IMM TIM23, and the presequences translocase-associated motor (PAM). The TOM complex consists of three cytosol-exposed receptors and a pore-forming core by the channel-forming protein Tom40 and three additional small Tom proteins (Hill *et al.*, 1998; Kiebler *et al.*, 1990; Mokranjac and Neupert, 2015; Shiota *et al.*, 2015). To ensure proper import, the translocases of the OMM and IMM have to transiently interact: when a protein passes the Tom40 channel on the side of the IMS, Tim50 binds as a receptor and hands the protein over to Tim23, which is closely associated with Tim17 (Albrecht *et al.*, 2006; Callegari *et al.*, 2020; Chacinska *et al.*, 2005), a mechanism that requires a functional electrochemical hydrogen ion gradient as part of an intact $\Delta\Psi_{mito}$ to further translocate proteins to the matrix (Gasser *et al.*, 1982; Kolansky *et al.*, 1982; Schleyer *et al.*, 1982). Whereas proteins with a hydrophobic stop-transfer signal are arrested during import to be laterally sorted into the IMM (Glick *et al.*, 1992; Schendzielorz *et al.*, 2018), precursors with a positively charged presequence targeted to be translocated into the matrix get fully imported by interaction with PAM in an ATP-dependent manner (Chen and Douglas, 1987; Eilers *et al.*, 1987; Pfanner and Neupert, 1986; Pfanner *et al.*, 1987b). It has been proposed that proline residues in the TM domain of the precursors are recognized during import by TIM23 so that the two destinations to the IMM or the matrix can be differentiated. Proline residues in the hydrophobic TM domains and the presence of charged residues C-terminally flanking the TM domain were shown to strongly favor the transfer of preproteins to the matrix, instead of the translocation arrest with lateral sorting into the IMM (Meier *et al.*, 2005). The presequences of both IMM-sorted and matrix-targeted preproteins is eventually cleaved off by matrix-localized proteases like the mitochondrial processing peptidase (MPP) or the inner-membrane metalloprotease overlapping activity with *m*-AAA proteases (OMA1) (Anand *et al.*, 2014), either during or after transport through the TIM23 complex (Conboy *et al.*, 1982; Greene *et al.*, 2012; Schmidt *et al.*, 1984). However, alternative mechanisms have been observed (Chacinska *et al.*, 2009; Rospert *et al.*, 1993; Waltner and Weiner, 1995).

1.3.1.2. The carrier pathway: import of multi-spanning IMM proteins

Many IMM proteins with multiple α-helical TM domains, like most carrier proteins, are synthesized without a cleavable presequences but contain internal targeting signals instead (Brix *et al.*, 1999; Endres *et al.*, 1999). The precursors interact and bind to cytosolic chaperones, such as the ATP-dependent heat-shock proteins (Hsp70/Hsp90). Although the exact import mechanism remains unclear, it is hypothesized that targeting components cooperate in binding of the ADP/ATP and phosphate carriers to the receptor Tom70 prior to sorting to the IMM (Humphries *et al.*, 2005; Young *et al.*, 2003). After the precursor is transferred to the central receptor Tom22, release into the Tom40 channel follows in a loop formation, with both termini still in the cytosol (Wiedemann *et al.*, 2001). Small IMS-resident TIM chaperones are recruited to the OMM by an N-terminal segment of Tom40 and eventually deliver the precursors to the carrier translocase of the IMM (TIM22) that further mediates lateral release and insertion driven by the forces of the inner membrane potential. It is speculated that insertion into the IMM includes a similar loop formation as seen for the OMM, since TIM22 forms a twin-translocase (Curran *et al.*, 2002; Rehling *et al.*, 2003; Vial *et al.*, 2002; Wiedemann *et al.*, 2001).

1.3.1.3. The MIA pathway: import and assembly of IMS proteins

The bacterial periplasm, the ER and the mitochondrial IMS contain numerous proteins with characteristic cysteine motifs that form intramolecular disulfide bonds (Herrmann and Riemer, 2014). In the IMS, such proteins do not contain cleavable targeting sequences and rely on the TOM complex and the oxidative protein folding machinery driven by oxidoreductase Mia40 (Chacinska *et al.*, 2004; Chatzi *et al.*, 2016; Fischer and Riemer, 2013; Naoé *et al.*, 2004). Small TIM chaperones for instance are typical IMS substrates (Milenkovic *et al.*, 2009) of Mia40, which cooperates with the sulfhydryl oxidase Erv1 or the FAD-dependent thiol oxidase ALR in a disulfide relay (Banci *et al.*, 2012; Mesecke *et al.*, 2005; Rissler *et al.*, 2005). In more detail: When an unfolded precursor from the cytosol passes the OMM in a reduced state via the Tom40 channel, it is quickly handed over to Mia40. Erv1 generates a disulfide bridge and transfers it to Mia40, which in turn forms a transient disulfide bridge with its substrate dependent on an internal cysteine-containing signal (Sideris *et al.*, 2009). By oxidizing cysteines in the precursors, Mia40 generates new disulfide bonds in the protein and the electrons are transferred from the oxidized substrates via Mia40 to Erv1 and finally to cytochrome c or molecular oxygen (Bien *et al.*, 2010; Bihlmaier *et al.*, 2007; Dabir *et al.*, 2007; Kawano *et al.*, 2009). The substrate spectrum of the MIA system was shown to be larger than initially expected and to contribute also to the biogenesis and quality control of IMM and matrix proteins. Examples are Tim17, Tim22 and the mitochondrial ribosomal subunit Mrp10. Whereas oxidation of Tim17 to form an intramolecular disulfide bond can be directly performed

by Erv1 (Ramesh *et al.*, 2016), formation of an intramolecular disulfide bond in Tim22 is generated by Mia40 before membrane integration can take place (Okamoto *et al.*, 2014; Wrobel *et al.*, 2016; Wrobel *et al.*, 2013). In the case of Mrp10, which contains an unusual proline-rich N-terminal MTS that enables interaction with and oxidation by Mia40 (Longen *et al.*, 2014) results in two disulfide bonds and is eventual import via the presequence pathway through TIM23 into the matrix. Moreover, some IMS-precursor proteins also use the presequence pathway after their initial membrane-anchors were cleaved off by proteases (**chapter 1.3.1.1.)** (Chen *et al.*, 1999; Nunnari *et al.*, 1993).

1.3.1.4. The OXA pathway: export of mitochondrial-encoded IMM proteins

The few mitochondrial-encoded proteins that are destined to be inserted into the IMM have to be exported from the matrix by the oxidase assembly (OXA) translocase (Hell *et al.*, 2001). Matrix ribosomes permanently attached to and interacting with Oxa1 and Mba1 of the OXA machinery in the IMM generate the mitochondrial-encoded proteins (Ott *et al.*, 2006; Pfeffer *et al.*, 2015; Prestele *et al.*, 2009; Preuss *et al.*, 2001), thereby facilitating insertion of the hydrophobic membrane proteins. In contrast to matrix and multi-spanning IMM proteins inserted by the presequence pathway and carrier pathway, respectively, protein insertion by the OXA machinery does not rely on the inner mitochondrial membrane potential but follows the positive-inside rule, as seen during insertion of nuclear-encoded mitochondrial proteins targeted to the IMM (Ott and Herrmann, 2010; Rojo *et al.*, 1999; Rojo *et al.*, 1995).

1.3.1.5. The β-barrel pathway: import of β-barrel OMM proteins

Whereas β-barrel proteins in the outer membrane of mitochondria and chloroplasts reflect the bacterial origin (Schmidt *et al.*, 2010), α-helical OMM proteins source from the eukaryotic cell and their precursors are not imported by one unique pathway. So far, mitochondria were predicted to contain only four types of β-barrel outer membrane proteins: the SAM complex channel Sam50, Tom40, the metabolite channel porin VDAC and Mdm10, which is part of the endoplasmic reticulum (ER)-mitochondria encounter structure (ERMES) (Walther *et al.*, 2009). The nuclear-encoded precursors are imported into mitochondria via the Tom40 channel of the TOM complex, bind to small TIM chaperones in the IMS, which are also implicated in the MIA pathway, and are eventually inserted into the OMM by the sorting and assembly machinery (SAM). During import, the receptor Tom22 and the peripheral membrane protein Sam37 link TOM and SAM into a transient supercomplex. Folding of the β-barrel occurs after Sam35 recognizes the sorting signal and hands the precursor over to Sam50, followed by Sam37-mediated release of the barrel into the lipid bilayer of the OMM (Klein *et al.*, 2012; Paschen *et al.*, 2003; Wiedemann *et al.*, 2003). If and how Tom40 can open laterally towards the lipid bilayer is still under debate (Guan *et al.*, 2021). In line with the ‘endosymbiosis theory’ the

central protein Sam50 and the basic mechanism of β-barrel sorting have been conserved from bacteria (BamA and BAM complex) to mitochondria and bacterial β-barrel proteins have been shown to be properly imported and assembled in mitochondria (Kozjak-Pavlovic *et al.*, 2011; Ulrich *et al.*, 2014; Walther *et al.*, 2009).

1.3.1.6. The MIM pathway: import of α-helical OMM proteins

Insertion of α-helical proteins into the OMM depends, like seen for IMM proteins, on the targeting signal that can have different positions either within or outside the TM domain of the precursors. Flanking positively charged amino acid residues in the TM segments with modest average hydrophobicity can function as both membrane anchors and mitochondrial targeting signals (Kanaji *et al.*, 2000; Shore *et al.*, 1995; Suzuki *et al.*, 2000; Waizenegger *et al.*, 2003). However, the exact recognition and targeting mechanisms are still under debate and insertion into the OMM independent of any known insertion machinery have been described (Kemper *et al.*, 2008; Meineke *et al.*, 2008; Setoguchi *et al.*, 2006). The protein insertase for signal-anchored and polytopic OMM proteins is the mitochondrial import complex (MIM), which itself consists of multiple copies of small single-spanning Mim1 and one copy of Mim2 (Wiedemann and Pfanner, 2017). Whereas polytopic α-helical proteins use the Tom70 receptor that cooperates with MIM for insertion (Becker *et al.*, 2011; Papić *et al.*, 2011), the majority of tail-anchored proteins is thought not to use a proteinaceous import machinery and their import may be assisted by the lipid composition of the membrane (Kemper *et al.*, 2008; Krumpe *et al.*, 2012; Setoguchi *et al.*, 2006). In the case of the signal-anchored proteins Tom20 and Tom70 a MIM-dependent insertion could be shown (Becker *et al.*, 2008; Dimmer *et al.*, 2012; Hulett *et al.*, 2008; Popov-Celeketić *et al.*, 2008). Precursors with an internal targeting signal like Mim1 and Tom22, whose C-termini are located in the IMS, both are imported by TOM receptors and the SAM complex (Keil and Pfanner, 1993; Papić *et al.*, 2013; Stojanovski *et al.*, 2007), although the final insertion steps differ. Interestingly, several examples revealed individual transport routes and insertion pathways for α-helical proteins into the OMM and future investigations are needed to draw a full picture of the exact OMM sorting and insertion mechanisms.

1.3.2. Mitochondrial quality control: proteolysis of mitochondrial proteins

Mitochondrial quality control is not only essential to maintain the cellular energy metabolism but also to control programmed cell death to avert disruptive mechanisms in a multicellular organism (Ni *et al.*, 2015; Truban *et al.*, 2017). It was described that at least 23 peptidases are exclusively localized within mitochondria, while others can shuttle between the cytosol and mitochondria (Quirós *et al.*, 2015) contributing to a continuous recycling of the mitochondrial proteome. It could be shown in yeast that 5-10% of the mitochondrial proteome is disintegrated

per generation time (Augustin *et al.*, 2005). Although proteins of the OMM are described to be degraded in the cytosol (Karbowski and Youle, 2011), the double-membrane organelle structure of mitochondria shields the IMS, IMM and matrix from the cytosol and demands an own degradation system for its sub-compartments. Interestingly, it was revealed that also IMS proteins can use Tom40 and the MIA pathway in the opposite direction to be retro-translocated into the cytosol for degradation by the proteasome when their oxidative folding is impaired (Bragoszewski *et al.*, 2013; Bragoszewski *et al.*, 2015). In order to break down proteins into small peptides or amino acids, ATP-dependent proteases within the IMS, IMM and the matrix exist, like AAA+ (ATPases associated with diverse cellular activities), for detailed description see (**chapter 1.3.2.2**). These use the energy derived from hydrolysis of ATP for complete unfolding of the substrate so that the protease can access the polypeptide bonds. Comparable to the removal of targeting signals of protein precursors during import into mitochondria, distinct processing peptidases also remove matrix targeting sequences or help to release active proteins from the IMM that are destined to be degraded by limited proteolysis. Hence, in contrast to the ATP-dependent proteases, proteolysis of the processing peptidases does not result in complete breakdown of the stably folded protein since only a limited number of cleavage sites is accessible to the enzyme (Goulet and Nepveu, 2004).

1.3.2.1. Proteasomal degradation of OMM proteins

It could be shown that most proteins of the OMM share functions in membrane dynamics and apoptosis (Karbowski and Youle, 2011) and if damaged are constantly sequestered from the OMM to the cytosol for proteasomal degradation via mitochondrial-associated degradation (MAD). Interestingly, this process shares central UPS factors with the ER-associated degradation (ERAD) machinery (Ravanelli *et al.*, 2020). In ERAD, secretory and integral membrane proteins are dislocated across the ER-membrane into the cytosol for degradation, since the ER itself does not contain corresponding protease-systems (Stevenson *et al.*, 2016; Sun and Brodsky, 2019). For mitochondria, typical OMM proteins that have been shown to be turned over by UPS include for instance dynamin-related protein 1 (Drp1) and mitofusins that are involved in mitochondrial fusion and fission (Cohen *et al.*, 2008; Karbowski *et al.*, 2007; Neutzner *et al.*, 2008; Neutzner *et al.*, 2007). But also, different anti- and pro-apoptotic proteins like BCL-1, BAX an MCL-1, see (**chapter 1.2.4**), undergo proteasomal degradation (Azad *et al.*, 2006; Benard *et al.*, 2010; Fu *et al.*, 2009; Yu *et al.*, 2008), either selectively (BAX), as regulatory event for expression and activation (BCL-2) or upon activation of apoptosis (MCL-1) (Breitschopf *et al.*, 2000; Cuconati *et al.*, 2003; Liu *et al.*, 2008; Nijhawan *et al.*, 2003). Comparable to the cytosolic degradation of integral membrane proteins in ERAD, most mitochondrial UPS substrates are membrane-anchored proteins that have to be extracted from the lipid bilayer in order to reach the proteasome. The AAA-ATPase p97 is able to extract ubiquitinated substrate proteins from cellular structures or multiprotein complexes and was

shown to be involved in turnover of OMM-associated Mitofusin 1 and MCL-1 (Stach and Freemont, 2017; Tanaka *et al.*, 2010; Xu *et al.*, 2011).

1.3.2.2. Proteolysis of IMS and matrix proteins

Mitochondrial proteases can be grouped in a family of more than 40 enzymes that are highly conserved and have different functions depending on the compartment within mitochondria they reside in and their catalytic activity, for review see (Deshwal *et al.*, 2020). The majority is involved in preserving mitochondrial proteostasis with regard to the mitochondrial unfolded protein response (UPR^{mt}), and participates in the stress-response system at multiple levels. The 18 currently known intrinsic mitochondrial proteases, or also termed mitochondrial peptidases, can be divided into four functional categories: processing peptidases, ATP-dependent peptidases, oligopeptidases, and other mitochondrial peptidases. Here, I will discuss only the best studied proteases, for an overview of the mitochondrial proteases and their associated functions see (**Table S1**). Of note, not all protease functions have been shown in mammals yet.

Among the first identified mitochondrial proteases were the processing peptidases that remove targeting signals from nucleus-encoded, newly imported proteins by limited proteolysis as an essential step of maturation (Mossmann *et al.*, 2012; Poveda-Huertes *et al.*, 2017), as seen for MPP within the matrix (Hawlitschek *et al.*, 1988; Ou *et al.*, 1989). In some cases, cleavage to remove the targeting signal of a protein precursor is followed by a second processing step involving the mitochondrial intermediate peptidase (MIP) (Kalousek *et al.*, 1988), which further removes eight additional amino acid residues (Isaya *et al.*, 1991; Isaya *et al.*, 1992; Kalousek *et al.*, 1992). In the IMS and IMM targeting signals of mitochondrial-encoded proteins are removed by the inner membrane peptidase (IMP) complex, also called IMMP, that can also further processes MPP-cleaved proteins from the matrix in order to remove their membrane-anchor (Burri *et al.*, 2005; Nunnari *et al.*, 1993; Pratje *et al.*, 1983).

Contrary to the presequence peptidases, ATP-dependent peptidases degrade proteins into small peptides and amino acids, which are released into in the IMS or matrix. So far, four ATP-dependent proteases are described in mammalian mitochondria that are all derived from bacterial ancestors: the LONP1 and CLPXP proteases in the matrix and two homologous AAA proteases in the IMM, whose subunits are homologous to bacterial FtsH, exposing their catalytic centers to opposite membrane surfaces (Leonhard *et al.*, 2000; Puchades *et al.*, 2019). Whereas LONP1 is involved in mtDNA maintenance, replication, mitochondrial adaptation to hypoxia and degradation of thermally denatured proteins (Bota and Davies, 2002; Hao *et al.*, 2018; Kunová *et al.*, 2017; Matsushima *et al.*, 2010), CLPXP is implicated in transcription/translation and ribosome assembly and turnover of misfolded proteins (Matsushima *et al.*, 2017; Szczepanowska *et al.*, 2016; Zhao, 2002). The *i*-AAA protease exerts activity at the IMS side and is composed of six yeast mtDNA escape 1-like (YME1L)

subunits (Leonhard *et al.*, 2000; Puchades *et al.*, 2017). The *m*-AAA protease in turn exerts activity at the matrix side and forms homo-oligomeric AFG3L2 (AFG3-like subunit 2) complexes or hetero-oligomeric complexes composed of homologous AFG3L2 or SPG7 (Paraplegin) subunits (Yta10/Afg3l2 and Yta12/Rca1 in yeast) and a third *m*-AAA protease subunit, AFG3L1, is expressed only in mice (Koppen *et al.*, 2007). Notably, both *i*-AAA and *m*-AAA proteases serve as quality control enzymes in the IMM, coordinate mitochondrial dynamics, and degrade membrane-integrated and peripherally-attached non-native and non-assembled polypeptides in a membrane topology-dependent manner (Arlt *et al.*, 1996; Gerdes *et al.*, 2012; Korbel *et al.*, 2004; Leonhard *et al.*, 1996; Leonhard *et al.*, 1999; Ohba *et al.*, 2020), and are associated with membrane scaffolds of the SPFH (stomatin, prohibitin, flotillin, HflC/K) family (Tatsuta and Langer, 2017; Wai *et al.*, 2016). Whereas the *i*-AAA protease YME1L and the processing peptidase PINK1/PGAM5-associated rhomboid-like protease (PARL), see (**chapter 1.5.4.2.**), assemble with the matrix SLP2 (stomatin-like protein 2) into the SPY (SLP2-PARL-YME1L) complex, *m*-AAA proteases assemble with membrane-anchored IMS prohibitin (PHB) ring complexes composed of multiple PHB1 and PHB2 subunits (Deshwal *et al.*, 2020). The substrate spectrum ranges from proteins involved in intramitochondrial lipid transfer, like STARD7 (by *i*-AAA) (Potting *et al.*, 2013; Potting *et al.*, 2010; Rainbolt *et al.*, 2013; Richter *et al.*, 2019; Saita *et al.*, 2018), to a ribosomal subunit (Nolden *et al.*, 2005). Thus, proteolysis for instance is associated with the dislocation of cytochrome c peroxidase 1 (Ccp1) from the IMM (by *m*-AAA) for further cleavage by cytochrome c peroxidase 1/Rhomboid 1 (Pcp1/Rbd1), the ortholog of mammalian rhomboid protease PARL (Esser *et al.*, 2002; Tatsuta *et al.*, 2007). Processing of optic atrophy 1 (OPA1) in mammals, see (**chapter 1.3.3.1**), (by both AAA proteases) results in mitochondrial membrane remodeling (Duvezin-Caubet *et al.*, 2007; Ehses *et al.*, 2009; Griparic *et al.*, 2007; Song *et al.*, 2007).

Additionally, many other different proteases were identified over the years (**Table S1**). One example is the metalloprotease OMA1, which is part of the quality control system in the IMM and can be activated following stress conditions and by self-cleavage. It shows overlapping function with *m*-AAA and *i*-AAA by cleaving OPA1 (Anand *et al.*, 2014; Ehses *et al.*, 2009; Käser *et al.*, 2003), leading to its inactivation and negative regulation of mitochondrial fusion (Head *et al.*, 2009). Thereby OMA1 can induce loss of mitochondrial membrane potential (Baker *et al.*, 2014). In hypoxia, YME1L degrades itself as well as OMA1, which results in limited OPA1 processing and allows fusion to proceed (MacVicar *et al.*, 2019). Interestingly, OMA1 also shares substrates with PARL, namely PINK1 and PGAM family member 5 (PGAM5) (Sekine *et al.*, 2012; Sekine *et al.*, 2019; Wai *et al.*, 2016), besides reciprocal processing of *i*-AAA YME1L (Rainbolt *et al.*, 2016). Thus, OMA1 plays a crucial role in mitochondrial quality control and is essential for regulating lipid metabolism and maintains body temperature and energy expenditure under cold-stress conditions (Baker *et al.*, 2014;

Zhang *et al.*, 2014). In the IMS, the proteases HTRA2/Omi and LACTB were described. Whereas HTRA2/Omi was shown to act in stress signaling and apoptosis (Martins *et al.*, 2002; Martins *et al.*, 2004; Radke *et al.*, 2008; Suzuki *et al.*, 2001; Verhagen *et al.*, 2002), LACTB is involved in phosphatidylethanolamine (PE) metabolism (Keckesova *et al.*, 2017).
Oligopeptidases degrade polypeptides into small peptides and amino acids (Desautels and Goldberg, 1982; Young *et al.*, 2001) but are only poorly characterized. Two examples are MEP (Neurolysin) in the IMS (Mossmann *et al.*, 2012; Teixeira and Glaser, 2013) and PITRM1 (PreP) in the matrix (Falkevall *et al.*, 2006; Taskin *et al.*, 2017). Their activity and subsequent export of the cleavage products out of mitochondria into the cytosol may prevent proteotoxic stress in mitochondria due to accumulation of peptides upon impaired proteolysis, thereby exhibiting signaling function to coordinate nuclear and mitochondrial gene expression (Arnold *et al.*, 2006; Young *et al.*, 2001). The mitochondrial proteolytic system highlights the importance of the spatial organization of proteolytic processes in the sub-compartments to maintain cellular health.

1.3.3. Mitochondrial dynamics-involved quality control: fusion and fission

In order to maintain mitochondrial homeostasis when cells experience metabolic or environmental stresses, mitochondria undergo reciprocally regulated fission and fusion events to isolate and remove irreversibly damaged structures as complementation of damaged systems (**Figure 2**). Fusion occurs when adjacent mitochondria are joined, while fission separates one mitochondrion into two. Both mechanisms are regulated by large GTPases that belong to the dynamin family and are conserved from yeast to mammals (Sabouny and Shutt, 2020), namely mitofusins and OPA1, that mediate OMM and IMM fusion, respectively, and Drp1, which is required for mitochondrial fission. Mitochondrial network remodeling is tightly controlled by regulated turnover of the involved proteins, as described above, with far reaching consequences for mitochondrial function resulting in physiological changes in the cell. These changes include the induction of apoptosis, autophagy and mitochondrial transport, especially in highly polarized cells such as neurons.

1.3.3.1. Mitochondrial fusion

Due to its high complexity, mitochondrial fusion requires coordinated function of GTPases in both mitochondrial membranes. Mitofusin 1 and 2 (MFN1, MFN2) form homo- and heteromeric complexes in the OMM to interact with surrounding mitochondria. The fusion of the OMMs is driven by GTP hydrolysis leading to a conformational change that brings the opposing membranes in contact with one another (Cao *et al.*, 2017; Qi *et al.*, 2016). MFN2 is also present in the ER and MAMs controlling tethering of the ER to mitochondria via interaction with mitochondrial-localized MFN1 and MFN2 (Basso *et al.*, 2018; de Brito and Scorrano, 2008;

Naon *et al.*, 2016), which is also involved in the fission process (Cohen *et al.*, 2018). In the IMM the membrane-anchored protein OPA1 together with the mitochondria-specific lipid cardiolipin are responsible for the fusion of the IMMs and cristae remodeling (Ban *et al.*, 2017; Delettre *et al.*, 2000; Song *et al.*, 2007; Tilokani *et al.*, 2018). Mutation in OPA1 can lead to the disease of autosomal-dominant optic atrophy, which is characterized by a degenerated optic nerve (Alexander *et al.*, 2000). A long and a short form of OPA1 have been described. Alternatively spliced long OPA1 (L-OPA1) can be proteolytically cleaved to short forms (S-OPA1) upon import into the IMM by stress-activated OMA1 and *i*-AAA YME1L (Anand *et al.*, 2014; Wang *et al.*, 2021). L-OPA1 interacts with cardiolipin on either side of the two IMM membranes, thereby tethering their fusion followed by OPA1-dependent GTP hydrolysis (Liesa *et al.*, 2009). S-OPA1 has been proposed to act as an enhancer for the L-OPA1-cardiolipin interaction and thus, fusion (DeVay *et al.*, 2009; Rujiviphat *et al.*, 2009). Whereas, mitofusin levels are regulated both transcriptionally and by UPS-controlled degradation, OPA1 is regulated post-transcriptionally and post-translationally (Wai and Langer, 2016).

In yeast, analog to mammals, two isoforms of mitochondrial genome maintenance 1 (Mgm1), the homolog of mammalian OPA1, are indispensable for normal mitochondrial morphology (Herlan *et al.*, 2003). The long isoform of Mgm1 is cleaved by the intramembrane protease Pcp1/Rbd1 in order to release a soluble form of the substrate, a mechanism which requires high matrix ATP levels and mitochondrial Hsp70 (Herlan *et al.*, 2004; McQuibban *et al.*, 2003; Sesaki *et al.*, 2003). Thereby, Pcp1/Rbd1 is involved in regulating the respiratory output in response to the energy status of the cell. A dysfunctional proteolytic regulation, deficiency or loss of fusion proteins leads to mitochondrial fragmentation (Ichishita *et al.*, 2008; Kanazawa *et al.*, 2008) and highlights once again the importance of correctly balanced proteolysis in mitochondria.

1.3.3.2. Mitochondrial fission

The process of mitochondrial fission requires initial replication of mtDNA in the matrix, which recruits the ER (Friedman *et al.*, 2011; Lewis *et al.*, 2016) and leads to constriction of the OMM at the MAMs before oligomerization of the soluble GTPase Drp1 follows. Drp1 is translocated from the cytosol to the potential mitochondrial fission sites (Karbowski *et al.*, 2007; Smirnova *et al.*, 2001; Wasiak *et al.*, 2007) and involves a number of mitochondrial-bound proteins including FIS1, MFF, MiD49 and MiD51 that aid in the recruitment process (Losón *et al.*, 2013). The tail-anchored protein FIS1, recently shown to be involved in lysosomal marking of the mitochondrial fission sites (Wong *et al.*, 2018), can act as mitochondrial receptor for Drp1 recruitment (Lackner *et al.*, 2009; Yoon *et al.*, 2003), but is not necessary for fission induction (Liesa *et al.*, 2019). Interestingly, in humans FIS1 was found to promote mitochondrial fragmentation both by activating fission and inhibiting fusion by preventing the GTPase activity of MFN1, MFN2, and OPA1 (Yu *et al.*, 2019), demonstrating the close connection between

fission and fusion processes, that are still not completely understood. Conformational changes by GTP hydrolysis of Drp1 subsequently causes further ER-mediated constriction of the OMM (Labrousse *et al.*, 1999; Smirnova *et al.*, 2001). Drp1 is regulated by posttranslational modifications, including phosphorylation, S-nitrosylation, ubiquitination and sumoylation (Cho *et al.*, 2009; Karbowski *et al.*, 2007; Nakamura *et al.*, 2006; Taguchi *et al.*, 2007; Wasiak *et al.*, 2007; Yonashiro *et al.*, 2006) and has been shown to be implicated in mitochondrial morphology, mitosis, apoptosis and linked disease. Whereas OMM constriction has been relatively well documented, the mechanism of IMM division is still unclear (Tilokani *et al.*, 2018). Recent work suggests a Ca^{2+}-dependent IMM constriction at the MAMs including a possible role of S-OPA1 in untethering the OMM from the IMM during fission (Chakrabarti *et al.*, 2017; Cho *et al.*, 2017). However, too less in known about the underlying details and further results are required to fully understand the fission process of the IMM.

1.4. Dysfunction of mitochondria and its role in various disorders including Parkinson's disease

Mitophagy maintains mitochondrial homeostasis and its impairment due to certain mutations, proteotoxic stress or simply age (mitophaging) contributes to an accumulation of dysfunctional mitochondria, which can cause various diseases such as Parkinson's disease (PD), Alzheimer's disease, cardiomyopathies and cancer (Bakula and Scheibye-Knudsen, 2020; Bernardini *et al.*, 2017; Fivenson *et al.*, 2017; Levine and Kroemer, 2019). Interventions that boost mitophagy have been shown to increase health and longevity in multiple model organisms ranging from yeasts to mice (Aparicio *et al.*, 2019; Palikaras *et al.*, 2015; Rana *et al.*, 2017; Ryu *et al.*, 2016; Schiavi *et al.*, 2015). For instance, in the nematode *Caenorhabditis elegans* inhibited mitophagy through loss of the mitophagy regulators dct-1 (NIX/BNIP3L homolog) or pink-1 (PINK1 homolog) results in an accumulation of dysfunctional mitochondria and increases the susceptibility to oxidative stress, heat stress, and starvation (Palikaras *et al.*, 2015). Further studies in the fruit fly *Drosophila melanogaster* revealed prolonged lifespan due to upregulation of the autophagy receptor p62 (Sequestosome 1) in middle-aged flies by enhanced mitochondrial fission and mitophagy (Aparicio *et al.*, 2019). In addition, overexpression of Drp1 in aging flies resulted in reversed age-related mitochondrial enlargement, restored mitochondrial respiratory function, and facilitated mitophagy (Rana *et al.*, 2017). Moreover, pharmacological activation of mitophagy through dietary supplementation of urolithin A was shown to prolong the lifespan in *C. elegans* and of aged mice (Ryu *et al.*, 2016).

After Alzheimer's disease, PD is the second most common neurodegenerative disorder and about 1% of the human population older than 60 years is affected (Sai *et al.*, 2012). Classical symptoms are displayed in movement impairments such as postural instability, rigidity, slowness of movement and tremor at rest (Jankovic, 2008) due to degeneration of

dopaminergic neurons in a region of the midbrain, the substantia nigra pars compacta. Many PD patients develop inclusion bodies inside of their neurons, the so-called Lewy bodies, consisting of abnormally accumulated ubiquitin-coupled α-synuclein. Since the disease is manifesting differently in every human body and there are PD patients not developing Lewy bodies and other people that possess Lewy bodies but do not show any signs of PD, it is still under debate when and on which basis a PD diagnosis can be given (Shulman *et al.*, 2011). Most Parkinson cases are classified as idiopathic (with an unknown cause) as only 10% of the patients carry genetic mutations, that can be inherited in an autosomal dominant or recessive mode (Bosco *et al.*, 2011). Especially, mutations in genes maintaining mitochondrial homeostasis have been linked to recessive Parkinsonism in patients, showing neurons with fragmented mitochondria, disturbed cristae structure, altered mitophagy and mutations in SNCA (α-synuclein), DJ-1, LRRK2, PINK1, Parkin, ATP13A2, PLA2G6, FBXO7, GIGYF2 and UCHL1 (Sai *et al.*, 2012; Selvaraj and Piramanayagam, 2019). Approximately, 27% of patients with early-onset PD carry mutations in LRRK2, Parkin, and GBA1 (Fraint *et al.*, 2018; Ryan *et al.*, 2019) but additional susceptibility genes have been found for all variants of Parkinson's disease over the recent years and need further investigation.

1.4.1. Clearance of defective mitochondria by mitophagy

Besides imbalances in mtDNA integrity and stability (Kujoth *et al.*, 2005; Linnane *et al.*, 1989; Trifunovic *et al.*, 2004), imbalances in mitochondrial proteostasis have been shown to cause mitochondrial dysfunction and trigger UPR^{mt}, which is also accompanied by rapid remodeling of the mitochondrial signature lipid cardiolipin. When ROS production exceeds the cellular antioxidant capacity or mitochondria display other functional damages, the cell needs to repair or eliminate the defective mitochondria immediately.

Removal of the whole organelle is achieved by selective mitophagy, which is characterized by the formation of a double-membrane structure, called autophagosome that is built around the defective organelle (Ding and Yin, 2012; Mizushima and Klionsky, 2007; Nakatogawa *et al.*, 2009; Yang and Klionsky, 2010). In response to various stimuli under distinct cellular contexts, several mitophagy signaling cascades were described in mammalian cells over the past years (Palikaras *et al.*, 2017; Wei *et al.*, 2015) and could be classified into ubiquitin-dependent and mitochondrial receptor-mediated mechanisms (Khaminets *et al.*, 2016; Pickles *et al.*, 2018) (**Figure 2**). The ubiquitin-dependent mechanism is also called PINK1/Parkin-mediated mitophagy and involves, as the name suggests, PINK1 and the ubiquitin protein ligase Parkin. Upon mitochondrial proteotoxicity or depolarization of $\Delta\Psi_{mito}$, for instance after usage of the uncoupling protonophore cyanide m-chlorophenyl hydrazone (CCCP), PINK1 accumulates on the mitochondrial surface and recruits the ubiquitin E3 ligase Parkin, which in turn ubiquitinates OMM proteins including voltage-dependent anion channel (VDAC) (Geisler *et al.*, 2010), MFN1/2 (Gegg *et al.*, 2010; Poole *et al.*, 2010) and Rho GTPase Miro (Wang *et al.*, 2011).

Such ubiquitinated OMM factors eventually undergo p97-dependent proteasomal degradation prior to mitophagy (Gegg *et al.*, 2010; Tanaka *et al.*, 2010; Xu *et al.*, 2011; Yoshii *et al.*, 2011). Additionally, autophagy receptor proteins like p62 and OPTN were described to bind ubiquitinated proteins on the defective organelle surface and trigger the recruitment of microtubule-associated protein 1 light chain 3 (LC3), which is integrated in the phagophore membranes (Ichimura *et al.*, 2008; Weil *et al.*, 2018) on the one hand, and on the other hand to interact with the autophagosomes through their LC3-interacting region (LIR) motifs, in order to facilitate and activate removal of the damaged mitochondrion (Harper *et al.*, 2018; Matsuda *et al.*, 2010; Ordureau *et al.*, 2014).

The mitochondrial receptor-mediated mitophagy could be shown to follow mostly hypoxia or occurs during erythropoiesis and involves mitophagy receptor proteins, such as the OMM proteins BCL-2-like protein 13 (BCL2L13), NIX (also called BCL2/adenovirus E1B-interacting protein 3-like, BNIP3L), BNIP3 and FUNDC1 (FUN14 domain-containing protein 1). Comparable to p62, these factors interact with the autophagosomes through their LIR motifs. Closed autophagosomes eventually fuse with lysosomes, in which enzymes digest the engulfed content (Gatica *et al.*, 2018; Hamacher-Brady *et al.*, 2007; Komatsu and Ichimura, 2010; Liu *et al.*, 2012; Murakawa *et al.*, 2015; Quinsay *et al.*, 2010; Rogov *et al.*, 2017). Besides canonical mitophagy, mitochondrial-derived vesicles (MDVs) were described as a mitochondrial quality control pathway that acts to remove oxidized proteins and lipids in mitochondria after ROS production (McLelland *et al.*, 2014) (**Figure 2**). MDVs share essential components with the mitophagy mechanism and dysfunction of MDVs was observed to result in premature mitophagy, which consequently impairs the hierarchical surveillance network of mitochondrial quality control, including the UPR^{mt}, mitochondrial fission and fusion, MDVs, and mitophagy (Sugiura *et al.*, 2014).

Impairment of mitochondrial function can lead to both induction of mitophagy and apoptosis and is highly controlled, depending on the stress level (Kubli and Gustafsson, 2012). Currently, the exact details underlying the ‘decision’ mechanism to distinguish between conquerable or fatal stress are not yet entirely understood. However, it is believed that the cell tries to restore mitochondrial function under mild impairment by fusion-mediated functional complementation and MDVs, or upon increased impairment by segregating damaged compartments from the mitochondrial network through fission and subsequent mitophagy first, before irreparable apoptosis is activated. Thus, mitophagy is so far seen as pro-survival mechanism beside fusion -mediated content mixing and MDVs (Liu *et al.*, 2020b). Various mitophagy pathways initiate the degradation process by targeting mitochondrial dynamics. MFN1 and MFN2 are ubiquitinated by Parkin upon mitochondrial depolarization, thereby abolishing fusion, promoting mitochondrial fragmentation, and facilitating mitophagy (Gegg *et al.*, 2010; Ziviani *et al.*, 2010).

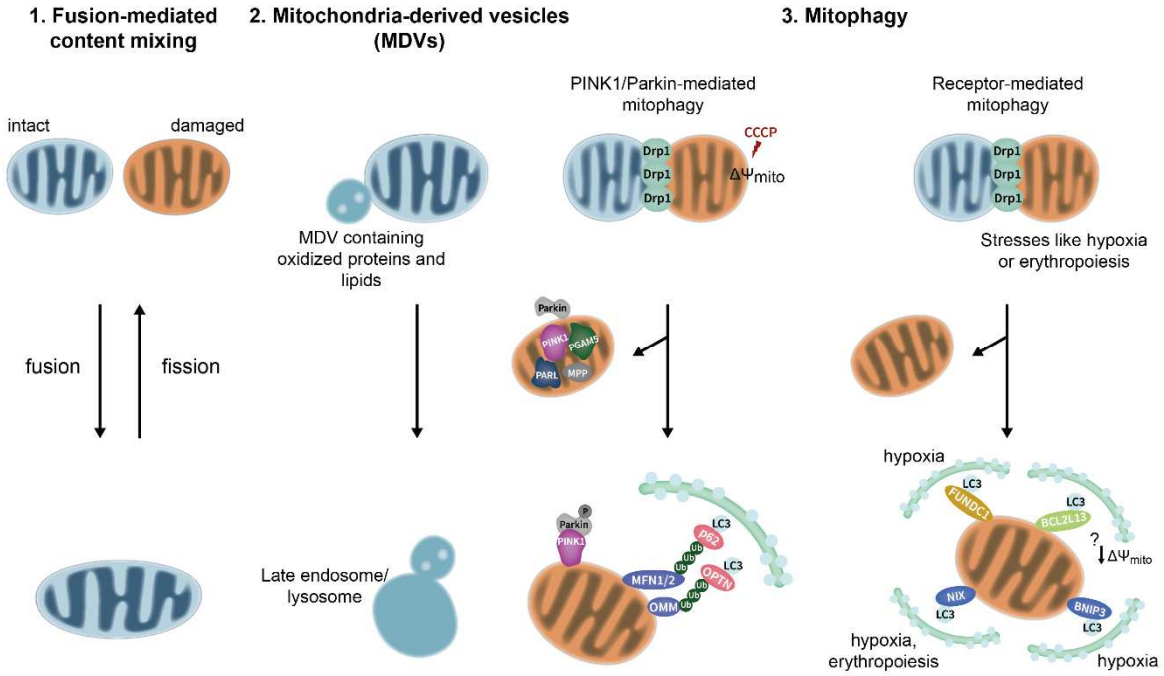

Figure 2 | Mitochondrial quality control pathways in mammals.

Schematic overview of the mitochondrial quality control network of surveillance mechanisms encompassing (1) fusion-mediated function complementation, (2) mitochondria-derived vesicles, and (3) mitophagy processes to protect mitochondrial homeostasis from increasing degrees of damage. Detailed explanation in the text. Adapted from (Liu *et al.*, 2020b).

A recent study revealed a novel function of Drp1 in affecting mitochondrial membrane potential (Cho *et al.*, 2019a), where under normal conditions, Drp1 was found to transiently reduce mitochondrial membrane potential at division sites in mammalian cells. Damaged mitochondria failed to restore the reduced membrane potential and therefore underwent mitophagy (Cho *et al.*, 2019a). However, future studies are needed to fully understand the detailed functions of Drp1 regulation upon mitochondrial damage and Drp1-mediated fission in mitophagy in different physiological contexts. Mitochondrial Rho GTPase Miro was described to be involved in mitochondrial movement along microtubules (Rice and Gelfand, 2006) and was found to be phosphorylated and ubiquitinated in a PINK1/Parkin-dependent manner upon mitochondrial depolarization in order to undergo proteasomal degradation (Wang *et al.*, 2011; Weihofen *et al.*, 2009). Without Miro at the mitochondrial surface, microtubules detach from damaged mitochondria and inhibit their movement in the cell, so that most probably, healthy and damaged mitochondria can be segregated from each other, with the former to be degraded by mitophagy. This process may play a particularly important role for cells that rely on efficient transport of mitochondria, such as neuronal cells, in which mitochondria are transported from the site of mitochondrial biogenesis, the cell soma, to the axon terminal with a high demand for energy (de Castro *et al.*, 2011).

1.4.2. PGAM5 in mitophagy, disease and ageing

Several regulators of mitophagy, including PINK1, Parkin and PGAM5, have been identified (Park *et al.*, 2018; Youle and Narendra, 2011). Mutations or deletions of these genes are implicated in abnormal mitophagy, which in turn has been observed in a variety of diseases, including ischemic injury, heart diseases and neurodegenerative diseases (Picca *et al.*, 2021; Shen *et al.*, 2021; Svaguša *et al.*, 2020). The 32 kDa protein PGAM5 belongs to a highly conserved phosphoglycerate mutase family and is a mitochondrial protein that lacks phosphotransferase function on phosphoglycerates, but retained activity as a serine/threonine protein phosphatase (Takeda *et al.*, 2009). It has been reported that in *Drosophila* deficiency in the ortholog of mammalian PGAM5 (dPGAM5) results in vulnerability to heat shock stress mainly because of increased apoptosis in certain neurons, suggesting the role for PGAM5 in apoptosis regulation (Ishida *et al.*, 2012). Several lines of evidence suggest that PGAM5 mediates apoptosis through the formation of the PGAM5-BAX-DRP1 complex and by interaction with anti-apoptotic BCL-X_L promoting its degradation (Wu *et al.*, 2014; Xu *et al.*, 2015; Zhuang *et al.*, 2013). Loss of PGAM5 causes increased mitochondrial fusion and decreased mitochondrial turnover, which results in the accumulation of damaged mitochondria characterized by elevated cellular ATP and ROS levels, enhanced mTOR and IRF/IFN-β signaling pathways, leading to cellular senescence (Yu *et al.*, 2020). Just recently it could be shown, that the KEAP1/PGAM5 complex senses mitochondrially generated superoxide and hydrogen peroxide in order to induce mitophagy. Moderate mitochondrial ROS production oxidates KEAP1, which breaks the interaction with PGAM5 leading to the inhibition of its proteasomal degradation. Further, accumulated PGAM5 was described to interfere with the processing of PINK1 and thereby enhancing the accumulation of PINK1 on the OMM with subsequent recruitment of Parkin (Zeb *et al.*, 2021). Eventually, loss of PGAM5 results in necroptosis, dopaminergic neuron degeneration and defects in growth and cell survival, establishing a molecular link between PGAM5 and the pathogenesis of PD, cardiac diseases (Cheng *et al.*, 2021). In general, it could be observed that depending on the mitochondrial stress level, PGAM5 can either stimulate cell survival or cell death. Under mild stress, PGAM5 maintains mitochondrial homeostasis by the induction of mitochondrial biogenesis and mitophagy, (Bernkopf *et al.*, 2018; Ma *et al.*, 2020). Under severe stress, PGAM5 promotes mitochondrial fission and regulates multiple death signals to induce cell death (Xu *et al.*, 2015; Yamaguchi *et al.*, 2019; Zhuang *et al.*, 2013). Taking the cell death-promoting role of PGAM5 into account, it is not surprising that the mitochondrial phosphatase became a popular target for developing therapies against the above-mentioned diseases, including colon, breast and cervical cancer (Wang *et al.*, 2012; Zhang *et al.*, 2019).

1.4.3. Subcellular localization of PGAM5: release and filaments

The localization of PGAM5 is a dynamic and stress responsive process, that is still not completely understood. PGAM5 contains an N-terminal non-cleaved mitochondrial targeting sequence that is also part of a TM segment that anchors the C-terminal phosphatase domain to the IMM (Lu *et al.*, 2014; Sekine *et al.*, 2012). Nevertheless, PGAM5 was also found to interact with several cytoplasmic proteins at the OMM, where its phosphatase domain is accessible from the cytosol, including the redox-regulated substrate adaptor and oxidative stress sensor KEAP1 (Lo and Hannink, 2006, 2008; Yamaguchi *et al.*, 2019). Up to now, PGAM5 was described to be partially released into the cytosol after cleavage by PARL and OMA1 (Sekine *et al.*, 2012; Wai *et al.*, 2016), generating a fragment missing the MTS (Bernkopf *et al.*, 2018; Saita *et al.*, 2017; Sekine *et al.*, 2012; Zhuang *et al.*, 2013). PARL-dependent mitochondrial release of PGAM5 that is thought to occur via proteasome-mediated rupture of the OMM through Parkin has been shown to trigger Wnt/β-catenin signaling (Bernkopf *et al.*, 2018; Rauschenberger *et al.*, 2017; Yamaguchi *et al.*, 2019). PGAM5 is known to form an equilibrium between dimeric and multimeric states (Chaikuad *et al.*, 2017) and catalytic activation of PGAM5 requires dodecamer formation (Ruiz *et al.*, 2019; Wilkins *et al.*, 2014). Furthermore, those dodecamers can assemble into long filaments in the cytoplasm, which were described to colocalize with microtubules (Ruiz *et al.*, 2019). In this process, the multimeric state of PGAM5 represents a molecular switch between mitofission/mitophagy and apoptosis. While PGAM5 multimers interact with FUNDC1 to initiate mitophagy and mitochondrial fission, PGAM5 dimers bind to BCL-X_L to prevent apoptosis (Ma *et al.*, 2020). Mitophagy however, can be regulated by PGAM5 also independent of Parkin through interaction and dephosphorylation of FUNDC1, which in turn interacts with LC3 in order to facilitate the engulfment of damaged mitochondria by autophagosomes (Liu *et al.*, 2012). In addition, PGAM5 influences mitochondrial division by dephosphorylating the mitochondrial fission factor Drp1. It could be shown, that function and localization of PGAM5 are regulated by syntaxin 17 (Stx17), a mitochondria-associated membrane protein implicated in mitochondrial dynamics in fed cells and autophagy in starved cells (Sugo *et al.*, 2018). Loss of Stx17 resulted in aggregation of PGAM5 within mitochondria and thereby failure of the dephosphorylation of Drp1, leading to mitochondrial elongation in healthy cells. Moreover, in Parkin-mediated mitophagy, Stx17 was shown to be a prerequisite for PGAM5 to interact with FUNDC1, highlighting the important role of the Stx17-PGAM5 axis in mitochondrial fission and PINK1/Parkin-mediated mitophagy (Sugo *et al.*, 2018). These observations led to further speculations if PGAM5 may be located at the contact sites between the inner and outer mitochondrial membranes, or if PGAM5 can shuttle between both membranes according to the cell state and mitochondrial membrane potential. Another model hypothesizes that PGAM5 is distributed on both the inner and outer mitochondrial membrane, but the proportion of distribution may differ (Sugo *et al.*, 2018). Further studies of PGAM5 outside of mitochondria

revealed that cleaved PGAM5 translocates to the nucleus and dephosphorylates nuclear serine/arginine-rich proteins during mitophagy and thus, coordinates cellular responses (Baba *et al.*, 2021). Nevertheless, the exact release mechanism of PGAM5 especially upon mitochondrial dysfunction needs to be further elucidated.

1.5. Intramembrane proteolysis and the involved protease classes

Almost ~30% of all known proteomes in all living organisms encode for membrane proteins that play important roles in a variety of biological processes as receptors, channels and transporters, are capable of mediating cell-cell and cell-environment interactions transferring chemical signals and molecules in and out of cells. Despite their significance in biology, medicine and their history in drug discovery – according to the Human Protein Atlas, about 70% of human drugs currently on the market target membrane proteins - our understanding of this important class of proteins is still fragmentary because of their highly hydrophobic nature and complex structural flexibility and dynamics, which complicate functional and structural studies (Chen *et al.*, 2013; Liu and Rost, 2001; Uhlén *et al.*, 2015).

An unusual group of proteases that can be found in all kingdoms of life cleaves peptide bonds of their membrane-anchored substrates in the plane of the lipid bilayer (Sun *et al.*, 2016). Back in the early 1990s this idea was controversially discussed, since it could not be explained how hydrolysis requiring a nucleophilic water molecule may occur in a water-limiting environment (Erez *et al.*, 2009). Today, intramembrane proteolysis is an appreciated and widely studied field, including research on structure, mechanism, regulation, and substrate identification. However, until today knowledge remains restricted when comparing to that of its soluble counterparts. Intramembrane proteases share common features as enzyme activity highly depends on surrounding lipids (Bondar and Lemieux, 2019) and as such enzymes are polytopic membrane proteins with their aqueous active sites buried several Ångstrom deep within the lipid bilayer. Up to now, fifteen intramembrane proteases have been described in humans that can be classified into four families according to the catalytic mechanism attacking the substrate carbonyl group: metalloproteases, aspartyl proteases, glutamyl proteases and rhomboid serine proteases. Among these families, two main functions can be distinguished, firstly, degradation of proteins as part of quality and abundance control in order to prevent cytotoxicity and secondly, activation and signaling as summarized in the term regulated intramembrane proteolysis (RIP) (Brown *et al.*, 2000). In general, membrane protease functions are as diverse as of soluble proteases and intramembrane proteolysis can be found in many biological processes such as intra- and extracellular signaling, for instance by activation of dormant ligands like growth factors (Fleck *et al.*, 2016), or transcription factors (Becker-Herman *et al.*, 2005), or by the degradation of bulk protein species (Erez and Bibi, 2009; Kühnle *et al.*, 2019; Lemberg, 2011). Intramembrane proteases are localized, except from peroxisomes, in every membrane-enclosed organelle in the cell as well as at the plasma

membrane (**Figure 3**) with the capability to cleave various types of membrane protein topologies (Kühnle *et al.*, 2019; Lemberg, 2011).

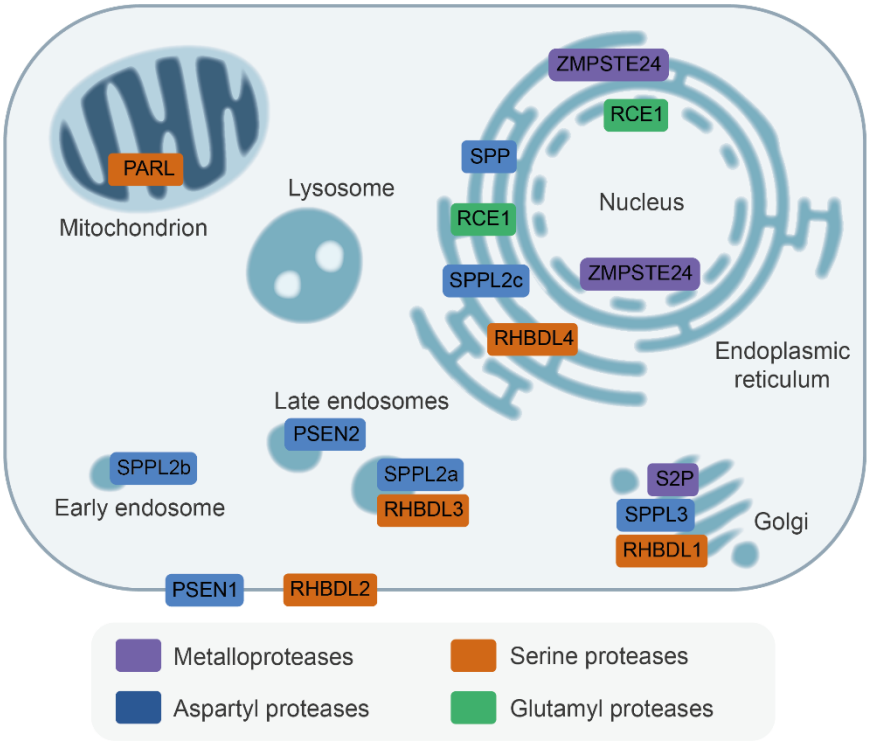

Figure 3 | Mammalian intramembrane proteases.
Schematic overview of the mammalian intramembrane proteases with their distribution and sub-cellular localization. Each of the four family classes has its own color code. Abbreviations of the proteases: PARL (PINK1/PGAM5-associated rhomboid-like), PSEN (presenilin), RCE1 (Ras-converting enzyme 1), RHBDL (rhomboid-like protein), S2P (site-2 protease), SPP (signal peptide peptidase), SPPL (SPP-like protease), ZMPSTE24 (zinc metalloproteinase Ste24 homolog).

1.5.1. Metalloproteases

The first reported intramembrane metalloprotease was the Golgi localized zinc site-2 protease (S2P) (Rawson *et al.*, 1997; Sakai *et al.*, 1996). S2P is conserved in metazoans and fungi but lost in yeast (Rawson *et al.*, 1997) and contains a HExxH metal binding motif that is characteristic for zinc metalloproteases (Hooper, 1994; Lewis and Thomas, 1999; Rawlings and Barrett, 1995; Rawson *et al.*, 1997). Active site histidine and glutamate residues coordinate the zinc ion to accomplish the nucleophilic attack on the substrate. Structural analysis from the archaea *Methanocaldococcus jannaschii* showed that S2P contains six TM domains and that the prosthetic zinc ion is coordinated between residue H54 and H58 in TM segment 2 and D148 in TM segment 4. Point mutations of the catalytic residues E55A, H54A, H58A, D148A were shown to abolish catalytic activity of the enzyme (Feng *et al.*, 2007). Substrate recognition and proteolysis by S2P requires a pre-processing (shedding) step, which

is performed by the site-1 protease (S1P, also MBTPS1) (Sakai *et al.*, 1998). Discovered was S2P as a key player in the control of sterol homeostasis (Rawson *et al.*, 1997). The sterol regulatory element binding protein (SREBP) is consecutively cleaved by S1P either in a luminal portion between two TM domains or in a protein's ectodomain and by S2P in the TM domain when trafficked to the Golgi to liberate a N-terminal fragment, which acts as a transcription factor crucial for sterol and fatty acid homeostasis. Besides SREBP, S2P has been reported to cleave the UPR factor ATF6 in response to ER stress (Ye *et al.*, 2000) and CREBH, which is implicated in the immune system as well as glucose and lipid metabolism (Ye *et al.*, 2000; Zhang *et al.*, 2016). Over the years 54 metalloprotease families in 15 'Clans' were described (Rawlings *et al.*, 2018).

1.5.1.1. ZMPSTE24 and OMA1

The yeast Ste24 homolog ZMPSTE24, also known as FACE1 or CAAX prenyl protease 1 homolog, was just recently added to the metalloprotease family 48 (M48) class of zinc metalloproteases (Kühnle *et al.*, 2019). ZMPSTE24 is an integral membrane protein with seven α-helices that create a barrel-shaped cavity within the membrane (Goblirsch and Wiener, 2020). In yeast Ste24 localizes to the inner nuclear membrane and the ER (Boyartchuk *et al.*, 1997). Although, only the barrel is buried in the bilayer and the catalytic zinc ion of the active site is situated right at the membrane surface, contrary to classical intramembrane proteases (Quigley *et al.*, 2013), peripheral membrane substrates access the active site cavity from within the membrane. ZMPSTE24 is conserved from yeast to humans and has been characterized for its processing of prelamin A (Fujimura-Kamada *et al.*, 1997). Mutations in the cleavage site of prelamin A or in ZMPSTE24 are associated with the accumulation of unprocessed prelamin A in laminopathies diseases (Barrowman *et al.*, 2012). One of the most severe forms is the Hutchinson-Gilford progeria syndrome, a premature aging disease (Barrowman *et al.*, 2012; Cenni *et al.*, 2018). Moreover, it was observed in yeast that Ste24 has a de-clogging capability by cleaving prematurely-fold and releasing stuck proteins of Sec61 in order to restore the flux of the translocon channel (Ast *et al.*, 2016; Kayatekin *et al.*, 2018). Whether in mammals similar mechanisms exist is yet to be discovered.

Interestingly, the IMM-localized intramembrane zinc metallopeptidase OMA1 (Ehses *et al.*, 2009; Head *et al.*, 2009), which is part of the mitochondrial quality control system, dormant under physiological conditions and activated in response to various mitochondrial stress situations, shows homology with ZMPSTE24 (Alavi, 2021). OMA1 also belongs to the metalloprotease family M48 and harbors a C-terminal M48 domain oriented towards the IMS, which is responsible for proteolytic activity, while the matrix-oriented N-terminal domain was described to fix OMA1 in the IMM and to sense changes in $\Delta\Psi_{mito}$ (Baker *et al.*, 2014; Käser *et al.*, 2003; Levytskyy *et al.*, 2017; López-Pelegrín *et al.*, 2013). OMA1 mutants lacking the positively charged N-terminal domain are unable to cleave the main substrate L-OPA1 in

response to loss of $\Delta\Psi_{mito}$ (Baker *et al.*, 2014). Besides OPA1, OMA1 was described to cleave the signaling peptide DELE1, which can elicit the integrated stress response, PGAM5 and PINK1, which are involved in necroptosis, mitophagy and apoptosis, as well as the intramitochondrial lipid transfer proteins STARD7, PRELID1, PRELID3B and TRIAP1, that forms heterodimers with PRELID1 and PRELID3B (Ohba *et al.*, 2020). Recently it could be shown that fluctuations in $\Delta\Psi_{mito}$, also called "flickering", activate OMA1 as a protective stress response against mitochondrial hyperfusion (Murata *et al.*, 2020). Additionally, OMA1 activation could be achieved by genetic knockdown of the mitochondrial scaffolding proteins PHB2 and SLP2 (Merkwirth *et al.*, 2008; Tondera *et al.*, 2009), which organize lipid microdomains and thereby control the activity of the AAA-proteases (Deshwal *et al.*, 2020). Strikingly, stress-activated OMA1 shares substrates with the rhomboid serine protease PARL (**chapter 1.5.4.2.**) and the *i*-AAA protease YME1L (**chapter 1.3.2.2.**), although PARL belongs to a very distinct protease family (Quirós *et al.*, 2015; Sekine *et al.*, 2019). Diseases associated with OMA1 malfunctioning are based on mitochondrial structure/function and cellular stress response (Gilkerson *et al.*, 2021), also including cancer (Daverey *et al.*, 2019).

1.5.2. Aspartyl proteases

The group of aspartyl intramembrane proteases comprises presenilin, signal peptide peptidase (SPP) and SPP-like (SPPL) proteases. Presenilin and SPP were described to contain nine TM segments and share a common YD/GxGD active site motif with two aspartyl residues located in TM6 and TM7 (Steiner and Haass, 2000; Weihofen *et al.*, 2002). Their last TM segment harbors a conserved PAL motif, which is crucial for catalytic activity (Sato *et al.*, 2008; Tolia *et al.*, 2008; Tomita *et al.*, 2001). Most aspartyl proteases require initial shedding of their substrate's ectodomain in order to proteolyze them eventually within the membrane (Lichtenthaler *et al.*, 2018).

1.5.2.1. Presenilin and the γ-secretase complex

Presenilins exist in two isoforms, presenilin 1 and 2 (PSEN1 and PSEN2), and were identified as the catalytic subunits of the γ-secretase complex, which is one of the most studied intramembrane protease-complex as it is genetically linked to early-onset Alzheimer's disease (AD) (De Strooper *et al.*, 1998; Levitan and Greenwald, 1995; Sherrington *et al.*, 1995; Wolfe *et al.*, 1999). Together with essential co-factors like Nicastrin, presenilin enhancer 2 (PEN2) and the anterior pharynx defective 1 (APH1), PSEN1 and PSEN2 cleave more than 100 substrates, including the amyloid precursor protein (APP) and Notch, a crucial signaling factor affecting cell proliferation and embryonic development (De Strooper *et al.*, 1999; Haapasalo and Kovacs, 2011; Hemming *et al.*, 2008; Levitan and Greenwald, 1995). The ectodomains of APP and Notch are first shed by the α-secretases ADAM10 or ADAM17 and/or β-secretase

such as BACE1 before the membrane-tethered substrate can undergo cleavage by γ-secretase (MacLeod *et al.*, 2015). APP can be cleaved by γ-secretase at multiple sites to create amyloid-β peptides of varying length such as Aβ42, which is an aggregation-prone species shown to form oligomers causing amyloid fibrillogenesis that is seen as the major constituent of senile amyloid plaques found in AD brains (Benilova *et al.*, 2012; Buxbaum *et al.*, 1998; Haass and Selkoe, 2007; Selkoe, 2004; Sinha *et al.*, 1999; Vassar *et al.*, 1999; Yan *et al.*, 1999). Thus, mutations also in the presenilins itself are directly linked to AD (Levy-Lahad *et al.*, 1995; Rogaev *et al.*, 1995) as they can increase the amount of toxic Aβ42 peptide (Borchelt *et al.*, 1996; Citron *et al.*, 1997). Additionally, it could be shown in rodent and human brain-derived microsomes that γ-secretase forms high molecular weight multiprotease complexes with α- or β-secretase, in order to enable efficient substrate processing by coupling shedding and intramembrane cleavage in the same physical complex (Chen *et al.*, 2015; Liu *et al.*, 2019). Comparable to APP, also Notch undergoes two sub-sequential processing steps, of which the second is executed by γ-secretase, leading to the release of the intracellular domain of Notch that acts as a transcription activating factor (Kopan and Goate, 2000). Recent cryo-electron microscopy (cryo-EM) of human γ-secretase in complex with APP or Notch revealed how the protease recognizes its substrates. The structural studies could show that the α-helical TM domains of APP and Notch are unwound in the enzyme prior to proteolytic cleavage, forming a hybrid β-sheet between PSEN1 and the substrate guiding the enzyme to the scissile peptide bond. This uncovers that both the substrate and the enzyme undergo critical conformational changes and mutations inhibiting the formation of this hybrid β-sheet were shown to hamper substrate processing (Yang *et al.*, 2019; Zhou *et al.*, 2019). The comparably wide substrate spectrum of y-secretase lead to the suggestion that the protease complex displays only loose substrate specificity and acts as a kind of ‘proteasome of the membrane’ (Kopan and Ilagan, 2004).

1.5.2.2. SPP and SPP-like proteases

Originally discovered as the protease clearing signal peptides from the ER membrane (Lemberg and Martoglio, 2002; Weihofen *et al.*, 2002), SPP and its four SPPL paralogs (SPPL2a, SPPL2b, SPPL2c and SPPL3) were independently annotated as presenilin homologues (Grigorenko *et al.*, 2002; Ponting *et al.*, 2002) but display an overall inverted topology compared to presenilin, which also impacts the substrate orientation (Weihofen *et al.*, 2002). It is currently believed that intramembrane proteases are selective for one substrate orientation, which is in line with the fact that presenilin exclusively accepts type I membrane proteins (N-terminus faces the extracellular/luminal side), whereas SPP is described to cleave TM domains with a type II orientation (N-terminus faces the cellular/cytoplasmic side) (Boname *et al.*, 2014; Chen *et al.*, 2014a; Friedmann *et al.*, 2004; Hsu *et al.*, 2019; Hsu *et al.*, 2015; Weihofen *et al.*, 2002). Contrary to presenilin, SPP does neither require co-factors for its

proteolytic activity (Narayanan *et al.*, 2007; Weihofen *et al.*, 2002), nor does it undergo endoproteolytic maturation (Friedmann *et al.*, 2004). The substrate list of SPP was greatly enlarged as it became obvious, hat SPP cleavage is not restricted to signal sequences. Substrate cleavage includes maturation of the cell surface histocompatibility antigen, non-classical HLA-E epitopes (Lemberg *et al.*, 2001), release of the mature core protein of hepatitis C virus (McLauchlan *et al.*, 2002) and heme oxygenase 1 (HO1) amongst a subset of other tail-anchored proteins (Boname *et al.*, 2014; Hsu *et al.*, 2015). SPP has been found to process FKBP8, a member of the immunophilin protein family and thereby promote cancer progression (Hsu *et al.*, 2019). Moreover, by cleaving Syntaxin-18, SPP could be connected with morphology control of the ER (Avci *et al.*, 2019) and with regulation of the UPR by processing XBP1u to control its abundance (Chen *et al.*, 2014a; Yücel *et al.*, 2019). Strikingly, SPP was found to function in a 500 kDa-complex together with the rhomboid pseudoprotease Derlin1 and the E3 ubiquitin ligase TRC8, in order to target ERAD substrates for degradation (Chen *et al.*, 2014a; Stagg *et al.*, 2009). In this complex, Derlin1 can act as a substrate receptor by recognizing the luminal domain of XBP1u and TRC8 ubiquitinates XBP1u to target it for proteasomal degradation (Boname *et al.*, 2014; Chen *et al.*, 2014a).

SPPL proteases localize to different compartments along the secretory pathway (**Figure 3**), share various mechanistic similarities with SPP, as they cleave type II membrane proteins (Mentrup *et al.*, 2017), and require prior ectodomain shedding, except for SPPL3 (Voss *et al.*, 2013). In terms of their physiological functions, SPPL proteases were shown to have specific roles in the immune system and in tumor development. A special role plays SPPL2c, which localizes to the ER and catalyzes certain tail-anchored proteins like SPP but is expressed exclusively in testis. Further research has linked SPPL2c to proteolysis of SNARE proteins and phospholamban in male germ cell development (Niemeyer *et al.*, 2019; Papadopoulou *et al.*, 2019).

1.5.3. Glutamyl proteases

Ras converting enzyme 1 (RCE1) is so far the only known member of the glutamyl intramembrane proteases (Manolaridis *et al.*, 2013), was first discovered together with yeast Ste24 (Barrowman and Michaelis, 2009; Boyartchuk *et al.*, 1997; Schmidt *et al.*, 1998) and is one of the latest additions to the intramembrane proteases catalogue. Comparable to ZMPSTE24, RCE1 localizes to the inner nuclear membrane and the ER (**Figure 3**) and cleaves proteins with a CAAX motif in order to release the -AAX tripeptide (Barrowman and Michaelis, 2009). The hydrophilic attack to process substrate peptide bonds is coordinated by glutamic acid and a histidine residue and instead of catalyzing substrates within their TM domains, RCE1 cleaves rather at the substrate C-terminus, in contrast to other intramembrane proteases (Manolaridis *et al.*, 2013). RCE1 homologs can be found in all kingdoms of life in the ABI (abortive infection) family of putative intramembrane proteases, which are

characterized by three conserved catalytic motifs (Manolaridis *et al.*, 2013; Pei and Grishin, 2001). Structural data was obtained from the archaea *Methanococcus maripaludis* that revealed eight conserved α-helical TM domains in RCE1 and two peripheral helices with its conserved catalytic motifs positioned at the top of a cavity, inside the membrane (Manolaridis *et al.*, 2013). In contrast to ZMPSTE24, RCE1 is described to have a wider substrate spectrum as it also cleaves all farnesylated or geranylgeranylated proteins (Manolaridis *et al.*, 2013). RCE1 substrates have been shown to be involved in cell physiology and cell signaling pathways and include Ras family proteins such as small GTPases, nuclear lamins, protein kinases and phosphatases (Gao *et al.*, 2009; Hampton *et al.*, 2018). Mice deficient for RCE1 were shown to develop dilated cardiomyopathy, which becomes lethal (Bergo *et al.*, 2004). Moreover, an increased induction of the oncogene K-Ras could be observed resulting in myeloproliferative disease and reduced survival (Wahlstrom *et al.*, 2008), despite being involved in proper function of photoreceptor cells in mice (Christiansen *et al.*, 2011).

1.5.4. Rhomboid serine proteases

Rhomboids, the most widespread and largest family of intramembrane proteases were first identified in a genetic screen that aimed to identify factors that are involved in the embryonic development of *D. melanogaster* and were named after the phenotype of rhomboid-shaped head skeletons upon mutation (Koonin *et al.*, 2003; Mayer and Nüsslein-Volhard, 1988; Urban *et al.*, 2001). Rhomboid serine proteases represent a conserved group of integral proteases cleaving a diverse set of TM proteins and known functions range from growth factor activation, as seen for epidermal growth factor (EGF) receptor signaling in *Drosophila,* and membrane remodeling to protein degradation (Bergbold and Lemberg, 2013; Freeman, 2008; Sturtevant *et al.*, 1993; Urban *et al.*, 2001). In contrast to intramembrane apartyl- and metalloproteases, rhomboid proteases do not require prior substrate shedding and cleave full-length membrane proteins (Lemberg, 2013).

1.5.4.1. Bacterial rhomboids

So far, the best understood rhomboid protease is the *Escherichia coli* rhomboid protease GlpG that is located in the plasma membrane, although until today no endogenous substrates or the physiological role of this enzyme are known and understood. The only phenotypes identified for *E. coli* GlpG mutants are an enhanced resistance to cefotaxime (Clemmer *et al.*, 2006) and reduced intestinal colonization in a murine model (Russell *et al.*, 2017). However, the molecular mechanisms underlying these phenotypes are unknown (Liu *et al.*, 2020a). Only a few substrates of bacterial rhomboids are known. For instance, the *Providencia stuartii* rhomboid AarA cleaves TatA (Stevenson *et al.*, 2007), an essential component of the twin-arginine translocation (Tat) system (Palmer and Berks, 2012) whose processing is critical for

the function of the Tat system-mediated quorum sensing (Stevenson *et al.*, 2007). In *Bacillus subtilis* the rhomboid YqgP cleaves the magnesium transporter MgtE under environmental conditions of low magnesium and high manganese or zinc and additionally functions as a substrate adaptor for the AAA protease FtsH (Began *et al.*, 2020). Interestingly, the active site of YqgP, but not its catalytic ability, is required for the interaction with FtsH and conjunctional cleavage of MgtE by FtsH, which resembles the function of derlins (**chapter 1.5.4.3.**) in eukaryotic ERAD (Kandel and Neal, 2020). While YqgP regulates the abundance of active MgtE, the *Shigella sonnei* rhomboids GlpG and Rhom7 have been shown to degrade orphan subunits by detecting unstable TM domains sourcing from a characteristic proline residue that, in the absence of complex partners, results in a destabilized membrane anchor (Liu *et al.*, 2020a). Despite the fact, that the catalytic core of rhomboid proteases is conserved with six TM domains including the active site GxSG/H catalytic motif forming a catalytic dyad in TM4 and TM6 (Lemberg *et al.*, 2005; Wang *et al.*, 2006), domain architecture and topology can differ, often extended by an additional TM domain and cytosolic domains, as observed for the mitochondrial rhomboid PARL (**see below**). GlpG has been used in numerous structural and mechanistic studies (Ticha *et al.*, 2018). To cleave peptide bonds in the hydrophobic environment of the membrane, an aqueous active site forms within the rhomboid domain that is capped at the surface by the flexible loop 5 and gated laterally by TM helix 5 (Wang *et al.*, 2006; Wu *et al.*, 2006). Both regions are proposed to regulate substrate entry, however, the extent of their mobility is under debate (Baker *et al.*, 2007; Cho *et al.*, 2019b; Wang and Ha, 2007; Xue and Ha, 2013).

1.5.4.2. Mammalian rhomboids

In mammals, rhomboids appear in all major cellular organelles, forming distinct phylogenic groups with distinct conserved functions: Five rhomboid proteases are described, namely rhomboid-related protein 1-4 (RHBDL1, RHBDL2, RHBDL3, RHBDL4) along the secretory pathway and PARL in the IMM (Kühnle *et al.*, 2019). For instance, plasma membrane-localized protease RHBDL2 is implicated in wound healing and cell adhesion by cleaving thrombomodulin, ephrin-B2 and ephrin-B3, for review see (Bergbold and Lemberg, 2013), as well as in epithelial homeostasis and cell motility by processing the interleukin-6 receptor, E-cadherin, N-cadherin and BCAM (Battistini *et al.*, 2019; Johnson *et al.*, 2017). The ER-localized RHBDL4 (also referred to as Rhbdd1) plays a major role in the ERAD machinery and cleaves its substrates either directly in the membrane, within luminal loops or within TM segments of polytopic membrane proteins (Fleig *et al.*, 2012). RHBDL4 was found to recognize ubiquitinated substrates in ERAD and to recruit the AAA-ATPase p97 in order to dislocate RHBDL4-generated cleavage fragments from the ER membrane into the cytosol for proteasomal degradation (Bergbold and Lemberg, 2013; Fleig *et al.*, 2012). Its broad substrate spectrum includes polytopic membrane proteins like the mutant form of opsin, single-spanning

type I membrane proteins such as pTα, TCRα or MPZ (Fleig *et al.*, 2012), as well as the soluble substrate MHC202 (Bock *et al.*, 2021). For RHBDL1 in the Golgi and RHBDL3 in late endosomes no substrates have been identified so far (Bergbold and Lemberg, 2013).

The IMM-localized rhomboid PARL, initially termed 'presenilin-associated rhomboid-like' originating from a Yeast-two-Hybrid artifact (Pellegrini *et al.*, 2001) and reassigned later, functions as a cellular safeguard of mitophagy (Cipolat *et al.*, 2006; Jeyaraju *et al.*, 2006) (**chapter 1.6**). While the spectrum of PARL substrates initially was limited to PINK1 and PGAM5 (Jin *et al.*, 2010; Meissner *et al.*, 2011; Sekine *et al.*, 2012), proteomics approaches in the last years identified four additional substrates (**Table 1**) (Saita *et al.*, 2017).

Table 1 | List of verified PARL substrates.

IMS: intermembrane space, IMM: inner mitochondrial membrane, OMM: outer mitochondrial membrane.

Name	Subcellular localizations	Regulatory functions	Additionally processed by	Reference
PINK1	IMM depolarization: OMM, cytoplasm	Mitophagy	MPP, *m*-AAA, CLPXP (AFG3L2), OMA1	(Deas *et al.*, 2011; Greene *et al.*, 2012; Jin *et al.*, 2010; Lin and Kang, 2010; Meissner *et al.*, 2011; Sekine *et al.*, 2019)
PGAM5	IMM depolarization: IMS, cytoplasm	Mitophagy, apoptosis/ necroptosis, Wnt signaling	OMA1	(Sekine *et al.*, 2012; Wai *et al.*, 2016)
Smac/DIABLO	IMM, cytoplasm	Apoptosis regulator, prevents the inhibitor of apoptosis protein (XIAP) from inhibiting its caspase targets		(Green and Kroemer, 2004; Jost *et al.*, 2009; Saita *et al.*, 2017)
STARD7	IMM, cytoplasm	Lipid carrier, transports phosphatidylcholine	MPP, OMA1	(Ohba *et al.*, 2020; Saita *et al.*, 2017; Saita *et al.*, 2018)
TTC19	IMM	Subunit of Ubiquinol Cytochrome c Reductase (UQCR, Complex III or Cytochrome bc1 complex)		(Saita *et al.*, 2017; Spinazzi *et al.*, 2019)
CLPB/Skd3	IMS, cytoplasm	Mitochondrial AAA+ protein disaggregase, AAA-ATPase chaperone		(Cupo and Shorter, 2020; Saita *et al.*, 2017; Thevarajan *et al.*, 2020)

However, also OPA1 and HtrA2/Omi have been suggested to be cleaved by PARL but the identification as a PARL substrate in mammals is still controversial. In the case of OPA1 a genetic interaction with PARL in mice and analogies with the yeast and *Drosophila* system (Cipolat *et al.*, 2006; McQuibban *et al.*, 2003) lead to the assumption of OPA1 being a substrate, although other studies have indicated that PARL is dispensable for OPA1 processing (Duvezin-Caubet *et al.*, 2007; Ehses *et al.*, 2009; Ishihara *et al.*, 2006). Also, in the case of HtrA2/Omi, analogies with the function of the PARL ortholog Rhomboid 7 in *Drosophila,* which also cleaves a PINK1 homolog, were taken as first basis for assumptions (Whitworth *et al.*, 2008), and knockout studies in mice assumed an interaction of PARL with the anti-apoptotic BCL-related protein HAX1 but not directly with HtrA2/Omi, and therefore proposed that HtrA2/Omi interacts with PARL via HAX1 (Chao *et al.*, 2008; Jeyaraju *et al.*, 2009; Yoshioka *et al.*, 2013). Nevertheless, no clear evidence is given until today, that clarifies OPA1 or HtrA2/Omi as PARL substrates (Spinazzi and De Strooper, 2016). Surprisingly, several of the recently found PARL substrates do not have defined TM segments, indicating that the substrate recognition mechanism is more complex than initially anticipated.

1.5.4.3. Rhomboid pseudoproteases

A group of catalytic inactive rhomboid proteases, called pseudoproteases, which are evolutionary and structurally related to active rhomboids, comprises iRhom 1 and 2, Derlin-1, -2, -3, RHBDD2, RHBDD3, TMEM115 and UBAC2 (Bergbold and Lemberg, 2013; Dulloo *et al.*, 2019; Lemberg and Adrain, 2016). iRhoms can be found throughout the metazoan kingdom and include some homologs that contain the full set of active site residues but with a conserved proline at the x-position of the rhomboid GxSG/H catalytic motif that silences their proteolytic activity (Lemberg and Freeman, 2007b; Zettl *et al.*, 2011). In *Drosophila* iRhom was shown to induce ERAD of EGF receptor ligands and by that act as a negative regulator of EGF-receptor signaling (Zettl *et al.*, 2011). iRhom pseudoproteases were found to be important regulators of transcellular signaling and innate immunity as they are essential factors for trafficking and activation of the metalloprotease ADAM17 (also called TACE) (Adrain *et al.*, 2012), which acts as sheddase of EGF-receptor ligands and cleaves the tumor necrosis factor TNFα that regulates immune cells (Lichtenthaler *et al.*, 2018).

Derlins, the second class of rhomboid-like pseudoproteases, are described as ERAD factors conserved from yeast to mammals (Greenblatt *et al.*, 2011; Knop *et al.*, 1996; Lemberg *et al.*, 2005; Oda *et al.*, 2006; Ye *et al.*, 2004) and employ substrate engagement, induce lipid distortion in retrotranslocation of ER membrane substrates (Neal *et al.*, 2018; Nejatfard *et al.*, 2021) and function as accessory factors for intramembrane proteases (Avci *et al.*, 2014; Chen *et al.*, 2014a). For instance, human Derlin-1 was shown to form a complex with SPP and TRC8 and to act as substrate adaptor recruiting the UPR regulator XBP1u for intramembrane proteolysis (Chen *et al.*, 2014a).

1.5.4.4. The lipid distortion effect of rhomboids

Lipid membranes contain hundreds of different lipid species and are the most important interfaces in biology as they provide the solvent for membrane proteins carrying out the most essential cellular functions. Optimal membrane protein function is only given with the correct lateral heterogeneities in the lipid distribution, appropriate lipid-dependent spontaneous curvature, and by specific lipid-protein interactions. However, so far only little is known about the mechanistical details how lipids tune protein function. Solving the question how lipids modulate the activity of membrane proteins is also key for detailed understanding of intramembrane proteolysis. For instance, Bovine rhodopsin was described to require highly elastic membranes composed of polyunsaturated lipids with negative spontaneous curvature for optimal function (Botelho *et al.*, 2002; Litman and Mitchell, 1996) and shows a headgroup specificity for phosphatidylethanolamine (PE) (Soubias *et al.*, 2006). In comparison to soluble enzymes, rhomboids process their substrates slowly, like other intramembrane proteases, due to complex binding and unwinding of the substrate TM domain prior to cleavage (Arutyunova *et al.*, 2014; Dickey *et al.*, 2013). Examining catalytic cleavage of rhomboids *in vitro* has been shown to be indeed dependent on the membrane composition (Kreutzberger *et al.*, 2019). It could be shown that rhomboids have a thinner hydrophobic band, a mismatch with the membrane thickness that can lead to membrane distortion (Bondar *et al.*, 2009; Killian, 1998) and thereby, reduces membrane viscosity. Thus, it has been suggested that diffusion through the lipid bilayer is the rate-determining step in rhomboid substrate cleavage (Kreutzberger *et al.*, 2019). Just recently, it could be shown that RHBDL2 can sense conformational changes in the membrane and cleaves the CRAC channel protein Orai1 when it is inappropriately activated, thus preventing false immunological signaling (Grieve *et al.*, 2021). Here, in collaboration with the Huster laboratory (Leipzig), we aim to further understand how lipids modulate the conformation of the membrane and thereby the activity of GlpG.

1.5.4.5. Molecular and mechanistic elements of mitochondrial PARL in comparison to other rhomboids

PARL possesses seven TM domains with the MTS-containing N-terminus located in the matrix and the C-terminus in the IMS. During import into the IMM, PARL undergoes constitutive α-cleavage in order to remove the MTS at amino acid positions 52-53 (α-site). However, a second developmentally controlled and self-regulated β-cleavage event at amino acids 77-78 (β-site) was described, releasing a short Pβ peptide that functions as a mitochondria-to-nuclei signaling factor whose sequence is conserved only in mammals (Sik *et al.*, 2004). To what extent β-cleavage alters PARL function, is still under debate since contradictory observations were made (Jeyaraju *et al.*, 2011; Lysyk *et al.*, 2021; Shi *et al.*, 2011; Shi and McQuibban, 2017).

PARL substrates have a N_{in}/C_{out} topology, whereas secretory pathway rhomboids cleave N_{out}/C_{in} TM segments of type I membrane proteins, but also cleavage in loops and TM domains of multi-span proteins have been reported (Fleig *et al.*, 2012). While rhomboid proteases in the eukaryotic secretory pathway have their active site opening towards the extracytoplasmic space, PARL has been suggested, consistent with the inverse substrate orientation, with an inverted topology (**Figure 4**) (Lemberg and Freeman, 2007a). Hence, its active site is supposed to face the mitochondrial matrix that in respect of its topology corresponds to the cytoplasm of other rhomboid proteases. PARL has a matrix targeting signal followed by an additional N-terminal TM domain. The structural consequences of this additional N-terminal TM segment, and if the loop corresponding to *E. coli* loop 5 serves as a cap to the matrix side, are not clear. Likewise, the mechanism of how PARL substrates are recognized and how this relates to the better studied bacterial rhomboids that may be governed by substrate TM helix stability and sequence features, remains to be investigated. Although a consensus sequence motif around the cleavage site of a bacterial rhomboid protease substrate has been identified (Akiyama and Maegawa, 2007; Strisovsky, 2016), it is not entirely clear how cognate substrate TM domains are selected. However, cleavage is specific, as indicated by a screen of the Freeman laboratory for substrates of the mammalian plasma membrane rhomboid protease RHBDL2, in which only a minor fraction of tested candidates was cleaved. Even for the *E. coli* rhomboid GlpG, where structures with substrate-mimicking peptide inhibitors provided first insights into the Michaelis complex (Cho *et al.*, 2016; Zoll *et al.*, 2014), the mechanism of how substrates are selected is controversially discussed.

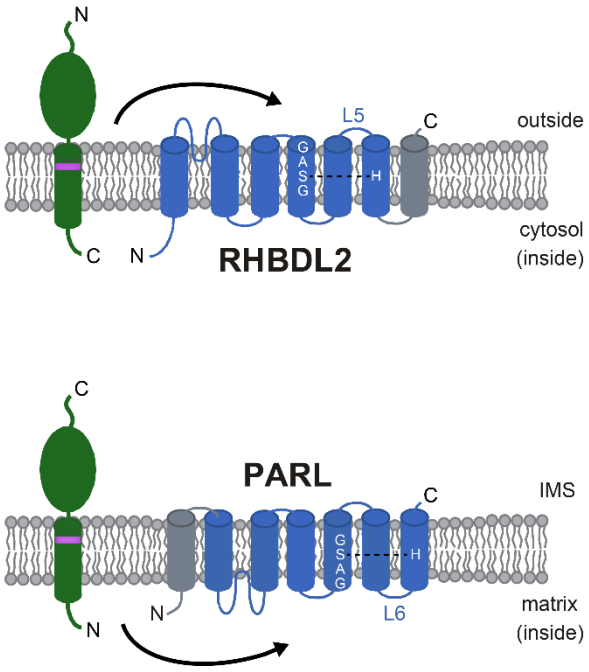

Figure 4 (Caption overleaf)

Figure 4 | Mitochondrial PARL has a flipped active site.
Compared to other rhomboids, PARL reveals a conserved additional TM domain (highlighted in grey) fused to the six-TM-spanning rhomboid core domain (blue) with an N-terminal MTS. Known PARL substrates have a N_{in}/C_{out} topology opposite to RHBDL2 substrates (N_{out}/C_{in}), supporting a model of a flipped PARL active site with an active site opening to the matrix. The active site motifs 'GASG' and 'H' form a catalytic dyad between TM helix 4 and 6 of the rhomboid domain. Cleavage site within substrate TM domain is depicted in magenta. L5: flexible loop 5; L6: flexible loop 6 corresponding to L5.

1.6. PARL cleaves PINK1 and PGAM5 in an inversely correlated manner

PARL knockout mice develop normally during embryogenesis but suffer from a progressive multisystem disorder a few weeks after birth (Cipolat *et al.*, 2006). When PINK1 is stabilized as for instance by disrupting the mitochondrial membrane potential with CCCP, PINK1 is no longer cleaved by PARL and accumulates at the OMM. Eventually, PINK1 becomes fully activated leading to the recruitment of Parkin and removal of damaged mitochondria by mitophagy (Youle and Narendra, 2011) (**chapter 1.4.1.**). Interestingly, by an ill-defined mechanism after the addition of CCCP another factor linked to mitochondrial homeostasis, the atypical Ser/Thr phosphatase PGAM5, is cleaved by PARL (Sekine *et al.*, 2012). PGAM5 was described to regulate mitophagy by stabilizing PINK1 under stress conditions (Lu *et al.*, 2014; Yan *et al.*, 2019). Consistent with this, it was shown that interactions of PINK1 and PGAM5 with a regulatory PARL complex, consisting of the matrix protein SLP2 and the inner membrane AAA-protease YME1L, are inversely correlated. In polarized mitochondria, this SLP2-PARL-YME1L (SPY) complex preferentially cleaves PINK1, while after mitochondrial depolarization, it preferentially cleaves PGAM5 (Wai *et al.*, 2016). PARL was found to cleave PGAM5 in the second half of the TM domain leading to the release of the C-terminal phosphatase domain into the IMS. Depending on the assay system, PARL cleavage has been mapped between amino acids F23-S24 (Lysyk *et al.*, 2021) or S24-A25 (Sekine *et al.*, 2012), respectively. As described in (**chapter 1.3.3.1**), a balanced level of two isoforms of yeast Mgm1 are mandatory to maintain mitochondrial morphology. Interestingly, the longer isoform of Mgm1 contains two conserved hydrophobic segments near its N-terminus of which the more C-terminal one is cleaved by Pcp1/Rbd1. Processing leads to a change of the hydrophobicity of the N-terminal segment and thereby modulates the ratio of the long and short isoforms, a pathway referred to as alternative topogenesis (Herlan *et al.*, 2004). It is still unknown what the exact cleavage determinants of PGAM5 are and how the constitutive cleavage is controlled by PARL in the SPY complex, also raising the possibility of whether PARL itself can sense polarization changes in the membrane or if co-factors exist, that function as voltage sensors monitoring the polarization of the IMM.

1.7. Aim of the thesis

PINK1 and PGAM5 cleavage by PARL is regulated in an inverse manner but the underlying mechanism explaining how the conditional cleavage of PGAM5 is achieved, still needs to be deciphered. Although up to now six PARL substrates are known, no clear consensus sequence became visible explaining what the exact cleavage determinants are (Saita *et al.*, 2017). Given the importance of PGAM5 in mitochondrial dynamics, cell-survival and health, I set out to find the cleavage determinants of this PARL substrate in a combination of mutational cell-based and cell-free PARL assays, including liquid-state NMR to study structural properties of the substrate TM domain. So, I ask what influence PGAM5 oligomerization and TM helix dynamics/helix-destabilizing residues have on PARL-catalyzed cleavage.

Moreover, among the challenges of deciphering how rhomboids find and cleave their substrates is to understand how they diffuse through viscous cell membranes crowded with other membrane proteins. To overcome the viscosity limit of the lipid environment, it has been suggested that the bacterial rhomboid protease GlpG thins its surrounding lipid belt (Kreutzberger *et al.*, 2019). Here, I contribute to the analysis of the lipid distortion effect of *E. coli* rhomboid GlpG wild-type (wt) and GlpG mutants with reduced catalytic activity in distinct lipid environments with different thickness by solid-state NMR.

2. Results

2.1 The human mitochondrial rhomboid PARL

The rhomboid protease PARL serves as safeguard of mitochondrial homeostasis and is processing PINK1 and PGAM5 in an inversely correlated manner, depending on the mitochondrial membrane potential. While the spectrum of PARL substrates initially was limited, recent proteomics approaches identified several PARL substrates including the apoptosis regulator Smac/DIABLO and the lipid carrier protein STARD7 (Saita *et al.*, 2017; Saita *et al.*, 2018). However, comparison of these PARL substrates does not reveal a clear consensus sequence, including PARL substrates that even lack defined TM segments, indicating that the substrate recognition mechanism is more complex than initially anticipated. Here, I investigate PARL substrate determinants on the example of PGAM5, which have not been rigorously studied yet.

2.1.1 Investigation of putative PARL substrates by SILAC

One of the major challenges in intramembrane protease research is the identification of native substrates, which is complicated by the fact of transient interaction between the enzyme and the substrate. Back in 2016 when I started my PhD project, only two verified substrates of the human mitochondrial rhomboid PARL were known, namely PINK1 and PGAM5 (Jin *et al.*, 2010; Meissner *et al.*, 2011; Sekine *et al.*, 2012). A well-established approach to identify putative substrates and interaction partners is a stable-isotope labeling with amino acids in cell culture (SILAC)-based proteomics approach (Ong *et al.*, 2002; Ong and Mann, 2006). This method has been used before successfully by others and in our laboratory to identify e.g. the zinc transporter Zrt1 as substrate of the SPP yeast homolog Ypf1 (Avci *et al.*, 2014) or to extend the list of tail-anchored proteins as substrates of SPP and SPPL2c (Avci *et al.*, 2019; Niemeyer *et al.*, 2019). SILAC mass-spectrometry allows to determine differences in protein abundance by using pairs of amino acids with different isotope composition. Based on their mass difference, peptides can afterwards be differentiated in a mass spectrometer. The here described SILAC bases on the idea of a PARL trapping approach using a doxycycline (dox)-inducible mouse PARL^{S275A}-GFP expressing T-REx cell line. Catalytic inactive PARL^{S275A} acts as a substrate trap by binding to and not processing endogenous substrates, so that upon solubilization from the membrane using a detergent, human PINK1 could be co-purified (Meissner *et al.*, 2015). Here, I analyze the results of four independent SILACs that were performed by the previous lab members Beate Hehn and Christabel Celia Kho. In brief, for this SILAC-protocol Hek293-T-REx cells were metabolically labelled with either ‘light’ (L) for the cells without an overexpression construct, ‘medium’ (M) for PARL-GFP or ‘heavy’ (H) for PARL^{S275A}-GFP overexpression construct (**Figure 5A**). Mass-spectrometry-based analysis of the trapped proteome of differentially labeled cells identified in sum 6746 peptides and 943

proteins of which 861 proteins were quantified. Proteins were normalized to GFP and filtered for mitochondrial proteins with the PERSEUS software (Tyanova *et al.*, 2016) and only those that appeared in at least two SILAC replicates, were considered for further analysis (**Figure 5B**). Proteins that are considered trapped substrates are enriched in the 'heavy' cell population and show high and positive log2-transformed H/M and H/L ratios. Additionally, putative substrates show decreased protein levels in the 'medium' population (negative M/L ratio), as they are processed by PARL wild type (wt). Analyzing the mass-spectrometry-based results, I found the following proteins as top hits for putative novel PARL substrates (**Table 2**); see for further results the extended table (**Table S2)**. Proteins that are considered interaction partners of PARL are enriched especially in the 'medium' cell population with a high and positive M/L ratio (**Table S3**).

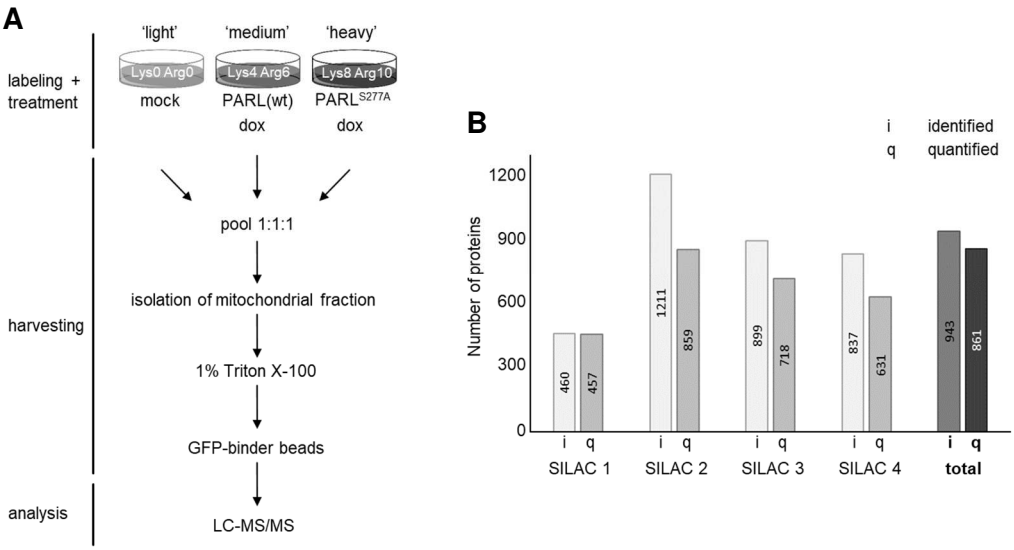

Figure 5 | SILAC-based substrate identification approach.

(A) Outline of the SILAC-based substrate identification approach using the PARL-trapping assay, in doxycycline (dox)-inducible mouse PARL-GFP or PARL^{S275A}-GFP expressing T-REx cells. Hek293-T-REx cells transfected with empty vector were used as control (mock). **(B)** Analysis of mass-spectrometry-derived data of identified (i) and quantified (q) proteins from the four SILAC-based approaches. Proteins contained in at least two replicates were used for further analysis. LC-MS/MS: liquid chromatography-mass spectrometry/mass spectrometry.

Initially, I aimed to identify novel PARL substrates with primarily one or multiple TM domains and putative PARL interaction partners. Since the Langer laboratory was already working on a proteomics approach to identify novel PARL interaction partners, and found PARL to interact with the scaffold SLP2, gene name STOML2, and the *i*-AAA protease YME1L in a proteolytic hub, the SPY-complex (Wai *et al.*, 2016), I decided to concentrate on novel substrates only. Of note, in our SILAC approach we could partially reproduce the results from the Langer laboratory, since beside SLP2 also YME1L was found enriched in the H/M ratios (**Table S2**). One top hit of the trapping approach was GHITM (growth hormone-inducible transmembrane)

protein, also known as MICS1, which has 6 predicted TM domains. However, when co-expressing GHITM-FLAG in Hek293T cells with either human PARL wt or catalytic inactive PARL^{S277A}, only full-length GHITM was detected (**Figure 6**). The protein levels of GHITM at 27 kDa stayed constant and no cleavage fragments appeared when different amounts of PARL wt or PARL^{S277A} were co-expressed with GHITM-FLAG. The slight reduction of the GHITM steady-state level at higher PARL expression was also observed for the catalytic PARL^{S277A} mutant, indicating that this effect is not caused by intramembrane proteolysis. Of note, I observed in this and other experiments that increasing the amount of ectopically expressed PARL over a certain threshold (roughly 300 ng), induces unspecific stress in mitochondria leading to decreased detection of PARL and the co-expressed substrate candidate, see for example (**Figure 6**). Likewise, no influence of PARL was observed in cycloheximide chase experiments to examine protein degradation after inhibition of protein translation, and also inhibition of the proteasome by epoxomicin did not stabilize any potential GHITM cleavage fragments (data not shown). Hence, I conclude that GHITM is not a physiological PARL substrate.

Further trapped putative substrates are the IMS-localized CLPB (caseinolytic peptidase B protein homolog), also known as HSP78 and Skd3, CSDE1 (Cold shock domain-containing protein E1) and catalase. Since for all three proteins no TM domain is predicted, rendering them soluble proteins, all were excluded from continuing validation.

Table 2 | Selected candidates of putative PARL substrates identified in the gain-of-function PARL-trapping approach using SILAC.

Average values			**Gene names**	**Protein names**	**Protein ID**
Ratio M/L	Ratio H/L	**Ratio H/M**			
-1.0851	0.2216	**1.5944**	**GHITM**	Growth hormone-inducible transmembrane protein	Q9H3K2
-0.8612	0.4994	**1.4975**	**CLPB**	Caseinolytic peptidase B protein homolog; Suppressor of potassium transport defect 3	Q9H078
-0.3133	0.3140	**0.9303**	**CSDE1**	Cold shock domain-containing protein E1	O75534
-0.2566	0.0438	**0.4196**	**CAT**	Catalase	P04040

While I was validating further putative PARL substrates, the Langer laboratory published in a very similar proteomics approach several PARL substrates including the apoptosis regulator Smac/DIABLO, the lipid carrier protein STARD7, the respiratory complex III-maintaining protein TTC19 and the regulatory AAA-ATPase chaperone/disaggregase CLPB (Saita *et al.*, 2017). Intriguingly, both TTC19 and CLPB are lacking a TM domain. Since the throughput of our proteomics approaches was limited, I decided to terminate further screenings and validation experiments for novel PARL substrates at this point and to concentrate on PGAM5 and its unexplored cleavage determinants and recognition mechanism by PARL, instead.

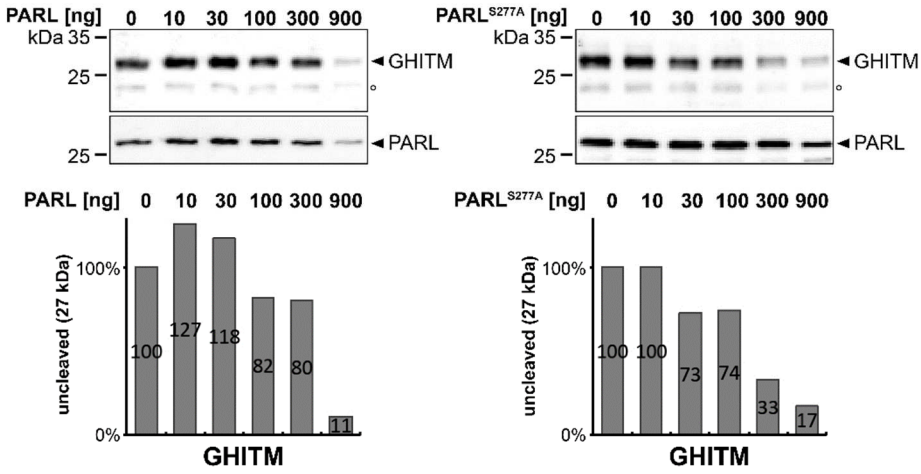

Figure 6 | GHITM-FLAG is not cleaved by PARL.

GHITM processing was analyzed in a cell-based gain-of-function assay and western blotting. Hek293T cells were co-transfected with GHITM-FLAG and different amounts of either PARL wt or catalytic inactive PARL^{S277A}. Lower panels show quantification of full-length GHITM (27 kDa) in relation to the starting condition of 0 ng PARL. Protein level of 0 ng PARL was set to 100%.

2.2 To study cleavage determinants in the PGAM5 TM domain unbiased: *in vitro* cleavage assay

Cell-based analyses often reaches technical limitations when performing ectopic overexpression of an enzyme, resulting in toxic effects unrelated to the catalytic activity, as seen for instance with PARL overexpression. Hence, I aimed to establish an *in vitro* cleavage assay with purified protein components that for instance, could also contribute to a more direct readout for the validation of PARL candidate substrates. In contrast to cellular assays, PARL-catalyzed cleavage in an *in vitro* assay is not biased by cellular events such as mitochondrial protein import, compartmentalization barriers, complex or interaction partners or any other regulatory processes. The most basic *in vitro* rhomboid assay relies on the detergent-solubilized protease and a known substrate TM domain in a physiological buffer system (Lemberg *et al.*, 2005). Based on this, reconstitution into lipid bilayers can be achieved but the lipid composition can affect rhomboid activity and needs to be chosen appropriately (Barniol-Xicota and Verhelst, 2018; Urban and Wolfe, 2005; Vinothkumar, 2011). Read-outs like cleavage fragments can be detected in gel-based assays by Coomassie staining, western-blot analysis or MALDI mass spectrometry. To map the cleavage site of a substrate, protein fragments can be analyzed by MALDI or EDMAN degradation.

To recreate substrate cleavage with purified proteases, the aim was to establish an expression system for eukaryotic rhomboid proteases in *Escherichia coli*. Human PARL (β-cleaved, also known as Δ77), either tagged with hexahistidine (His6) at the N- or C-terminus was expressed in Rosetta 2 (Novagen), a derivate of the BL21 strain which is designed to enhance the expression of eukaryotic proteins that contain codons rarely used in *E. coli* (**Figure S1A**).

Preliminary results showed, that we managed to express small amounts of active recombinant PARL as judged by activity-based labeling with the ActivX TAMRA-FP serine hydrolase probe (Thermo Fisher Scientific), (**Figure S1B**). This probe binds to the catalytic amino acids in correctly folded active sites of serine proteases, comparable to a protease inhibitor but is fused to a fluorescent probe, whose light emission can be detected. Purified, active *E. coli* rhomboid GlpG was used as control and rhomboid activity was inhibited by the serine protease inhibitor 3,4-Dichloroisocoumarin (DCI). Moreover, pilot experiments with CHAPS- and DDM-solubilized recombinant human PARL expressed in *E. coli* showed signs of activity by cleavage of a chimeric model substrate (MBP-PGAM5). This fusion construct contains the substrate TM domain of interest between an N-terminal *E. coli* maltose binding protein (MBP) and a C-terminal fusion of *E. coli* thioredoxin 1 (TrxA), followed by a triple FLAG-tag and a His6-tag (**Figure 7A and S1C**). However, the observed activity of human PARL in *E. coli* membranes was not always reproducible and varied between the different batches. Consistent with this, neither MBP-PINK1 nor MBP-PGAM5 cleavage could be detected when co-expressing His6-PARL wt and catalytic inactive His6-PARL^{S277A} in *E. coli* (**Figure S1D**). To exclude any putative background cleavage by the endogenous *E. coli* rhomboid GlpG, a *Δglpg* knockout strain (JW5687) (Baba *et al.*, 2006) was used for this experiment. Since GlpG is not essential for *E. coli*, the strain exhibited normal growth (Maegawa *et al.*, 2005). Further analysis with this strain and detailed trials to enhance PARL expression using different tags, like a GST-tag or other expression vector systems, like pGEX-4T-1, were examined in the master thesis of Josephine Bock, I co-supervised. The main bottleneck is to solubilize the rhomboid proteases from the membranes of the expression organism and to purify it in an enzymatically active state. Since, we always reached only minor activity of human PARL in the *E. coli* membranes using various combinations of different strains, vector systems and tags, and never managed to maintain enzymatic activity after purification, we collaborated with the Lemieux laboratory (University of Alberta, Canada), who managed to purify active recombinant DDM-solubilized human PARL from the secretory pathway of the yeast *Pichia pastoris* using peptide-based fluorescent substrates (Lysyk et al., 2021). In order to study PARL cleavage of its native substrates, chimeric MBP-PGAM5 (**Figure 7A**) was expressed in and purified from *E. coli*. Since we faced problems purifying a fusion protein with the PINK1 TM domain in earlier studies in this lab due to perturbing interactions with SDS (data not shown), I concentrated on the substrate TM domain of PGAM5 as my model substrate. Incubation of the 64 kDa MBP-PGAM5 with PARL wt but not catalytic inactive PARL^{S277A} in an appropriate DDM-containing cleavage buffer, resulted in an expected band shift revealing a 44 kDa N-terminal and a 20 kDa C-terminal cleavage fragment, resolved by SDS-PAGE and visualized by Coomassie staining (**Figure 7B**). In order to map the PARL cleavage site in MBP-PGAM5 containing the PGAM5 wt TM domain, cleavage fragments were separated in SDS-PAGE and blotted to a PDVF membrane. The band putatively containing the C-terminal cleavage fragment was cut out and sent for

EDMAN sequencing. Cleavage was indeed successful and the cleavage site could be mapped between Phe-23 and Ser-24, which is one amino acid upstream from the so far determined cleavage site between Ser-24 and Ala-25 (Sekine *et al.*, 2012), as shown in (**Figure 7C**) and published in our collaborative paper with the Lemieux laboratory (Lysyk *et al.*, 2021).

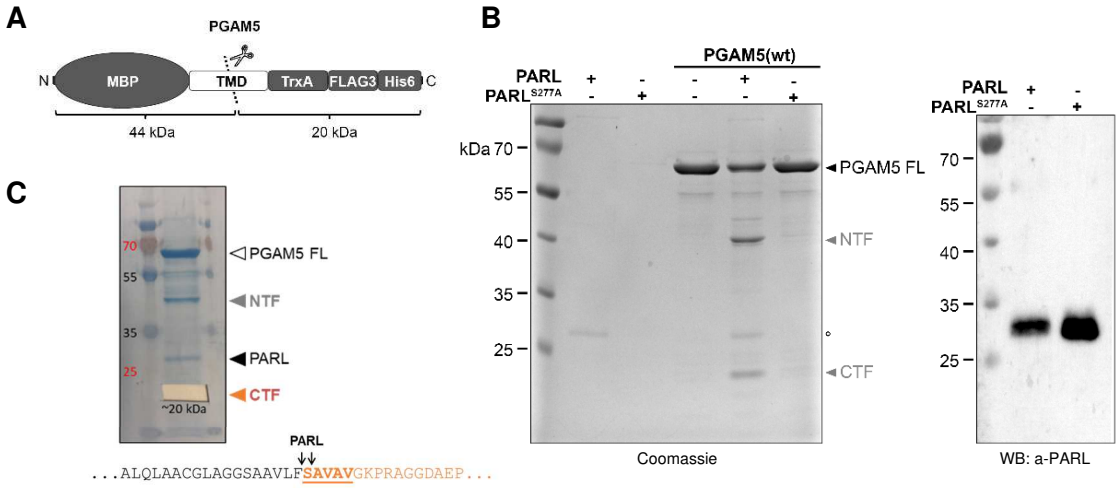

Figure 7 | Purified human PARL cleaves chimeric MBP-PGAM5.
(A) Schematic representation of the chimeric MBP-PGAM5 substrate construct, containing the PGAM5 TM domain (amino acids 1-46) N-terminally fused to maltose binding protein (MBP) with a C-terminal fusion containing thioredoxin 1 (TrxA), 3xFLAG and 6xHis tag. **(B)** *in vitro* cleavage assay using DDM-solubilized human PARL wt (β-cleaved, Δ77) and its catalytic inactive mutant PARL^{S277A} purified from *P. pastoris.* Since substoichiometric amount of PARL is not visible in the Coomassie-stained gel, equal protein load was controlled by WB (right panel). PGAM5 FL: MBP-PGAM5 full length, NTF: N-terminal cleavage fragment, CTF: C-terminal cleavage fragment, circle: minor contamination from PARL preparation. PARL-dependent alternative cleavage fragments appeared as side-effects of the detergent background. **(C)** The C-terminal cleavage fragment (CTF) was analyzed by EDMAN sequencing revealing cleavage within the PGAM5 TM domain one amino acid upstream from the so far determined cleavage site. The recovered sequence is underlined.

Taken together, these results show that purified DDM-solubilized PARL recapitulates key aspects of intramembrane proteolysis of PGAM5. However, the biophysical properties of the lipid bilayer cannot be reproduced in a detergent-micelle system. Although in collaboration with the Lemieux laboratory good amounts of active human PARL could be purified from *P. pastoris,* upscaling to high amounts needed for instance for solid-state NMR (see below), is still a bottleneck. Whereas activity of reconstituted PARL in proteoliposomes could be detected using small peptide-based substrates (Lysyk *et al.*, 2021), which do not have to fully-insert into the lipid bilayer, also co-reconstitution of the TM substrates alongside PARL into a lipid environment remains a challenging future project.

2.2.1 The *E. coli* rhomboid GlpG as model to study enzyme-substrate interactions in a membranous environment

For a full mechanistic analysis of rhomboid-catalyzed cleavage a robust *in vitro* assay in a membrane environment is key. However, for PARL the assay development still faces technical limitations (see above). Hence, I shifted my attempts to a simpler to handle model rhomboid protease and by this could also contribute to approach a new readout to study enzyme-substrate interactions in a membranous environment. As part of our DFG-funded research consortium (Research Unit 2290 “Understanding Intramembrane Proteolysis”), I collaborated with the group of Daniel Huster (Leipzig), who performed solid-state NMR of the *E. coli* rhomboid GlpG with the model substrate LacYTM2, which contains the second TM region of *E. coli* lactose permease (LacY) (Maegawa *et al.*, 2005). The aim was to record substrate-enzyme interactions in membranes of different thickness, since it was previously described, that the rhomboid fold can distort surrounding lipids in the membrane to overcome the viscosity-imposed speed limit of membrane diffusion (Kreutzberger *et al.*, 2019). Moreover, dynamics measurements revealed a dynamic hotspot of GlpG at the N-terminal part of TM domain 5 and the adjacent loop 5, indicating that this region is important for substrate gating. In addition, relaxation dispersion experiments suggest that TM domain 5 is in conformational exchange between an open and a closed conformation (Shi *et al.*, 2019). Understanding the principle of substrate recognition using GlpG as model might also contribute to the understanding of enzyme-substrate interaction of human PARL.

Lipids modulate the activity of membrane proteins, including intramembrane proteases, and catalytic cleavage highly depends on the composition of the viscose environment of a membrane where substrate diffusion is much slower as compared to the cytosol (Urban and Wolfe, 2005). Recently, it has been described that GlpG has a membrane thinning effect on its surrounding lipids to overcome the viscosity limit of membrane protein diffusion (Kreutzberger *et al.*, 2019). If a mismatch between the hydrophobic thickness of the rhomboid and the surrounding membrane exists, unfavorable free energy is created that can be balanced in three different ways. First, the proteins can adjust their α-helical content to the thickness of the membrane or second, the proteins can cluster to minimize the interaction with the lipids and/or third, the lipids can adjust their chain lengths to match the thickness of the membrane protein (Killian, 1998; Soubias *et al.*, 2008; Soubias *et al.*, 2015; Vogel *et al.*, 2003). For GlpG molecular dynamics (MD) simulations pointed to a membrane thinning capability up to 4 Å (Bondar, 2019).

Results given here will be presented in this form or in a slightly modified version in our joint manuscript that is just in preparation. I purified in total 266.3 mg of active GlpG-His6 from 50 L *E. coli* culture using our DDM-micelle based approach. The purification success was controlled by visualization of the individual purification steps via SDS-PAGE with subsequent Coomassie staining (**Figure 8A**) and spectrophotometric measurement of the protein amount. Enzymatic

activity of purified GlpG-His6 was controlled on different levels. First, by incubation of GlpG with the TAMRA-FP serine hydrolase probe in presence of increasing amounts of the serine protease inhibitor 3,4-dichloroisocoumarin (DCI), resulting in an expected decrease of the TAMRA-FP signal (**Figure 8B**). Second, in our DDM-micelle-based *in vitro* cleavage assay using purified GlpG-His6 and the chimeric model substrate MBP-Spitz, comparable to MBP-PGAM5 (**chapter 2.2**), but containing the *Drosophila* Spitz TM domain that was shown to be cleaved by GlpG before (Lemberg *et al.*, 2005; Urban *et al.*, 2002; Urban and Wolfe, 2005). I purified in total 33 mg MBP-Spitz out of 6 L culture (**Figure S2A**) and as expected, incubation of GlpG-His6 with MBP-Spitz revealed an N- and C-terminal cleavage fragment (**Figure 8C**). Additionally, GlpG was tested by our collaborators for purity using MALDI-TOF-MS. Spectra revealed very good signal to noise ratios that are indicative for an intact primary sequence of the GlpG-His6 protein construct (**Figure S2B**). Last, GlpG activity was tested using the fluorogenic kinetic substrate LacYTM2_fluo (Ticha *et al.*, 2017) and EDANS fluorescence was monitored. LacYTM2_fluo contains the fluorescence resonance energy transfer (FRET)-donor EDANS N-terminal of the cleavage site and the FRET-acceptor DABCYL C-terminal of the cleavage site. When DABCYL and EDANS are in close proximity, the EDANS signal will be quenched and no fluorescence can be detected. Continuous increase of the EDANS fluorescence over time, when GlpG-His6 is present, indicates substrate cleavage and thus protease activity of GlpG (**Figure S2C**).

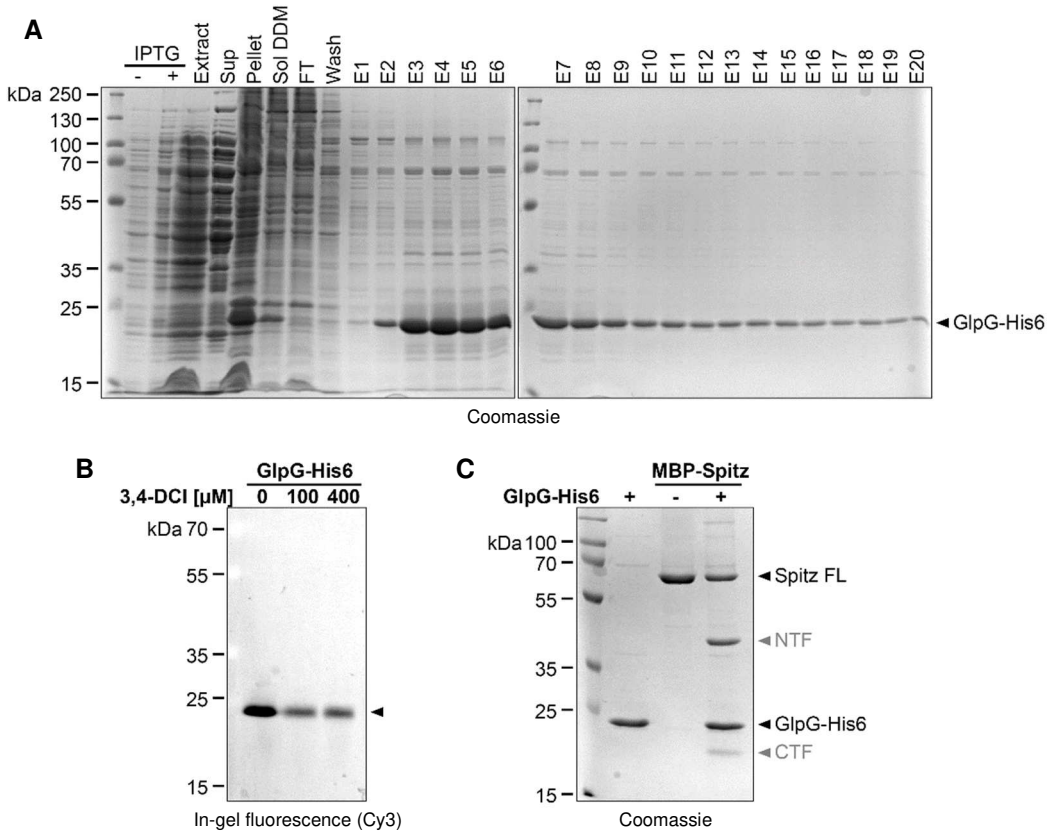

Figure 8 (Caption overleaf)

Figure 8 | Purified GlpG is active and cleaves the model substrate MBP-Spitz.
(A) Representative Coomassie-stained gel of each purification step after nickel-nitrilotriacetic acid (Ni-NTA) affinity purification. C-terminally His6-tagged GlpG was expressed in *E. coli* with 0.3 mM IPTG and solubilized from the membranes with 1.5% DDM. Aliquots were resolved by SDS-PAGE in gels containing 12% acrylamide. Sup: supernatant, Sol DDM: DDM-solubilized fraction, FT: flow through, E1-E20: elution fraction 1-20. **(B)** Activity of purified GlpG-His6 was measured by labelling with the TAMRA-FP serine hydrolase probe in presence of 3,4-dichloroisocoumarin (DCI) followed by SDS-PAGE and fluorescent imaging. **(C)** *in vitro* cleavage assay using DDM-solubilized GlpG-His6 and the chimeric substrate MBP-Spitz. Incubation for 2 h at 30°C resulted in an expected shift revealing an N- and C-terminal cleavage fragment, resolved by SDS-PAGE and visualized by Coomassie staining. Spitz FL: MBP-Spitz full length, NTF: N-terminal cleavage fragment, CTF: C-terminal cleavage fragment.

Further, purified GlpG was reconstituted with or without the model substrate LacYTM2 (Maegawa *et al.*, 2005) into multilamellar lipid stacks by our collaborators, using a protein to lipid ratio of 1:100 (Schmidt *et al.*, 2017) with the respective spin-labeled lipids to perform ^{2}H NMR and stationary ^{31}P NMR. Measurements of the average acyl chain length (L_C) was performed at pH 7, where GlpG is enzymatically active and at pH 4, where it can bind to its substrate but lacks enzymatic activity (Dickey *et al.*, 2013). GlpG reconstituted into the three saturated model membranes DLPC (dilauroylphosphocholine, C12:0, L_C = 9.6 Å), DMPC (dimyristoylphosphocoline, C14:0, L_C = 11.8 Å), and DPPC (dipalmitoylphosphocholine/cholesterol (2/1, mol/mol, C16:0, L_C = 19.9 Å), revealed the optimal chain length for GlpG to be in the range of the DMPC membrane system with a L_C = 11.8 Å, deduced from unchanged L_C values for the membrane system alone compared to DMPC with GlpG at pH 7 and pH 4 in combination with or without the substrate LacYTM2 (**Figure 9A**). Whereas the thinner DLPC membranes showed a small increase in acyl chain length at both pHs, the thick DPPC/cholesterol membranes showed a small decrease in presence of GlpG, which was slightly enhanced in combination with LacYTM2 (**Figure 9A, upper panels**). Since saturated lipids have limited relevance in biological membranes that mostly harbor 16 to 18 carbons, GlpG was also reconstituted into physiologically more relevant monounsaturated POPC (palmitoyloleoylphosphocholine). The POPC chain length (L_C = 12.2 Å) is comparable to the one of DMPC (L_C = 11.8 Å) and as speculated, no alterations were induced by the presence of GlpG (**Figure 9A, lower right**). The complex reconstitution protocol for GlpG needs tightly controlled parameters to ensure, amongst others, that no traces of DDM remained after reconstitution. ^{31}P NMR spectra were additionally used to exclude signals from undesired phospholipid species. Interestingly, two signals revealed traces of PE (phosphatidylethanolamine) and PG (phosphatidylglycerol) (Schiller *et al.*, 2007), which are predominant lipids in the *E. coli* membrane and were co-purified during my preparation. This was raising the question if there is an essential role of those lipids for GlpG activity like e.g., as important co-factors that, in a lipid mix, would have a more drastic impact on the membrane properties. Indeed, GlpG reconstituted into *E. coli*-like 3:1 (mol/mol) POPE/POPG mixture revealed a pronounced thinning effect of ≥1.0 Å for both POPE and POPG species (**Figure 9B-D**).

Lastly, we asked if GlpG mutants with highly reduced activity (Baker *et al.*, 2007) would also modify POPE/POPG membranes to the same extend. For this, I generated six different GlpG mutants and tested their expression efficiency (**Figure S2D-E**). GlpG W136A and R137A are mutated in the conserved WR motif in loop 1 (Urban *et al.*, 2001), which is known to stabilize the sideways hairpin-like membrane-submerged structure of the loop (Wang *et al.*, 2006). G257A and G261A are mutated in the GxxxG helix dimerization motif within TM segment 6 (Russ and Engelman, 2000), and the mutants Y138A and K191A were already suggested to have an influence on membrane thinning and interaction with DMPC (Bondar, 2019; Vinothkumar, 2011). As of yet, I could successfully purify two of them, namely R137A (in total 40.4 mg out of 12 L culture) and G261A (in total 48.8 mg out of 6 L culture) (**Figure S2F-G**), so that corresponding solid-state NMR could be performed. Whereas R137A shows a similar reduction of both POPE and POPG chain length, the G261A mutant reduced the length of POPE even by 1.5 Å and the length of POPG by 1.2 Å (**Figure 9E-F**). Since GlpG is highly active also in DMPC and POPC membranes and the inactive GlpG mutants also thin POPE/POPG bilayers, this data suggests that the membrane thinning of *E. coli*-like membranes does not result from the catalytic activity of GlpG but its special tertiary structure and the specific interactions with PE and PG headgroups. In summary, this collaboration could show that the activity of the rhomboid GlpG is related to membrane thickness irrespective of the lipid headgroups and the optimal lipid chain window was found to be 11.8 - 12.9 Å, highlighting the essential properties of an appropriate lipid environment on protein function.

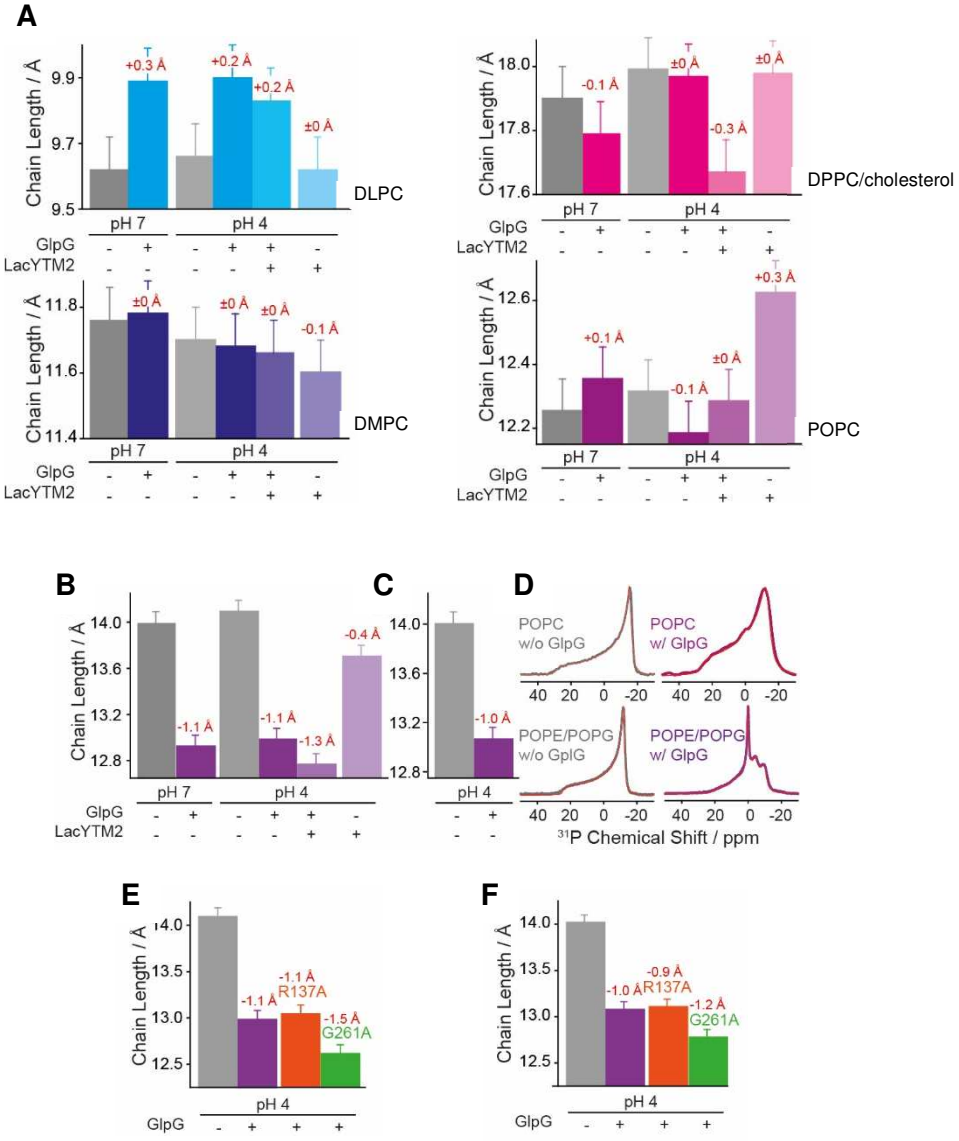

Figure 9 | Influence of GlpG on lipid chain lengths in different membranes, lipid analytics and GlpG activity.
Data recorded by Huster laboratory. **(A)** Average acyl chain length of DLPC, DMPC, DPPC/cholesterol, and POPC membranes in the absence (gray bars) and in the presence of GlpG and the GlpG substrate LacYTM2 (colored bars) at pH 7 and 4. Average acyl chain length of POPE **(B)**, POPG **(C)** in mixed membranes of POPE/POPG (3:1, mol/mol) in the absence (gray bars) and in the presence of GlpG and the GlpG substrate LacYTM2 (colored bars). **(D)** Stationary ^{31}P NMR spectra of POPC (top) and POPE/POPG membranes (bottom) in the absence and in the presence of GlpG. Impact of the GlpG mutations R137A and G261A on the chain length of POPE **(E)** and POPG **(F)**.

2.3 Requirements for PARL-catalyzed PGAM5 cleavage

Due to hydrophobicity of the lipid bilayer, single-spanning rhomboid substrates have to adopt a helical structure that prevents their hydrophilic peptide backbone from contact with the membrane core (Cymer *et al.*, 2015). Substrate helices therefore have to transiently unfold near the protease active site, prior to cleavage by proteases (Moin and Urban, 2012; Strisovsky *et al.*, 2009). Research on TM helix flexibility could show that for certain intramembrane protease substrates impaired TM helix flexibility negatively affected the rate of cleavage and that glycine residues allow maximal peptide backbone dynamics. Thereby flexibility of the TM helix contributes to selectivity (Lemberg and Martoglio, 2004). Since PARL was described to cleave its canonical substrates more to the center of their TM domains (Lemberg and Freeman, 2007b), it is important to study how substrate helix dynamics influence PARL-catalyzed cleavage. Recently, it could be shown in an *in vitro* assay, that PGAM5 is cleaved with the highest efficiency compared to PINK1 and Smac (Lysyk *et al.*, 2021), highlighting PGAM5's beneficial substrate properties as study object for PARL-catalyzed cleavage. So, I aim to solve the question how PARL-catalyzed cleavage of PGAM5 is controlled with regard to certain TM helix residues and the structural properties of the PGAM5 TM domain. The following chapters contain the key data of my PhD project. Results shown here, are presented in this form or in a slightly modified version in my first-author preprint (Siebert *et al.*, bioRxiv, doi: https://doi.org/10.1101/2021.11.19.469224v2).

2.3.1 Phenylalanine in P1 position enables efficient PGAM5 processing by PARL but is not strictly required

Our previous analysis of the PINK1 TM helix in cell-based assays showed that two conserved glycine residues are key for PARL-catalyzed cleavage (Meissner *et al.*, 2011). However, recent multiplex substrate profiling indicated a preference of PARL for phenylalanine in P1 (Lysyk *et al.*, 2021). Nevertheless, several substrates including PINK1 show other residues in P1 and an alignment of all so far known PARL substrates does not reveal an obvious consensus sequence (**Figure 10A**). Along those lines, serine-24 in the PGAM5 cleavage site region is not conserved across evolution (**Figure 10B**) and mutation to phenylalanine or tryptophan reduces PARL-catalyzed processing in tissue culture cells (Sekine *et al.*, 2012; Sugawara *et al.*, 2020). Hence, I asked whether analogue to PINK1, a less defined signature of amino acid residues keeps the PGAM5 TM helix in a metastable conformation, thereby enabling cleavage by PARL. So, I expressed FLAG-tagged human PGAM5 wt and different TM domain mutants in Hek293-T-REx cells expressing a doxycycline-inducible PARL-specific shRNA (Meissner *et al.*, 2011) and analyzed processing efficiency at different PARL levels by western blotting. Of note, this study bases on C-terminally tagged PGAM5-FLAG constructs, since tagging PGAM5 at its N-terminus, or deleting the MTS, results in an obligatory cytosolic and occasionally nucleic pool

(Bernkopf *et al.*, 2018). At the beginning of this project, microscopy to verify the correct intracellular localization of the PGAM5 constructs was planned by utilizing fluorescent protein tags like GFP or CFP. Tagging PGAM5 at the C-terminus with GFP or CFP resulted in mitochondrial localization (data not shown) but abolished PARL-catalyzed cleavage (**Figure S3**), most probably because the fluorescent PGAM5 constructs accumulated at the OMM or they were correctly imported into mitochondria but the PARL-cleavage site was shielded from being processed by the fluorescent-tag. To increase the turnover of the 32-kDa full length form of PGAM5 to the processed 28-kDa species, the oxidative phosphorylation uncoupler CCCP, which disrupts the IMM potential and thereby stimulates PGAM5 processing (Matsuda *et al.*, 2010; Narendra *et al.*, 2010), as well as ectopically expressed PARL were added (**Figure 10C**). Levels of cleaved PGAM5 could be significantly enhanced by overexpression of PARL wt but not its catalytic-inactive mutant PARL^{S277A}. Of note, in this control endogenous PARL is still present in both PARL wt and PARL^{S277A} overexpression conditions to provide a readout for the indirect effect of protein overexpression (**Figure 10D**). This is consistent with previous reports, in which knockdown of PARL prevented processing of PGAM5 wt in unstressed cells and significantly reduced generation of processed PGAM5 in presence of CCCP (Sekine *et al.*, 2012) (**Figure 10C**). As mentioned before, I examined wt and mutant PGAM5 TM domains in an *in vitro* cleavage assay based on detergent-solubilized recombinant human PARL (**Figure 7**) (Lysyk *et al.*, 2021), additional to human tissue culture. Since it is not known to what extend the amino acid sequence surrounding the scissile peptide bond in mammalian rhomboid substrates influences cleavage specificity, I started analyzing the F23A mutant of PGAM5, which removes the bulky amino acid at P1 that had been shown in a peptide-based multiplex *in vitro* assay to be favored (Lysyk *et al.*, 2021). In the Hek293-T-REx cell-based gain- and loss-of-function assay, I observed that PGAM5^{F23A} is slightly less processed than PGAM5 wt at endogenous PARL level but the difference did not reach significance (**Figure 10C**). In order to verify mitochondrial targeting, immunofluorescence microscopy analysis was performed for all PGAM5-FLAG constructs evaluating co-localization of the endogenous translocase of outer membrane subunit TOM20 (green) and ectopically expressed PGAM5-FLAG (magenta). Immunofluorescence analysis revealed that mitochondrial targeting of PGAM5^{F23A} was not affected by the mutation (**Figure 10E**). Surprisingly, PGAM5^{F23A} gets extensively cleaved when PARL is overexpressed and in the three conditions when the IMM potential is disrupted by CCCP (**Figure 10B**).

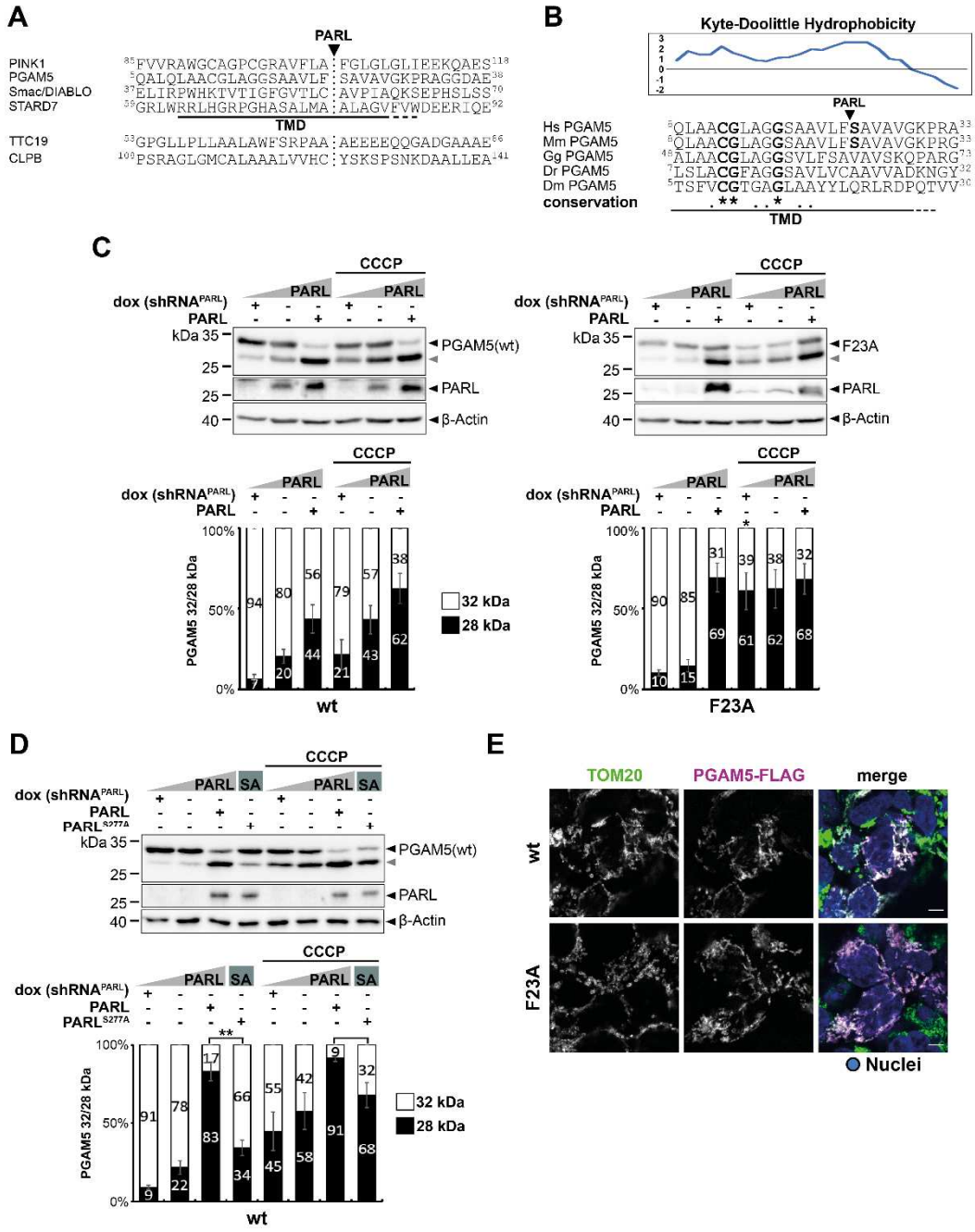

Figure 10 | Bulky residue in P1 position shows only modest influence on PGAM5 processing in cells.

(A) TM segments of so far identified PARL substrates (Deas *et al.*, 2011; Jin *et al.*, 2010; Meissner *et al.*, 2011; Saita *et al.*, 2017; Sekine *et al.*, 2012; Shi *et al.*, 2011). **(B)** Multi-sequence alignment reveals that C12, G13 and G17 are conserved between PGAM5 from *Home sapiens* (Hs), *Mus musculus* (Mm), *Gallus gallus* (Gg), *Danio rerio* (Dr) and *Drosophila melanogaster* (Dm). The predicted hydrophobic transmembrane domain (TMD) is underlined. The hydrophobicity plot of the relevant region in human PGAM5 is shown [using the scale of (Kyte and Doolittle, 1982), with a window size of 7] indicating the potential TMD boundaries. Arrowhead indicates the PARL cleavage site as determined by (Lysyk *et al.*, 2021). **(C)** PGAM5 processing was analyzed in a cell-based gain- and loss-of-function assay and western blotting. Whereas knockdown of endogenous PARL by doxycyclin (dox)-induced expression of a PARL-specific shRNA prevents PGAM5 cleavage, ectopic expression of PARL increased processing. PGAM5 processing was further stimulated by treating cells with the mitochondrial uncoupling agent CCCP. Grey triangle: 28 kDa cleavage fragment. Lower panel shows quantification of PGAM5 32/28 kDa distribution (n = 3, mean ± SEM). Significant changes versus wt PGAM5-FLAG are indicated with black stars (*p ≤ 0.05; unpaired two-tailed t-test). **(D)** Ectopic expression of PARL wt but not the catalytic-inactive PARL^{S277A}, leads to increased processing. Grey triangle: 28 kDa cleavage fragment. Lower panel shows quantification of PGAM5 32/28 kDa distribution (n = 3, means ± SEM). Significant changes comparing PARL and PARL^{S277A} overexpression without and with CCCP treatment are indicated with black stars (*p ≤ 0.05, **p ≤ 0.01; unpaired two-tailed t-test). **(E)** Immunofluorescence analysis examines mitochondrial targeting of ectopically expressed PGAM5-FLAG constructs (purple)

co-stained with endogenous TOM20 (green); cell nuclei are stained with Hoechst (blue). Scale bar, 5 µm; immunofluorescence analysis performed by Elena Heuten (Lemberg lab).

To determine if certain PGAM5 mutants become a better substrate for the stress-activated metalloprotease OMA1, I performed control experiments under *OMA1* knockdown using a specific siRNA. Indeed, when compared to the PGAM5 wt construct, processing of F23A by OMA1 was enhanced (**Figure 11A**). OMA1 is known to cleave PINK1 and PGAM5 under certain stress-conditions and is regulated by SLP2 as part of the SPY complex (Sekine *et al.*, 2012; Wai *et al.*, 2016). Consistent with the cell-based PARL assay, the F23A mutant was also cleaved by purified PARL as efficient as the MBP-PGAM5 wt fusion protein. The N-terminal cleavage fragment of 44 kDa appeared already after 30 min of incubation and increased in a comparable manner to the wt construct (**Figure 11B**). For the semi-quantitative progression, I tested 30°C to be the most appropriate temperature with the best ratio between the amount of cleavage fragments and velocity of the process (**Figure 11C**). Taking the *in vitro* results and the cell-based analysis into consideration, these results show that a phenylalanine in the P1 position may help to enable efficient PGAM5 processing when PARL activity is limiting but is not a strict requirement. Since the PGAM5 construct with a mutated P1 position (F23A) does not show decreased cleavage but interestingly, enhanced cleavage under PARL overexpression and the induction of mitochondrial stress by CCCP, I suggest that additional cleavage determinants exist that dominate substrate selection.

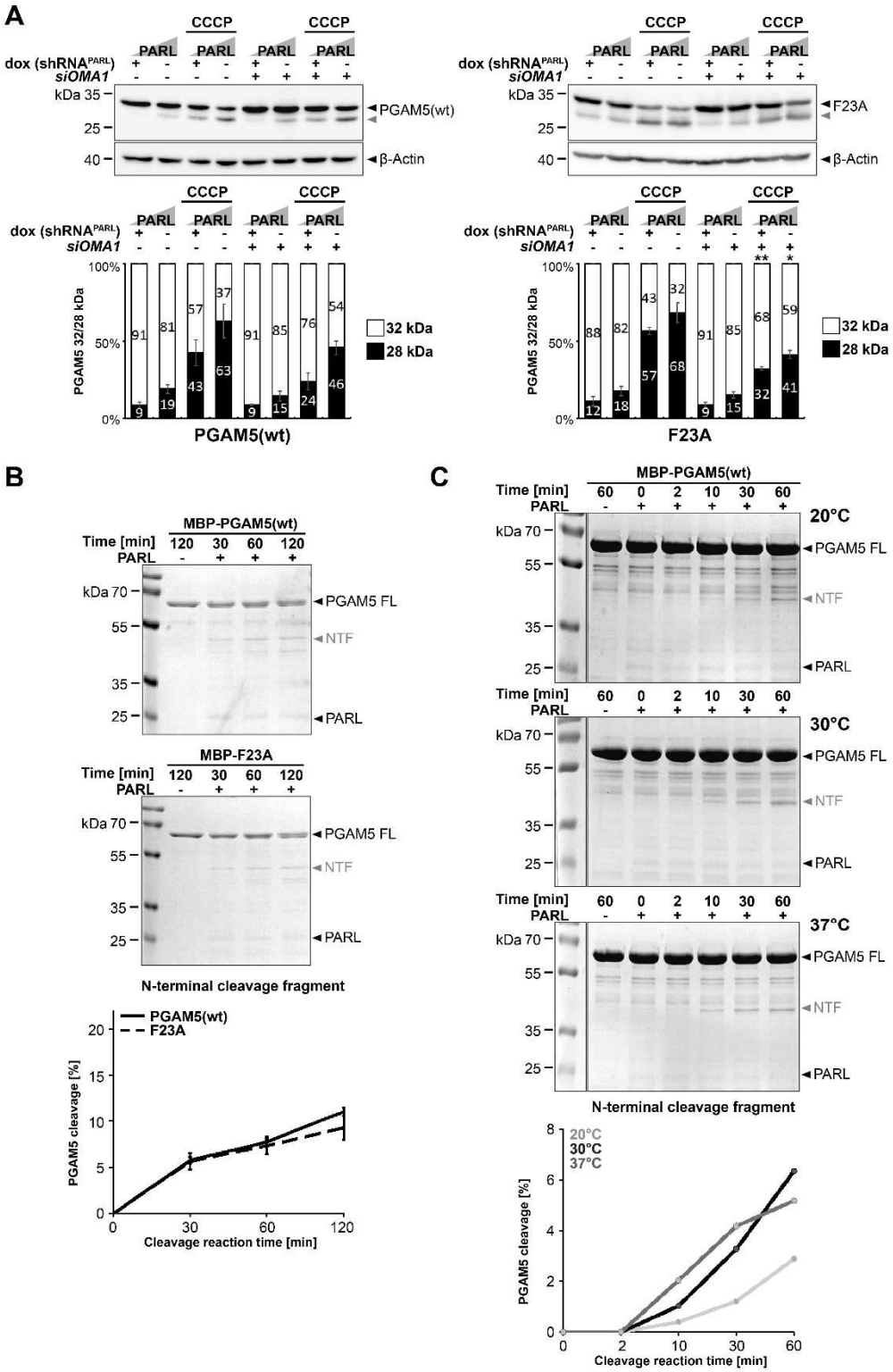

Figure 11 | Phenylalanine in P1 position enhances cleavage by OMA1 under stress.

(A) For *OMA1* knockdown, cells were transiently transfected with either a non-targeting siRNA or an *OMA1*-specific siRNA for 48 hours before transient transfection of the PGAM5-FLAG constructs. PGAM5 cleavage was stimulated by treating cells with CCCP. Grey triangle: 28 kDa cleavage fragment. Lower panels show quantification of PGAM5 32/28 kDa distribution (n = 3, means ± SEM). Significant changes versus cells transfected with non-targeting siRNA are indicated with black stars (*p ≤ 0.05, **p ≤ 0.01; unpaired two-tailed t-test). **(B)** Incubation of DDM-solubilized and purified recombinant PARL with MBP-PGAM5 (as outlined in Figure 8A) leads to generation of an N-terminal cleavage (NTF) fragment as resolved by SDS-PAGE and staining with Coomassie blue. Of note, the 20 kDa C-terminal cleavage fragment did not become visible under the experimental conditions and therefore the N-terminal cleavage fragment was used for quantification, lower panel (n = 3, means ± SEM). PARL-dependent alternative

cleavage fragments appeared as side-effects of the detergent background. FL: MBP-PGAM5 full length. **(C)** Incubation of recombinant PARL with MBP-PGAM5 at 20°C, 30°C and 37°C shows a temperature optimum of 30°C for the in vitro cleavage assay. Lower panel shows quantification of the N-terminal cleavage fragment at 20°C, 30°C and 37°C.

2.3.2 PARL-catalyzed cleavage of PGAM5 is influenced by multiple TM residues

In a next step, I aimed to determine the influence of two conserved glycine and certain hydrophilic amino acid residues in the TM domain of PGAM5 (**Figure 10B**) on PARL-catalyzed cleavage. Thus, I mutated these residues to the hydrophobic amino acid leucine or phenylalanine (**Figure 12A**). Although the exact influence on TM domain stability cannot be predicted, biophysical studies suggest a stabilizing effect of the helix conformation (Deber and Li, 1995), which may counteract recognition of the scissile peptide bond by the rhomboid active site, as described for γ-secretase (Langosch and Steiner, 2017).

Mutations in the PGAM5 TM domain were placed N- and C-terminal of the cleavage site. Both, single mutations C-terminal of the cleavage site, namely G29L and P31L, as well as a G29L/P31L double mutant did not significantly reduce PARL-catalyzed cleavage, with a tendency of G29L/P31L to a slightly reduced processing efficiency (**Figure 12B** and **Figure 13A**). Immunofluorescence analysis confirmed that mitochondrial targeting of these PGAM5 constructs was not affected by the mutations (**Figure 13B**), indicating that the modest reduction is caused by direct effects on PARL-catalyzed processing. However, while for PINK1 mutation of a single glycine C-terminal of the cleavage site was sufficient to block processing (Meissner *et al.*, 2011), for PGAM5$^{G29L/P31L}$ the observed reduction of PARL-catalyzed cleavage was minor only. This highlights once again the possibility for alternative cleavage determinants in the rest of the TM helix. Surprisingly, I could show that a C12L mutation in the N-terminal portion of the PGAM5 TM domain is cleaved more efficiently than PGAM5 wt, whereas G13L, G16L, G17L and the double mutant GG16/17LL show decreased cleavage when compared to PGAM5 wt (**Figure 12B** and **Figure 13A**). Additional to the restricted cleavage, immunofluorescence analysis revealed that for the G13L, G16L and GG16/17LL mutants a certain fraction is mistargeted to the ER (**Figure 13B**). Thus, unambiguous analysis in cells is not possible and dually localized mutants were excluded from further experiments in human tissue culture. As it has been observed before, a S24F mutation reduced PARL-catalyzed processing (Sekine *et al.*, 2012) and (**Figure 12B** and **Figure 13A**). Taken together these results show that multiple features of the PGAM5 TM helix influence PARL-catalyzed cleavage. Strikingly, mutating Ser-18 to leucine hampered processing, even at PARL overexpression and CCCP-stimulation (**Figure 12B** and **Figure 13A**) but targeting to mitochondria was not affected (**Figure 13B**). For a direct comparison of PGAM5 wt, S18L and S24F cleavage at endogenous PARL level without and with CCCP treatment, see (**Figure 13C**), confirming the pronounced effect on PARL-catalyzed cleavage.

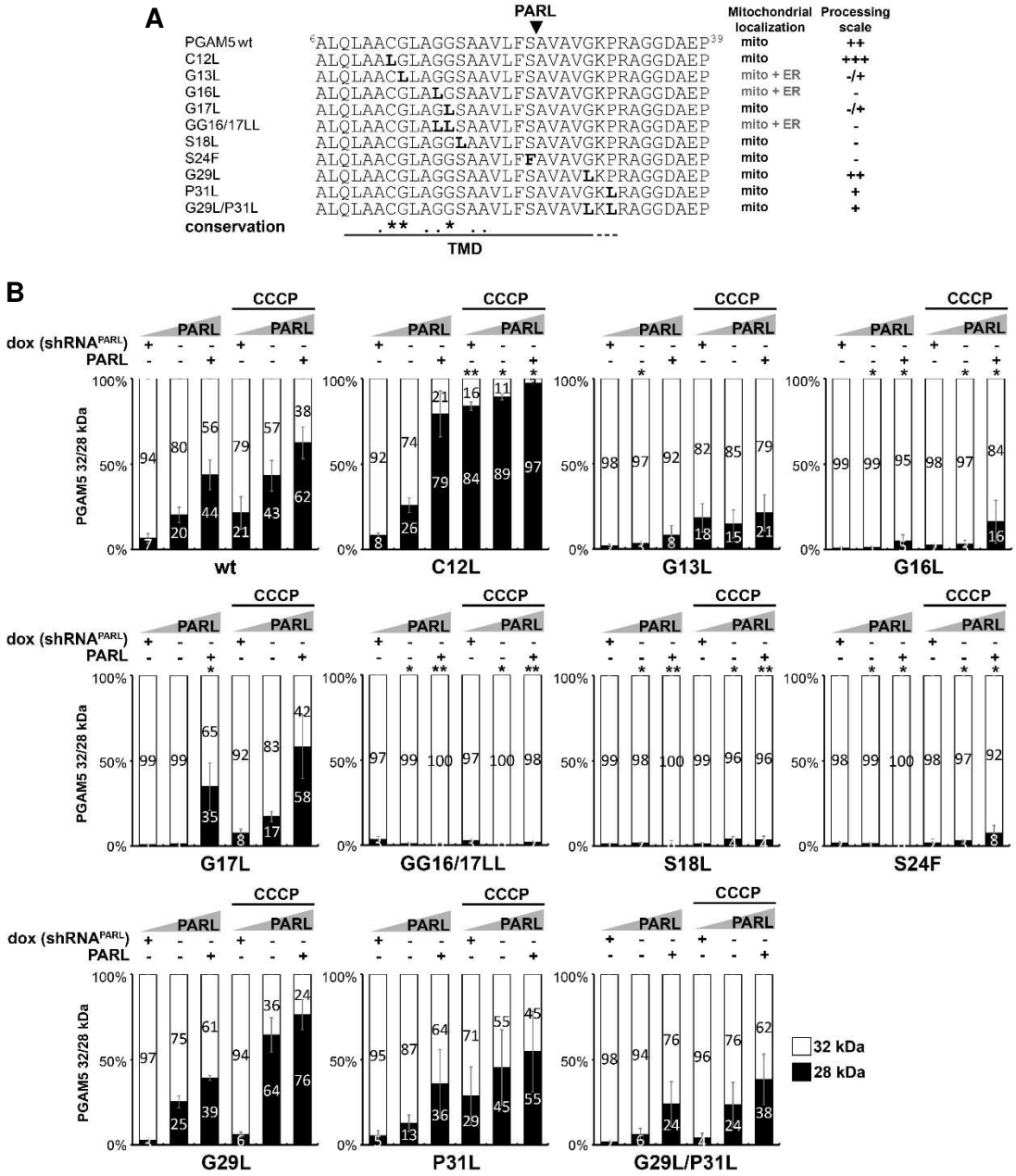

Figure 12 | PARL-catalyzed cleavage of PGAM5 depends on conserved TM residues (part I).

(A) Amino acid sequences of PGAM5 TM domain leucine mutants used in this study, including S24F previously analyzed by (Sekine *et al.*, 2012). **(B)** Quantification of PGAM5 32/28 kDa distribution upon PARL knockdown, endogenous levels or PARL over-expression without or with CCCP treatment (n = 3, means ± SEM). Significant changes versus wt PGAM5-FLAG are indicated with black stars (*p ≤ 0.05, **p ≤ 0.01; unpaired two-tailed t-test).

However, the chimeric *in vitro* substrate MBP-PGAM5 with the S18L mutation in the TM domain was cleaved by detergent-solubilized PARL with the same efficiency as the wt construct (**Figure 14A**). Thus, I speculate that the effect caused by the TM domain mutations is at least partially dependent on the context of the lipid bilayer and consequently any semi-quantitative detergent-based cleavage assays are only suitable to reveal influence of the primary amino acid sequence surrounding the cleavage site (Lysyk *et al.*, 2021). Likewise, the G17L and S24F mutants, which reduced PARL-catalyzed cleavage of PGAM5 in cells and G13L and GG16/17LL, which had a dual localization in cells, did not show striking changes in

cleavage tested in DDM-micelles when compared to the wt TM domain of PGAM5 (**Figure 14A**). Accordingly, my observations indicate that PARL-catalyzed cleavage of PGAM5 is determined by multiple TM features. The strongest inhibition is observed by S18L leading to inhibition of cleavage in the cell-based PARL gain- and loss-of-function assay. Interestingly, this position is not conserved outside vertebrates and for example in the fruit fly *Drosophila melanogaster* a leucine residue is found (**Figure 14B**), which would predict that cleavage by the PARL orthologue Rhomboid-7 is hampered. Strikingly, ectopic expression of FLAG-tagged *D. melanogaster* PGAM5 in human cells, which is correctly localizing to mitochondria (**Figure 14C**), resulted in significantly decreased cleavage by PARL when compared to human PGAM5 wt at endogenous PARL level (**Figure 12B and Figure 13A**). However, processing efficiency was higher when compared to the S18L mutant of human PGAM5 (**Figure 12B and Figure 13A**). This points to the inhibiting property of leucine in a TM domain within the lipid bilayer and might be balanced by compensatory factors such as additional charged TM residues in *D. melanogaster* PGAM5, namely Arg-22 and Arg-24 (**Figure 10B**). However, the length of the TM region in *D. melanogaster* is reduced by 4-5 residues like in *Aedes aegypti* (yellow fever mosquito) and *Caenorhabditis elegans* (nematode) and it remains elusive which amino acid residues are essential for cleavage by rhomboid proteases across the animal kingdom. Most PGAM5 TM residues are not shared between species and thus, seem not to underly a strong selective pressure. In addition to Gly-13 and Gly-17, Cys-12 is shared between various species (**Figure 10B**), albeit not to 100%. For instance, among vertebrates *Xenopus laevis* (African clawed frog) and *Bufo bufo* (common toad) do not contain a cysteine at this position and neither do *A. aegypti* or *C. elegans*. Interestingly, mutation of Cys-12 to leucine caused an unexpected increase of PARL-catalyzed cleavage of human PGAM5 in my cell-based assay and I got interested if this effect might alter substrate selection when further mutating Cys-12 to a serine **(Figure 15A**), which is more hydrophilic than leucine and closer to the chemical properties of cysteine. C12S was correctly targeted to mitochondria (**Figure 15B**) and strikingly, this mutation even further increased processing significantly, especially at endogenous PARL level (**Figure 15C-D**) when compared to C12L (**Figure 12B and Figure 13A**). To confirm that the enhanced cleavage was PARL-dependent and not induced by OMA1 activity, I again performed control experiments under *OMA1*-knockdown and could validate PARL-catalyzed processing (**Figure 15E-F**).

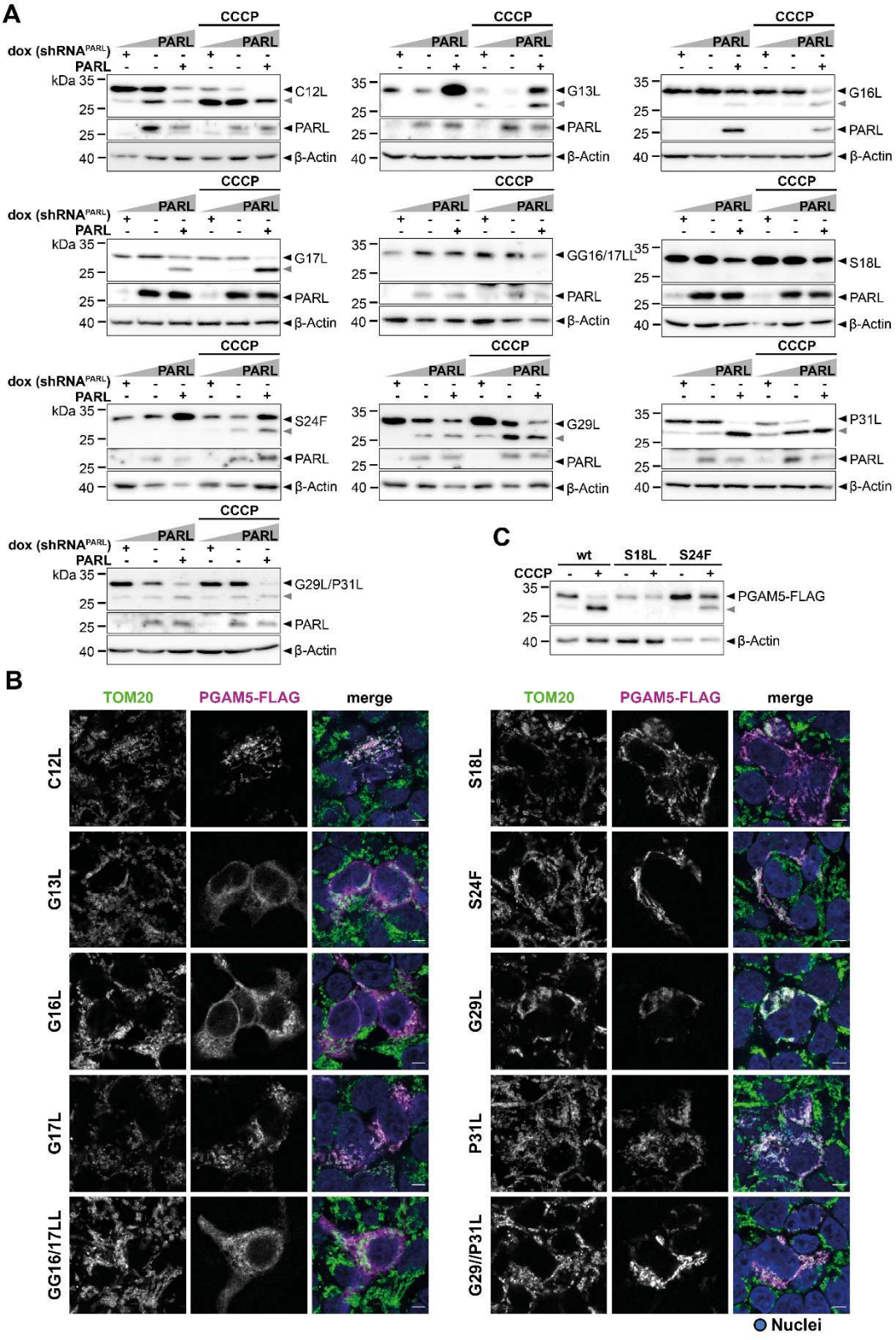

Figure 13 | PARL-catalyzed cleavage of PGAM5 depends on conserved TM residues (part II).

(A) Corresponding cell-based PARL gain- and loss-of-function assay examined in western blot analysis. Grey triangle: 28 kDa cleavage fragment. **(B)** Immunofluorescence analysis examines mitochondrial targeting of ectopically expressed mutant PGAM5-FLAG constructs (purple) co-stained with endogenous TOM20 (green); cell nuclei are stained with Hoechst (blue). Scale bar, 5 µm; immunofluorescence analysis performed by Elena Heuten (Lemberg lab). **(C)** Direct comparison of PGAM5 wt, S18L and S24F cleavage at endogenous PARL level without and with CCCP treatment. My samples reloaded by Elena Heuten (AG Lemberg).

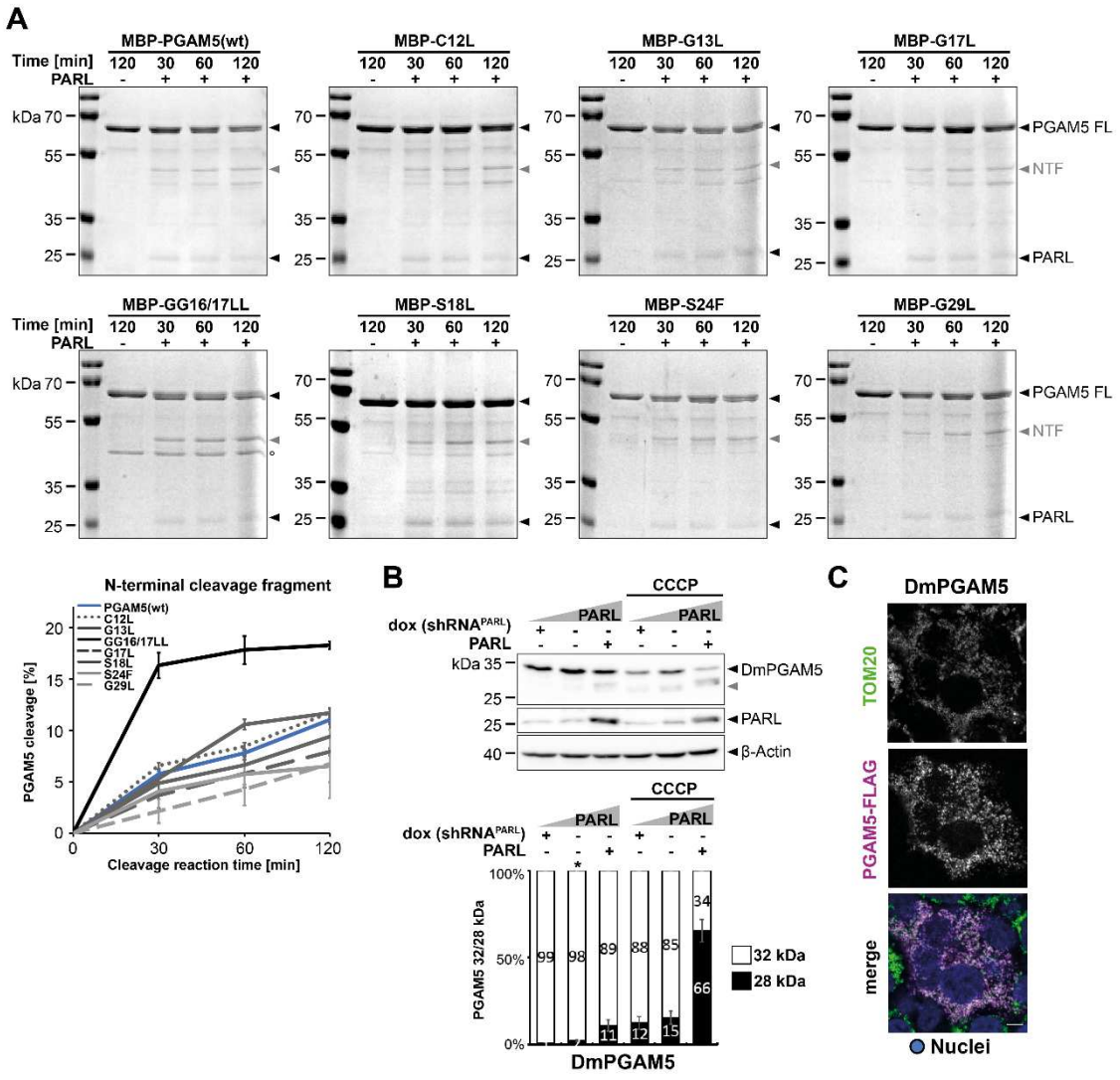

Figure 14 | PARL-catalyzed cleavage of PGAM5 depends on conserved TM residues (part III).

(A) Incubation of detergent-solubilized and purified recombinant PARL with MBP-PGAM5 leads to generation of an N-terminal cleavage fragment (NTF) as resolved by SDS-PAGE and staining with Coomassie blue. Circle: contaminating band from MBP-PGAM5 purification that is especially pronounced for GG16/17LL. PARL-dependent alternative cleavage fragments appeared as side-effects of the detergent background. FL: MBP-PGAM5 full length. Lower left panel shows quantification of N-terminal cleavage fragment as indicated (n = 3, means ± SEM). **(B)** Corresponding cell-based gain- and loss-of-function assay ectopically expressing *D. melanogaster* PGAM5-FLAG with quantification of PGAM5 32/28 kDa distribution in the lower panel (n = 3, means ± SEM). Grey triangle: 28 kDa cleavage fragment. Significant changes versus human wt PGAM5-FLAG are indicated with black stars (*p ≤ 0.05; unpaired two-tailed t-test). **(C)** Immunofluorescence analysis examines mitochondrial targeting of ectopically expressed mutant PGAM5-FLAG constructs (purple) co-stained with endogenous TOM20 (green); cell nuclei are stained with Hoechst (blue). Scale bar, 5 µm; immunofluorescence analysis performed by Elena Heuten (Lemberg lab).

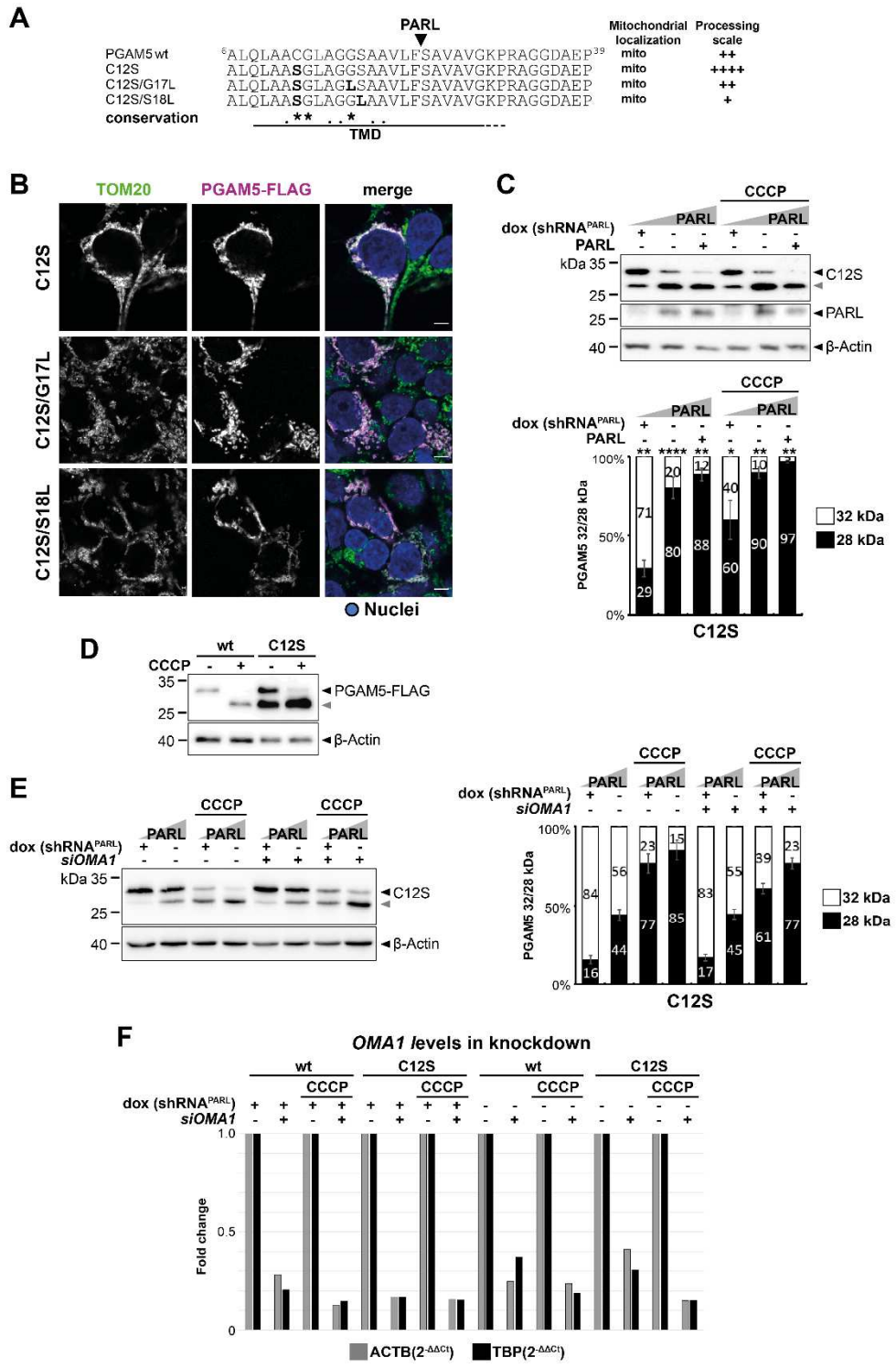

Figure 15 | N-terminal substrate feature in PGAM5 is important for PARL-catalyzed cleavage (part I).

(A) Amino acid sequences of PGAM5 C12S TM domain mutants used in this study. **(B)** Immunofluorescence analysis examines mitochondrial targeting of ectopically expressed mutant PGAM5-FLAG constructs (purple) co-stained with endogenous TOM20 (green); cell nuclei are stained with Hoechst (blue). Scale bar, 5 µm; immunofluorescence analysis performed by Elena Heuten (Lemberg lab). **(C)** Mutation of C12 to serine further increases processing efficiency in cell-based PARL gain- and loss-of function assay. Grey triangle: 28 kDa cleavage fragment. Lower panel shows the quantification of PGAM5 32/28 kDa distribution (n = 3, means ± SEM). Significant changes versus wt PGAM5-FLAG are indicated with black stars (*p ≤ 0.05, **p ≤ 0.01, ***p ≤ 0.001, ****p ≤ 0.0001; unpaired two-tailed t-test). **(D)** Direct comparison of PGAM5 wt, and C12S cleavage at endogenous PARL level without and with CCCP treatment. My samples reloaded by Elena Heuten (AG Lemberg). **(E)** For *OMA1* knockdown, cells were transiently transfected with either a non-targeting siRNA or an *OMA1*-specific siRNA for 48 hours before transient transfection of the PGAM5-FLAG construct. PGAM5 cleavage was stimulated by treating cells with CCCP. Grey triangle: 28 kDa cleavage

fragment. Right panel shows quantification of PGAM5 32/28 kDa distribution (n = 3, means ± SEM). No significant changes versus cells transfected with non-targeting siRNA were observed (unpaired two-tailed t-test). **(F)** *OMA1* levels are knocked down by transient transfection of *OMA1*-specific siRNA. Normalization of relative gene expression by comparison to the reference genes β-Actin (ACTB) and TATA-box binding protein (TBP).

Interestingly, I could observe that substrate features act independently from each other and show additive effects when combining C12S with the processing-inhibiting G17L or S18L mutation. The double mutants C12S/G17L and C12S/S18L showed significantly decreased cleavage efficiency when compared to C12S (**Figure 16A**).

Disulfide (S-S) bond formation is crucial for the biogenesis and structure of many mitochondrial proteins that are localized in the IMS and the IMM, like seen for Tim22 (Wrobel *et al.*, 2016). Since PGAM5 forms oligomers, I asked whether PGAM5 might also form disulfide bridges with Cys-12 and if mutating this position to leucine or serine might alter disulfide bridging and therefore enhance PARL catalyzed-cleavage. To this end, I overexpressed PGAM5 wt and C12S in my cell-based PARL gain- and loss-of-function assay and performed gel electrophoresis under reducing (dithiothreitol, DTT) and non-reducing conditions. Both, PGAM5 wt and the mutant C12S looked comparable and did not show any higher molecular weight assemblies in the non-reducing conditions (**Figure 16B**). This result suggests, that PGAM5 does not form any S-S bonds and the influence of Cys-12 may affect the recognition by PARL by a different mechanism. Consistent with this hypothesis, the only TM domain mutant that showed a slightly increased cleavage in the *in vitro* PARL assay when compared to wt MBP-PGAM5 was the C12S mutant (**Figure 16C**). Judging mutagenesis of hydrophilic TM residues in the cell-based and in the *in vitro* assay, I could reveal that PARL-catalyzed cleavage of PGAM5 is influenced both by TM residues N-terminal and C-terminal of the scissile peptide bond. Here, especially Cys-12 plays a prominent role assuming a relevant ‘long-range’ influence, in contrast to *E. coli* GlpG, which recognizes a specific sequence closely surrounding the substrate cleavage site (Strisovsky *et al.*, 2009).

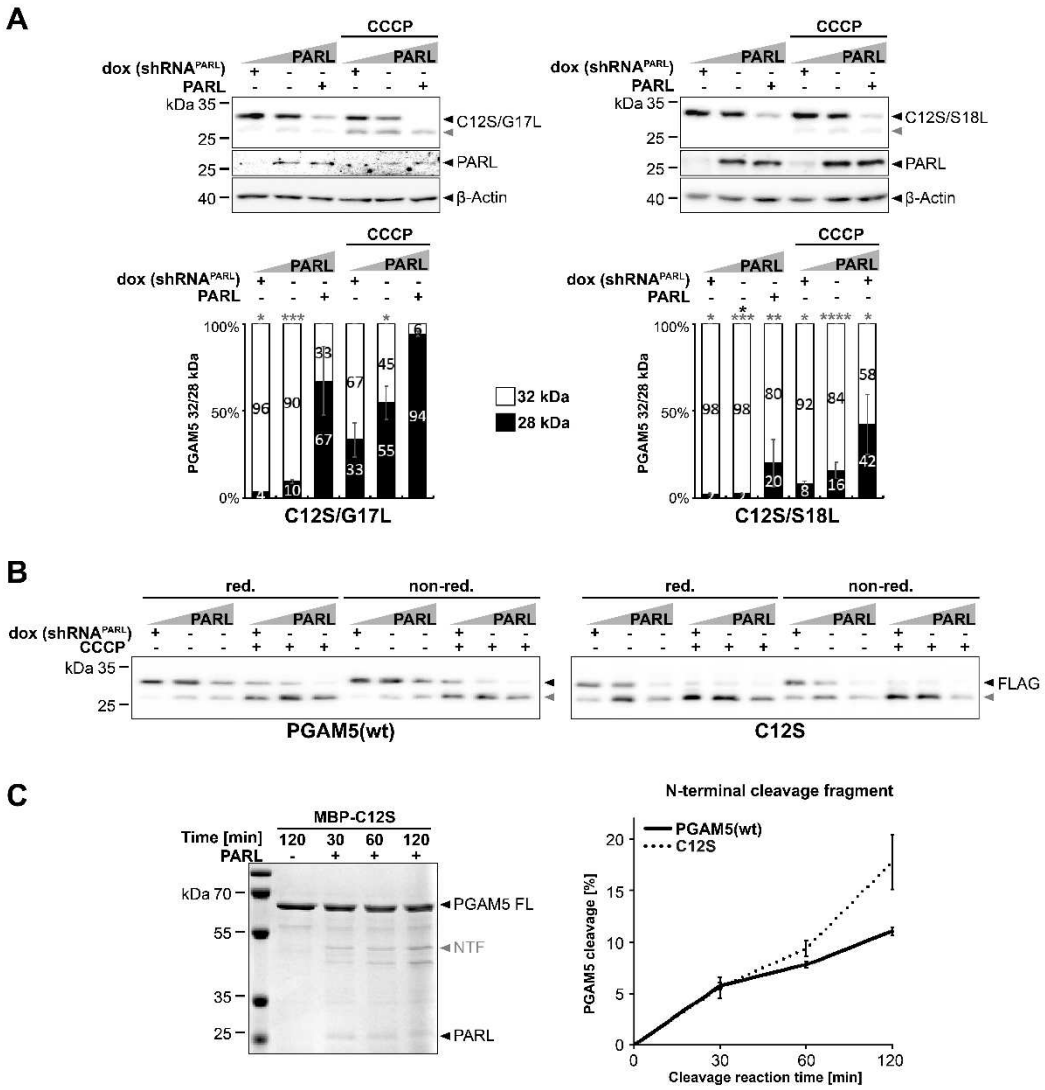

Figure 16 | N-terminal substrate feature in PGAM5 is important for PARL-catalyzed cleavage (part II).
(A) C12 acts independent of G17 and S18. Double mutants with the C12S mutation show decreased cleavage efficiency. Lower panel shows quantification of PGAM5 32/28 kDa distribution upon PARL knockdown, endogenous levels or PARL over-expression without or with CCCP treatment (n = 3, means ± SEM). Grey triangle: 28 kDa cleavage fragment. Significant changes versus wt PGAM5-FLAG are indicated with black stars, significant changes versus PGAM5^{C12S}-FLAG are indicated with grey stars (*p ≤ 0.05, **p ≤ 0.01, ***p ≤ 0.001, ****p ≤ 0.0001; unpaired two-tailed t-test). **(B)** Putative disulfide (S-S) bond formation of PGAM5 wt and C12S samples was tested in reducing (red.) or non-reducing (non-red.) sample buffer conditions. **(C)** Incubation of recombinant PARL with MBP-PGAM5^{C12S} leads to more efficient generation of the N-terminal cleavage fragment (NTF) when compared with the wt construct (n = 3, means ± SEM; see **Figure 14A** for comparison). PARL-dependent alternative cleavage fragments appeared as side-effects of the detergent background. FL: MBP-PGAM5 full length.

2.3.3 Structural properties of the PGAM5 TM domain

As part of our DFG-funded research consortium (Research Unit 2290 “Understanding Intramembrane Proteolysis”), I set out to further analyze whether the different cleavage efficiencies observed for the PGAM5 mutants are caused by structural or dynamic effects, in collaboration with Dr. Mara Silber and Dr. Claudia Muhle-Goll from KIT Karlsruhe (Germany). All data was recorded by Mara Silber and jointly interpreted in our team. In brief, the structure

of PGAM5 wt and the C12L, C12S and G17L mutant TM domains (residue 2 to 35) were analyzed by CD spectroscopy and liquid-state NMR using aqueous trifluoroethanol (TFE), a model that is believed to mimic biophysical properties of a water-filled intramembrane protease active site cavity (Pester *et al.*, 2013b; Yücel *et al.*, 2019). Circular dichroism (CD) spectroscopy revealed that all TM domains showed a moderate content of α-helical structure in the range of 33-38% in this solvent, indicating that it is a suitable model situation to study unfolding of the PARL substrate TM helix (**Figure 17A**). Mutation of the central glycine G17 to a hydrophobic leucine slightly increased helicity when compared to wt, whereas mutation of C12 to either Ser or Leu did not result in explicit secondary structure changes. NMR secondary chemical shifts are dependent on the protein secondary structure and are used as sensitive reporters. For instance, Cα atoms in α-helices tend to have positive secondary chemical shifts, whereas Hα atoms in α-helices tend to have negative secondary chemical shifts. The final values were calculated as difference between measured Hα or Cα chemical shifts and the respective chemical shifts in random coil peptides (Schwarzinger *et al.*, 2001; Wishart and Sykes, 1994; Wishart *et al.*, 1992). In the model situation of 80% TFE/water the PGAM5 TM domain is divided into two distinct α-helical parts, amino acid residues R4-C12, N-terminally three residues longer than the predicted TM part and S18-V28 with negative Hα and positive Cα secondary chemical shifts (**Figure 17B**). The central part, G13-G17, had no preference for a defined secondary structure, leading to the generation of a hinge-like loop. Thus, our analysis under the TFE/water model situation reveals the PGAM5 TM domain to contain a kink in the region of the PARL active site splitting it into two helices, with the longer C-terminal end harboring the scissile peptide bond, instead of being a straight single helix.

Next, in order to analyze stability of this unusual TM domain our collaborators studied which amide protons in the PGAM5 TM domain were protected against deuterium exchange performing hydrogen-deuterium (H/D) exchange analysis to record short consecutive $^{1}H^{1}H$-TOCSY experiments and to follow the intensities of the HN-Hα cross-peaks. H/D exchange gives information about the solvent accessibility in various parts of a molecule, and thus the tertiary structure of a protein (Englander *et al.*, 1997; Wales and Engen, 2006). Here, exchanges monitored probed for stable hydrogen bonds. Although the exchange of several residues could not be determined due to spectral overlap, two regions in the PGAM5 TM domain could be marked that showed reduced deuterium exchange (**Figure 17C**). Amino acids Q8-C12 in the N-terminal helix and A19-V28 in the C-terminal helix revealed slowed down exchange that was interrupted by the region G13-G17 showing immediate exchange without involvement in stable hydrogen bonds. This is in line with the analysis of secondary chemical shifts pointing towards this region without a defined secondary structure and may serve as a hinge. The mutants C12S and C12L only marginally affected secondary structure, because chemical shift changes were small and dispersed over the entire TM domain (**Figure 17B**). Whereas, mutation of C12 to leucine showed disturbances within the N-terminal helix that

cannot be easily interpreted in terms of secondary structure changes, mutation to serine seems to slightly destabilized the entire helical TM domain. G17L seemed to induce α-helical structure in the central part G13-L17 with strong alterations in both Hα and Cα secondary chemical shifts. Since changes in secondary structure caused by the mutants were in total unobtrusive, our collaborators calculated their 3D structures. For this, the 20 best structures each were condensed to a bundle superposed onto the C-terminal helix (**Figure 17D**). No further major structural changes could be detected for either the N- or C-terminal helix between the four PGAM5 TM peptides and the extent of their helicity did not vary. With regard to the observed different cleavage efficiencies in my cell-based PARL gain- and loss-of-function assay this was intriguing, and taking the TFE/water model into account we considered simple local structure changes as possible explanations. Since the orientation of the N-terminal helix with respect to the C-terminal one was not well defined for all four bundles as judged by superposition, we wondered whether the orientation was fully arbitrary or whether certain conformations were preferred. Looking at the bundle from the top, when the C-terminal helix was aligned along the -z axis, the wt fanned out into two possible conformation ranges where two angle ranges of ~60° each were devoid of structures (**Figure 17E**). Interestingly, the mutants C12S and C12L, which are cleaved stronger than PGAM5 wt in human cells, showed also restricted conformational variability. Aside from two structures in C12L, the angle region devoid of structures for those two mutants was much more pronounced. The area of possible conformations of C12S overlapped with one of the conformational regions in the wt whereas the bundle in C12L was turned by roughly 90°. On the contrary, G17L that is cleaved less than PGAM5 wt in cells stabilizes the beginning of the C-terminal helix elongating it on one hand and restricting the possible mutual orientations of the two helical parts. Most likely due to this elongation, G17L had a distribution of possible orientations that was distinct from the other three by roughly 120°. Taken together, these results in the TFE/water model indicate that the N-terminal feature in the PGAM5 TM domain affects TM substrate dynamics and thereby may enable or hamper bending into the PARL active site. However, we note that these conclusions remain speculative, since the measurements were done in the absence of structural data derived from the PGAM5 TM domain and PARL in a physiological lipid bilayer.

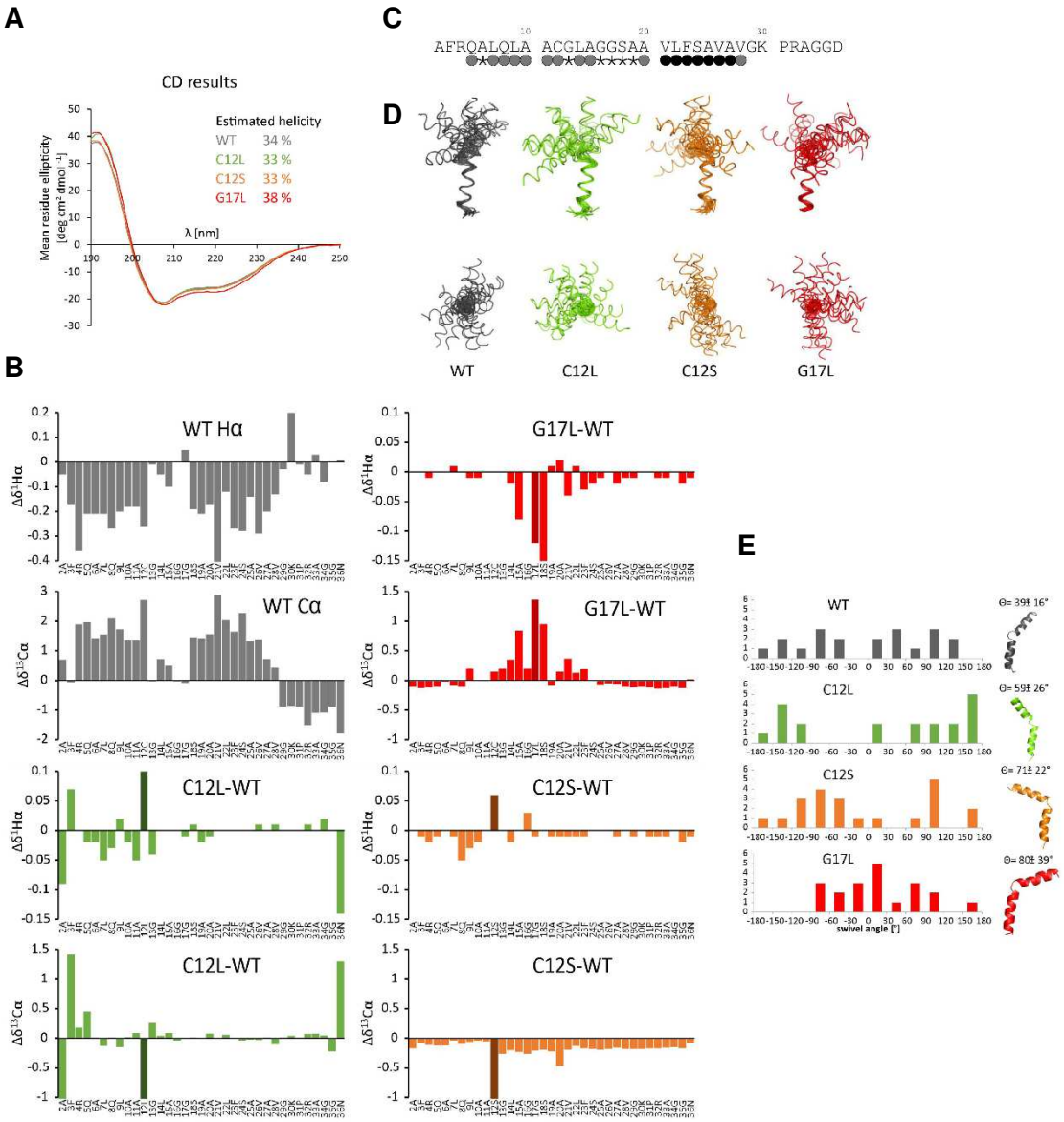

Figure 17 | Properties of the PGAM5 TM domain.

Data recorded by Dr. Mara Silber (KIT Karlsruhe). **(A)** CD results of wt and three mutants; values are scaled to wt. **(B)** Random coil chemical shifts were subtracted from experimental values of Hα and Cα respectively. Negative secondary chemical shifts of Hα and positive secondary shifts of Cα indicate α-helical structure. For C12L, C12S and G17L deviations from wt secondary chemical shifts are shown. Negative values for Hα and positive values for Cα suggest a more helical structure compared to wt. **(C)** Hydrogen-deuterium exchange of wt TM domain shows stable H-bonds directly before the cleavage site and at the N-terminus between Q8 an C12. Hydrogen bonds at the helix termini and between G13 and G17 are significantly weakened. Black dots indicate fast exchange, grey dots slow exchange. Some exchange rates could not be determined due to peak overlap, these residues are marked by an asterisk. **(D)** All structures aligned from residue 20 to 25, L22Hα defined as x-axis. Black: wt, green: C12L, orange: C12S, red: G17L. Upper panel front view, lower panel top view. **(E)** The swivel angle is defined by the rotation of the N-terminal helix relative to the Hα atom of L22 as reference in the C-terminal helix. Swivel angles of the 20 best structures were grouped in 30° segments, frequency distributions are given above. Right: The bend angle is defined as the angle between the axis through the N-terminal and the C-terminal helix. Bend angles and representative structures are given above.

2.3.4 The substrate's juxtamembrane region influences cleavage efficiency

It was recently shown, that a negatively charged motif C-terminally to the TM anchor in the so called 'juxtamembrane' (JM) region of the PARL substrates PINK1 and STARD7, serves as sorting signal for mitochondrial import and release and facilitates PARL-catalyzed cleavage (Saita *et al.*, 2018; Sekine *et al.*, 2019). A PINK1 mutant lacking this negative motif, namely PINK1^{3EA}, fails to accumulate on depolarized mitochondria and is degraded by the stress-activated metalloprotease OMA1 instead (Sekine *et al.*, 2019). OMA1 cleaves PGAM5 under mitochondrial stress conditions and is regulated by SLP2 as part of the SPY complex (Sekine *et al.*, 2012; Wai *et al.*, 2016). Since OMA1 and PARL share the substrates PINK1 and PGAM5, it is important to understand the underlying regulation and to reveal additional cleavage determinants. Thus, I was wondering if in addition to the PGAM5 TM domain, PARL-catalyzed cleavage may be also influenced by its C-terminal portion facing the IMS.

In contrast to PINK1 and STARD7, PGAM5 is lacking such a pronounced cluster of negatively charged amino acids at the same position (**Figure 18A**) and I therefore asked whether introducing negative charges to the PGAM5 JM region might increase PARL-catalyzed processing as well. Mutating two glycine residues C-terminal of the TM helix to glutamic acid did not change processing in unstressed cells, but under depolarizing stress using CCCP, PGAM5$^{GG34/35EE}$ was significantly more cleaved when compared to PGAM5 wt (**Figure 18B-C**), while correctly localizing to mitochondria as judged by immunofluorescence (**Figure 18D**). Control experiments under *OMA1* knockdown could confirm PARL-catalyzed cleavage and no significant role of OMA1 activity (**Figure 18E**). In order to compare and illustrate the differences between the JM region of PINK1 and PGAM5 on PARL-catalyzed cleavage, I generated a PINK1 mutant lacking two of the three negative charges in the C-terminal TM domain motif and analyzed it in parallel to PGAM5 in my cell-based gain- and loss-of-function assay, before (Sekine *et al.*, 2019) were publishing their data. As observed for PINK1^{3EA}, I could show that PINK1$^{EE112/113AV}$ also showed significantly increased processing under PARL overexpression and the CCCP induction conditions (**Figure S4A**), while correctly localizing to mitochondria (**Figure S4B**). Additional bands around 62 kDa and 50 kDa could be detected, which is likely due to OMA1 processing, as described before (Sekine *et al.*, 2019). To gain a better understanding of subcellular localization of the uncleaved and cleaved PINK1 and PGAM5 charge mutants in comparison to its wt counterparts, I performed subcellular fractionation experiments. Fractionation revealed that the release into the cytosol of PGAM5$^{GG34/35EE}$ was enhanced with the highest increase of 2.3-fold at endogenous PARL level when compared to PGAM5 wt (**Figure S5A-B**). The cytosolic portion of wt and mutant PGAM5-FLAG showed more or less equal distribution of uncleaved and cleaved protein (**Figure S5C**). In subcellular fractionation of PINK1-FLAG expressing cells, the PINK1$^{EE112/113AV}$ cleavage fragments in the cytosolic fractions seem to have a smaller molecular weight and run slightly lower, which might result from degradational processes involving the proteasome (**Figure S6A**). Comparable to

the PGAM5-like character that was described for the import arrest mutant PINK1^{3EA} in (Sekine *et al.*, 2019), PINK1$^{EE112/113AV}$ showed enhanced release to the cytosol when compared to PINK1 wt with the highest increase of 3.3-fold at the condition of PARL overexpression and simultaneous CCCP-treatment (**Figure S6B**). In comparison to PINK1 wt, the released PINK1-FLAG portion showed on average about 50% more cleaved protein in PINK1$^{EE112/113AV}$ (**Figure S6C**). From these observations I conclude that substrates like PINK1 or STARD7 can be seen as 'fast' processing substrates, including a fast release into the cytosol, whereas PGAM5 is lacking the advantageous negative charges in the JM region and may be processed in unstressed mitochondria by PARL with a slower kinetic.

Interestingly, also the N-terminal TM domain region in front of the PARL cleavage site differs between PINK1, STARD7 and PGAM5 with regard to charged amino acid residues. Whereas PINK1 and STARD7 contain positively charged residues, PGAM5 displays a neutral TM domain region, (ignoring weak positively charged cysteine residues in all substrates), (**Figure 19A**). I was wondering, if introducing positive charges into the N-terminal TM domain part of PGAM5 might also increase cleavage efficiency. Therefore, I exchanged Cys-12 and Gly-13, which are shared between various species (**Figure 19B**) to the positively charged amino acids arginine and histidine. As observed for the single mutants C12L and C12S, also PGAM5$^{CG12/13RH}$ was cleaved significantly stronger than PGAM5 wt (**Figure 19B**), while still correctly localizing to mitochondria (**Figure 19C**), in contrast to single mutant G13L that had a dual localization (**Figure 13B**). When directly comparing to C12S, CG12/13RH cleavage efficiency did not significantly increase further, except from the PARL knockdown condition. Although, a role of OMA1 activity cannot be excluded for this mutant, these results highlight once again the important role of Cys-12 and Gly-13 in the N-terminal region of the PGAM5 TM domain for PARL-catalyzed cleavage.

An additional idea to study the determinants for PARL-catalyzed cleavage was to create JM domain swap mutants between the 'fast' processing substrate PINK1 and the 'slow' processing substrate PGAM5. For this, I aimed to generate two chimeric constructs after the following principle (**Figure S7**): The first construct PINK1-PGAM5$^{32-71}$-FLAG contained the N-terminal part of PINK1 including its TM domain (residues 1-111), with the JM region of PGAM5 (residues 32-71) in the middle part, followed by the C-terminal part of PINK1 including the remaining kinase domain (residues 152-581). The second construct PGAM5-PINK1$^{112-151}$-FLAG contained the N-terminal part of PGAM5 including its TM domain (residues 1-31), with the JM region of PINK1 (residues 112-151) in the middle part, followed by the C-terminal part of PGAM5 including the phosphatase domain (residues 72-289). Whereas cloning of the first construct failed, I could successfully generate the second construct and transfected it in Hek293T and Hek293-T-REx cells. Repeatedly, in neither of both cell lines PGAM5-PINK1$^{112-151}$ was expressing (data not shown), so that we decided to neglect the domain swap approach at this point.

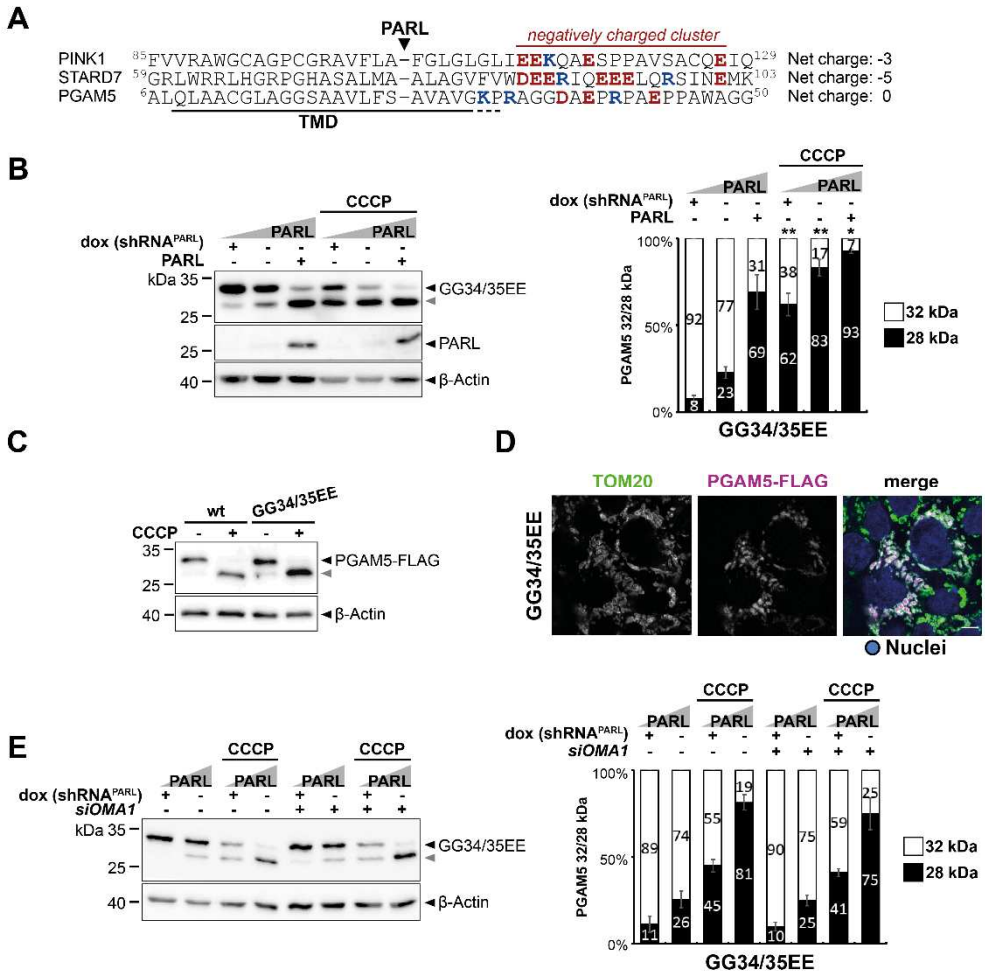

Figure 18 | Negative charges in the substrate's juxtamembrane region influence cleavage efficiency.

(A) Negatively charged cluster in juxtamembrane (JM) region of PINK1 and STARD7 but not PGAM5. Net charge in JM region of negatively charged amino acids (red) and positively charged amino acids (blue). **(B)** Corresponding analysis of PGAM5 cleavage in the cell-based PARL gain- and loss-of-function assay. Grey triangle: 28 kDa cleavage fragment. Panel on the right shows quantification of PGAM5 32/28 kDa distribution upon PARL knockdown, endogenous levels or PARL over-expression without or with CCCP treatment (n = 3, means ± SEM). Significant changes versus wt PGAM5-FLAG are indicated with black stars (*p ≤ 0.05, **p ≤ 0.01; unpaired two-tailed t-test). **(C)** Direct comparison of PGAM5 wt, and GG34/35EE cleavage at endogenous PARL level without and with CCCP treatment. My samples reloaded by Elena Heuten (AG Lemberg). **(D)** Immunofluorescence analysis examines mitochondrial targeting of ectopically expressed mutant PGAM5-FLAG constructs (purple) co-stained with endogenous TOM20 (green); cell nuclei are stained with Hoechst (blue). Scale bar, 5 µm; immunofluorescence analysis performed by Elena Heuten (Lemberg lab). **(E)** For *OMA1* knockdown, cells were transiently transfected with either a non-targeting siRNA or an *OMA1*-specific siRNA for 48 hours before transient transfection of the PGAM5-FLAG construct. PGAM5 cleavage was stimulated by treating cells with CCCP. Grey triangle: 28 kDa cleavage fragment. Right panel shows quantification of PGAM5 32/28 kDa distribution (n = 3, means ± SEM). No significant changes versus cells transfected with non-targeting siRNA were observed (unpaired two-tailed t-test).

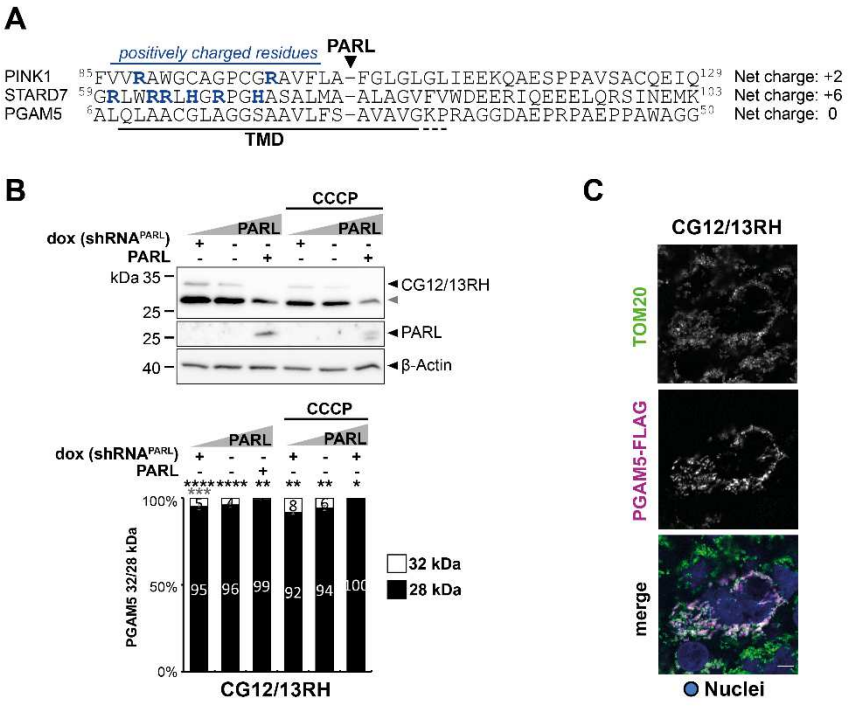

Figure 19 | PGAM5 lacks positive charges in the N-terminal TM domain region.

(A) Positively charged N-terminal TM doamin region of PINK1 and STARD7 but not PGAM5. Net charge in N-terminal region; positively charged amino acids (blue). **(B)** Corresponding analysis of PGAM5 cleavage in the cell-based PARL gain- and loss-of-function assay. Grey triangle: 28 kDa cleavage fragment. Lower panel shows quantification of PGAM5 32/28 kDa distribution upon PARL knockdown, endogenous levels or PARL over-expression without or with CCCP treatment (n = 3, means ± SEM). Significant changes versus wt PGAM5-FLAG are indicated with black stars, significant changes versus PGAM5^{C12S}-FLAG are indicated with grey stars (*p ≤ 0.05, **p ≤ 0.01, ***p ≤ 0.001, ****p ≤ 0.0001; unpaired two-tailed t-test), see **Figure 15** for comparison. **(C)** Immunofluorescence analysis examines mitochondrial targeting of ectopically expressed mutant PGAM5-FLAG constructs (purple) co-stained with endogenous TOM20 (green); cell nuclei are stained with Hoechst (blue). Scale bar, 5 µm; immunofluorescence analysis performed by Elena Heuten (Lemberg lab).

2.3.5 Formation of the PGAM5 higher order structure prevents PARL-catalyzed cleavage

The slower kinetics of PGAM5 as PARL substrate in unstressed mitochondria may allow PGAM5 to be imported into mitochondria and form oligomers via its C-terminal dimerization domain and an N-terminal WDPNWD-multimerization motif (Chaikuad *et al.*, 2017) (**Figure 20A**). Since it is commonly thought that other intramembrane proteases, as seen for γ-secretase, cleave their substrates only in a monomeric state (Fernandez *et al.*, 2016; Jung *et al.*, 2014; Perrin *et al.*, 2020; Winkler *et al.*, 2015), I set out to examine whether PGAM5 processing is affected by its higher order structure. Hence, I generated a monomeric PGAM5$^{\Delta C}$ (Δ278-289) mutant lacking its C-terminal dimerization domain and a multimerization-deficient PGAM5^{AAxxAA} mutant, lacking the WDPNWD-motif (Chaikuad *et al.*, 2017), and tested both in my cell-based PARL gain- and loss-of-function assay. Immunofluorescence analysis revealed that mitochondrial targeting of these PGAM5 constructs was not affected by the mutations (**Figure 20B**). Strikingly, both mutants were significantly more processed by PARL when

compared to PGAM5 wt and enhanced cleavage occurred even in the absence of CCCP (**Figure 20C-D**). Thus, cleavage of these mutants seems to be uncoupled from the physiological activation mechanism. Additional ectopic expression of PARL and treatment with CCCP could further increase cleavage. Control experiments under *OMA1* knockdown confirmed PARL-catalyzed cleavage and no significant role of OMA1 activity (**Figure 20E**). Of note: Cells ectopically expressing PGAM5$^{\Delta C}$ had to be incubated with the proteasome inhibitor MG132 in the *OMA1* knockdown experiment, since this mutant is cleaved so rapidly and the prolonged experimental procedure of siRNA knockdown otherwise resulted in protein levels under the detection limit. For an additional detection control see (**Figure S8A**). Thus, the results for PGAM5$^{\Delta C}$ in the *OMA1* knockdown control resemble more an endpoint assay instead of a steady-state analysis and the before observed enhanced cleavage compared to PGAM5 wt became less visible. Nevertheless, the control still revealed the important information that OMA1 played no significant role in cleavage of monomeric PGAM5$^{\Delta C}$. To understand if the oligomeric state influences PARL-catalyzed processing independent of the determinants within the TM domain, I generated double mutants combining monomeric PGAM5$^{\Delta C}$ with the G17L and S18L TM domain mutations that were localizing correctly to mitochondria (**Figure 21A**). Indeed, PGAM5$^{\Delta C\text{-}G17L}$ and PGAM5$^{\Delta C\text{-}S18L}$ showed a significantly decreased cleavage efficiency (**Figure 21B**) when compared to PGAM5$^{\Delta C}$ alone (**Figure 20C**). Thus, this observation suggests that the oligomeric state of PGAM5 influences PARL-catalyzed processing independent of the determinants within the TM domain. In a next step, I asked whether CCCP may increase PGAM5 processing by disassembling its oligomers, thereby making PGAM5 monomers susceptible for PARL-catalyzed cleavage. For this, I analyzed PGAM5 ectopically expressed in Hek293T cells untreated or treated with CCCP by blue-native (BN)-PAGE. I could reveal a reduction of higher molecular weight assemblies of PGAM5 wt in the range of 500 kDa over time (**Figure 21C**) and as expected, no higher molecular weight assemblies for PGAM5$^{\Delta C}$ and PGAM5^{AAxxAA} (data not shown). Moreover, I observed an increase of monomeric and processed PGAM5 by BN-PAGE, which is in line with the PARL-catalyzed PGAM5 as shown in control SDS-PAGE. Adding a second dimension by two-dimensional PAGE (2D-PAGE) could resolve the 500 kDa assemblies of PGAM5 wt into smaller fragments around 60 kDa and 35 kDa, which corresponds roughly to the size of a PGAM5 dimer and monomer, respectively (**Figure S8B**). Taken together, these results reveal that PGAM5 processing is governed by an oligomeric switch that in healthy mitochondria prevents PARL-catalyzed cleavage and upon depolarization of the IMM disassembly enables the conversion of higher molecular weight assemblies to its soluble form, resulting in subsequent cleavage because of a suitable TM domain.

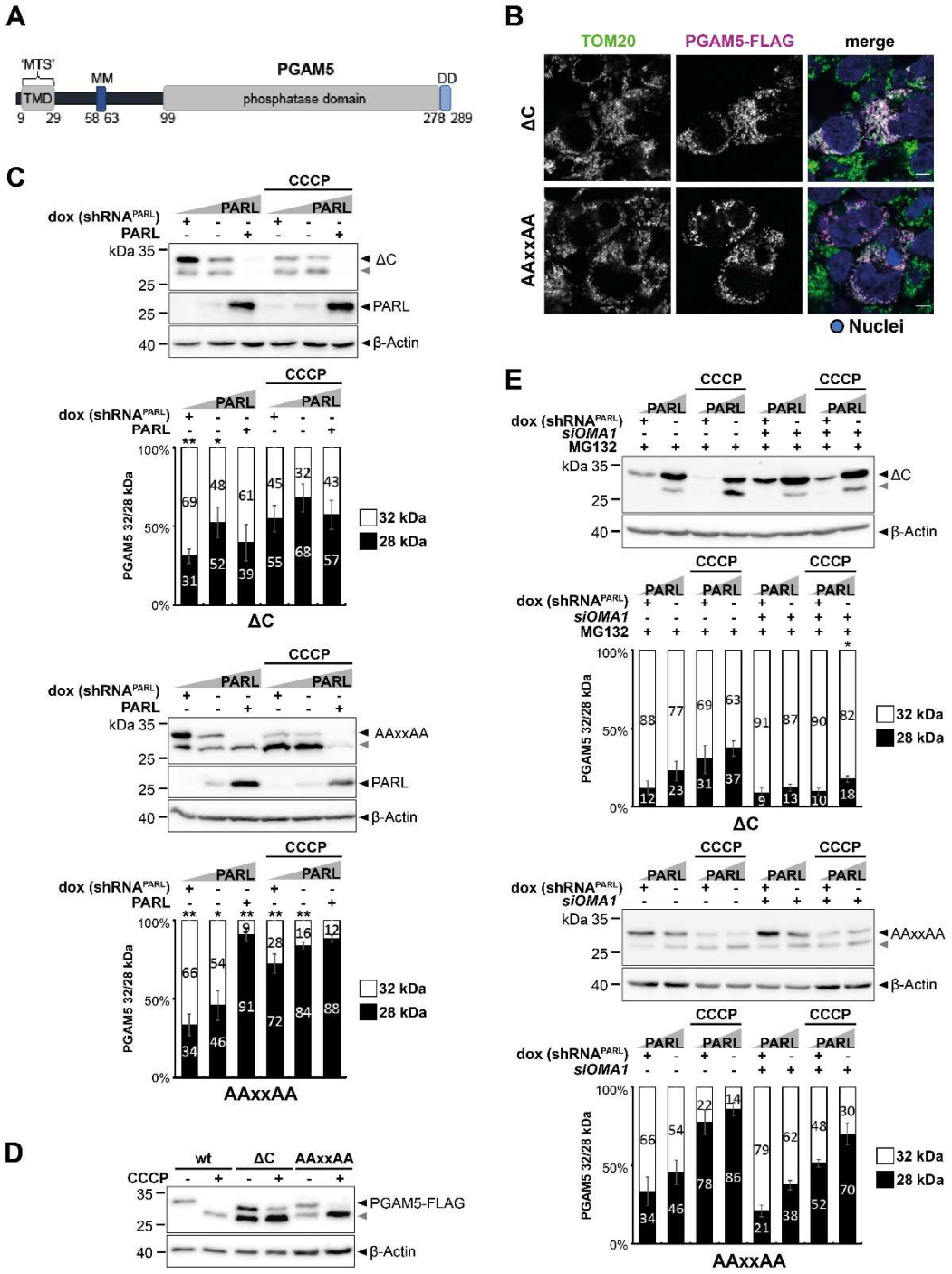

Figure 20 | Formation of the PGAM5 higher order structure prevents PARL-catalyzed cleavage (part I).

(A) Schematic representation of PGAM5 domain structure. Indicating TM domain (TMD) with function as matrix targeting signal (MTS), WDxxWD multimerization motif (MM) and C-terminal dimerization domain (DD). **(B)** Immunofluorescence analysis examines mitochondrial targeting of ectopically expressed mutant PGAM5-FLAG constructs (purple) co-stained with endogenous TOM20 (green); cell nuclei are stained with Hoechst (blue). Scale bar, 5 µm; immunofluorescence analysis performed by Elena Heuten (Lemberg lab). **(C)** Processing of monomeric PGAM5$^{\Delta C}$ and multimerization-deficient PGAM5^{AAxxAA} analyzed in the cell-based PARL gain- and loss-of-function assay. Grey triangle: 28 kDa cleavage fragment. Lower panels show quantification of PGAM5 32/28 kDa distribution (n = 3, means ± SEM). Significant changes versus wt PGAM5-FLAG are indicated with black stars (*p ≤ 0.05, **p ≤ 0.01; unpaired two-tailed t-test). **(D)** Direct comparison of PGAM5 wt, ΔC and AAxxAA cleavage at endogenous PARL level without and with CCCP treatment. My samples reloaded by Elena Heuten (AG Lemberg). **(E)** For *OMA1* knockdown, cells were transiently transfected with either a non-targeting siRNA or an *OMA1*-specific siRNA for 48 hours before transient transfection of the PGAM5-FLAG constructs. PGAM5 cleavage was stimulated by treating cells with CCCP. PGAM5$^{\Delta C}$ was

additionally treated with 2 µM MG132 for 24 h before harvesting. Grey triangle: 28 kDa cleavage fragment. Lower panels show quantification of PGAM5 32/28 kDa distribution (n = 3, means ± SEM). No significant changes versus cells transfected with non-targeting siRNA were observed (unpaired two-tailed t-test).

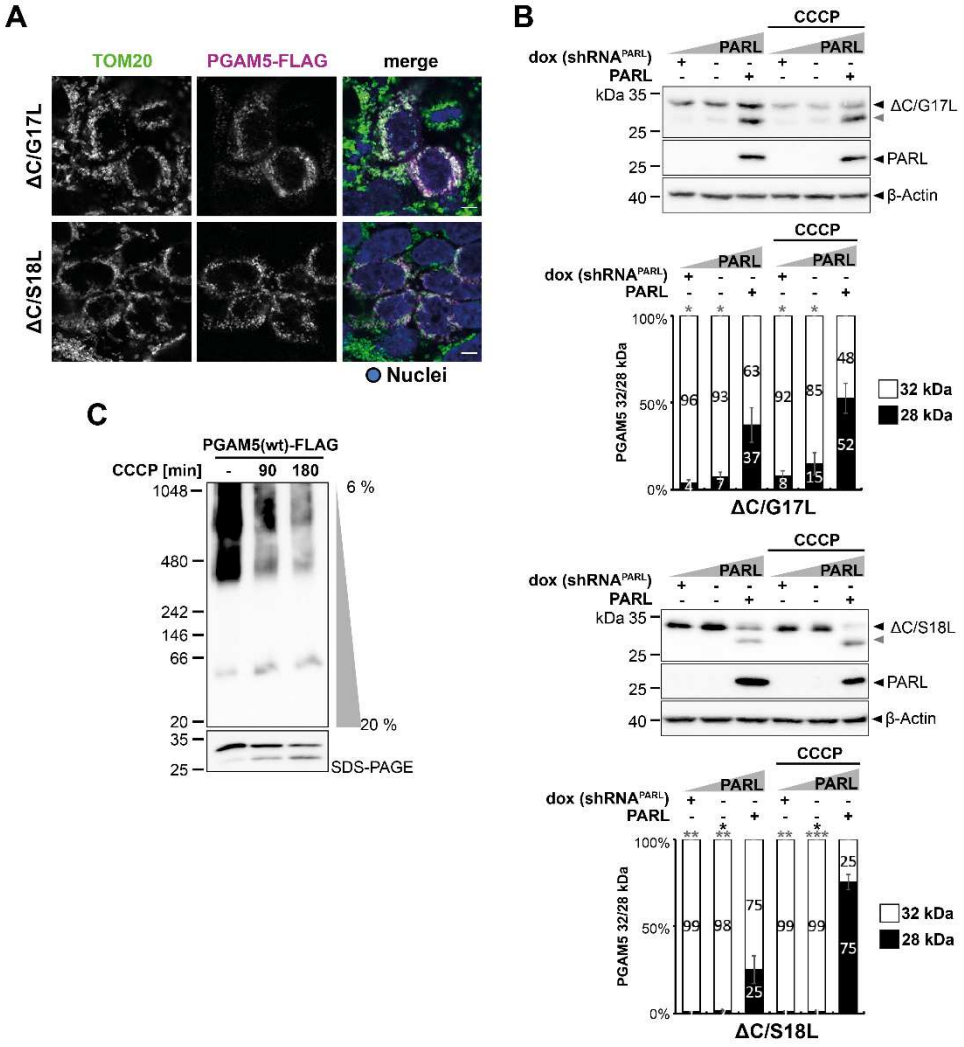

Figure 21 | Formation of the PGAM5 higher order structure prevents PARL-catalyzed cleavage (part II).
(A) Immunofluorescence analysis examines mitochondrial targeting of ectopically expressed mutant PGAM5-FLAG constructs (purple) co-stained with endogenous TOM20 (green); cell nuclei are stained with Hoechst (blue). Scale bar, 5 µm; immunofluorescence analysis performed by Elena Heuten (Lemberg lab). **(B)** Corresponding analysis of monomeric PGAM5 double mutants PGAM5$^{G17L/\Delta C}$ and PGAM5$^{S18L/\Delta C}$ additionally containing TM domain mutations G17L and S18L. Grey triangle: 28 kDa cleavage fragment. Lower panels show quantification of PGAM5 32/28 kDa distribution (n = 3, means ± SEM). Significant changes versus wt PGAM5-FLAG are indicated with black stars, significant changes versus PGAM5$^{\Delta C}$-FLAG are indicated with grey stars (*p ≤ 0.05, **p ≤ 0.01, ***p ≤ 0.001; unpaired two-tailed t-test). **(C)** Analysis of PGAM5 higher molecular weight structures in BN-PAGE upon treatment with 10 µM CCCP for 90 min and 180 min.

3. Discussion

In this study, I investigated the requirements for PARL-catalyzed cleavage of PGAM5 to gain insight into its cleavage mechanism and how cleavage is accelerated by uncoupling the mitochondrial membrane potential. I could show that the N-terminal portion of the PGAM5 TM domain plays a special role and is a critical determinant for PARL-catalyzed processing. Strikingly, I obtained PGAM5 mutants with highly increased cleavage by PARL uncoupling it from its native regulation, besides cleavage resistant forms. Analysis of the PGAM5 TM helix structure by NMR indicates that instead of a single straight TM helix, PGAM5 harbors two split helices with a hinge-like loop in between. Based on this analysis, I suggest that mutations within the N-terminal or C-terminal helix alter the interaction with PARL or bending into the PARL active site. Moreover, I found that a balanced net charge in the C-terminal JM region prevents PGAM5 from being cleaved in a premature state by PARL so that cleavage-resistant PGAM5 oligomers can assemble upon mitochondrial import. Under mitochondrial stress such as observed by uncoupling the membrane potential, I propose a model in which PGAM5 disassembles at the IMM by an unknown mechanism into monomers that are efficiently cleaved by PARL to trigger PGAM5's downstream activities. Taken together, my findings indicate that the substrate recognition mechanism of PARL relies on different substrate features with hierarchical importance and include a membrane-potential-dependent oligomeric switch.

3.1 PARL substrate discovery

Throughout the recent years in total six PARL substrates have been discovered. Whereas PINK1 (Deas *et al.*, 2011; Jin *et al.*, 2010; Meissner *et al.*, 2011) and PGAM5 (Sekine *et al.*, 2012) were found in functional cell-based experiments, STARD7, Smac/DIABLO, CLPB and TTC19 were first identified by proteomics approaches (Saita *et al.*, 2017). Surprisingly, the two latter do not contain a TM domain making PARL a new addition to the group of rhomboids that are capable to also cleave soluble substrates. Whereas, GlpG has so far only been described to cleave soluble substrates *in vitro* (Lazareno-Saez *et al.*, 2013; Wang *et al.*, 2006; Xue and Ha, 2012), the mammalian secretory-pathway rhomboid RHBDL4 was shown to process soluble substrates in cell-based assays (Bock *et al.*, 2021; Tang *et al.*, 2022).

When investigating putative PARL substrates by SILAC, we could reproduce the identification of CLPB. Recent studies could narrow down the PARL cleavage site in CLPB between amino acid C126 and Y127, between a 35-amino acid hydrophobic stretch and an ankyrin-repeat domain (Cupo and Shorter, 2020; Saita *et al.*, 2017). Interestingly, a recent proteomics approach also pointed towards the multipass IMM protein GHITM as PARL substrate due to differential regulation of protein expression in Parl$^{-/-}$ mouse brain mitochondria (Spinazzi *et al.*, 2019). However, in line with my HEK-cell-based data that failed a clear confirmation of GHITM

as PARL substrate, further validation will be required. Since PARL can cleave single-spanning membrane proteins as well as soluble proteins, the question remains open if also polytopic substrates exist.

Overall, identification of PARL substrates is challenging and underlies different biological and technical limitations. Some putative substrates might only temporarily interact with PARL or display an induced interaction at certain cellular conditions. For instance, crosslinking approaches might help to overcome issues of short and/or weak interaction between enzyme and substrate. Moreover, it should be taken into account that the PARL complex partners of the SPY-complex may be involved in certain substrate-interactions as well. Apart from that, substrate validation is often performed by transiently overexpressing tagged protein candidates. Tagging a functional protein at the wrong terminus or with a too bulky tag, can result in unfunctional, misfolded proteins, hampered complex formation or even inhibits correct subcellular localization and transport (Bräuer *et al.*, 2019; Einhauer and Jungbauer, 2001; Waugh, 2005).

3.2 PARL processing and substrate release are of high biological importance

Human PGAM5 was described to have two protein isoforms, PGAM5-L and PGAM5-S, which originate from alternative splicing of a 3' exon of the PGAM5 transcript and are similar in the first 239 amino acids. Strikingly, the short isoform of PGAM5 has not been detected in any other mammal except from humans so far (Cheng *et al.*, 2021; Lo and Hannink, 2006). Since PGAM5-L and PGAM5-S have similar molecular weights, full-length PGAM5 detection of human samples by standard western blot analysis shows PGAM5-L and PGAM5-S as mixture in one band around 32 kDa. The lower band around 28 kDa corresponds to the PARL-catalyzed cleaved L-PGAM5 species (Lo and Hannink, 2006; Sekine *et al.*, 2012). PGAM5 can be found in an equilibrium between dimeric and multimeric states (Chaikuad *et al.*, 2017; Ruiz *et al.*, 2019), depending on its biological function as result of mitochondrial quality control. So far, the impact of the oligomeric state of PGAM5 on PARL-catalyzed cleavage has not been addressed yet. Detachment from its membrane anchor followed by release of cleaved PGAM5 into the cytoplasm is an important but yet ill-defined mechanism that affects various actions from control of mitophagy via DRP1 to mitochondrial biogenesis via Wnt signaling (Bernkopf *et al.*, 2018; Saita *et al.*, 2017; Sekine *et al.*, 2012; Wai *et al.*, 2016; Yamaguchi *et al.*, 2019; Zhuang *et al.*, 2013). The cytosolic pool of PGAM5 was shown to assemble into symmetric rings, which can further polymerize into filaments that were described to co-localize with microtubules (Chaikuad *et al.*, 2017; Ruiz *et al.*, 2019). Discussion is still ongoing, if PGAM5 filaments are initially generated inside the mitochondria or whether this phenomenon links PGAM5 to stress-induced retrograde trafficking of mitochondria. Together with PINK1, Smac/DIABLO and STARD7, PGAM5 belongs to four out of six known PARL substrates that were found to be dually localized in mitochondria and the cytosol under various cellular

conditions. This fact substantiates the critical role of PARL-catalyzed processing for the localization of its substrates. Whereas PARL-mediated cleavage during mitochondrial import partitions STARD7 to the cytosol and the IMS (Saita *et al.*, 2018), release of the conditional substrate PGAM5 after cleavage by PARL still remains fragmentary and demands further research.

3.3 The development of a PARL *in vitro* cleavage assay is challenging

Expression and purification of enzymatically active eukaryotic intramembrane proteases is demanding, due to their low abundance in the cell and their multiple membrane-spanning TM domains. For instance, overexpression has to be tightly titrated as it can result in proteotoxic effects dependent or independent of the catalytic activity, as partially seen for human PARL. These are experimental obstacles that leave scientists with a limited set of *in vitro* assays to study intramembrane cleavage mechanisms and to measure kinetics. Although *E. coli* expression systems are in general well established and used in multiple approaches to study intramembrane proteolysis, they also have their limitations. Overexpression of membrane proteins often results in inclusion bodies, which complicates subsequent isolation without disrupting the protein structure (Drew *et al.*, 2003). Also, the bacterial folding machinery is not as efficient as the eukaryotic counterpart, often resulting in a saturation of the translocation machinery with toxic effects (Klepsch *et al.*, 2011). However, the human rhomboids RHBDL2 and *Drosophila* Rhomboid-4 were already successfully expressed and purified in the *E. coli* expression system (Baker and Urban, 2015; Cordier and Lemberg, 2017).

One key component in the experimental set-up of human PARL purification is to isolate the rhomboid free from any contaminating or potentially interacting proteases. Since mitochondria in general are loaded with proteases in all sub-compartments as part of the huge mitochondrial proteolytic network and PARL in human cells forms the SPY-complex with the metalloprotease YME1L, purification directly from mitochondria is obstructive. In a recent study, PARL was expressed in a bacterial lysate-based cell-free expression system with subsequent reconstitution into liposomes containing a defined mixture of phospholipids and cardiolipin, leaving recombinant PARL with some basic activity (Saita *et al.*, 2018). This result suggests that the bacterial translation machinery is sufficient for protein expression and the problematic step in PARL purification might be to find the correct lipid composition or detergent environment that retains rhomboid activity. Another limitation is that cell-free translation systems are comparably cost-intensive and difficult to use for large-scale productions of mammalian rhomboid. Therefore, we collaborated with the Lemieux laboratory, in which human PARL lacking the MTS could be successfully expressed and purified from the secretory pathway of the yeast *P. pastoris* (Lysyk *et al.*, 2021). Yeast, as classical unicellular eukaryotic model organism combines advantages of bacteria, like low-cost cultivation requirements, high growth

speed and easy genetic manipulation with various features of higher eukaryotes, including certain phosphorylation.

3.3.1 The lipid environment influences rhomboid activity

In contrast to soluble proteases, intramembrane proteases require the appropriate membrane environment after purification to be folded correctly and exhibit catalytic activity. Hence, for purification suitable detergents have to be used to solubilize the recombinant enzyme. The right detergent and the appropriate conditions need to be experimentally worked out and cannot be predicted as every intramembrane protease has its own characteristics and requirements depending on its structure and membranous background. In our studies, the rather mild water-soluble nonionic detergent DDM was the most suitable for solubilizing rhomboids and preserving their catalytic activity.

Lipid addition and reconstitution experiments with the *E. coli* rhomboid GlpG indicate that full proteolytic activity requires certain phospholipids (Urban and Wolfe, 2005). Likewise, we could show that the activity of DDM-solubilized human PARL is highly influenced by cardiolipin (Lysyk *et al.*, 2021), a lipid enriched in the mitochondrial inner membrane, which affects stability and activity of membrane protein complexes (Dudek, 2017; Houtkooper and Vaz, 2008). The bacterial membrane contains only minor amounts of cardiolipin (Oursel *et al.*, 2007).

Although up to now, using the secretory pathway of the yeast expression system turned out to be the most suitable one to purify active human PARL, it is still of future interest to further improve PARL purification, especially in terms of upscaling and make usage of alternative expression systems like cell-free systems, or tissue-culture based systems like the baculovirus-insect cell system. The baculovirus-insect cell system is known for high yield recombinant protein expression of mammalian membrane proteins with significant eukaryotic post-translational modifications (Jarvis, 2009). Previous studies reported promising expression of human membrane proteins such as a homotrimeric ion channel and different membrane transporters (Chen *et al.*, 2013; Tschantz *et al.*, 2008). Thus, one option could be to express human PARL in the insect cell background utilizing a biotin-streptavidin system. The biotin-streptavidin interaction is one of the strongest non-covalent biological interactions (Chaiet and Wolf, 1964) and is widely used for affinity purification with denaturing (Rybak *et al.*, 2004; Sano *et al.*, 1997) or non-denaturing purification protocols (Lin *et al.*, 2020). In order to approach the ideal *in vitro* assay, reconstitution of enzyme and substrate into proteoliposomes or nanobodies is essential to be able to perform structural studies in order to understand enzyme-substrate interactions in a membrane and evaluate kinetics of human PARL. Therefore, high amounts of purified and active rhomboid are required. Moreover, during co-reconstitution of enzyme and substrate, premature cleavage of the substrate needs to be inhibited to prevent its loss before measurements or disturbances by unwanted cleavage products. One versatile option is to work with pH-shifts either in different and/or within the same samples using

appropriately adjusted buffers. Whereas GlpG is enzymatically active at pH 7, it can bind to its substrate but lacks enzymatic activity at pH 4 (Dickey *et al.*, 2013). Since for PARL the assay development still faces technical limitations, I converted analyses in a lipid environment to the simpler *E. coli* rhomboid model GlpG.

In this collaborative project, in which I contributed to a co-authorship, we investigated the lipid distortion effect of the *E. coli* rhomboid GlpG and two catalytic-inactive mutants reconstituted in different lipid environments, without or with the model substrate LacYTM2, to further understand the enzyme-substrate interaction mechanistically. Since all eukaryotic rhomboids share the bacterial 6-TM domain core, it is highly likely that all rhomboids also share specific mechanistic patterns when it comes to enzyme-substrate interactions influenced by the surrounding lipids. New insights could contribute to gain understanding how also the mitochondrial rhomboid PARL influences surrounding lipids and interacts with its substrates in the plane of the membrane. Therefore, I expressed and purified GlpG-His6 and its mutants that were analyzed by our collaboration partners of the Huster lab in Leipzig with different biochemical/biophysical approaches including MALDI-MS and solid-state NMR. The results suggest that GlpG activity is related to membrane thickness irrespective of the lipid headgroup composition *in vitro* and found the optimal lipid chain length to be between ~11.8 – 12.9 Å. Substrate cleavage of GlpG outside the optimal lipid chain length window appeared to be much slower or was essentially abolished. Interestingly, our results revealed a specific interaction of GlpG with PE and PG lipids, which were co-purified from my *E. coli* preparations. Although, in comparison to its eukaryotic counterparts, GlpG is not known to require cofactors for its catalytic activity (Urban and Wolfe, 2005), the strong interaction to PE and PG lipids highlights once again, how important lipids are for the correct establishment of membrane proteins in their hydrophobic environment and thus, how they contribute to the enzymatic capabilities of an intramembrane protease.

Solid-state NMR of GlpG without or with its model substrate LacYTM2 was performed in different lipid membranes of varying lipid chain length. Due to the specific and apparently strong interaction of GlpG with its native PE and PG lipids in the *E. coli* membrane, all measurements contained the rhomboid bound to these specific lipids. Thus, in a next step it would be interesting to perform the exact same experiments but lacking PE and PG bound to GlpG. During Ni-NTA affinity purification it is not possible to get rid of those lipids. Either, there is a way to remove the phospholipids after purification by enzymatic reaction, for instance by using phospholipases or it could be worth to try a cell-free expression system to perform *in vitro* translation. As discussed above, this system is comparably cost-intensive for the production of high protein amounts. Nevertheless, it would solve the problem of co-purified bacterial lipids and allows to study the lipid distortion effect and enzymatic activity of GlpG without PE and PG lipids. Since both GlpG mutants used in this study, namely R137A and G261A, display only strongly reduced enzymatic activity but are no ‘catalytic-dead’ mutants, in

a next step it could be of interest to repeat the measurements with the catalytic-inactive mutant S201A and compare the thinning effect between GlpG wt and the already tested mutants. Since LacYTM2 displays the GlpG cleavage site outside of the TM domain, it would be interesting to record enzyme-substrate interactions with a model substrate like chimeric MBP-Spitz, which harbors the cleavage site within its TM domain. However, because of the higher molecular weight compared to LacYTM2, co-reconstitution with PARL might be technically more complex.

Although currently, detergent micelle-based *in vitro* cleavage assays are the most robust approach to study intramembrane proteolysis, for a holistic understanding a full-recapitulation of events in the membrane is required. For the *E. coli* rhomboid protease GlpG assays in proteoliposomes were already used in multiple studies (Arutyunova *et al.*, 2018; Moin and Urban, 2012; Ticha *et al.*, 2017). It is known that substrate TM helices have to transiently unfold near the protease active site, prior to cleavage by proteases. Hence, the assay conditions have a profound influence on the cleavage rate. Whereas substrates and non-substrates showed equally stable TM helices in phospholipid proteoliposomes and therefore hampered cleavage by GlpG, the detergent micelle was described as a more active-site-like mimicking aqueous system for GlpG that supported increased destabilization of substrate TM helices and facilitated cleavage (Moin and Urban, 2012). When it comes to GlpG substrate sequence features, it was found that the positioning of helix-destabilizing residues relative to the cleavage site plays an important role. So, analysis using the model substrate LacYTM2 *in vivo* and *in vitro* showed that a hydrophilic region was encompassing the cleavage site and that helix-destabilizing residues were located in the downstream hydrophobic region, resulting in the conclusion that GlpG prefers residues with a small side chain and a negative charge at the P1 and P1' sites respectively (Akiyama and Maegawa, 2007). However, in my study I did not observe any differences in the cleavage efficiency of purified MBP-PGAM5 TM domain mutants in DDM-micelles when compared to MBP-PGAM5 wt, indicating that for this substrate the overall TM helix stability is less crucial than for the previously analyzed GlpG substrates.

Studying PGAM5 TM helix characteristics in liquid-state NMR by our collaborators revealed that PGAM5 has an unstructured hinge-like region at the center of its TM helix. In general, cleavage efficiency of TM domains is highly influenced by the environment, in which TM domains interact with water for instance via intrahelical hydrogen-bonds. For the γ-secretase substrate amyloid-precursor-protein APP-C99, which harbors a di-glycine hinge in its TM helix, it could be shown that embedding the TM domain in an isotropic solvent, a large micelle or a lipid bilayer, removes a kink at the di-glycine hinge and alters cleavage efficiency (Dominguez *et al.*, 2014; Lemmin *et al.*, 2014; Pester *et al.*, 2013a). Speculating that such a kink does also exist at the di-glycine G16-G17 hinge-like region in MBP-PGAM5 and working in our micelle-based *in vitro* assay removes that potential kink, then this effect may also result in an altered cleavage efficiency by PARL. Hence, the loss of such a kink might mask alterations in PARL-

catalyzed cleavage between the MBP-PGAM5 TM domain mutants, so that no differences could be detected compared to MBP-PGAM5 wt.

I speculate that the differential cleavage that could be observed in human tissue culture given by the PGAM5 TM domain mutants, is most likely a lipid-dependent effect that needs an appropriate membranous environment, which cannot be mimicked sufficiently in DDM-micelles. (The effect observed in cells will be discussed in more detail in the next paragraph.) Recapitulating, the bottleneck remains to obtain sufficient amounts of purified and active human PARL that can be reconstituted together with purified PGAM5 into a membranous environment using bicelles or proteoliposomes. As soon as this can be achieved, PARL-PGAM5 kinetics and interaction dynamics could be examined in enhanced cleavage assays, also in combination with solid-state NMR.

3.4 Is intramembrane cleavage of PGAM5 affected by TM helix dynamics?

Proteolytic cleavage within a TM domain is mechanistically more complex than proteolysis within an aqueous environment (Langosch and Steiner, 2017). Restricted lateral diffusion of the substrate and its hampered capability to freely rotate within the lipid bilayer complicate the cleavage mechanism in addition to the limited availability of water. Thus, interaction between the rhomboid protease and its substrate with subsequent intramembrane cleavage is seen as multi-step process. Prior to cleavage, translocation of the helical substrate TM domain from the lipid bilayer towards the rhomboid protease active site is required so that the scissile peptide of the substrate can to bind into a water-filled catalytic cleft. It is commonly believed, that the TM helix of rhomboid substrates initially dock onto a membrane-integral exosite of the enzyme, a process that may be associated with structure-encoded global motions of the substrate TM helix (Strisovsky *et al.*, 2009). Access of the catalytic residues to the cognate cleavage site motif followed by processing of the substrate is given by unwinding of the bound TM helix (Cho *et al.*, 2019b; Strisovsky, 2016). Known substrate cleavage sites in the case of bacterial and eukaryotic secretory pathway rhomboids like *E. coli* GlpG and the human plasma membrane rhomboid RHBDL2, map at the N-terminal TM domain boundary (Johnson *et al.*, 2017; Stevenson *et al.*, 2007) and processing efficiency is largely determined by the primary sequence (Strisovsky *et al.*, 2009). Hence, cleavage sites are facing the outside of the cell and most likely gain access to the catalytic center from the top of the enzyme. This assumes that substrate unfolding happens between the scissile peptide bond and the hydrophobic TM helix, followed by a sharp turn in the protein main chain (Ha *et al.*, 2013) while the TM helix may remain bound to the exosite (Ha *et al.*, 2013; Strisovsky *et al.*, 2009). RHBDL2 cleaves substrates not only at single sites after small amino acid residues within the N-terminal region of their TM domain but also in the immediate juxtamembrane region (Johnson *et al.*, 2017). Consistent with this juxtamembrane cleavage, RHBDL2 does not require helix-destabilizing residues in its substrate TM domains for functional processing. For instance, unlike most

rhomboid substrates, thrombomodulin does not contain helix-destabilizing residues but has a cytosolic domain instead that acts as a cleavage determinant. The cytoplasmic region of thrombomodulin is even sufficient to transform otherwise non-cleavable proteins into rhomboid substrates (Lastun *et al.*, 2016; Lohi *et al.*, 2004). A comparable observation could be made for the yeast PARL orthologue Pcp1/Rbd1 that also does not require helix-breaking residues in the cleaved hydrophobic region of its substrate Mgm1. TM segments of non-substrates became cleavable by Pcp1/Rbd1 when put in place of the authentic rhomboid cleavage region of Mgm1 (Schäfer *et al.*, 2010). In contrast to the outwards orientation of bacterial and secretory pathway rhomboids (Lemberg and Freeman, 2007b), human PARL, like yeast Pcp1/Rbd1, is predicted to have an inverted active site facing the mitochondrial matrix and cleaves its canonical substrates towards the C-terminal portion of their TM domains (**Figure 4**). Therefore, the whole context of an intramembrane protease of interest, regarding the cell organelle and its function at certain cellular conditions with the specific topology and lipid environment of the membrane, has to be taken into account. Whereas, recognition of juxtamembrane motifs and/or tails may be sufficient to drive substrate interaction and cleavage for some intramembrane proteases, in the absence of such motifs, TM helix stability and unwinding may play a more prominent role (**Figure 22**).

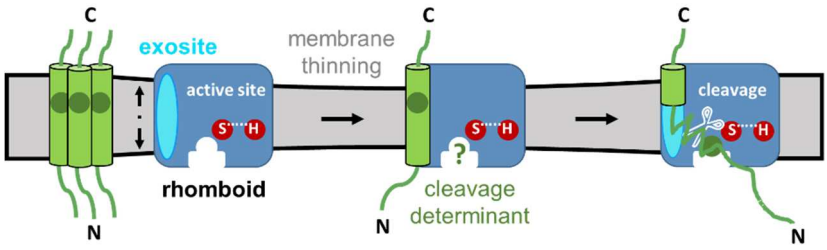

Figure 22 | Hypothetical model of rhomboid-catalyzed cleavage with regard to PARL-like topology.
Certain cellular signals might activate an oligomeric switch of the so far inactivated substrates releasing monomers from the oligomeric assembly. This enables recognition and conditional cleavage by the rhomboid protease, which thins its surrounding membrane lipids. After docking of the substrate TM domain to a putative rhomboid exosite, access of the catalytic residues to the cognate cleavage site motif is given by unwinding of the bound TM helix followed by processing of the substrate. The exact cleavage determinants are still unknown for mammalian rhomboids.

In line with this, I now show that the preference of a bulky amino acid in the P1 position of PGAM5, namely F23 (Lysyk *et al.*, 2021), only results in modest effects and leads to the speculation that the cleavage rate may be governed by TM helix dynamics. Conserved helix-destabilizing glycine residues in the C-terminal portion of the PINK1 TM domain were found to be highly important for effective PARL-catalyzed cleavage (Meissner *et al.*, 2011). However, substitution of the putative equivalent helix-destabilizing residues in PGAM5, G29 and P31, did only mildly influence PARL-catalyzed cleavage and the critical residues were found in the N-terminal half of the substrate TM domain, instead. One possible explanation is that according

to our structures these residues are located outside the helical region. Taking our results into consideration, this suggests that TM domain dynamics are influenced by multiple features, making it difficult to predict.

Since membrane-altering agents can influence rhomboid substrate cleavage including the position of cleavage sites (Urban and Moin, 2014), it remains an open and interesting question whether CCCP-induced disruption of $\Delta\Psi_{mito}$ can modulate membrane properties and hence the accessibility of the PGAM5 TM domain. This effect might contribute to the two slightly varying cleavage site determinations in PGAM5 between S24-A25 (Sekine *et al.*, 2012) and F23-S24 (Lysyk *et al.*, 2021), depending on the assay background of human tissue culture or a cell-free *in vitro* assay, respectively. Mutations in the TM domain of PGAM5 may also drive a shift of the PARL cleavage site, for instance by +1 or -1 amino acid, which may be sufficient to maintain processing since rhomboid proteases do not have such a strict sequence selectivity as has, for example, trypsin.

The TFE/water model system used for NMR analysis mimics important biophysical aspects of an intramembrane protease active site (Pester *et al.*, 2013b; Yücel *et al.*, 2019). Here, our collaborators observed no significant secondary structure changes for the mutants C12S, C12L, and G17L. This finding was surprising in regard to the striking differences in the efficiency of PARL-catalyzed cleavage observed in living cells and suggests that not primarily TM helix stability determines the cleavage rate. Moreover, our collaborators revealed that PGAM5 harbors a pronounced hinge-like loop of five amino acid residues at the center of its TM domain between G13 and G17, which is several residues apart from the scissile peptide bond. Such a non-continuous feature, instead of a straight TM helix, can be observed in other intramembrane protease substrates, including the bacterial twin arginine transport system protein TatA and mammalian APP-C99 (Barrett *et al.*, 2012; Leeuw *et al.*, 2001), of which TatA shows an even more pronounced kink in the protein main chain compared to APP-C99. This leads to an almost rectangular arrangement of the TM domain and the following amphipathic helix (Rodriguez *et al.*, 2013). Glycine and proline were shown to have the strongest destabilizing effect of all amino acids on model TM helices with regard to their helicity in detergent micelles (Li and Deber, 1994; Liu and Deber, 1998) and glycine was found twice as abundant in TM helices than in water-soluble helices (Baeza-Delgado *et al.*, 2013), highlighting its importance in the functional role of TM domains. Whereas the hinge-like region of the *P. stuartii* rhomboid substrate TatA is formed by G-S-P, the pronounced APP-C99 hinge displays a G-G (di-glycine) sequence (Langosch *et al.*, 2015). Glycine seems to comprise also a major role for PGAM5, since the hinge-like region is formed between G13 and G17, containing a di-glycine motif with G16-G17 (**chapter 2.3.3.**). Recently, it could be shown that modulation of the hinge flexibility in the TM domain of APP-C99 alters cleavage by γ-secretase (Götz *et al.*, 2019; Lemmin *et al.*, 2014; Pester *et al.*, 2013a) and affects substrate-enzyme interaction (Silber *et al.*, 2020). Since I observed decreased cleavage of the PGAM5 mutants

G16L, G17L and GG16/17LL when compared to PGAM5 wt in tissue culture cells (**Figure 12B and 13A**), I speculate that also here the hinge flexibility might have been altered due to the mutations resulting in decreased processing efficiency, as observed for APP-C99 and γ-secretase.

3.4.1 The PGAM5 TM domain and its intermitted helix

Interestingly, the PGAM5 TM domain with its zoned amphipathic N-terminal helix resembles to a greater degree the bacterial TatA, which harbors a N-terminal TM helix (also termed helix-α1) separated by a short hinge-like region from an amphipathic helix (helix-α2) that in turn ends with an unstructured, polar, C-terminal region (White *et al.*, 2010). The amphipathic helix of TatA is described to lie along the membrane surface and undergo topology changes in which the helix becomes membrane-spanning, related to the function and biological needs of the cell (Gouffi *et al.*, 2004). Of note: TatA from *E. coli* is homologous to TatA from *P. stuartii*, which is synthesized as an inactive pre-protein with an eight amino acid N-terminal extension that needs to be cleaved off by the *P. stuartii* rhomboid AarA to activate TatA. Interestingly, *E. coli* TatA lacking these eight amino acids is not cleaved by the *E. coli* rhomboid GlpG, although the *P. stuartii* TatA in turn can functionally substitute for *E. coli* TatA and requires processing by GlpG to be active in *E. coli* (Fritsch *et al.*, 2012). Given the structural resemblance of the PGAM5 and TatA TM domains, a comparable cleavage mechanism as seen for *P. stuartii* TatA bending into the active site of *E. coli* GlpG is likely for PGAM5 and PARL, albeit due to PARL's predicted topology in an inverted orientation (**Figure 23**).

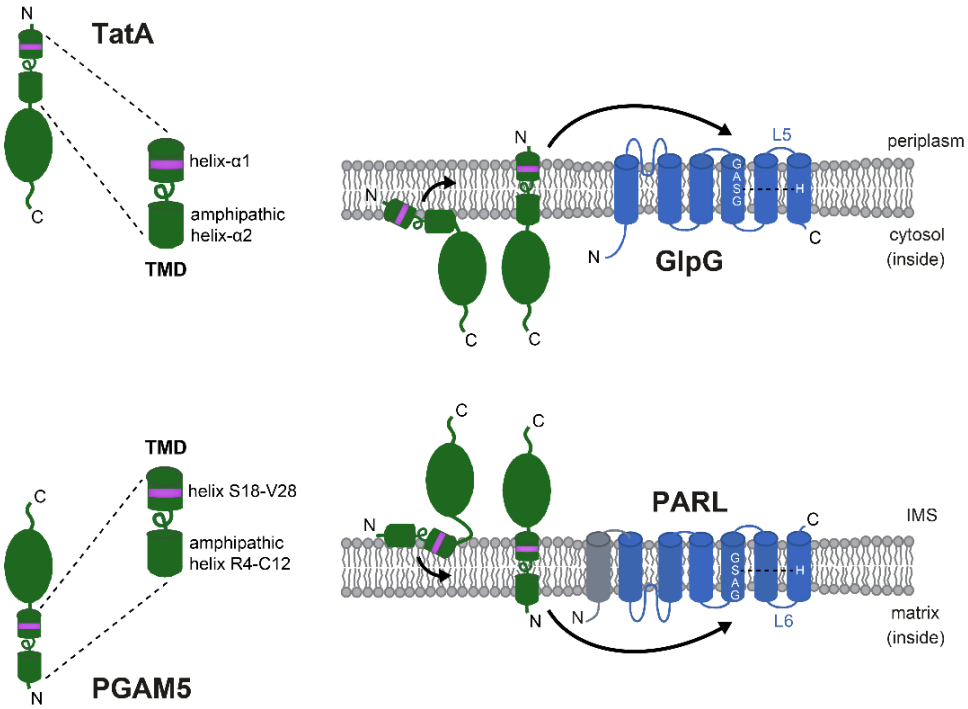

Figure 23 (Caption overleaf)

Figure 23 | Hypothetical model of TatA and PGAM5 TM domain movement prior cleavage.
Upper panel represents *P. stuartii* TatA prior *E. coli* GlpG-catalyzed cleavage after import into the membrane from the cytosol. The C-terminal amphipathic helix-α2 of the TatA TM domain lies along the membrane surface and becomes membrane-spanning after topology changes. Helix-α2 enters the GlpG active site either laterally or from an opening towards the periplasm. Cleavage site (A8-A9) (Strisovsky *et al.*, 2009) within helix-α1 is depicted in magenta. Accordingly, lower panel represents human PGAM5 prior PARL-catalyzed cleavage after import into the IMM from the IMS. The N-terminal amphipathic helix (R4-C12) of the PGAM5 TM domain lies along the membrane surface and becomes membrane-spanning after topology changes due to disruption of $\Delta\Psi_{mito}$. The amphipathic helix eventually enters the PARL active site either laterally or as predicted from an opening towards the matrix. Cleavage site (F23-S24) within helix S18-V28 is depicted in magenta. L5: flexible loop 5; L6: flexible loop 6 corresponding to L5.

In more detail, the N-terminal helix from R4 to C12 in the PGAM5 TM domain has an amphipathic character with R4, Q5, Q8, and C12 aligned on one side of the helix while the C-terminal helix from S18 to V28 shows strong hydrophobicity. In the used TFE/water model, both helices are bent by more than 30° resulting in a strong tilt with respect to the membrane normal and a putative submerged orientation of the amphipathic N-terminal helix in lipid bilayers. Extrapolation from structural details observed in the *E. coli* GlpG crystal structure are difficult due to the additional seventh TM domain and inverted topology of PARL. Thus, we used the AlphaFold (Jumper *et al.*, 2021) model of PARL (**Figure 24**) to develop a hypothesis how the intramembrane protease may interact with the PGAM5 substrate TM span. The catalytic S277 and H335 face a water-filled cavity like GlpG that in the case of PARL is predicted to open towards the mitochondrial matrix. Contrary to GlpG that cuts within the N-terminal unfolded region adjacent to the TM helix as seen in TatA, LacYTM2, Spitz and Gurken (Strisovsky *et al.*, 2009), PARL cuts in the C-terminal end of the TM domain within the most stable part towards the middle of the second TM helix. Based on this speculative model (**Figure 24**), we may envision how the PGAM5 TM domain binds to a putative PARL exosite. We speculate that upon unfolding of the N-terminal helix prior to processing by PARL, the PGAM5 cleavage site (F23-S24) (Lysyk *et al.*, 2021) in the C-terminal helix moves from its position in the plane of the membrane transiently into the matrix to reenter the membrane-embedded catalytic cleft. Interestingly, in our liquid-state NMR analysis of PGAM5 different swivel angles and thus different possible orientations of the N-terminal amphipathic TM helix could be observed. Given the different processing efficiencies observed for PGAM5 TM mutants, I speculate that altered directions of the cone opening might influence the efficiency by which mutant PGAM5 TM domains bend into the PARL active site. However, the TFE/water model of our liquid-state NMR analysis is a technical compromise and in future it will be interesting to study structure of the PGAM5 TM span reconstituted in bicelles, multilamellar vesicles or proteoliposomes to get further insights into the structural and dynamic properties of PGAM5 within a membranous system.

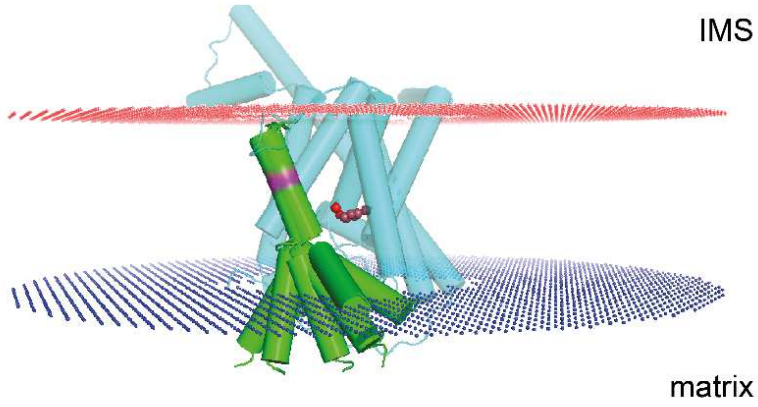

Figure 24 | Hypothetical model of the PGAM5 TM domain bound by a putative PARL exosite.
Model of PARL generated by Dr. Claudia Muhle-Goll using AlphaFold, entry Q9H300. Catalytic S277 and H335 are depicted in red facing the water-filled cavity of PARL, which opens to the matrix. Insertion depth for PARL AlphaFold model and the helical PGAM5 TM domain examined by NMR into the IMM was determined with the OPM server (Lomize *et al.*, 2012). The amphipathic helix of PGAM5 is shown here with a submerged orientation that allows the charged and hydrophilic sidechains to be placed within the lipid headgroup area. Cleavage site within the C-terminal helix of PGAM5 TM domain (F23-S24) is depicted in magenta. Red area: upper lipid layer towards mitochondrial IMS, blue area: lower lipid layer towards mitochondrial matrix.

3.5 A negatively charged juxtamembrane region accelerates PARL-catalyzed cleavage

The recognition mechanism of intramembrane protease substrates is not only influenced by properties within TM domain but also substrate features outside the membrane plane. In line with this is the observation that the yeast PARL orthologue Pcp1/Rbd1 recognizes C-terminally to the cleavage site a stretch of negatively charged amino acids in the IMS region of its substrate Mgm1. Mutational alterations of this region led to strong processing defects (Schäfer *et al.*, 2010). Recently, a similar negatively charged cluster was suggested to influence the fate of the PARL substrates PINK1 and STARD7 (Saita *et al.*, 2018), while the conditional substrate PGAM5 is lacking such a negative patch and shows a neutral net charge in its juxtamembrane region (**Figure 18**). In the case of PINK1 the negatively charged cluster is required for PINK1 import arrest, recognition and subsequent cleavage of the mitochondrial import intermediate by PARL. Interestingly, a PINK1 mutant lacking this motif (PINK1^{3EA}) gets constantly imported instead of accumulating on depolarized mitochondria and perturbs the biological equilibrium to such an extent that the stress-activated metalloprotease OMA1 starts processing PINK1^{3EA} (Sekine *et al.*, 2019). Here, I show that introducing negative charges into the juxtamembrane region of PGAM5 correlates with enhanced CCCP-induced PARL cleavage and release into the cytoplasm. Thus, I speculate that the absence of this feature complicates binding to a putative IMS-exposed PARL exosite and thereby allows the conditional cleavage of PGAM5.

3.6 PGAM5 multimerization prevents processing

The exact mechanism of how recognition and conditional cleavage of PGAM5 by PARL is achieved in response to mitochondrial stress, has not been resolved yet. The intramembrane protease γ-secretase is a multi-subunit protease complex (Wolfe, 2019) and has been shown to cleave its substrates only in a monomeric state (Jung *et al.*, 2014; Winkler *et al.*, 2015). Like in the γ-secretase substrate APP-C99, it is believed that TM domain dimerization restricts bending into the active site, which is gated by the γ-secretase complex partner Nicastrin (Bolduc *et al.*, 2016; Petit *et al.*, 2019; Urban, 2016). Until now, it has been unclear if also PARL has a preference for substrates in a certain state of assembly. Like γ-secretase, PARL is embedded in a multiprotein assembly known as the SPY-complex (Wai *et al.*, 2016), and substrate gating may be similarly controlled and influenced by the oligomeric state of its substrates.

In this work, I reveal that PGAM5 processing is affected by its oligomeric state, that in response to mitochondrial stress enables recognition and conditional cleavage of PGAM5 by PARL, as it has been observed before (Sekine *et al.*, 2012) potentially acting as an oligomeric switch. Interestingly, PARL-catalyzed processing of the monomeric form of PGAM5 resembles other rhomboid family proteins in protein quality control, as for instance bacterial *S. sonnei* GlpG and Rhom7 as well as mammalian ERAD rhomboid RHBDL4 remove orphan subunits of multiprotein complexes (Began *et al.*, 2020; Fleig *et al.*, 2012; Knopf *et al.*, 2020; Liu *et al.*, 2020a). Moreover, it is uncertain how the mitochondrial membrane potential influences the oligomeric state of PGAM5 and further, to what extent it may influence the TM domain position within the IMM. An active and undisturbed $\Delta\Psi_{mito}$ might facilitate fixation of PGAM5 in the membrane, for instance under involvement of an AAA-ATPase that constantly pulls the PGAM5 TM domain towards the IMS, thus assisting oligomerization (with regard to the relatively low hydrophobicity of the PGAM5 TM domain). When $\Delta\Psi_{mito}$ is disrupted, the TM domain of PGAM5 might be able to slide out onto the matrix side, followed by recognition and PARL-catalyzed cleavage. The ability of AAA-ATPases to perform mechanical work and dislocation of moderately hydrophobic TM segments could be shown for instance by the *m*-AAA protease in yeast *S. cerevisiae*, which pulls the Ccp1 TM domain to the matrix prior to processing by the rhomboid protease Pcp1/Rbd1 in the IMM (Botelho *et al.*, 2013; Esser *et al.*, 2002; Tatsuta *et al.*, 2007). In line with the procaryotic ancestors of mitochondria, a comparable mechanism was described for CLPX in the ATP-dependent bacterial protease CLPXP, where enzyme-mediated unfolding of stable substrate TM domains requires mechanical pulling by the enzyme in combination with a transient stochastic reduction in protein stability (Aubin-Tam *et al.*, 2011; Maillard *et al.*, 2011).

3.6.1 Different stressors to induce mitophagy

To study the conditional cleavage of PGAM5 in living cells, it is mandatory to induce mitochondrial stress. PGAM5 cleavage was observed to increase already with the amount of experienced cell stress due to over-confluency or longer cultivation and handling, 'in-culture senescence' (own observations and personal communication). In turn, it could be observed that disruption of mitochondrial homeostasis by deletion of PGAM5 lead to cell senescence in mice *in vitro* and *in vivo,* due to hampered phosphorylation of DRP1 with subsequent decrease in mitochondrial fission/turnover, and elevated cellular ATP and ROS levels (Yu *et al.*, 2020). This work bases on disruption of $\Delta\Psi_{mito}$ with the uncoupling protonophore CCCP (**Figure 25**). Inducing mitochondrial stress at different levels will alter the subsequent stress responses, including activation of mitophagy, and might help to finetune also the induction of PGAM5 cleavage. Besides relatively harsh chemicals that are known to strongly induce PGAM5 cleavage, namely the uncouplers of oxidative phosphorylation CCCP and its counterpart carbonyl cyanide-p-trifluoromethoxyphenylhydrazone (FCCP) as well as the electron transfer chain inhibitors Antimycin A and Oligomycin, also proteotoxic stress in the IMS and matrix can induce mitochondrial stress responses. Since CCCP affects various biological processes, the electron transport chain complex III and ATP synthase inhibitors Antimycin A and Oligomycin, respectively, were also used to induce mitophagy (Lazarou *et al.*, 2015) and were recently shown to result in a time-dependent decrease in Tom20 in a manner similar to that induced by CCCP with cleavage of PGAM5 and its release into the cytosol in HeLa cells (Yamaguchi *et al.*, 2019). A mutant form of endonuclease G, EndoG^{N174A} was described to misfold and form protein aggregates in the IMS and thereby activate stress reactions (Radke *et al.*, 2008). Other studies could show that PINK1/Parkin-dependent mitophagy can be activated upon accumulation of misfolded proteins in the mitochondrial lumen when overexpressing the misfolded matrix protein ΔOTC, a deletion mutant of ornithine carbamoyltransferase (Jin and Youle, 2013). Alternatively, the HSP90 inhibitor Gamitrinib-triphenylphosphonium (G-TPP) can interfere with mitochondrial protein folding and induces PINK1 accumulation, ubiquitin phosphorylation, Parkin activation and its recruitment to mitochondria (Fiesel *et al.*, 2017) (**Figure 25**). Since I observed PARL-catalyzed cleavage of PGAM5 only after disruption of $\Delta\Psi_{mito}$ (**Figure S9**), I speculate that primarily the uncoupled membrane potential is sensed and not general mitochondrial stress.

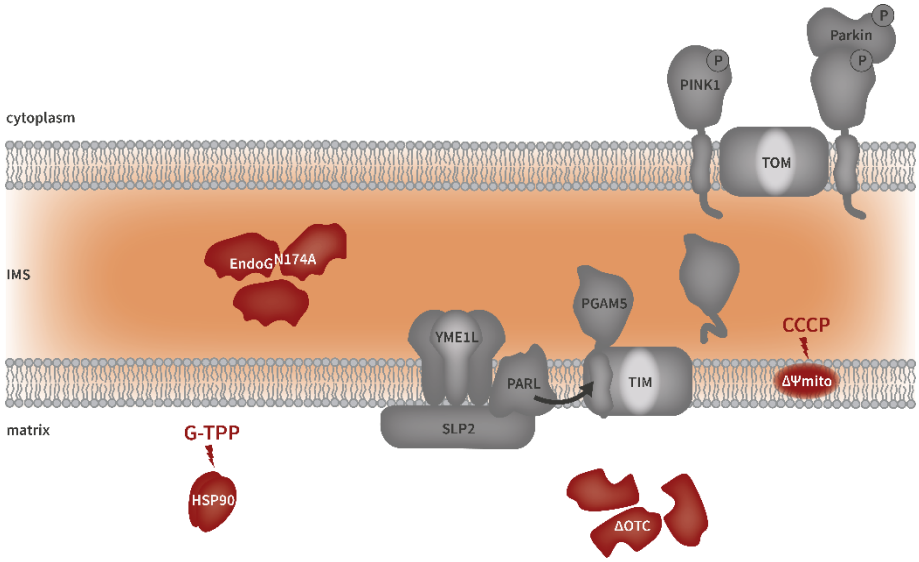

Figure 25 | Schematic overview of different stressors to induce mitophagy.
G-TPP interferes with mitochondrial protein folding in the matrix and induces PINK1 accumulation; EndoG^{N174A} misfolds and forms protein aggregates in the IMS resulting in stress reactions; the misfolded matrix protein ΔOTC leads to accumulation of misfolded proteins in the mitochondrial lumen; CCCP induces disruption of $\Delta\Psi_{mito}$.

3.7 Model of PARL-catalyzed PGAM5 cleavage in comparison to PINK1

PARL cleaves PINK1 in healthy mitochondria as an import intermediate and PGAM5 in damaged mitochondria as fully imported protein in an inversely correlated manner depending on the stress level (**Figure 26**). I hypothesize, that this different outcome is determined primarily by the speed of processing. PINK1 is rapidly processed as import intermediate because of a negative charged cluster in its juxtamembrane region and a suitable TM helix, leading to the constant release of a C-terminal cleavage fragment into the cytoplasm (Yamano and Youle, 2013). In contrast, PGAM5 is inserted into the IMM as a homodimer or even in a multimeric state, which prevents cleavage by PARL rendering PGAM5 a slowly processed substrate. This allows PGAM5 to maintain its membrane anchored form until IMM depolarization or other forms of mitochondrial stress trigger its disassembly into monomers that eventually undergo PARL-catalyzed cleavage (**Figure 26**). Contrary to that, the PGAM5 mutants C12S and C12L are more efficiently cleaved by PARL also in absence of the uncoupling protonophore CCCP, which leads to the speculation that they might be cleaved before they can dimerize. Thus, monomeric forms of IMM proteins, like seen with other cellular proteins, are more prone to cleavage and degradation (Juszkiewicz and Hegde, 2018). In my study, I observed PGAM5 mutants that showed enhanced processing when compared to PGAM5 wt but still behaved different than PINK1, suggesting that the fate of PGAM5 and PINK1 is determined by multiple factors. With regard to the important role of PGAM5 in mitochondrial dynamics, detailed mechanistic research on the cleavage requirements for the rhomboid protease PARL can contribute to a multifaceted understanding of disease-promoting mechanisms.

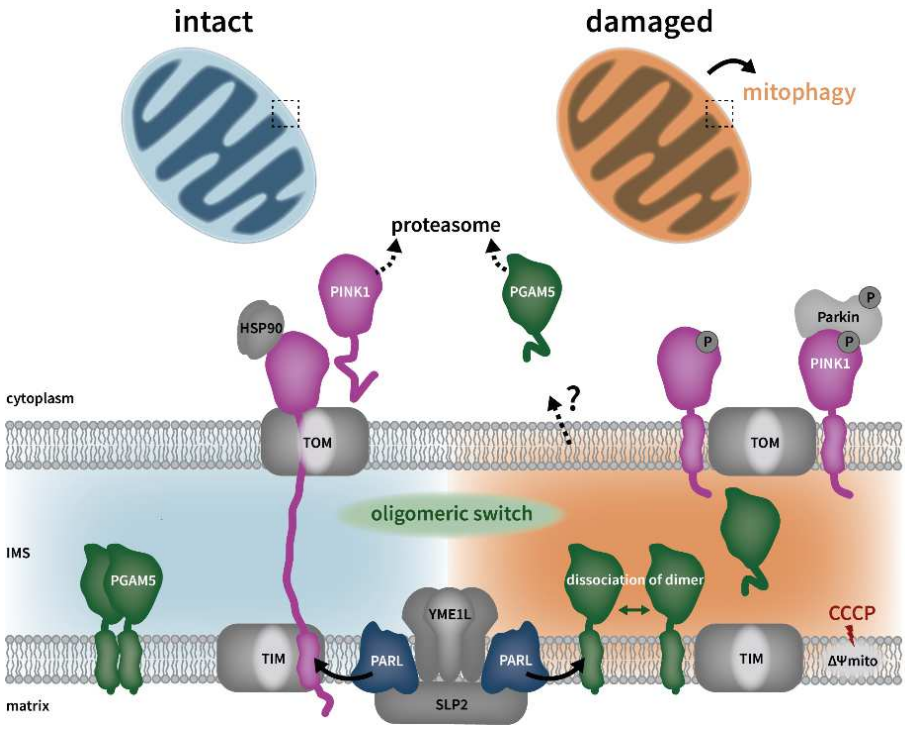

Figure 26 | Model of PARL-catalyzed PGAM5 cleavage in comparison to PINK1.
Depending on mitochondrial stress, PARL cleaves PINK1 (as an import intermediate) and PGAM5 (as fully imported protein) in an inversely correlated manner. Upon disruption of $\Delta\Psi_{mito}$, PGAM5 dimers or even oligomers disassemble into monomeric forms representing an "oligomeric switch" before getting processed by PARL. A portion of cleaved PGAM5 is released into the IMS, while another portion is released via a so far unknown mechanism into the cytoplasm where it undergoes proteasomal degradation.

3.8 Future perspectives

In this study, I reveal that the substrate recognition mechanism of PGAM5 by PARL relies on different substrate features with hierarchical importance, including a $\Delta\Psi_{mito}$-dependent oligomeric switch. Since there is no clear consensus sequence in all so far know PARL substrates, future studies on cleavage determinants may continue to include and link the observations to the co-evolution of rhomboids and their substrates by comparing prokaryotic and eukaryotic counterparts. The molecular mechanism of how PARL recognizes PGAM5 as conditional substrate is still unknown and raises the question if a voltage sensor in the IMM exist that is monitoring $\Delta\Psi_{mito}$. Thus, future studies should include the identification of a voltage-sensing component in this complex circuit. Since the IMM scaffold protein PHB2 was found to promote mitophagy by the PARL-PGAM5-PINK1 axis (Yan *et al.*, 2019), it is attractive to speculate that prohibitins may function as voltage sensors for the state of IMM polarization and are thereby involved in the oligomeric switch of PGAM5 cleavage. Alternatively, the membrane potential may be sensed by specialized TM domains as observed in voltage-sensing phosphatases (Okamura *et al.*, 2018). I envision a voltage sensor as a regulative capacity in the PARL substrate pool, either in the substrates itself or in substrate interactors, that are so far unknown. Although PGAM5 itself contains only one TM domain with positively

charged amino acid residues solely at the end of its C-terminus, combined TM domains of oligomeric PGAM5 might be able to function as such a sensor. Perhaps there might be other regions PGAM5 that could contribute to a comparable function.

All known PARL substrates play key roles in mitochondrial homeostasis and are linked to various diseases (Capo-Chichi *et al.*, 2015; Chen *et al.*, 2014b; Cheng *et al.*, 2011; Cheng *et al.*, 2021; Deas *et al.*, 2009; Ghezzi *et al.*, 2011; Horibata and Sugimoto, 2010; Jin *et al.*, 2010; Kanabus *et al.*, 2015; Saunders *et al.*, 2015; Wortmann *et al.*, 2015; Yang *et al.*, 2015). Their maturation and/or proper function relies on correct PARL-catalyzed cleavage, highlighting the importance of a detailed mechanistic understanding of their processing.

4. Materials & Methods

4.1 Materials

4.1.1 Equipment

Table 3 | List of equipment used.

Equipment	Supplier
Centrifuge 5415R	Eppendorf
Centrifuge 5417R	Eppendorf
Centrifuge 5810R	Eppendorf
Centrifuge Sorvall RC 6 Plus	Thermo Scientific
Centrifuge Universal 320	Hettich Zentrifugen
Electrophoresis Power Supply – EPS 301, 600, 601	GE Healthcare
Erlenmeyer flasks	Schott
F9S-4x1000y rotor	FiberLite Piramoon Techn., Inc.
F10-6x500y rotor	FiberLite Piramoon Techn., Inc.
Gel documentation GelDoc XR+	BioRad
Genesys 10S UV-Vis Spectrophotometer	Thermo Scientific
HERAcell 150i CO_2 incubator	Thermo Scientific
Heraeus Pico17 centrifuge	Thermo Scientific
Infors HT Multitron	Infors-AG, CH
Infors HT Orbitron	Infors-AG, CH
Laminar flow HeraSafe KS	Thermo Scientific
LAS4000	FujiFilm
Micropulser electroporation device	BioRad
Mini gel chamber	BioRad
Mini TransBlot.cell	BioRad
Multiple gel caster	Amersham Biosciences
NanoDrop™2000 Spectrophotometer	Thermo Scientific
Neubauer chamber	Heinz Herenz Medizinaltechnik
^{3}Prime Thermal Cycler	Techne
Pipettes (2 µL, 20 µL, 200 µL, 1000 µL)	Gilson
Labinco L28 Test-tube rotator	Labinco
RC-2-U (Shaker)	Adolf Kühner AG, Basel, CH
Robocycler Gradient 96	Stratagene
Rotator SB3	Stuart, Cole-Parmer, UK
Satorius CP64-0CE fine scale	Sartorius
Shaker DOS-10L	NeoLab
Shaker DRS-12	NeoLab
SI Analytics Lab 845 pH meter	Xylem Analytics

T-Personal 48 Thermal cycler	Biometra
Thermomixer comfort	Eppendorf
Thermomixer 5436	Eppendorf
Ti45 rotor	Beckman Instruments
Ti70 rotor	Beckman Instruments
UV transilluminator UVT-20 L	Herolab GmbH Laborgeräte
Zeiss LSM780 confocal microscope	Zeiss
Zeiss Axio Observer Z widefield microscope	Zeiss

4.1.2 Consumables

Table 4 | List of consumables used.

Consumable	Supplier
Ampliseal™ transparent microplate sealer	Greiner bio-one
Cell Scraper, 2-position blade, blade length: 1.7 cm	Sarstedt
Cover glasses, Ø12 mm	Kühnle GmbH
Cryotubes,1.8 mL	Simport
Cuvettes, 10 x 4 x 45 mm	Sarstedt
Fluoromount-G	SouthernBiotech
Immobilon-P Membrane 0.45 µm PVDF	Merck Millipore
Microscope slide, 26x76 mm	Heinz Herenz Hamburg
Micro Tube 1.5 mL	Sarstedt
Micro Tube 2.0 mL	Sarstedt
BD Microlance™ (27G x ¾", 0.4 mm x 19 mm)	Becton Dickinson
Pipet tips (10 µL, 200 µL, 1000 µL)	Sarstedt
Polycarbonate centrifuge tubes	Beckman Instruments
Safe seal tube 1.5 mL	Sarstedt
Syringes (1 mL, 2 mL, 10 mL, 50 mL)	Becton Dickinson
TC dish 100, Standard	Sarstedt
TC dish 150, Standard	Sarstedt
TC plate, 6 Well, Standard F	Sarstedt
TC plate, 12 Well, Standard F	Sarstedt
TC plate, 24 Well, Standard F	Sarstedt
TC plate, 96 Well, Standard F	Sarstedt
Tube 15 mL, 120 x 17 mm, PP	Sarstedt
Tube 50 mL, 144 x 28 mm, PP	Sarstedt
Whatman paper, 3 mm	Whatman
8-well microscopy chambers	ibidi

4.1.3 Chemicals

Table 5 | List of chemicals used.

Chemical	Supplier
3-((3-cholamidopropyl)dimethylammonio)-1-propanesulfonate (CHAPS)	AppliChem
3,4-Dichlor-isocumarin serine protease inhibitor	Sigma-Aldrich
4-(2-hydroxyethyl)-1-piperazineethanesulfonic acid (HEPES)	Sigma-Aldrich
6-Aminohexanoic acid	Sigma-Aldrich
4,4,5,5-d_4-L-Lysine•HCl	Silantes
$^{13}C_6{}^{15}N_2$-L-Lysine•HCl	Silantes
$^{13}C_6$-L-Arginine•HCL	Silantes
$^{13}C_6{}^{15}N_4$-L-Arginine•HCL	Silantes
Acetic acid	Carl Roth
Acrylamide/bisacrylamide Rotiphorese R 30 (37.5:1)	Carl Roth
Acrylamide Bis-AA Mix (40%, 32:1, 40% T, 3% C)	Sigma-Aldrich
ActivX Desthiobiotin-FP Serine Hydrolase Probe	Thermo Scientific
ActivX TAMRA-FP Serine Hydrolase Probe	Thermo Scientific
Agarose, electrophorese grade	AppliChem
Ammonium persulfate (APS)	AppliChem
Ampicillin Natriumsalz	AppliChem
Blasticidin S-HCl (10 mg/mL)	Thermo Scientific
Bromophenol blue	Chroma Waldeck GmbH
Carbonyl cyanide m-chlorophenyl hydrazone (CCCP)	Sigma-Aldrich
Chloramphenicol	AppliChem
cOmpleteTM Protease Inhibitor, EDTA-free	Roche
Coomassie Brilliant blue G-250	AllpiChem
Cycloheximide	AppliChem
Dialyzed FBS	Gibco, Life Technologies
Dimethyl sulfoxide (DMSO)	AppliChem
Dithiothreitol (DTT)	AppliChem
Dulbecco's Modified Eagle Medium (DMEM)	Gibco, Life Technologies
Epoxomicin	CalBiochem
Ethanol	Zentralbereich, INF, HD
Ethidium bromide solution 0.07%	AppliChem
Ethylene glycol teraacetic acid (EGTA)	Carl Roth GmbH + Co. KG
Ethylenediamineteraacetic acid (EDTA)	Merck
Fetal bovine serum (FBS)	Gibco, Life Technologies
GeneRulerTM 1 kb DNA ladder	Thermo Scientific
Geneticin™ (G418 Sulfate)	Gibco, Life Technologies

Glucose monohydrate	AppliChem
GlutaMAX™, 100x	Gibco, Life Technologies
L-Glutamine (200 mM)	Gibco, Life Technologies
Glycerol	Sigma-Aldrich
Glycine	Sigma-Aldrich
Hoechst 33342 (bisBenzimide H 33342 trihydrochloride)	Sigma-Aldrich
Hydrochloric acid	Carl Roth
Hygromycin B	Thermo Scientific
Isopropanol	AppliChem
Kanamycin sulfate	AppliChem
Magnesium acetate ($Mg(OAc)_2$)	AppliChem
Magnesium chloride ($MgCl_2$)	AppliChem
Methanol	AppliChem
MG132	CalBiochem
n-Dodecyl-β-D-Maltopyranoside (DDM)	Anatrace
N-ethylmaleimide (NEM)	AppliChem
N,N,N',N'-tetramethylethylendiamine (TEMED)	Sigma-Aldrich
Nonfat dried milk powder	AppliChem
Opti-Minimal Essential Medium (MEM)®	Gibco, Life Technologies
Paraformaldehyde	Riedel-de Haën
Penicillin-Streptomycin, 10,000 U/mL	Gibco, Life Technologies
Phenylmethansulfonylfluorid (PMSF)	AppliChem
Polyethylene glycol 3350 or 8000, (PEG)	Sigma-Aldrich
Polyethylenimine (PEI)	Polyciences, Inc.
Poly-L-Lysine solution, MW 150,000-300,000, 0.01%	Sigma-Aldrich
Potassium acetate (KOAc)	AppliChem
Potassium chloride (KCl)	AppliChem
Potassium dihydrogen phosphate (KH_2PO_4)	Riedel-deHaen
Potassium hydroxide (KOH)	AppliChem
PageRuler Plus Prestained Protein Ladder	Thermo Scientific
Protein G Sepharose 4 Fast Flow	GE Healthcare
RNase, DNase-free	AppliChem
Sodium carbonate (Na_2CO_3)	AppliChem
Sodium chloride (NaCl)	Bernd Kraft GmbH
Sodium dihydrogen phosphate (NaH_2PO_4)	AppliChem
Sodium dodecyl sulfate (SDS)	AppliChem
Sodium hydroxide (NaOH)	AppliChem
Sodium pyruvate (100 mM)	Gibco, Life Technologies
D-Sucrose	AppliChem
Trichloroacetic acid (TCA)	AppliChem
Tris	Carl Roth
Bis-Tris	Carl Roth

Tricine	Carl Roth
Triton X-100, 10%, peroxide free	AppliChem
Trypsin-EDTA (0.05%), phenol red	Gibco, Life Technologies
Tryptone	Becton Dickinson GmbH
Tween-20	AppliChem
β-mercaptoethanol	Sigma-Aldrich
WesternBright ECL HRP substrate	Advansta
Yeast extract	Carl Roth GmbH + Co.KG
Zeocin™ Selection Reagent	Invivogen

4.1.4 Buffers and media

Table 6 | List of buffer and media compositions.

Buffer/Medium	Ingredient	Content
Anode buffer (10x), BN	Bis-Tris, pH 7.0	500 mM
Blocking solution	TBS-T	1x
	Non-fat dried milk powder	5% (w/v)
Blotting buffer, wet blot	Tris	25 mM
	Glycine	192 mM
	Methanol	20% (v/v)
BN-sample buffer (40x)	6-Aminohexanoic acid	500 mM
	Bis-Tris, pH 7.0	100 mM
	Coomassie G-250	5% (w/v)
BN-transfer buffer	Tris	25 mM
	Glycine	150 mM
	SDS	0.02% (v/v)
	Methanol	20% (v/v)
Cathode buffer dark-blue (10x), BN	Tricine, pH 7.0	500 mM
	Bis-Tris	150 mM
	Coomassie G-250	0.2% (w/v)
Cathode buffer light-blue (10x), BN	Tricine, pH 7.0	500 mM
	Bis-Tris	150 mM
	Coomassie G-250	0.02% (w/v)

Cleavage buffer, *in vitro*	Tris, pH 8.0	50 mM / 20mM
	NaCl	150 mM
	Glycerol	10% (v/v)
	DDM	0.3% (w/v)
Coomassie staining solution	Coomassie Brilliant Blue-G250	0.2% (w/v)
	Methanol	50% (v/v)
Coomassie destaining solution	Methanol	40% (v/v)
	Acetic acid	20% (v/v)
	Acetic acid	20% (v/v)
Elution buffer (D), *in vitro*	HEPES, pH 7.4	50 mM
	NaCl	300 mM
	Glycerol	10% (v/v)
	Imidazole	400 mM
	DDM	0.05% (w/v)
Fixation solution, BN	Methanol	40%
	Acetic acid	10%
Gel buffer (3x), BN	6-Aminohexanoic acid	200 mM
	BisTris-Cl, pH 7.0	150 mM
Hypotonic buffer, SILAC	HEPES-KOH, pH 7.4	0.01 M
	$MgCl_2$	0.0015 M
	KOAc	0.01 M
	DTT	0.5 µL/mL
	Roche complete	¼ tablet/10 mL
	PMSF	few crystals
IF antibody solution	IF blocking buffer	99.9%
	Triton X-100	0.1% (v/v)
	antibody	x µL
IF blocking buffer	FBS	20% (v/v)
	PBS, 10x	1x
	H_2O	
IF fixation buffer, 25 mL	Paraformaldehyde	4% (w/v)
	NaOH, 1 M	0.002 M
	PBS, 10x	1.1 mL

	PBS, 1x	13.5 mL
	H_2O	10 mL
Isolation buffer (hypotonic)	D-Sucrose	250 mM
	Tris-Cl, pH 7.4	10 mM
	HEPES, pH 7.4	10 mM
	EGTA	0.1 mM
	Roche complete	¼ tablet/10 mL
	PMSF	few crystals
LB (Luria-Bertani) liquid medium, 1 L (pH 7.0)	Tryptone	10 g
	NaCl	10 g
	Yeast extract	5 g
	NaOH for pH adjustment	x mL
	H_2O	to 1 L
LB agar, 1 L	LB liquid medium	1 L
	Agar	15 g/L
Laemmli buffer (10x)	Tris-HCl, pH 6.8	0.25 M
	Glycine	1.92 M
	SDS	1% (w/v)
Lysis buffer (A), *in vitro*	HEPES, pH 7.4	20 mM
	NaCl	150 mM
	$MgCl_2$	5 mM
	Glycerol	10% (v/v)
	PMSF	1 mM
	β-mercaptoethanol	5 mM
Phosphate-buffered saline (PBS) (pH 7.4)	NaH_2PO_4	0.01 M
	KH_2PO_4	0.0014 M
	KCl	0.0027 M
	NaCl	0.14 M
PBS-EDTA	PBS	1x
	EDTA, pH 8.0	0.001 M
	Glucose	0.2 g/L
PVDF stripping solution, harsh	Tris-HCl, pH 7.4	0.0625 M
	SDS	2% (w/v)

SDS-sample buffer (4x), Laemmli	Tris-HCl, pH 6.8	0.2 M
	EDTA, pH 8.0	0.04 M
	Glycerol	20% (v/v)
	SDS	8% (w/v)
	Bromophenol blue	0.01% (w/v)
	β-mercaptoethanol	20% (v/v)
SILAC medium, light labelling	DMEM, 500 mL	1x
	dialyzed FBS	10% (v/v)
	Penicillin/Streptomycin	1% (v/v)
	GlutaMAX	1% (v/v)
	Arg (100 mg mL^{-1})	0.430 mL
	Lys (100 mg mL^{-1})	0.750 mL
SILAC medium, medium labelling	DMEM, 500 mL	1x
	dialyzed FBS	10% (v/v)
	Penicillin/Streptomycin	1% (v/v)
	GlutaMAX	1% (v/v)
	$^{13}C_6$-L-Arg•HCl (100 mg mL^{-1})	0.431 mL
	4,4,5,5-d_4-L-Lys•HCl (100 mg mL^{-1})	0.755 mL
SILAC medium, heavy labelling	DMEM, 500 mL	1x
	dialyzed FBS	10% (v/v)
	Penicillin/Streptomycin	1% (v/v)
	GlutaMAX	1% (v/v)
	$^{13}C_6{}^{15}N_4$-L-Arg•HCl (100 mg mL^{-1})	0.439 mL
	$^{13}C_6{}^{15}N_2$-L-Lys•HCl (100 mg mL^{-1})	0.760 mL
Semi-dry blotting buffer (10x)	Tris-HCl, pH 7.5	0.48 M
	Glycine	0.39 M
Semi-dry blotting buffer (1x)	10x Semi-dry blotting buffer	10% (v/v)
	Methanol	20% (v/v)
	H_2O	70% (v/v)
Solubilization buffer, IP	HEPES-KOH, pH 7.4	50 mM
	NaCl	150 mM
	$Mg(OAc)_2$	2 mM
	EGTA, pH 8.0	1 mM
	Glycerol	10% (v/v)
	Triton X-100	1% (v/v)
	Roche complete	¼ tablet/10 mL

	PMSF	few crystals
Solubilization buffer (B), *in vitro*	HEPES, pH 7.4	50 mM
	NaCl	150 mM
	$MgCl_2$	5 mM
	Glycerol	10% (v/v)
	PMSF	1 mM
	β-mercaptoethanol	5 mM
Solubilization buffer (2.5x), BN	Tris-Cl, pH 7.5	20 mM
	NaCl	50 mM
	$MgCl_2$	1.5 mM
	EGTA	1 mM
	Glycerol	10% (v/v)
	Triton X-100	2.5% (v/v)
Storage buffer	Tris-HCl, pH 7.4	0.01 M
	$CaCl_2$	0.1 M
	Glycerol	15% (v/v)
TAE buffer, pH 7.8 (50x)	Tris-HCl, pH 7.5	2 M
	EDTA, pH 8.0	0.5 M
Tris-buffered saline (TBS)	Tris-HCl, pH 7.4	0.01 M
	NaCl	0.15 M
TBS-T	TBS	1x
	Tween-20	0.1% (v/v)
TSS (2x)	PEG (3350 or 8000)	20% (w(v)
	DMSO	10% (v/v)
	$MgCl_2$, pH 6.5	100 mM
	in LB-medium	
Wash buffer (C), *in vitro*	HEPES, pH 7.4	50 mM
	NaCl	300 mM
	Glycerol	10% (v/v)
	Imidazole	50 mM
	DDM	0.05% (w/v)

4.1.5 Lists of antibodies

Table 7 | List of primary antibodies.

Primary antibody	Species	Source	Dilution	Cat #
β-actin (AC-15)	mouse, monoclonal	Sigma-Aldrich	1:4000	A1978
AIF	mouse, monoclonal	Santa Cruz	1:500	sc-13116
FLAG (M2)	mouse, monoclonal	Sigma-Aldrich	1:1000	F1804
GFP	rabbit, polyclonal	Abcam	1:1000	ab6556
GFP	mouse, monoclonal	Roche	1:1000	11814460001
His5 (Penta His)	mouse, monoclonal	Qiagen	1:1000	34660
MBP	mouse, monoclonal	New England BioLabs	1:10000	E8032S
TOM20 (FL-145)	rabbit, polyclonal	Santa Cruz	1:200	sc-11415
TOM20 (F-10)	mouse, monoclonal	Santa Cruz	1:400	sc-17764
PGAM5	mouse, monoclonal	Thermo Fisher	1:1000	CL0624
PARL	rabbit, polyclonal	Abcam	1:300	ab45231
PARL	rabbit, polyclonal	Rockland	1:1000	600-401-J27

Table 8 | List of secondary antibodies.

Secondary antibody	Conjugation	Source	Dilution	Cat #
donkey-α-rabbit IgG (H+L)	Horseradish peroxidase	Dianova	1:10000	711-035-152
donkey-α-mouse IgG (H+L)	Horseradish peroxidase	Dianova	1:10000	715-035-150
goat-α-mouse IgG (H+L)	Alexa Fluor® 488	Invitrogen	1:500	A-11029
goat-α-rabbit IgG (H+L)	Alexa Fluor® 633	Invitrogen	1:500	A-21070

4.1.6 Commercial Kits

Table 9 | List of commercial Kits used.

Kit	Supplier	Cat #
LipofectamineTM RNAiMAX transfection reagent	Invitrogen	13778030
NucleoSpin RNA isolation Kit	Macherey-Nagel	740955.50
NucleoSpin Gel and PCR Clean-up Kit	Macherey-Nagel	740609.250
NucleoBond plasmid Kit	Macherey-Nagel	740588.250
NucleoBond PC100 Midi-Prep Kit	Macherey-Nagel	740573.100
KOD Hot Start DNA Polymerase	Merck Millipore	71068-3
RevertAid First Strand cDNA Synthesis Kit	Thermo Scientific	K1622
SensiFASTTM SYBR No-ROX Kit	Bioline	BIO-98005

4.1.7 Plasmids

Table 10 | List of expression vectors (Amp: ampicillin, Cm: chloramphenicol, Kan: kanamycin).

Plasmid name	Resistance	Vector	Internal #	Source
pBAD24_His6-PARLbeta	Amp	pBAD24	HD1127	Baptiste Cordier
pBAD24_His6-S277A-PARLbeta	Amp	HD1127	HD1370	This study
pBAD33_MBP-PINK1	Cm	pBAD33	HD1337	(Bock, 2018)
pBAD33_MBP-PGAM5	Cm	pBAD33	HD1335	(Bock, 2018)
pcDNA3.1(+)	Amp	-	Pla7	Invitrogen
pcDNA3.1_GHITM-FLAG	Amp	Pla7	HD930	(Schwager, 2015)
pcDNA3.1_PGAM5-FLAG	Amp	pcDNA3.1	HD957	(Sekine *et al.*, 2012)
pcDNA3.1_C12L-PGAM5-FLAG	Amp	HD957	HD1385	This study
pcDNA3.1_C12S/G17L-PGAM5-FLAG	Amp	HD957	HD1368	This study
pcDNA3.1_C12S-PGAM5-FLAG	Amp	HD957	HD1217	This study
pcDNA3.1_C12S/S18L-PGAM5-FLAG	Amp	HD957	HD1365	This study
pcDNA3.1_CG12/13RH-PGAM5-FLAG	Amp	HD957	HD1504	This study
pcDNA3.1_G13L-PGAM5-FLAG	Amp	HD957	HD1238	This study
pcDNA3.1_G16L-PGAM5-FLAG	Amp	HD957	HD1344	This study
pcDNA3.1_G17L-PGAM5-FLAG	Amp	HD957	HD1345	This study
pcDNA3.1_GG16/17LL-PGAM5-FLAG	Amp	HD957	HD1229	This study
pcDNA3.1_S18L-PGAM5-FLAG	Amp	HD957	HD1233	This study
pcDNA3.1_F23A-PGAM5-FLAG	Amp	HD957	HD1671	This study
pcDNA3.1_S24F-PGAM5-FLAG	Amp	HD957	HD958	(Sekine *et al.*, 2012)
pcDNA3.1_G29L-PGAM5-FLAG	Amp	HD957	HD1216	This study
pcDNA3.1_P31L-PGAM5-FLAG	Amp	HD957	HD1245	This study
pcDNA3.1_G29L/P31L-PGAM5-FLAG	Amp	HD957	HD1248	This study
pcDNA3.1_GG34/35EE-PGAM5-FLAG	Amp	HD957	HD1464	This study
pcDNA3.1_ΔC-PGAM5-FLAG	Amp	pcDNA3.1	HD1390	This study
pcDNA3.1_ΔC/G17L-PGAM5-FLAG	Amp	HD1390	HD1474	This study
pcDNA3.1_ΔC/S18L-PGAM5-FLAG	Amp	HD1390	HD1417	This study
pcDNA3.1_AAxxAA-PGAM5-FLAG	Amp	HD957	HD1503	This study
pcDNA3.1_DmPGAM5-FLAG	Amp	pcDNA3.1	HD1693	This study
pcDNA3.1_PGAM5-PINK1$^{112\text{-}151}$-FLAG	Amp	pcDNA3.1	HD1492	This study
pcDNA3.1_PINK1-FLAG	Amp	pFLAG-N1	HD31	(Meissner *et al.*, 2015)
pcDNA3.1_EE112/113AV-PINK1-FLAG	Amp	HD31	HD1480	This study
pcDNA3.1_EndoG-N174A-3xFLAG	Amp	pcDNA3.1	HD1508	This study
pcDNA3.1_ΔOTC-3xFLAG	Amp	pcDNA3.1	HD876	Lemberg lab
pCFP-N1-PGAM5	Kan	pCFP-N1	HD1303	Alireza Pouya
pCFP-N1-C12S-PGAM5	Kan	pCFP-N1	HD1319	Alireza Pouya
pCFP-N1-S18L-PGAM5	Kan	pCFP-N1	HD1325	Alireza Pouya
pEGFP-N1	Kan	-	Pla186	Clontech

pEGFP-N1_PGAM5-GFP	Kan	Pla186	HD1302	Alireza Pouya
pET25b(+)	Amp	-	CA118	Novagen
pET25b(+)_GlpG-His6	Amp	pET25b(+)	Pla121	(Lemberg *et al.*, 2005)
pET25b(+)_GlpG-G257A-His6	Amp	Pla121	HD1653	This study
pET25b(+)_GlpG-G261A-His6	Amp	Pla121	HD1654	This study
pET25b(+)_GlpG-K191A-His6	Amp	Pla121	HD1652	This study
pET25b(+)_GlpG-R137A-His6	Amp	Pla121	HD1650	This study
pET25b(+)_GlpG-W136A-His6	Amp	Pla121	HD1649	This study
pET25b(+)_GlpG-Y138A-His6	Amp	Pla121	HD1651	This study
pET25b(+)-MBP-PGAM5	Amp	pET25b(+)	HD1179	Baptiste Cordier
pET25b(+)-MBP-C12L-PGAM5	Amp	HD1179	HD1396	This study
pET25b(+)-MBP-C12S-PGAM5	Amp	HD1179	HD1218	This study
pET25b(+)-MBP-C12S/G17L-PGAM5	Amp	HD1179	HD1371	This study
pET25b(+)-MBP-C12S/S18L-PGAM5	Amp	HD1179	HD1366	This study
pET25b(+)-MBP-G13L-PGAM5	Amp	HD1179	HD1192	Baptiste Cordier
pET25b(+)-MBP-G16L-PGAM5	Amp	HD1179	HD1346	This study
pET25b(+)-MBP-G17L-PGAM5	Amp	HD1179	HD1347	This study
pET25b(+)-MBP-GG16/17LL-PGAM5	Amp	HD1179	HD1194	Baptiste Cordier
pET25b(+)-MBP-S18L-PGAM5	Amp	HD1179	HD1307	This study
pET25b(+)-MBP-F23A-PGAM5	Amp	HD1179	HD1670	This study
pET25b(+)-MBP-S24F-PGAM5	Amp	HD1179	HD1195	This study
pET25b(+)-MBP-G29L-PGAM5	Amp	HD1179	HD1193	Baptiste Cordier
pET25b(+)-MBP-P31L-PGAM5	Amp	HD1179	HD1246	This study
pET25b(+)-MBP-G29L/P31L-PGAM5	Amp	HD1179	HD1247	This study
pET25b(+)-MBP-Spitz	Amp	pET25b(+)	HD1306	This study
pET25b(+)_PARLbeta-His6	Amp	pET25b(+)	HD987	Baptiste Cordier
pET25b(+)_S277A-PARLbeta-His6	Amp	HD987	HD1079	Baptiste Cordier
pET28a(+)	Kan	-	HD986	Novagen
pET28a(+)_His6-PARLbeta	Kan	pET28a(+)	HD989	Baptiste Cordier
pET28a(+)_His6-S277A-PARLbeta	Kan	HD989	HD1231	This study

4.1.8 *E. coli* strains

Table 11 | List of *E. coli* strains used in this study.

Strain	Genotype	Purpose
DH5α	F–, Φ80lacZΔM15 Δ(lacZYA-argF)U169, recA1, endA1, hsdR17, phoA, supE44, thi-1, gyrA96, relA1	Plasmid amplification
BL21(DE)pLysS	F–, ompT, hsdSB (rB–, mB–), dcm, gal, λ(DE3), pLysS, Cm^R	expression: GlpG

Rosetta 2 (DE)	F–, ompT, hsdSB (rB– mB–), dcm, gal, λ(DE3), pRARE2, Cm^R	expression: PARL, chimeric substrates
JW5687	F–, Δ(araD-araB)567, ΔlacZ4787(::rrnB-3), λ-, ΔglpG757::kan, rph-1, Δ(rhaD-rhaB)568, hsdR514	co-expression *in vivo*

4.1.9 Software and databases

Table 12 | List of software and databases used.

Name and version	Source/Reference
EndNote, v.X9	Clarivate Analytics
Fiji (ImageJ), 64 bit, v.2.0.0.-rc49/1.51a	(Schindelin *et al.*, 2012)
Ensembl	(Yates *et al.*, 2020)
Clustal Omega	(Sievers *et al.*, 2011)
UniProt	(The UniProt, 2021)
I-TASSER	(Roy *et al.*, 2010)
ExPASy ProtScale	(Gasteiger *et al.*, 2003)
TMHMM Server, v. 2.0	(Krogh *et al.*, 2001)
AlphaFold	(Jumper *et al.*, 2021)
OPM server	(Lomize *et al.*, 2012)
GraphPad Prism, v.9.1.2.226	GraphPad Software, Inc.
Illustrator CC2021	Adobe Systems
InDesign CC2021	Adobe Systems
Perseus, v.1.5.1.6	(Tyanova *et al.*, 2016)
Microsoft Office Professional Plus 2016, v.16.0.14131.20278	Microsoft

4.2 Molecular biology methods

4.2.1 Polymerase Chain Reaction

Polymerase chain reaction (PCR)-based amplification of plasmid or genomic DNA was prepared as given below.

Table 13 | Standard PCR reaction setup.
Components, volumes, and final concentrations for standard PCR reaction.

Component	Volume	Final Concentration
10x KOD Hot Start DNA polymerase buffer	5.0 µL	1x
25 mM $MgSO_4$	3.0 µL	1.5 mM
dNTPs (2 mM each)	5.0 µL	0.2 mM
forward primer (10 µM)	1.5 µL	0.3 µM
reverse primer (10 µM)	1.5 µL	0.3 µM
template DNA	50 ng (plasmid DNA) 30 ng (genomic DNA)	
KOD DNA polymerase (1 U/µL)	1 µL	0.02 U/µL
ddH_2O	to 50 µL	

Table 14 | PCR cycle conditions.
Temperature, times, and cycle numbers for PCR-based amplification.

Step	Temperature	Time (min:s)	Cycle
initial denaturation	95°C	2:00	1 x
amplification			
denaturation	95°C	0:20	
annealing	lowest primer T*m*°C	0:20	30 x
extension	70°C	0:20/kb	
final extension	70°C	10:00	1 x
final hold	4°C	∞	1 x

The obtained PCR product was separated by gel electrophoresis on a 1.0% (w/v) agarose gel in 1x TAE buffer containing 0.001% (v/v) ethidium bromide at 100 V/cm for appropriate time. For size determination, 5 µL 1 kB DNA Ladder was used as marker. DNA was visualized and documented using the GelDoc® XR+ gel imager and accompanying software (BioRad). If required, the DNA band of correct size was excised from the gel on a UV transilluminator and purified using the Gel and PCR clean-up Kit according to the manufacturer's protocol. DNA was eluted in 20 µL ddH_2O.

4.2.2 Generation of expression constructs

All primers to clone the constructs (**Table 10**) used in this study, are listed in (**Table 15**). Construction of pcDNA3.1-GHITM-FLAG, pcDNA3.1-PARL, pcDNA3.1-PINK1-FLAG, pcDNA3.1-PGAM5-FLAG and pcDNA3.1-PGAM5^{S24F}-FLAG expression plasmids for human tissue culture have been described previously (Meissner *et al.*, 2011; Schwager, 2015; Sekine *et al.*, 2012). Mutations in the transmembrane domain and juxtamembrane region of PGAM5 and PINK1 were introduced by site-directed mutagenesis following the protocol of the Stratagene's QuikChange® Site-Directed Mutagenesis Kit (Agilent Technologies), see (**Table 16**). For PGAM5 lacking the C-terminal tail (ΔC), primers to PCR amplify EcoRI-PGAM5 (amino acids 1-277) from pcDNA3.1-PGAM5-FLAG (HD957) were designed, adding an early FLAG-tag with stop codon and XbaI restriction site to clone the new insert into pcDNA3.1 between EcoRI and XbaI, see (**chapter 4.2.1** and **Table 15**). Drosophila PGAM5 (ID: Pgam5-RA cds) was ordered as custom DNA oligo gBlock (Integrated DNA Technologies, IDT), containing the codon-optimized coding sequence with a FLAG-tag surrounded by an EcoRI and XbaI restriction site, to clone into pcDNA3.1 between EcoRI and XbaI. PGAM5-PINK1$^{112-151}$-FLAG and EndoG^{N174A}-3xFLAG were ordered as custom DNA oligo gBlocks (Integrated DNA Technologies, IDT) surrounded by an EcoRI and XbaI restriction site, to clone into pcDNA3.1 between EcoRI and XbaI. All pcDNA3.1-constructs were verified by sequencing (GATC/Eurofins) using CMV-fwd, and pcDNA3.1-RP primers (**Table 15**).

Recombinant substrates (MBP-PGAM5, MBP-Spitz) and enzymes (GlpG-His6, PARL-His6) for the detergent-micelle based *in vitro* system, were cloned using the pET-vector system (Novagen). The sequence of the human PGAM5 transmembrane (TM) region (amino acids 1-46) and of the *D. melanogaster* Spitz TM region (amino acids 133-174) were cloned into *E. coli* expression vector pET25b(+) (Novagen) between SpeI and KpnI restriction sites with an N-terminal maltose-binding protein (MBP) and C-terminal Thioredoxin 1 (TrxA) followed by a triple FLAG-tag (3xFLAG) and a C-terminal hexahistidine (His6)-tag. Corresponding PINK1 and PGAM5 TM domain constructs were generated in a pBAD33 vector (Guzman *et al.*, 1995) as described in the master thesis of (Bock, 2018). Construction of the pET25b(+)-GlpG *E. coli* expression plasmid has been described in (Lemberg *et al.*, 2005). The sequence of β-cleaved human PARL was cloned into the *E. coli* expression vectors pET25(b)+ and pET28a(+) (Novagen) between NdeI and KpnI restriction sites with a C-terminal His6-tag, and between NdeI and HindIII restriction sites with a N-terminal His6-tag, respectively. Generation of the pBAD24_His6-PARL construct was described in the master thesis of (Bock, 2018). Point mutations in PARL and GlpG were introduced by site-directed mutagenesis according to Stratagene's QuikChange® protocol. All pET- and pBAD-constructs were verified by sequencing (GATC/Eurofins) using MBP-fwd, T7-fwd, pET-RP and pBAD-FP primers, respectively (**Table 15**).

Table 15 | Primer sequences for the generation of PGAM5, PINK1, PARL and GlpG expression constructs.
Fwd: forward, Rev: reverse.

Primer name	Sequence (5' → 3')
GlpG-G257A_quik_fwd	GCACACATCGCCGCATTAGCCGTGGGT
GlpG-G257A_quik_rev	ACCCACGGCTAATGCGGCGATGTGTGC
GlpG-G261A_quik_fwd	GGGTTAGCCGTGGCATTAGCGATGGCT
GlpG-G261A_quik_rev	AGCCATCGCTAATGCCACGGCTAACCC
GlpG-K191A_quik_fwd	TATGTGCAGCAAGCATTCAGCGGGCCG
GlpG-K191A_quik_rev	CGGCCCGCTGAATGCTTGCTGCACATA
GlpG-R137A_quik_fwd	TTTGAGTTCTGGGCATACTTCACCCAC
GlpG-R137A_quik_rev	GTGGGTGAAGTATGCCCAGAACTCAAA
GlpG-W136A_quik_fwd	AAATTTGAGTTCGCACGTTACTTCACC
GlpG-W136A_quik_rev	GGTGAAGTAACGTGCGAACTCAAATTT
GlpG-Y138A_quik_fwd	GAGTTCTGGCGTGCATTCACCCACGCG
GlpG-Y138A_quik_rev	CGCGTGGGTGAATGCACGCCAGAACTC
hPARLB-S277A_quik_fwd	TCACTTGGTGCAGCTGGTGCCATCA
hPARLB-S277A_quik_rev	TGATGGCACCAGCTGCACCAAGTGA
PGAM5-AAxxAA_quik_fwd	GGCCCCGGTGTCGCGGCCCCCAACGCGGCCAGGCGAGAAC CA
PGAM5-AAxxAA_quik_rev	TGGTTCTCGCCTGGCCGCGTTGGGGGCCGCGACACCGGGGCC
PGAM5-C12L_quik_fwd	CAGCTGGCGGCCCTAGGGCTGGCCGGG
PGAM5-C12L_quik_rev	CCCGGCCAGCCCTAGGGCCGCCAGCTG
PGAM5-C12S_quik_fwd	CAGCTGGCGGCCAGTGGGCTGGCCGGG
PGAM5-C12S_quik_rev	CCCGGCCAGCCCACTGGCCGCCAGCTG
PGAM5-G13L_quik_fwd	GCCCCCGGCCAGTAGGCAGGCCGCCAG
PGAM5-G13L_quik_rev	CTGGCGGCCTGCCTACTGGCCGGGGGC
PGAM5-CG12/13RH_quik_fwd	CAGCTGGCGGCCCGCCACCTGGCCGGGGGC
PGAM5-CG12/13RH_quik_rev	GCCCCCGGCCAGGTGGCGGGCCGCCAGCTG
PGAM5-G16L_quik_fwd	TGCGGGCTGGCCCTAGGCTCGGCCGCC
PGAM5-G16L_quik_rev	GGCGGCCGAGCCTAGGGCCAGCCCGCA
PGAM5-G17L_quik_fwd	GGGCTGGCCGGGCTATCGGCCGCCGTG
PGAM5-G17L_quik_rev	CACGGCGGCCGATAGCCCGGCCAGCCC
PGAM5-GG16/17LL_quik_fwd	AGAGCACGGCGGCCGATAGTAGGGCCAGCCCGCAGGCC
PGAM5-GG16/17LL_quik_rev	GGCCTGCGGGCTGGCCCTACTATCGGCCGCCGTGCTCT
PGAM5-S18L_quik_fwd	CTGGCCGGGGGCCTAGCCGCCGTGCTC
PGAM5-S18L_quik_rev	GAGCACGGCGGCTAGGCCCCCGGCCAG
PGAM5-F23A_quik_fwd	GCCGCCGTGCTCGCCTCGGCCGTGGCG
PGAM5-F23A_quik_rev	CGCCACGGCCGAGGCGAGCACGGCGGC
PGAM5-G29L_quik_fwd	GCGCGCGGCTTTAGTACCGCCACGGCCGAGAAGA
PGAM5-G29L_quik_rev	TCTTCTCGGCCGTGGCGGTACTAAAGCCGCGCGC
PGAM5-G29L/P31L_quik_fwd	GCGGTACTAAAGCTGCGCGCAGGCGGG

PGAM5-G29L/P31L_quik_rev	CCCGCCTGCGCGCAGCTTTAGTACCGC
PGAM5-P31L_quik_fwd	GCGGTAGGGAAGCTGCGCGCAGGCGGG
PGAM5-P31L_quik_rev	CCCGCCTGCGCGCAGCTTCCCTACCGC
PGAM5-GG34/35EE_quik_fwd	AAGCCGCGCGCAGAGGAGGACGCGGAGCCA
PGAM5-GG34/35EE_quik_rev	TGGCTCCGCGTCCTCCTCTGCGCGCGGCTT
PINK1-EE112/113AV_quik_fwd	CTGGGCCTCATCGCGGTAAAACAGGCGGAG
PINK1-EE112/113AV_quik_rev	CTCCGCCTGTTTTACCGCGATGAGGCCCAG
SpeI_Spitz-TMD_fwd	atatACTAGTAAGAGGCCGCGTCCGATGTTG
Spitz-TMD_KpnI_rev	atatGGTACCGGCCTTCTTGGCAGCCCGCTGC
CMV-F_fwd	CGCAAATGGGCGGTAGGCGT
MBP_seq_fwd	CATGGTCCAACATCGACAC
pcDNA3.1-RP_rev	CAAACAACAGATGGCTGGC
pET-RP_rev	CTAGTTATTGCTCAGCGG
T7_fwd	TAATACGACTCACTATAGGG

Table 16 | PCR cycle setting for site-directed mutagenesis.

Step	Temperature	Time (min:s)	Cycle
initial denaturation	95°C	2:00	1 x
amplification			
denaturation	95°C	0:20	
annealing	70°C	0:20	25 x
extension	70°C	3:30	
final extension	70°C	10:00	1 x
final hold	4°C	∞	1 x

After PCR, DpnI (20 U/µL) enzyme was directly added to the PCR product and incubated for 1 h at 37°C to digest the non-mutated, parental dsDNA template. 10-17 µL of the DpnI-digested DNA was used for transformation into chemical-competent DH5α *Escherichia coli* cells, plated on LB-agar plates containing ampicillin and grown overnight at 37°C. Bacterial colonies from this plate were used to inoculate 4 mL LB medium containing ampicillin (at 100 µg/mL) and incubated overnight at 37°C on an orbital shaker at 120 rpm (RC-2-U, Adolf Kühner AG) or alternatively at 200 rpm (Infors HT Orbitron, Infors-AG, CH). Two mL of this culture were used for plasmid DNA preparation using the plasmid purification Kit of Macherey-Nagel according to the manufacturer's protocol. Mutated DNA was verified by sequencing (Eurofins Genomics, formerly GATC) using the sequencing primers listed in (**Table 15**).

4.2.3 Restriction digest

For cloning purposes, 2 µg of vector DNA and the entire purified PCR product, see (**chapter 4.2.1**) were cleaved by double-digestion using the required restriction site specific enzymes.

Therefore, 10 units of each restriction enzyme were used in appropriate buffer as specified by the supplier in a final volume of 50 µL. Restriction digest was performed for at least 1 hour at 37°C.

4.2.4 Purification of DNA fragments

Restriction enzyme-digested vector DNA fragments were separated by agarose gel electrophoresis on a 1% (w/v) agarose gel in 1x TAE buffer containing ethidium bromide at 100 V/cm for appropriate time. Vector DNA of correct size was excised from the gel, purified and eluted in 25 µL ddH_2O (Gel and PCR Clean-up Kit, Macherey- Nagel) according to manufacturer's instructions. Double-digested insert DNA was purified by column purification using the same Kit.

4.2.5 Ligation

To determine the ratio of vector to insert, purified DNA concentration was measured using the NanoDrop™2000 Spectrophotometer (Thermo Scientific). Vector and insert DNA were mixed to a total of 200 ng in a 1:5 ratio with a total volume of 20 µL. Additionally, 2 µL 10x T4 ligase buffer and 1 µL T4 ligase were added and the reaction was filled up to 20 µL with ddH_2O. Ligation was performed overnight at 16°C in a Thermomixer (Eppendorf).

4.2.6 Preparation of competent cells for transformation

4.2.6.1 Preparation of chemical competent *E. coli* (storage)

For the preparation of chemical competent *E. coli*, the bacteria were streaked out on a LB-agar plate lacking antibiotics and were incubated overnight at 37°C. The next day, a pre-culture was set up with 20-25 mL of LB medium inoculated with a single colony from this plate and incubated overnight at 37°C. The pre-culture was used to inoculate one liter of LB medium in a 5-liter narrow-neck baffled conical flask and grown at 30°C with shaking at 180 rpm (Infors HT Multitron) until OD_{600} was 0.6 (Genesys 10S UV-Vis Spectrophotometer). All following steps were performed at 4°C. The bacterial culture was centrifuged for 10 min at 3500 ×g using a F9S-4x1000y rotor (Sorvall RC 6 Plus centrifuge) and the supernatant was discarded. The pellet was carefully resuspended in 50 mL 100 mM $MgCl_2$, transferred to a 500 mL centrifuge bottle and incubated on ice for 30 min. Afterwards, bacterial culture was centrifuged for 10 min at 6000 ×g using a F10-6x500y rotor (Sorvall RC 6 Plus centrifuge), the supernatant was discarded, and the pellet was resuspended in 100 mL 100 mM $CaCl_2$. The culture was again incubated on ice for 30 min prior to centrifugation for 10 min at 6000 ×g. The resulting pellet was resuspended in 5-10 mL storage buffer, aliquoted to 100 µL/tube, flash frozen in liquid nitrogen and stored at -80°C.

4.2.6.2 Preparation of chemical competent *E. coli* with 2x TSS

The day before transformation, *E. coli* Rosetta 2 (DE3) or *E. coli* BL21(DE3)pLysS cells (both Novagen) were streaked out on a LB-agar plate containing 34 µg/mL chloramphenicol (Cm) and incubated overnight at 37°C. The next day, a liquid culture was set up with 10 mL of LB-Cm medium inoculated with a pool of colonies from this plate and incubated 4-5 h over day at 37°C and 120-150 rpm agitation. The cells were harvested by centrifugation at 3500 rpm for 10 min at 4°C and the cell pellet was resuspended in 1 mL 2x TSS medium. From this mixture 50 µL were taken for transformation, see (**chapter 4.2.7.1**).

4.2.6.3 Preparation of electro-competent *E. coli* (storage)

At day one, a pre-culture was set up with 20 to 25 mL of LB medium devoid of antibiotics and inoculated with one colony of overnight grown bacteria from a LB-plate. The pre- culture was incubated overnight at 37°C. The next day, 2 liters of LB-medium in two 5-liter narrow-neck baffled conical flasks were inoculated with the overnight grown 20-25 mL bacterial pre-culture and grown with shaking at 180 rpm (Infors HT Multitron) at 30°C until OD_{600} reached 0.4 (Genesys 10S UV-Vis Spectrophotometer). At this point, the culture was put on ice, transferred to two 1-liter centrifuge-bottles and centrifuged for 15 min at 3,700 x g at 4°C (F9S-4x1000y rotor, Sorvall RC 6 Plus centrifuge). Each pellet was resuspended with 25 mL 10% (v/v) glycerol, transferred to a 500 mL centrifuge-bottle and filled to 500 mL with 10% (v/v) glycerol. Following centrifugation for 15 min at 6,000 ×g at 4°C (F10-6x500y rotor, Sorvall RC 6 Plus centrifuge), each pellet was resuspended with 25 mL 10% (v/v) glycerol, pooled, and filled up to 500 mL with 10% (v/v) glycerol. Bacterial cells were again centrifuged for 15 min at 6,000 ×g at 4°C and the supernatant was discarded. The pellet was resuspended in 15 mL 10% (v/v) glycerol, aliquoted to 100 µL/tube, flash frozen in liquid nitrogen and finally stored at -80°C.

4.2.7 Transformation

4.2.7.1 Transformation into chemical competent *E. coli* cells

For transformation of DNA into chemically competent cells, 50 µL chemical-competent *E. coli* (DH5α, Rosetta 2 or BL21) were mixed with 3 µL plasmid or up to 10 µL of a ligation mixture and incubated on ice for 20 min followed by a heat shock at 42°C for 45 s. The reaction was shortly cooled down on ice. For recovery (all resistances except ampicillin), 500 µL LB medium without antibiotics was added and cells were incubated for 30 to 60 min at 37°C in a heat block, shaking at 800 rpm. Cells were spun down for 2 min at 500 ×g, 400 µL of supernatant was removed and the pellet was carefully resuspended in the remaining volume. Cells were plated on LB-agar plates containing the respective antibiotics to select for cells that have successfully incorporated the plasmid. Plates were incubated overnight at 37°C.

4.2.7.2 Transformation into electro-competent *E. coli* cells

Electro-competent DH5α cells were thawed on ice. Then, 50 µL of cells were mixed with 5 µL ligation mixture and transferred to a pre-chilled cuvette. Afterwards, electroporation was performed for 5 ms with a pulse of ~2.5 kV using the Micropulser electroporation device (BioRad). Immediately after electroporation, 500 µL of LB-medium without antibiotics was added to the cuvette and the content was transferred to a 1.5 mL tube. Cells were recovered and further processed as described before (**chapter 4.2.7.1**).

4.2.8 DNA plasmid purification

Single bacterial colonies were used to inoculate 4 mL LB-medium containing construct specific antibiotics and were grown overnight at 37°C with constant shaking of at 120-150 rpm. To pellet cells, 2 mL of overnight cultures were centrifuged at 11,000 ×g for 1 min at room temperature. Plasmid DNA was purified from the cell pellet by alkaline extraction (NucleoSpin plasmid Kit, Macherey-Nagel) following the manufacturer's protocol. DNA was eluted in 30 µL ddH_2O and stored at -20°C until further use.

4.2.9 Measuring DNA concentrations

Concentrations of plasmid or genomic DNA were measured using the NanoDrop™2000 Spectrophotometer (Thermo Scientific) reading the absorbance at 260 nm where 1 AU at OD_{260} corresponds to 50 µg double-stranded DNA. Purity of DNA was estimated using the absorbance ratio at 260 and 280 nm considering a ratio of ~1.8 as pure DNA.

4.2.10 Expression and purification of recombinant proteins

Recombinant substrates (MBP-PGAM5, MBP-Spitz) and enzymes (GlpG-His6, PARL-His6) for the detergent-micelle based *in vitro* system were expressed as His-tag fusion proteins using the pET-vector system (Novagen) with an isopropyl-β-D-thiogalactopyranosid (IPTG)-inducible T7 promotor. Expression was performed in either *E. coli* Rosetta 2 (DE3) (Novagen) for substrates and human PARL, or in *E. coli* BL21(DE3)pLysS cells (Novagen) for GlpG. The vector was transformed into the respective chemical competent *E.coli* cells, grown in LB medium (Miller) containing 100 µg/mL ampicillin and 34 µg/mL chloramphenicol at 37°C. A preculture in liquid LB-medium containing the antibiotics was grown overnight or for up to 4 h over day at 37°C and 120-150 rpm agitation. The main cultures (1 L culture each in a 5 L baffled conical flask) were inoculated with the preculture to an OD_{600} at 0.025 and were grown for up to 2 h at 37°C and 120-150 rpm agitation. Expression of the protein was induced with 0.3 mM IPTG at OD_{600} 0.3 and expressed, either for 2-3 h at 37°C (substrates), or overnight (~20 hours) at 16°C (enzymes). Cells were harvested by centrifugation at 3500 rpm for 15 min at 4°C and resuspended in Lysis buffer (A). Prior to lysis, 200 µg/mL lysozyme, 1 mM PMSF

and benzonase (2.5 ku, Merck Millipore) were added and cells were lysed using Emulsiflex (Avestin) with a maximum pressure of 15 kPSI (100 MPa). Crude membranes were obtained by ultracentrifugation at 29000 rpm for 45 min at 4°C. The membrane pellet was resuspended in Solubilization buffer (B). The His6-tagged proteins were solubilized from the crude membranes with 1.5 % DDM for 1 hour on a rotating wheel at room temperature (RT) (substrates) or at 4°C (enzymes). Extraction of His6-tagged proteins from membrane debris was done by ultracentrifugation at 29000 rpm for 1 hour at 4°C. Cleared extract was batch incubated with Ni-NTA beads (Macherey-Nagel) for 1 hour on a rotating wheel at RT (substrates) or 4°C (enzymes) for His-tag affinity purification. Bound His6-tagged proteins were washed with Wash buffer (C) 50 mM HEPES pH 7.4, 300 mM NaCl, 10% glycerol (v/v), 50 mM imidazole, 0.05% DDM and eluted with Elution buffer (D). Determination of fractions containing purified His6-tagged proteins was established by SDS-PAGE running 12% acrylamide gels, which were visualized through Coomassie staining. If required, the His6-tagged protein was concentrated using an Amicon® Ultra Filter (Merck) with 10 kDa MWCO at 4°C.

4.2.11 Co-expression of rhomboid proteases and substrates in *E. coli*

For co-expression of human PARL and chimeric substrates in *E. coli*, expression vectors with different compatible replicons had to be chosen. In contrast to the separately expressed pET-vector constructs, the co-expressed fusion proteins were expressed under the control of an arabinose-inducible promoter. Therefore, human His6-PARL wt was cloned into pBAD24 (pBR322/ColE1 ori) and the chimeric substrates MBP-PINK1 (amino acids 70-137) and MBP-PGAM5 (amino acids 1-46) were cloned into pBAD33 (p15A ori). The catalytic inactive mutant His6-PARL^{S277A} was generated by site-directed mutagenesis following the protocol of the Stratagene's QuikChange® Site-Directed Mutagenesis Kit (Agilent Technologies). Freshly 2x TSS-transformed *E. coli* JW5687 (*ΔglpG*757::kan) cells (**chapter 4.2.6.2**) were inoculated in a 25 mL preculture in LB medium with the appropriate antibiotics and grown in a baffled conical flask with at 37°C with 140 rpm shaking. The main culture was inoculated with the preculture to an OD_{600} of 0.025 and was grown at 37°C and 140 rpm agitation for 2-3 h. Expression of rhomboids and substrates was induced with 2% L-arabinose at OD_{600} 0.3 and expressed overnight (~20 hours) at 16°C. Samples were taken for SDS-PAGE analysis and subsequent western blotting.

4.2.12 Measuring protein concentrations

Total protein concentrations were measured using the NanoDrop^{TM}2000 Spectrophotometer (Thermo Scientific) reading the absorbance at 280 nm where 1 Abs at OD_{280} corresponds to 1 mg/mL protein after blanking with elution buffer. Protein purity was estimated using the absorbance ratio at 260 and 280 nm considering a ratio of 0.5-0.55 as pure protein. Of note:

Purified proteins were in general kept in the elution buffer. Since the elution buffer contains the detergent DDM and high concentrations of salt and imidazole, traditional methods to determine protein concentration like the Bradford-test and even the BCA-test (Lowry-assay except bicinchoninic acid), failed in my study. Detergents, already at low levels, disturb the Bradford-test because the detergent also binds to the protein and competes with the dye for binding sites or displace it from the protein, which prevents the color reaction (Friedenauer and Berlet, 1989). Test methods after Lowry or the BCA-test are in general less sensitive to detergents (Noble *et al.*, 2007), but using the NanoDrop™ 280 nm absorbance measurement still resulted in the most appropriate concentration determination in my study.

4.2.13 Detergent-micelle based *in vitro* cleavage assay

For MBP-PGAM5 cleavage by PARL-His6, 5 µg (4 µM) of *E. coli* purified MBP-PGAM5 was incubated with either 0.44 µg (0.7 µM) PARL-His6 or 0.44 µg (0.7 µM) catalytic inactive PARL^{S277A}-His6 purified from *P. pastoris* for 1.5 h at 30°C in cleavage buffer, as published in (Lysyk *et al.*, 2021) in a total volume of 20 µL. For MBP-Spitz cleavage by GlpG-His6, 5 µg of *E. coli* purified substrate was incubated with 5 µg GlpG-His6 for 2 h at 37°C in cleavage buffer and a total volume of 20 µL. Cleavage reactions were stopped by adding 2x SDS-sample buffer. PARL and GlpG activity was inhibited by adding 3,4-Dichlor-isocumarin (3,4-DCI) serine protease inhibitor to a final concentration of 1000 µM. Determination of peptide cleavage was established by SDS-PAGE using 12% acrylamide gels, which were visualized through Coomassie staining.

4.2.14 TAMRA-FP labelling

To estimate correct protein folding and thus catalytic activity of rhomboid-containing *E. coli* membranes or purified PARL and GlpG, 1-5 µM purified enzyme or 10 µL rhomboid-containing *E. coli* membranes were incubated with 0.5 µM TAMRA-FP Serine Hydrolase probe in cleavage buffer in a total reaction volume of at least 10 µL. The mixture was incubated for 2 h at 37°C protected from light and the reaction was stopped by adding 2x SDS-sample buffer. Determination of stained protein was established by SDS-PAGE with a running tank covered from light, using 12% acrylamide gels, which were visualized using the LAS4000 system with a green light source (532 nm, Ex/Em: 552/575nm) and a Cy®3 filter to detect the emitted fluorescence of the TAMRA-FP probe.

4.2.15 N-terminal sequencing by Edman degradation

In total, 8-16 µg of *E. coli* purified MBP-PGAM5 was incubated with 0.4 µg of *P. pastoris* purified PARL for 2 h at 37°C in cleavage buffer. Protein fragments were separated by SDS-PAGE running 12% acrylamide gels and transferred to a PVDF membrane by wet blot (glycine buffer).

Protein fragments were stained with Coomassie overnight, the membrane containing the C-terminal cleavage fragment (CTF) was cut out and the CTF was analyzed in four cycles by Edman degradation (TOPLAB), as published in (Lysyk *et al.*, 2021).

4.2.16 Reconstitution of GlpG into lipid membranes

Reconstitution of GlpG into membranes was performed by Dr. Oskar Engberg from the Huster lab, Institute for Medical Physics and Biophysics, Leipzig and will be described in the joint publication.

4.3 Cell biology methods

4.3.1 Cell culture of mammalian cells

Human embryonic kidney (Hek) 293T (ATCC CRL-3216TM) and Hek293 Flp-In T-REx (ATCC CRL-1573TM) cells were maintained in Dulbecco's modified Eagle's medium (DMEM) supplemented with 10% (v/v) fetal bovine serum (FBS). Stably expressing Hek293-T-Rex cells were additionally supplemented with 1% (v/v) GlutaMAX, 1% (v/v) sodium-pyruvate and 5 µg/mL blasticidine (Gibco) and 500 µg/mL geneticin-G418 (Gibco). Cells were grown as monolayers in 10 cm cell culture dishes at 37°C and 5% CO_2. For passaging, medium was first aspirated and cells were washed with 10 mL pre-warmed PBS followed by treatment with 0.05% Trypsin-EDTA to detach cells. In order to stop trypsinization, 9 mL warm DMEM + 10% (v/v) FBS was added to the cells. The cells were triturated by pipetting up and down several times and split at the desired dilution depending on growth status and purpose. In general, cells for experiments were seeded to 70-80% confluency for the next day (dilution 1:5) in 6-well plates, 10 cm or 15 cm culture dishes or 1:10 in ibidi microscopy chambers. For maintenance, cells were split 1:10 twice a week.

4.3.2 Transient transfection of mammalian cells

The protocol for transient transfection was adapted from (Durocher *et al.*, 2002). Cells were seeded in 15 cm or 10 cm culture dishes, 6-well plates or 8-well ibidi microscopy chambers at desired density as described before, see (**chapter 4.3.1**). Transfection was performed the day after cell seeding using the reagent volumes as given in (**Table 17**).

Table 17 | Transient transfection of mammalian cells.
Volumes used for transient transfection of mammalian cells of different cell culture plate types. P/S: penicillin/streptomycin.

	15 cm dish	10 cm dish	6-well plate	8-well ibidi
Cell dilution and volume	1:5 / 25 mL	1:5 / 10 mL	1:5 / 2 mL	1:10 / 0.3 mL
total DNA	30 µg	12 µg	2 µg / well	0.2 µg / well
DMEM + 1% P/S	3,750 µLL	1,500 µLL	250 µL	50 µL
Polyethylenimine (PEI)	75 µL	30 µL	5 µL	1 µL
DMEM + 5% FBS + 1% P/S	11,250 µL	4,500 µLL	750 µL	150 µL
DMEM + 10% FBS + 1% P/S	25 mL	10 mL	2 mL	250 µL

For regular testing of the transfection efficiency, a plasmid expressing free GFP (pEGFP-N1) was co-transfected. Plasmid DNA was pre-mixed with 10 µL water. To this mixture, the respective volume of DMEM containing 1% (v/v) Penicillin/Streptomycin (P/S) supplemented with 1 mg/mL 25 kD linear polyethylenimine (PEI) was added. This mix was thoroughly vortexed and incubated at room temperature (RT) for 10 min allowing DNA-PEI complexes to form. Afterwards, DMEM + 5% (v/v) FBS + 1% (v/v) P/S was added and further incubated for 5 min at RT. Medium on cells was removed and the transfection mix was carefully applied. Cells were incubated at 37°C, 5% CO_2 for 4 h before replacing the transfection mix with the respective volume of DMEM + 10% (v/v) FBS + 1% (v/v) P/S and for Hek293-T-Rex cells containing additionally 1% (v/v) GlutaMAX and 1% (v/v) sodium-pyruvate and the respective antibiotics. Usually, cells were harvested 24-36 h post transfection or optionally treated 16-20 h post transfection. For steady state analysis, inhibitors or vehicle control were directly added to the cells during medium exchange. In general, the amount of plasmid containing the substrate did not exceed 50% (v/v), and plasmid harboring the protease gene was 15% (v/v) of total DNA volume. The DNA amount in each well was held constant by adding empty pcDNA3.1(+) vector.

4.3.3 siRNA knockdown

For the knockdown of OMA1 (UniGene ID Hs.425769), Hek293-T-Rex shPARL cells were transfected with small-interfering RNA (siRNA)-oligonucleotides (Ambion, Austin, TX, USA) using the Thermo Scientific RNAiMAX transfection Kit according to the manufacturer's protocol. Oligonucleotides, Silencer™ Select NegCtrl #1 (4390843) and Silencer™ Select OMA1 (s41777) were resuspended to a final 20 µM stock in nuclease-free water and frozen at -20°C until use. Cells were seeded onto poly-L-lysine (PLL)-coated 6-well or 12-well plates in DMEM + 10% (v/v) FBS + 1% (v/v) GlutaMAX + 1% (v/v) sodium-pyruvate with 5 µg/mL blasticidine + 500 µg/mL G418. For transfection, 20 nM siRNA and the RNAiMAX transfection

reagent were each mixed with half the volume of Opti-MEM followed by vortexing and incubation at RT for 5 min. The Opti-MEM-RNAiMAX mix was added to the siRNA, mixed by pipetting up and down and incubated for 15 min at RT. Afterwards, the transfection mix was applied onto the cells. After 24 h, medium was exchanged to fresh DMEM + 10% (v/v) FBS + 1% (v/v) P/S + 1% (v/v) GlutaMAX + 1% (v/v) sodium-pyruvate with 5 µg/mL blasticidine + 500 µg/mL G418 and cells were harvested 72 h after siRNA transfection.

4.3.4 Disruption of the inner mitochondrial membrane potential

To block mitochondrial import and induce cleavage of PGAM5, the inner mitochondrial membrane potential was disrupted by incubating the cells with 10 µM of the uncoupling ionophore carbonyl cyanide m-chlorophenyl hydrazone (CCCP) up to 3 h before harvesting. The stock solution was prepared in DMSO and cells not treated with CCCP were incubated with DMSO only.

4.3.5 Inhibition of the proteasome

Proteolytic activity of the proteasome was inhibited by incubating the cells with either 2 µM MG132 overnight (16-24 h) or with 5 µM epoxomicin for 2-8 h prior to harvesting. The stock solutions were prepared in DMSO and cells not treated with the proteasome inhibitors were incubated with DMSO only.

4.3.6 Inhibition of protein synthesis with cycloheximide

To study protein stability in gain-of-function or loss-of-function chase assays, protein synthesis was inhibited by treating cells with cycloheximide. For this, a stock solution of 10 mg/mL (w/v) cycloheximide in water was freshly prepared and diluted to a final concentration of 100 µg/mL (w/v) in DMEM + 10% (v/v) FBS. After addition of the compound onto the cells, lysates were prepared at specific time points and protein abundance was analyzed by western blotting. Timepoint 0 was immediately harvested and did not receive cycloheximide.

4.4 Biochemical methods

4.4.1 Preparation of total cell lysate

For human whole cell lysates, cells were directly lysed in SDS-sample buffer. First, cells were washed with 1 mL PBS/well (6-well plate) before adding 300 µL 1x SDS-sample buffer containing 5% (v/v) β-mercaptoethanol. Lysates were heated at 65°C for 15 min with agitation at 1250 rpm in a heating block (Thermomixer comfort, Eppendorf) followed by centrifugation for 2 min at 11,000 ×g (Centrifuge 5415R, Eppendorf). Samples were either directly applied to sodium dodecyl sulfate polyacrylamide gel electrophoresis (SDS-PAGE) or frozen at -20°C.

For *E. coli* total cell lysates, 1 mL of culture was harvested by centrifugation for 2 min at 11,000 x g, supernatant was discarded and the cell pellet resuspended in 100 µL 2x SDS-sample buffer containing 10% (v/v) β-mercaptoethanol. Lysates were heated at 95°C for 15 min with agitation at 1250 rpm in a heating block, followed by centrifugation for 2 min at 11,000 ×g and either direct use in SDS-PAGE or storage at -20°C.

In order to check for disulfide (S-S) bonds in PGAM5, 1x SDS-sample buffer was prepared either with 20 mM DTT (reducing), instead of β-mercaptoethanol or without DTT (non-reducing). 60 mM NEM was added to the sample buffer in order to alkylate reduced thiol groups (mainly upon DTT treatment) and to quench free DTT in the reduced sample. Thereby reduced and non-reduced samples can be loaded side by side avoiding free DTT to diffuse and interfere with the oxidized proteins. Whereas, samples containing DTT in the sample buffer were heated at 65°C as described above, samples under the non-reducing condition, were heated at 37°C for 10 min with agitation at 1250 rpm in a heating block (Thermomixer comfort, Eppendorf) followed by centrifugation for 2 min at 11,000 ×g (Centrifuge 5415R, Eppendorf).

4.4.2 SDS-PAGE

Protein samples were separated by reducing Tris-glycine sodium dodecyl sulfate (SDS)-polyacrylamide gel electrophoresis (PAGE) according to (Laemmli, 1970). Typically, 15 µL human total cell lysate from cells with overexpressed protein and 20 µL for the detection of endogenous protein were loaded. For *E. coli* samples, 5-10 µL of the -/+ IPTG lysates were loaded and 20 µL for all fractions of the protein purification as well as for incubated samples of the *in vitro* cleavage assays. SDS-gels (**Table 18**) were first run at constant voltage of 60 V for 30 min followed by running at constant current of 22 mA per gel until the bromophenol front was leaking out from the gel. Protein bands were visualized by western blotting.

Table 18 | Composition of Tris-glycine SDS gels.

Component	Separation gel (10%)	(12%)	Stacking gel (4%)
30% Acrylamide solution	3 mL	3.6 mL	0.5 mL
2 M Tris-HCl, pH 8.8	1.8 mL	1.8 mL	-
0.5 M Tris-HCl, pH 6.8	-	-	0.3 mL
20% (v/v) SDS	45 µL	45 µL	15 µL
10% (v/v) APS	80 µL	80 µL	50 µL
TEMED	8 µL	8 µL	5 µL
H_2O	4.2 mL	3.5 mL	2.15 mL

4.4.3 BN-PAGE

Blue Native (BN)-PAGE allows to resolve protein complexes in the range of 10 kDa to 10000 kDa (Schagger *et al.*, 1994). Commonly gradient gels are used, as described in (**Table 19**). If not indicated differently, all steps were performed on ice or at 4°C. Mitochondrial enriched crude membranes of Hek293T cells ectopically expressing PGAM5-FLAG constructs were obtained by cell disruption followed by differential centrifugation, see (**chapter 4.4.9**).
The mitochondrial enriched crude membranes were incubated in solubilization buffer supplemented with EDTA-free complete protease inhibitor cocktail (1xPI, Roche) and 1 mM PMSF. After removal of the insoluble fraction by centrifugation at 14000 rpm, the supernatant was combined with a 1/40 volume of BN-sample buffer before subjection onto BN-PAGE in self-casted Bis-Tris 6-20% acrylamide (AA-Bis, 40%, 32:1) gradient gels. Gels were run for 1 h at 150 V with the dark-blue cathode buffer, and then continued at 230 V for 2-3 h after changing to the light-blue cathode buffer. Afterwards, gels were incubated for 15 min in BN-transfer buffer and were transferred at 100 mA for 70 min onto a PVDF membrane (Immobilon-P, 0.45 µM pore size, Merck Millipore) using the semi-dry blotting system. The PVDF membrane was incubated in fixation solution, destained in methanol and washed in water. Protein bands were visualized as described in (**chapter 4.4.6**).

Table 19 | Composition of Tris-Tricine BN gels.

Component	Separation gel (6%)	(20%)	Stacking gel (4%)
Acrylamide AA-Bis, 40%	0.9 mL	3.0 mL	0.3 mL
3x Gel buffer	2.0 mL	2.0 mL	1.0 mL
80% (v/v) Glycerol	-	1.5 mL	-
10% (v/v) APS	50 µL	30 µL	40 µL
TEMED	5 µL	3 µL	4 µL
H_2O	3.1 mL	80 µL	1.7 mL

4.4.4 2D-PAGE

Two-dimensional (2D)-PAGE with material from a BN-PAGE adds a second analytical dimension and allows to resolve single proteins from initial protein complexes. BN-PAGE of PGAM5-FLAG expressing Hek293T cells was performed as described before. Gel pieces of interest were cut out and horizontally infused into the stacking gel area of a standard SDS-PAGE gel, that was subsequently run under standard conditions, as described in (**chapter 4.4.2**) and analyzed by Western blotting.

4.4.5 Coomassie staining

For staining SDS-gels with Coomassie Brilliant blue G-250, gels were quickly washed in tap water and then incubated for 30 min in Coomassie Brilliant blue G-250 staining solution on an orbital shaker with a maximum speed of 95 rpm. After rinsing the gels with tap water, destaining solution was applied. As soon as the destaining solution turns dark blue, it was changed several times, briefly washing with water in between the steps (2-3 h in total). The destained gels were kept in tap water and imaged with the LAS4000 system (DIA tray).

4.4.6 Western blotting and protein detection

The semi-dry western blotting method was used for protein transfer onto methanol-activated PVDF membrane using blotting machines made inhouse. Transfer was achieved using 1x Semi-dry blotting buffer at 100 mA per gel for 70 min at RT. Afterwards, the membrane was immersed in 5% (w/v) milk/TBS-T blocking solution for 30 min at RT followed by incubation with the primary antibody at indicated dilution in 2 mL blocking solution overnight at 4°C. The membrane was washed three times for 10 min with 10 mL TBS-T and the secondary antibody in TBS-T was applied for 1 h at RT. The membrane was then washed twice for 10 min with TBS-T and finally rinsed for 10 min in TBS. For protein band visualization, the membrane was incubated for max 3 min with enhanced chemiluminescent solution before imaging with the LAS4000 system.
Western blotting via the wet blot method was used only in order to analyze the C-terminal cleavage fragment of MBP-PGAM5 in N-terminal sequencing by Edman degradation, using 1x blotting buffer at 100 mA per chamber for 1 h at 4°C.

4.4.7 Immunofluorescence staining and image acquisition

HEK293T cells were plated in 24-well plate on PLL-coated 12 mm cover glass. Cells were transfected with 125 ng of plasmid and total plasmid levels were adjusted to 500 ng with empty plasmid. For immunofluorescence analysis, cells were chemically fixed with 4% formaldehyde (16% formaldehyde diluted in PBS) for 15 min, washed 3x in PBS followed by permeabilization and blocking in PBS containing 0.1% Triton X-100 and 20% fetal calf serum (TPBS-FCS) for 45 min. Subsequently, the fixed cells were probed with anti-TOM20 antibody diluted 1:400 and anti-FLAG antibody diluted 1:500 in TPBS-FCS for one hour and washed 3x in PBS. After staining with fluorescently labelled secondary antibodies Alexa Fluor 488 goat anti-mouse and Alexa 633 goat anti-rabbit, both diluted 1:500 in TPBS-FCS for 1 h, the slides were washed 3x in PBS, followed by Hoechst staining 1 µg/mL in PBS for 10 min. After washing 3x with PBS, the cover glasses were mounted with Fluoromount-G on microscope slides. Samples were imaged with a LSM780 system (Carl Zeiss) using 405, 488, and 633 nm laser lines, a Plan-

APOCHROMAT 63x 1.4NA oil objective (Carl Zeiss) and pinhole settings of 1AU with the Zeiss ZEN 2010 software. Image processing was performed using ImageJ (http://rsb.info.nih.gov/ij/).

4.4.8 Co-immunoprecipitation for SILAC

As performed by Beate Hehn and Christabel Celia Kho, Lemberg laboratory, ZMBH: For co-immunoprecipitation, cells were washed with 1x PBS and incubated with PBS-EDTA for 5 min at 4°C to detach them via scraping. Cells were transferred to a chilled tube on ice and centrifuged (Centrifuge 5415R, Eppendorf) for 3 min at 500 ×g at 4°C to pellet cells. The supernatant was aspirated and the pellet was lysed in 1 mL solubilization buffer containing PMSF, complete protease inhibitor cocktail and 1% (v/v) Triton X-100. Cells were lysed for 30 min on ice followed by centrifugation (Centrifuge 5415R, Eppendorf) for 15 min at full speed (21780 ×g) at 4°C to pellet the Triton-insoluble fraction. The supernatant was transferred to a fresh tube and diluted 1:2 with solubilization buffer without detergent to dilute the Triton X-100 concentration to 0.5 % (v/v) before affinity purification. The lysate was precleared by incubation with Protein G Sepharose beads shaking for 2 h at 4°C on a rotator. For immunoprecipitation, lysate was spun for 3 min at 4,000 ×g at 4°C (Centrifuge 5415R, Eppendorf), transferred to a clean tube and incubated with GFP-binder beads (Stoecklin laboratory, ZMBH, Heidelberg) for 4 h at 4°C on a rotator. The beads were washed three times with solubilization buffer containing 0.1% (v/v) Triton X-100 and immunoprecipitates were collected by centrifugation for 3 min at 4000 ×g at 4°C. Protein was eluted from GFP-binder beads in 2x SDS-sample buffer at 14000 rpm and 65°C in a heating block.

4.4.9 Subcellular fractionation

In order to enrich for mitochondrial membranes, subcellular fractionation was performed by cell disruption followed by differential centrifugation. In brief, cells were detached from 6-well plates or 10 cm dishes by applying PBS-EDTA and scraping, transferred to a chilled tube on ice, followed by centrifugation for 5 min at 500 ×g and 4°C (Centrifuge5415R, Eppendorf). The supernatant was discarded and the cell pellet resuspended in hypotonic isolation buffer. After 10 min of incubation at 4°C, cells were lysed by passing six times through a 27-gauge needle (BD Microlance™ 3, 27G x 3/4'', 0.4 mm x 19 mm) attached to a 1 mL syringe. Cellular debris and nuclei were discarded after centrifugation at 200 ×g for 5 min at 4°C. The supernatant was spun at 10000 ×g for 10 min and 4°C, resulting in a mitochondrial-enriched membrane pellet and a supernatant, referred to as cytosolic fraction. The cytosolic supernatant was transferred to a fresh tube on ice, precipitated with 10% (v/v) trichloracetic acid and spun at full speed (21780 ×g) for 2 min at 4°C to harvest the precipitate, which was washed with acetone at RT and resuspended in 1x SDS-sample buffer. The mitochondrial membrane pellet was kept on ice, washed in isolation buffer, spun at 10000 ×g for 10 min at 4°C and resuspended in 1x

SDS-sample buffer. Before analyzing in SDS-PAGE, samples were heated at 65°C for 15 min with agitation at 1250 rpm in a heating block.

4.4.10 Stable isotope labelling with amino acids in cell culture (SILAC)

Since the identification of native substrates of proteases is a challenging task, stable isotope labelling with amino acids in cell culture (SILAC)-based proteomics to identify new PARL substrates was used. *The experiments were performed by Beate Hehn and Christabel Celia Kho in the Lemberg laboratory (ZMBH) between 2015 and 2016, based on a PARL-trapping approach.*

For the triple gain-of-function SILAC approach, membrane fractions of doxycycline-inducible Hek293-T-REx cells stably expressing mouse wild-type PARL-GFP were compared to cells stably expressing the catalytic inactive mutant PARL^{S275A}-GFP and mock transfected cells as control. Here, control cells were light labelled (Arg/Lys, R0K0), PARL wt was labelled with medium isotopes of arginine and lysine ($^{13}C_6$-L-Arg and 4,4,5,5-d_4-L-Lys), and the cells overexpressing PARL^{S275A} were labelled with heavy amino acids ($^{13}C_6{}^{15}N_4$-L-Arg and $^{13}C_6{}^{15}N_2$-L-Lys). For each approach, three 15 cm culture plates per labelling condition were used. In order to ensure proper incorporation of amino acids, cells were grown in medium supplemented with the respective amino acid isotopes, antibiotics, and dialyzed FBS for at least 5 passages. At the day of harvest, cells were washed with ice-cold 1x PBS, harvested in PBS-EDTA (2 mL/plate) and transferred to a 50 mL tube on ice. Cells were centrifuged for 10 min at 400 ×g at 4°C (Universal 320, Hettich Zentrifugen) and the pellet was resuspended in ice-cold hypotonic buffer (1 mL/plate) supplemented with PMSF and protease inhibitor cocktail (Roche). At this point, cells with the different labelling (light, medium or heavy) were pooled at 1:1:1 ratio and kept on ice for 10 min. For lysis, cells were passed 5 times through a 27-Gauge needle (see 6.4.8) followed by centrifugation for 15 min at 400 ×g at 4°C to remove cell debris and nuclei. Pure mitochondrial pellets were obtained by ultracentrifugation using the 70Ti rotor (Beckman Coulter) for 20 min at 100,000 ×g and 4°C. The obtained mitochondrial pellet was then solubilized with solubilization buffer containing 1% Triton X-100, followed by incubation on ice for about 50 min. After another centrifugation at 100,000 ×g for 20 min the supernatant was split into halves of the volume and diluted in the solubilization buffer until it contained a final concentration of 0.5% Triton X-100. 30 µL GFP-binder beads were added to the sample, followed by an overnight incubation at 4°C in the rotating wheel. The next day, the samples were washed 3 times with 0.1% Triton X-100 for 10 min at 4°C with agitation. Afterwards, the beads were resuspended in 30 µL 2x SDS-sample buffer, incubated at 65°C for 15 min at 1200 rpm shaking. *Mass spectrometry analysis was performed by Dr. Bernd Heßling and Dr. Thomas Ruppert from the Core Facility of Mass Spectrometry and Proteomics at the ZMBH.* Data analysis was performed by using the software PERSEUS (Max Planck Institute of

Biochemistry). Prediction of TM helices in proteins was performed using the TMHMM Server (v. 2.0, Technical University of Denmark).

4.4.11 Matrix Assisted Laser Desorption/Ionization Mass Spectrometry (MALDI-MS)

MALDI-MS analysis was performed by Dr. David Ulbricht from the Huster laboratory, Institute for Medical Physics and Biophysics, Leipzig and will be described in the joint publication.

4.4.12 Kinetic measurements in DDM-micelles

Kinetic measurements were performed by Dr. David Ulbricht from the Huster laboratory, Institute for Medical Physics and Biophysics, Leipzig and will be described in the joint publication.

4.4.13 CD spectroscopy, liquid-state NMR and H/D exchange

The atomic coordinates and experimental data used for structure calculation have been deposited in the Protein Data Bank (www.wwpdb.org) and BMRB (https://bmrb.io/). PGAM5 WT: 7QAM, 34681; C12L: 7QAL, 34680; C12S: 7QAO, 34682; G17L: 7QAP, 34683. *CD spectroscopy, liquid-state NMR and H/D exchange of PGAM5 TM helices was performed and analyzed by Dr. Mara Silber. Supervision Dr. Claudia Muhle-Goll, Institute for Biological Interfaces 4, Karlsruhe Institute of Technology.*

4.4.14 ^{2}H NMR spectroscopy and stationery ^{31}P NMR measurements

^{2}H NMR spectroscopy was performed by Dr. Oskar Engberg from the Huster laboratory, Institute for Medical Physics and Biophysics, Leipzig and will be described in the joint publication.

4.4.15 Quantitative real-time PCR (qRT-PCR)

Quantitative real-time PCR was used to assess the mRNA level of OMA1 in Hek293-T-REx shPARL cells. Therefore, RNA was isolated with the RNA isolation Kit according to the manufacturer's protocol from confluent cells from one well of a 6-well plate. Purified RNA was eluted in 60 µl RNAse-free H_2O and the concentration and purity were determined using the NanoDrop™2000 Spectrophotometer. For reverse transcription, 2 µg RNA were converted into cDNA using the RevertAid First Strand cDNA Synthesis Kit and stored at -20°C assuming a concentration of 100 ng/µL. The pipetting scheme and incubation times are given in (**Table 20**).

Table 20 | Composition of reaction mixture and incubation times for cDNA synthesis.

Component	Volume/Amount
RNA	2 µg
Random Hexamer Primer	1 µL
H_2O	up to 12 µL
incubation at 65°C for 5 min	
5x reaction buffer	5 µl
Riboblock	1 µl
NTPs 10 mM	2 µl
RevertAid Reverse Transcriptase	1 µl
incubation at 25°C for 5 min	
incubation at 42°C for 60 min	
incubation at 70°C for 5 min	

12.5 ng cDNA were used for quantitative RT-PCR (**Table 21**) in one well of a 384-well plate using the SensiFAST™ SYBR No-ROX Kit according to the manufacturer's proto- col and the following pipetting scheme (**Table 22**).

Table 21 | Primers used for qRT-PCR. Fwd: forward, Rev: revers.

Gene/Primer name		Sequence (5' → 3')
β-Actin (ACTB)	fwd	CACCATTGGCAATGAGCGGTTC
	rev	AGGTCTTTGCGGATGTCCACGT
TATA-box binding protein (TBP)	fwd	CCGGCTGTTTAACTTCGTT
	rev	ACGCCAAGAAACAGTGATGC
OMA1_p1	fwd	TCCTCACAATGATTTGGGCCAT
	rev	CACAAGCCTTTGCAGCAAGC

Table 22 | Composition of reaction mixture for RT-PCR.

Component	Volume/Amount
SYBR Green	5.0 µL
Primer mix (10 µM)	0.4 µL
cDNA	4.0 µL
H_2O	to 10 µL

The reaction mixture was scaled up according to needs and pipetted into a 384-well plate using filter tips with regular tip exchanges to minimize contamination and pipetting errors. The plate was sealed with the Ampliseal™ microplate sealer and then centrifuged at 1111 ×g (Centrifuge

5810R, Eppendorf) for 5 min at RT to remove air bubbles. mRNA quantification was determined using the LightCycler480 Instrument II (Roche) with the cycle settings listed in (**Table 23**).

Table 23 | Cycle settings for qRT-PCR.

Step	Temperature		Time (min:s)	Ramping (°C/s)	Cycle
Denaturation	95°C		2:00	4.8	
Amplification	95°C		0:05	4.8	40 x
	57°C		0:10	2.5	
Melt Curve	72°C		0:25	4.8	1 x
	95°C		5:00	4.8	1 x
	60°C		1:00	2.5	1 x
	97°C	acquisition	0:05	0.11	1 x
Cool-down	40°C		10:00	2.5	1 x

Each reaction was performed in technical triplicate, β-actin (ACTB) and TATA-box binding protein (TBP) were used as reference genes for normalization. For the relative quantification of mRNA levels of OMA1, the delta delta Ct method was used to calculate relative fold change of gene expression. Each reaction has a certain Ct (cycle threshold) value, which is the cycle number required to detect a fluorescent signal above background. First, the difference between gene of interest and housekeeping gene, here ACTB and TBP were calculated, and secondly the difference between the PARL-knockdown background and endogenous PARL level were calculated in PGAM5 wt-FLAG and PGAM5^{C12S}-FLAG expressing Hek293-T-Rex cells, untreated or treated with CCCP.

4.4.16 Data processing and statistical analysis

Microscopy images were processed using Fiji/ImageJ. Image manipulations included cropping, adjustment of brightness and contrast, and background subtraction. Quantification of the intensity of western blot bands was performed using Fiji/ImageJ and all statistical analyses were performed using the GraphPad Prism (v.9.1.2.226) software. Differences between two means was determined by unpaired two-tailed t-test. Data are represented as mean ± SEM from at least three independent biological replicates. Significance levels: *p ≤ 0.05, **p ≤ 0.01, ***p ≤ 0.001, ****p ≤ 0.0001.

5. References

Abe, Y., Shodai, T., Muto, T., Mihara, K., Torii, H., Nishikawa, S., Endo, T., and Kohda, D. (2000). Structural basis of presequence recognition by the mitochondrial protein import receptor Tom20. Cell *100*, 551-560.

Adrain, C., Zettl, M., Christova, Y., Taylor, N., and Freeman, M. (2012). Tumor necrosis factor signaling requires iRhom2 to promote trafficking and activation of TACE. Science *335*, 225-228.

Akiyama, Y., and Maegawa, S. (2007). Sequence features of substrates required for cleavage by GlpG, an Escherichia coli rhomboid protease. Mol. Microbiol. *64*, 1028-1037.

Alavi, M.V. (2021). OMA1—An integral membrane protease? Biochimica et Biophysica Acta (BBA) - Proteins and Proteomics *1869*, 140558.

Albeck, J.G., Burke, J.M., Aldridge, B.B., Zhang, M., Lauffenburger, D.A., and Sorger, P.K. (2008). Quantitative analysis of pathways controlling extrinsic apoptosis in single cells. Mol Cell *30*, 11-25.

Alberts, B., Johnson, A., Lewis, J., Morgan, D., Raff, M., Roberts, K., Walter, P., Wilson, J., and Hunt, T. (2015). Molecular biology of the cell, Sixth edition edn (New York, NY: Garland Science Taylor and Francis Group).

Albrecht, R., Rehling, P., Chacinska, A., Brix, J., Cadamuro, S.A., Volkmer, R., Guiard, B., Pfanner, N., and Zeth, K. (2006). The Tim21 binding domain connects the preprotein translocases of both mitochondrial membranes. EMBO reports *7*, 1233-1238.

Alexander, C., Votruba, M., Pesch, U.E., Thiselton, D.L., Mayer, S., Moore, A., Rodriguez, M., Kellner, U., Leo-Kottler, B., Auburger, G.*, et al.* (2000). OPA1, encoding a dynamin-related GTPase, is mutated in autosomal dominant optic atrophy linked to chromosome 3q28. Nat Genet *26*, 211-215.

Allan, C.M., Awad, A.M., Johnson, J.S., Shirasaki, D.I., Wang, C., Blaby-Haas, C.E., Merchant, S.S., Loo, J.A., and Clarke, C.F. (2015). Identification of Coq11, a new coenzyme Q biosynthetic protein in the CoQ-synthome in Saccharomyces cerevisiae. J Biol Chem *290*, 7517-7534.

Anand, R., Wai, T., Baker, M.J., Kladt, N., Schauss, A.C., Rugarli, E., and Langer, T. (2014). The i-AAA protease YME1L and OMA1 cleave OPA1 to balance mitochondrial fusion and fission. The Journal of cell biology *204*, 919-929.

Aparicio, R., Rana, A., and Walker, D.W. (2019). Upregulation of the Autophagy Adaptor p62/SQSTM1 Prolongs Health and Lifespan in Middle-Aged Drosophila. Cell Rep *28*, 1029-1040.e1025.

Arlt, H., Tauer, R., Feldmann, H., Neupert, W., and Langer, T. (1996). The YTA10-12 complex, an AAA protease with chaperone-like activity in the inner membrane of mitochondria. Cell *85*, 875-885.

Arnold, I., Wagner-Ecker, M., Ansorge, W., and Langer, T. (2006). Evidence for a novel mitochondria-to-nucleus signalling pathway in respiring cells lacking i-AAA protease and the ABC-transporter Mdl1. Gene *367*, 74-88.

Arutyunova, E., Jiang, Z., Yang, J., Kulepa, A.N., Young, H.S., Verhelst, S., O'Donoghue, A.J., and Lemieux, M.J. (2018). An internally quenched peptide as a new model substrate for rhomboid intramembrane proteases. Biol Chem.

Arutyunova, E., Panwar, P., Skiba, P.M., Gale, N., Mak, M.W., and Lemieux, M.J. (2014). Allosteric regulation of rhomboid intramembrane proteolysis. EMBO J *33*, 1869-1881.

Ast, T., Michaelis, S., and Schuldiner, M. (2016). The Protease Ste24 Clears Clogged Translocons. Cell *164*, 103-114.

Aubin-Tam, M.-E., Olivares, Adrian O., Sauer, Robert T., Baker, Tania A., and Lang, Matthew J. (2011). Single-Molecule Protein Unfolding and Translocation by an ATP-Fueled Proteolytic Machine. Cell *145*, 257-267.

Augustin, S., Nolden, M., Müller, S., Hardt, O., Arnold, I., and Langer, T. (2005). Characterization of Peptides Released from Mitochondria: EVIDENCE FOR CONSTANT PROTEOLYSIS AND PEPTIDE EFFLUX *. Journal of Biological Chemistry *280*, 2691-2699.

Avci, D., Fuchs, S., Schrul, B., Fukumori, A., Breker, M., Frumkin, I., Chen, C.Y., Biniossek, M.L., Kremmer, E., Schilling, O.*, et al.* (2014). The Yeast ER-Intramembrane Protease Ypf1 Refines Nutrient Sensing by Regulating Transporter Abundance. Mol Cell *56*, 630-640.

Avci, D., Malchus, N.S., Heidasch, R., Lorenz, H., Richter, K., Nessling, M., and Lemberg, M.K. (2019). The intramembrane protease SPP impacts morphology of the endoplasmic reticulum by triggering degradation of morphogenic proteins. J Biol Chem *294*, 2786-2800.

Azad, N., Vallyathan, V., Wang, L., Tantishaiyakul, V., Stehlik, C., Leonard, S.S., and Rojanasakul, Y. (2006). S-nitrosylation of Bcl-2 inhibits its ubiquitin-proteasomal degradation. A novel antiapoptotic mechanism that suppresses apoptosis. J Biol Chem *281*, 34124-34134.

Baba, T., Ara, T., Hasegawa, M., Takai, Y., Okumura, Y., Baba, M., Datsenko, K.A., Tomita, M., Wanner, B.L., and Mori, H. (2006). Construction of Escherichia coli K-12 in-frame, single-gene knockout mutants: the Keio collection. Molecular systems biology *2*, 2006.0008.

Baba, T., Tanimura, S., Yamaguchi, A., Horikawa, K., Yokozeki, M., Hachiya, S., Iemura, S.-I., Natsume, T., Matsuda, N., and Takeda, K. (2021). Cleaved PGAM5 dephosphorylates nuclear serine/arginine-rich proteins during mitophagy. Biochimica et Biophysica Acta (BBA) - Molecular Cell Research *1868*, 119045.

Baeza-Delgado, C., Marti-Renom, M.A., and Mingarro, I. (2013). Structure-based statistical analysis of transmembrane helices. Eur Biophys J *42*, 199-207.

Baker, M.J., Lampe, P.A., Stojanovski, D., Korwitz, A., Anand, R., Tatsuta, T., and Langer, T. (2014). Stress-induced OMA1 activation and autocatalytic turnover regulate OPA1-dependent mitochondrial dynamics. The EMBO journal *33*, 578-593.

Baker, R.P., and Urban, S. (2015). Cytosolic extensions directly regulate a rhomboid protease by modulating substrate gating. Nature *523*, 101-105.

Baker, R.P., Young, K., Feng, L., Shi, Y., and Urban, S. (2007). Enzymatic analysis of a rhomboid intramembrane protease implicates transmembrane helix 5 as the lateral substrate gate. Proc. Natl. Acad. Sci. USA *104*, 8257-8262.

Bakula, D., and Scheibye-Knudsen, M. (2020). MitophAging: Mitophagy in Aging and Disease. Frontiers in cell and developmental biology *8*, 239-239.

Ballard, K.J., and Holt, S.J. (1968). Cytological and cytochemical studies on cell death and digestion in the foetal rat foot: the role of macrophages and hydrolytic enzymes. J Cell Sci *3*, 245-262.

Ban, T., Ishihara, T., Kohno, H., Saita, S., Ichimura, A., Maenaka, K., Oka, T., Mihara, K., and Ishihara, N. (2017). Molecular basis of selective mitochondrial fusion by heterotypic action between OPA1 and cardiolipin. Nature cell biology *19*, 856-863.

Banci, L., Bertini, I., Calderone, V., Cefaro, C., Ciofi-Baffoni, S., Gallo, A., and Tokatlidis, K. (2012). An Electron-Transfer Path through an Extended Disulfide Relay System: The Case of the Redox Protein ALR. Journal of the American Chemical Society *134*, 1442-1445.

Barniol-Xicota, M., and Verhelst, S.H.L. (2018). Stable and Functional Rhomboid Proteases in Lipid Nanodiscs by Using Diisobutylene/Maleic Acid Copolymers. Journal of the American Chemical Society *140*, 14557-14561.

Barrett, P.J., Song, Y., Van Horn, W.D., Hustedt, E.J., Schafer, J.M., Hadziselimovic, A., Beel, A.J., and Sanders, C.R. (2012). The amyloid precursor protein has a flexible transmembrane domain and binds cholesterol. Science *336*, 1168-1171.

Barrowman, J., and Michaelis, S. (2009). ZMPSTE24, an integral membrane zinc metalloprotease with a connection to progeroid disorders. Biol Chem *390*, 761-773.

Barrowman, J., Wiley, P.A., Hudon-Miller, S.E., Hrycyna, C.A., and Michaelis, S. (2012). Human ZMPSTE24 disease mutations: residual proteolytic activity correlates with disease severity. Hum Mol Genet *21*, 4084-4093.

Basso, V., Marchesan, E., Peggion, C., Chakraborty, J., von Stockum, S., Giacomello, M., Ottolini, D., Debattisti, V., Caicci, F., Tasca, E.*, et al.* (2018). Regulation of ER-mitochondria contacts by Parkin via Mfn2. Pharmacological Research *138*, 43-56.

Battistini, C., Rehman, M., Avolio, M., Arduin, A., Valdembri, D., Serini, G., and Tamagnone, L. (2019). Rhomboid-Like-2 Intramembrane Protease Mediates Metalloprotease-Independent Regulation of Cadherins. International Journal of Molecular Sciences *20*.

Becker-Herman, S., Arie, G., Medvedovsky, H., Kerem, A., and Shachar, I. (2005). CD74 is a member of the regulated intramembrane proteolysis-processed protein family. Mol Biol Cell *16*, 5061-5069.

Becker, T., Pfannschmidt, S., Guiard, B., Stojanovski, D., Milenkovic, D., Kutik, S., Pfanner, N., Meisinger, C., and Wiedemann, N. (2008). Biogenesis of the mitochondrial TOM complex: Mim1 promotes insertion and assembly of signal-anchored receptors. J Biol Chem *283*, 120-127.

Becker, T., Wenz, L.S., Krüger, V., Lehmann, W., Müller, J.M., Goroncy, L., Zufall, N., Lithgow, T., Guiard, B., Chacinska, A.*, et al.* (2011). The mitochondrial import protein Mim1 promotes biogenesis of multispanning outer membrane proteins. J Cell Biol *194*, 387-395.

Began, J., Cordier, B., Brezinova, J., Delisle, J., Hexnerova, R., Srb, P., Rampirova, P., Kozisek, M., Baudet, M., Coute, Y.*, et al.* (2020). Rhomboid intramembrane protease YqgP licenses bacterial membrane protein quality control as adaptor of FtsH AAA protease. EMBO J, e102935.

Benard, G., Neutzner, A., Peng, G., Wang, C., Livak, F., Youle, R.J., and Karbowski, M. (2010). IBRDC2, an IBR-type E3 ubiquitin ligase, is a regulatory factor for Bax and apoptosis activation. Embo j *29*, 1458-1471.

Benilova, I., Karran, E., and De Strooper, B. (2012). The toxic Aβ oligomer and Alzheimer's disease: an emperor in need of clothes. Nat Neurosci *15*, 349-357.

Bergbold, N., and Lemberg, M.K. (2013). Emerging role of rhomboid family proteins in mammalian biology and disease. Biochim Biophys Acta, doi: 10.1016/j.bbamem.2013.1003.1025.

Bergo, M.O., Lieu, H.D., Gavino, B.J., Ambroziak, P., Otto, J.C., Casey, P.J., Walker, Q.M., and Young, S.G. (2004). On the Physiological Importance of Endoproteolysis of CAAX Proteins: HEART-SPECIFIC RCE1 KNOCKOUT MICE DEVELOP A LETHAL CARDIOMYOPATHY*. Journal of Biological Chemistry *279*, 4729-4736.

Bernardini, J.P., Lazarou, M., and Dewson, G. (2017). Parkin and mitophagy in cancer. Oncogene *36*, 1315-1327.

Bernkopf, D.B., Jalal, K., Bruckner, M., Knaup, K.X., Gentzel, M., Schambony, A., and Behrens, J. (2018). Pgam5 released from damaged mitochondria induces mitochondrial biogenesis via Wnt signaling. J Cell Biol *4*, 1383–1394.

Bien, M., Longen, S., Wagener, N., Chwalla, I., Herrmann, J.M., and Riemer, J. (2010). Mitochondrial disulfide bond formation is driven by intersubunit electron transfer in Erv1 and proofread by glutathione. Mol Cell *37*, 516-528.

Bihlmaier, K., Mesecke, N., Terziyska, N., Bien, M., Hell, K., and Herrmann, J.M. (2007). The disulfide relay system of mitochondria is connected to the respiratory chain. The Journal of cell biology *179*, 389-395.

Blow, D.M., Birktoft, J.J., and Hartley, B.S. (1969). Role of a Buried Acid Group in the Mechanism of Action of Chymotrypsin. Nature *221*, 337-340.

Bock, F.J., and Tait, S.W.G. (2020). Mitochondria as multifaceted regulators of cell death. Nature Reviews Molecular Cell Biology *21*, 85-100.

Bock, J. (2018). Biochemical characterization of rhomboid proteases. Master thesis (AG Lemberg), 60.

Bock, J., Kühnle, N., Knopf, J.D., Landscheidt, N., Lee, J.-G., Ye, Y., and Lemberg, M.K. (2021). Rhomboid protease RHBDL4 promotes retrotranslocation of aggregation-prone proteins for degradation. bioRxiv, 848754.

Bolduc, D.M., Montagna, D.R., Gu, Y., Selkoe, D.J., and Wolfe, M.S. (2016). Nicastrin functions to sterically hinder γ-secretase–substrate interactions driven by substrate transmembrane domain. Proceedings of the National Academy of Sciences *113*, E509-E518.

Boname, J.M., Bloor, S., Wandel, M.P., Nathan, J.A., Antrobus, R., Dingwell, K.S., Thurston, T.L., Smith, D.L., Smith, J.C., Randow, F.*, et al.* (2014). Cleavage by signal peptide peptidase is required for the degradation of selected tail-anchored proteins. J Cell Biol *205*, 847-862.

Bondar, A.N. (2019). Mechanisms by Which Lipids Influence Conformational Dynamics of the GlpG Intramembrane Protease. J Phys Chem B *123*, 4159-4172.

Bondar, A.N., del Val, C., and White, S.H. (2009). Rhomboid protease dynamics and lipid interactions. Structure *17*, 395-405.

Bondar, A.N., and Lemieux, M.J. (2019). Reactions at Biomembrane Interfaces. Chem Rev *119*, 6162-6183.

Borchelt, D.R., Thinakaran, G., Eckman, C.B., Lee, M.K., Davenport, F., Ratovitsky, T., Prada, C.M., Kim, G., Seekins, S., Yager, D.*, et al.* (1996). Familial Alzheimer's disease-linked presenilin 1 variants elevate Abeta1-42/1-40 ratio in vitro and in vivo. Neuron *17*, 1005-1013.

Bosco, D.A., LaVoie, M.J., Petsko, G.A., and Ringe, D. (2011). Proteostasis and movement disorders: Parkinson's disease and amyotrophic lateral sclerosis. Cold Spring Harbor perspectives in biology *3*, a007500-a007500.

Bota, D.A., and Davies, K.J.A. (2002). Lon protease preferentially degrades oxidized mitochondrial aconitase by an ATP-stimulated mechanism. Nature Cell Biology *4*, 674-680.

Botelho, A.V., Gibson, N.J., Thurmond, R.L., Wang, Y., and Brown, M.F. (2002). Conformational Energetics of Rhodopsin Modulated by Nonlamellar-Forming Lipids. Biochemistry *41*, 6354-6368.

Botelho, S.C., Tatsuta, T., von Heijne, G., and Kim, H. (2013). Dislocation by the m-AAA protease increases the threshold hydrophobicity for retention of transmembrane helices in the inner membrane of yeast mitochondria. J Biol Chem *288*, 4792-4798.

Boyartchuk, V.L., Ashby, M.N., and Rine, J. (1997). Modulation of Ras and a-factor function by carboxyl-terminal proteolysis. Science *275*, 1796-1800.

Bragoszewski, P., Gornicka, A., Sztolsztener, M.E., and Chacinska, A. (2013). The ubiquitin-proteasome system regulates mitochondrial intermembrane space proteins. Mol Cell Biol *33*, 2136-2148.

Bragoszewski, P., Wasilewski, M., Sakowska, P., Gornicka, A., Böttinger, L., Qiu, J., Wiedemann, N., and Chacinska, A. (2015). Retro-translocation of mitochondrial intermembrane space proteins. Proceedings of the National Academy of Sciences *112*, 7713.

Branda, S.S., and Isaya, G. (1995). Prediction and identification of new natural substrates of the yeast mitochondrial intermediate peptidase. J Biol Chem *270*, 27366-27373.

Bräuer, M., Zich, M.T., Önder, K., and Müller, N. (2019). The influence of commonly used tags on structural propensities and internal dynamics of peptides. Monatshefte für Chemie - Chemical Monthly *150*, 913-925.

Breitschopf, K., Haendeler, J., Malchow, P., Zeiher, A.M., and Dimmeler, S. (2000). Posttranslational modification of Bcl-2 facilitates its proteasome-dependent degradation: molecular characterization of the involved signaling pathway. Mol Cell Biol *20*, 1886-1896.

Brix, J., Rüdiger, S., Bukau, B., Schneider-Mergener, J., and Pfanner, N. (1999). Distribution of binding sequences for the mitochondrial import receptors Tom20, Tom22, and Tom70 in a presequence-carrying preprotein and a non-cleavable preprotein. J Biol Chem *274*, 16522-16530.

Brown, M.S., Ye, J., Rawson, R.B., and Goldstein, J.L. (2000). Regulated intramembrane proteolysis: a control mechanism conserved from bacteria to humans. Cell *100*, 391-398.

Burri, L., Strahm, Y., Hawkins, C.J., Gentle, I.E., Puryer, M.A., Verhagen, A., Callus, B., Vaux, D., and Lithgow, T. (2005). Mature DIABLO/Smac Is Produced by the IMP Protease Complex on the Mitochondrial Inner Membrane. Molecular Biology of the Cell *16*, 2926-2933.

Buxbaum, J.D., Liu, K.N., Luo, Y., Slack, J.L., Stocking, K.L., Peschon, J.J., Johnson, R.S., Castner, B.J., Cerretti, D.P., and Black, R.A. (1998). Evidence that tumor necrosis factor alpha converting enzyme is involved in regulated alpha-secretase cleavage of the Alzheimer amyloid protein precursor. J Biol Chem *273*, 27765-27767.

Callegari, S., Cruz-Zaragoza, L.D., and Rehling, P. (2020). From TOM to the TIM23 complex – handing over of a precursor. Biological Chemistry *401*, 709-721.

Calvo, S.E., Clauser, K.R., and Mootha, V.K. (2016). MitoCarta2.0: an updated inventory of mammalian mitochondrial proteins. Nucleic acids research *44*, D1251-D1257.

Cao, Y.-L., Meng, S., Chen, Y., Feng, J.-X., Gu, D.-D., Yu, B., Li, Y.-J., Yang, J.-Y., Liao, S., Chan, D.C.*, et al.* (2017). MFN1 structures reveal nucleotide-triggered dimerization critical for mitochondrial fusion. Nature *542*, 372-376.

Capo-Chichi, J.M., Boissel, S., Brustein, E., Pickles, S., Fallet-Bianco, C., Nassif, C., Patry, L., Dobrzeniecka, S., Liao, M., Labuda, D.*, et al.* (2015). Disruption of CLPB is associated with congenital microcephaly, severe encephalopathy and 3-methylglutaconic aciduria. J Med Genet *52*, 303-311.

Capponi, A.M., Rossier, M.F., Davies, E., and Vallotton, M.B. (1988). Calcium stimulates steroidogenesis in permeabilized bovine adrenal cortical cells. J Biol Chem *263*, 16113-16117.

Carafoli, E. (2004). Calcium signaling: a historical account. Biol Res *37*, 497-505.

Carneiro, B.A., and El-Deiry, W.S. (2020). Targeting apoptosis in cancer therapy. Nat Rev Clin Oncol *17*, 395-417.

Cenni, V., D'Apice, M.R., Garagnani, P., Columbaro, M., Novelli, G., Franceschi, C., and Lattanzi, G. (2018). Mandibuloacral dysplasia: A premature ageing disease with aspects of physiological ageing. Ageing research reviews *42*, 1-13.

Chacinska, A., Koehler, C.M., Milenkovic, D., Lithgow, T., and Pfanner, N. (2009). Importing mitochondrial proteins: machineries and mechanisms. Cell *138*, 628-644.

Chacinska, A., Lind, M., Frazier, A.E., Dudek, J., Meisinger, C., Geissler, A., Sickmann, A., Meyer, H.E., Truscott, K.N., Guiard, B*., et al.* (2005). Mitochondrial Presequence Translocase: Switching between TOM Tethering and Motor Recruitment Involves Tim21 and Tim17. Cell *120*, 817-829.

Chacinska, A., Pfannschmidt, S., Wiedemann, N., Kozjak, V., Sanjuán Szklarz, L.K., Schulze-Specking, A., Truscott, K.N., Guiard, B., Meisinger, C., and Pfanner, N. (2004). Essential role of Mia40 in import and assembly of mitochondrial intermembrane space proteins. The EMBO journal *23*, 3735-3746.

Chaiet, L., and Wolf, F.J. (1964). THE PROPERTIES OF STREPTAVIDIN, A BIOTIN-BINDING PROTEIN PRODUCED BY STREPTOMYCETES. Arch Biochem Biophys *106*, 1-5.

Chaikuad, A., Filippakopoulos, P., Marcsisin, S.R., Picaud, S., Schroder, M., Sekine, S., Ichijo, H., Engen, J.R., Takeda, K., and Knapp, S. (2017). Structures of PGAM5 Provide Insight into Active Site Plasticity and Multimeric Assembly. Structure *25*, 1089-1099 e1083.

Chakrabarti, R., Ji, W.-K., Stan, R.V., de Juan Sanz, J., Ryan, T.A., and Higgs, H.N. (2017). INF2-mediated actin polymerization at the ER stimulates mitochondrial calcium uptake, inner membrane constriction, and division. Journal of Cell Biology *217*, 251-268.

Chao, J.-R., Parganas, E., Boyd, K., Hong, C.Y., Opferman, J.T., and Ihle, J.N. (2008). Hax1-mediated processing of HtrA2 by Parl allows survival of lymphocytes and neurons. Nature *452*, 98-102.

Chatzi, A., Manganas, P., and Tokatlidis, K. (2016). Oxidative folding in the mitochondrial intermembrane space: A regulated process important for cell physiology and disease. Biochim Biophys Acta *1863*, 1298-1306.

Chen, A.C., Kim, S., Shepardson, N., Patel, S., Hong, S., and Selkoe, D.J. (2015). Physical and functional interaction between the α- and γ-secretases: A new model of regulated intramembrane proteolysis. J Cell Biol *211*, 1157-1176.

Chen, C.-y., Malchus, N.S., Hehn, B., Stelzer, W., Avci, D., Langosch, D., and Lemberg, M.K. (2014a). Signal peptide peptidase functions in ERAD to cleave the unfolded protein response regulator XBP1u. The EMBO journal *33*, 2492-2506.

Chen, G., Han, Z., Du, F., Chen, Y., Chen, L., Wu, H., Huang, L., Zhou, C., Cai, X., Fu, C*., et al.* (2014b). A regulatory signaling loop comprising the PGAM5 phosphatase and CK2 controls receptor-mediated mitophagy. Molecular cell *54*, 362-377.

Chen, H., Shaffer, P.L., Huang, X., and Rose, P.E. (2013). Rapid screening of membrane protein expression in transiently transfected insect cells. Protein Expr Purif *88*, 134-142.

Chen, W.J., and Douglas, M.G. (1987). Phosphodiester bond cleavage outside mitochondria is required for the completion of protein import into the mitochondrial matrix. Cell *49*, 651-658.

Chen, X., Van Valkenburgh, C., Fang, H., and Green, N. (1999). Signal peptides having standard and nonstandard cleavage sites can be processed by Imp1p of the mitochondrial inner membrane protease. J Biol Chem *274*, 37750-37754.

Cheng, J., Zhu, Y., He, S., Lu, Y., Chen, J., Han, B., Petrillo, M., Wrzeszczynski, K.O., Yang, S., Dai, P*., et al.* (2011). Functional mutation of SMAC/DIABLO, encoding a mitochondrial proapoptotic protein, causes human progressive hearing loss DFNA64. American journal of human genetics *89*, 56-66.

Cheng, M., Lin, N., Dong, D., Ma, J., Su, J., and Sun, L. (2021). PGAM5: A crucial role in mitochondrial dynamics and programmed cell death. European journal of cell biology *100*, 151144.

Cherradi, N., Rossier, M.F., Vallotton, M.B., and Capponi, A.M. (1996). Calcium stimulates intramitochondrial cholesterol transfer in bovine adrenal glomerulosa cells. J Biol Chem *271*, 25971-25975.

Chipuk, J.E., Bouchier-Hayes, L., and Green, D.R. (2006). Mitochondrial outer membrane permeabilization during apoptosis: the innocent bystander scenario. Cell Death Differ *13*, 1396-1402.

Cho, B., Cho, H.M., Jo, Y., Kim, H.D., Song, M., Moon, C., Kim, H., Kim, K., Sesaki, H., Rhyu, I.J.*, et al.* (2017). Constriction of the mitochondrial inner compartment is a priming event for mitochondrial division. Nature Communications *8*, 15754.

Cho, D.H., Nakamura, T., Fang, J., Cieplak, P., Godzik, A., Gu, Z., and Lipton, S.A. (2009). S-nitrosylation of Drp1 mediates beta-amyloid-related mitochondrial fission and neuronal injury. Science *324*, 102-105.

Cho, H.M., Ryu, J.R., Jo, Y., Seo, T.W., Choi, Y.N., Kim, J.H., Chung, J.M., Cho, B., Kang, H.C., Yu, S.-W.*, et al.* (2019a). Drp1-Zip1 Interaction Regulates Mitochondrial Quality Surveillance System. Molecular Cell *73*, 364-376.e368.

Cho, S., Baker, R.P., Ji, M., and Urban, S. (2019b). Ten catalytic snapshots of rhomboid intramembrane proteolysis from gate opening to peptide release. Nat Struct Mol Biol *26*, 910-918.

Cho, S., Dickey, S.W., and Urban, S. (2016). Crystal Structures and Inhibition Kinetics Reveal a Two-Stage Catalytic Mechanism with Drug Design Implications for Rhomboid Proteolysis. Mol Cell *61*, 329-340.

Christiansen, J.R., Kolandaivelu, S., Bergo, M.O., and Ramamurthy, V. (2011). RAS-converting enzyme 1-mediated endoproteolysis is required for trafficking of rod phosphodiesterase 6 to photoreceptor outer segments. Proceedings of the National Academy of Sciences of the United States of America *108*, 8862-8866.

Cipolat, S., Rudka, T., Hartmann, D., Costa, V., Serneels, L., Craessaerts, K., Metzger, K., Frezza, C., Annaert, W., D'Adamio, L.*, et al.* (2006). Mitochondrial rhomboid PARL regulates cytochrome c release during apoptosis via OPA1-dependent cristae remodeling. Cell *126*, 163-175.

Citron, M., Westaway, D., Xia, W., Carlson, G., Diehl, T., Levesque, G., Johnson-Wood, K., Lee, M., Seubert, P., Davis, A.*, et al.* (1997). Mutant presenilins of Alzheimer's disease increase production of 42-residue amyloid beta-protein in both transfected cells and transgenic mice. Nat Med *3*, 67-72.

Clemmer, K.M., Sturgill, G.M., Veenstra, A., and Rather, P.N. (2006). Functional characterization of Escherichia coli GlpG and additional rhomboid proteins using an aarA mutant of Providencia stuartii. Journal of bacteriology *188*, 3415-3419.

Cohen, M.M., Leboucher, G.P., Livnat-Levanon, N., Glickman, M.H., and Weissman, A.M. (2008). Ubiquitin-proteasome-dependent degradation of a mitofusin, a critical regulator of mitochondrial fusion. Mol Biol Cell *19*, 2457-2464.

Cohen, S., Valm, A.M., and Lippincott-Schwartz, J. (2018). Interacting organelles. Current opinion in cell biology *53*, 84-91.

Conboy, J.G., Fenton, W.A., and Rosenberg, L.E. (1982). Processing of pre-ornithine transcarbamylase requires a zinc-dependent protease localized to the mitochondrial matrix. Biochem Biophys Res Commun *105*, 1-7.

Cordier, B., and Lemberg, M.K. (2017). Probing the Activity of Eukaryotic Rhomboid Proteases In Vitro. Methods Enzymol *584*, 99-126.

Cox, D.A., Conforti, L., Sperelakis, N., and Matlib, M.A. (1993). Selectivity of inhibition of Na(+)-Ca2+ exchange of heart mitochondria by benzothiazepine CGP-37157. J Cardiovasc Pharmacol *21*, 595-599.

Cribbs, J.T., and Strack, S. (2007). Reversible phosphorylation of Drp1 by cyclic AMP-dependent protein kinase and calcineurin regulates mitochondrial fission and cell death. EMBO Rep *8*, 939-944.

Cuconati, A., Mukherjee, C., Perez, D., and White, E. (2003). DNA damage response and MCL-1 destruction initiate apoptosis in adenovirus-infected cells. Genes Dev *17*, 2922-2932.

Cupo, R.R., and Shorter, J. (2020). Skd3 (human ClpB) is a potent mitochondrial protein disaggregase that is inactivated by 3-methylglutaconic aciduria-linked mutations. Elife *9*.

Curran, S.P., Leuenberger, D., Oppliger, W., and Koehler, C.M. (2002). The Tim9p-Tim10p complex binds to the transmembrane domains of the ADP/ATP carrier. The EMBO journal *21*, 942-953.

Cymer, F., Heijne, G., and White, S.H. (2015). Mechanisms of integral membrane protein insertion and folding. Journal of molecular biology *427*, 999-1022.

Dabir, D.V., Leverich, E.P., Kim, S.K., Tsai, F.D., Hirasawa, M., Knaff, D.B., and Koehler, C.M. (2007). A role for cytochrome c and cytochrome c peroxidase in electron shuttling from Erv1. Embo j *26*, 4801-4811.

Daverey, A., Levytskyy, R.M., Stanke, K.M., Viana, M.P., Swenson, S., Hayward, S.L., Narasimhan, M., Khalimonchuk, O., and Kidambi, S. (2019). Depletion of mitochondrial protease OMA1 alters proliferative properties and promotes metastatic growth of breast cancer cells. Scientific Reports *9*, 14746.

Davies, K.M., Strauss, M., Daum, B., Kief, J.H., Osiewacz, H.D., Rycovska, A., Zickermann, V., and Kühlbrandt, W. (2011). Macromolecular organization of ATP synthase and complex I in whole mitochondria. Proc Natl Acad Sci U S A *108*, 14121-14126.

de Brito, O.M., and Scorrano, L. (2008). Mitofusin 2 tethers endoplasmic reticulum to mitochondria. Nature *456*, 605-610.

de Castro, I.P., Martins, L.M., and Loh, S.H. (2011). Mitochondrial quality control and Parkinson's disease: a pathway unfolds. Mol Neurobiol *43*, 80-86.

de Koning, P.J., Tesselaar, K., Bovenschen, N., Colak, S., Quadir, R., Volman, T.J., and Kummer, J.A. (2010). The cytotoxic protease granzyme M is expressed by lymphocytes of both the innate and adaptive immune system. Mol Immunol *47*, 903-911.

De Strooper, B., Annaert, W., Cupers, P., Saftig, P., Craessaerts, K., Mumm, J.S., Schroeter, E.H., Schrijvers, V., Wolfe, M.S., Ray, W.J.*, et al.* (1999). A presenilin-1-dependent gamma-secretase-like protease mediates release of Notch intracellular domain. Nature *398*, 518-522.

De Strooper, B., Saftig, P., Craessaerts, K., Vanderstichele, H., Guhde, G., Annaert, W., Von Figura, K., and Van Leuven, F. (1998). Deficiency of presenilin-1 inhibits the normal cleavage of amyloid precursor protein. Nature *391*, 387-390.

Deas, E., Plun-Favreau, H., Gandhi, S., Desmond, H., Kjaer, S., Loh, S.H., Renton, A.E., Harvey, R.J., Whitworth, A.J., Martins, L.M.*, et al.* (2011). PINK1 cleavage at position A103 by the mitochondrial protease PARL. Hum Mol Genet *20*, 867-879.

Deas, E., Plun-Favreau, H., and Wood, N.W. (2009). PINK1 function in health and disease. EMBO Mol Med *1*, 152-165.

Deber, C.M., and Li, S.C. (1995). Peptides in membranes: helicity and hydrophobicity. Biopolymers *37*, 295-318.

Delettre, C., Lenaers, G., Griffoin, J.M., Gigarel, N., Lorenzo, C., Belenguer, P., Pelloquin, L., Grosgeorge, J., Turc-Carel, C., Perret, E.*, et al.* (2000). Nuclear gene OPA1, encoding a mitochondrial dynamin-related protein, is mutated in dominant optic atrophy. Nat Genet *26*, 207-210.

den Brave, F., Engelke, J., and Becker, T. (2021). Quality control of protein import into mitochondria. Biochemical Journal *478*, 3125-3143.

Desautels, M., and Goldberg, A.L. (1982). Liver mitochondria contain an ATP-dependent, vanadate-sensitive pathway for the degradation of proteins. Proc Natl Acad Sci U S A *79*, 1869-1873.

Deshwal, S., Fiedler, K.U., and Langer, T. (2020). Mitochondrial Proteases: Multifaceted Regulators of Mitochondrial Plasticity. Annual Review of Biochemistry *89*, 501-528.

DeVay, R.M., Dominguez-Ramirez, L., Lackner, L.L., Hoppins, S., Stahlberg, H., and Nunnari, J. (2009). Coassembly of Mgm1 isoforms requires cardiolipin and mediates mitochondrial inner membrane fusion. Journal of Cell Biology *186*, 793-803.

Dickey, S.W., Baker, R.P., Cho, S., and Urban, S. (2013). Proteolysis inside the Membrane Is a Rate-Governed Reaction Not Driven by Substrate Affinity. Cell *155*, 1270-1281.

Dimmer, K.S., Papić, D., Schumann, B., Sperl, D., Krumpe, K., Walther, D.M., and Rapaport, D. (2012). A crucial role for Mim2 in the biogenesis of mitochondrial outer membrane proteins. J Cell Sci *125*, 3464-3473.

Dimroth, P., Kaim, G., and Matthey, U. (2000). Crucial role of the membrane potential for ATP synthesis by F(1)F(o) ATP synthases. J Exp Biol *203*, 51-59.

Ding, W.-X., and Yin, X.-M. (2012). Mitophagy: mechanisms, pathophysiological roles, and analysis. Biological Chemistry *393*, 547-564.

Dolmetsch, R.E., Xu, K., and Lewis, R.S. (1998). Calcium oscillations increase the efficiency and specificity of gene expression. Nature *392*, 933-936.

Dominguez, L., Meredith, S.C., Straub, J.E., and Thirumalai, D. (2014). Transmembrane Fragment Structures of Amyloid Precursor Protein Depend on Membrane Surface Curvature. Journal of the American Chemical Society *136*, 854-857.

Drag, M., and Salvesen, G.S. (2010). Emerging principles in protease-based drug discovery. Nature reviews. Drug discovery *9*, 690-701.

Drew, D., Fröderberg, L., Baars, L., and de Gier, J.W. (2003). Assembly and overexpression of membrane proteins in Escherichia coli. Biochim Biophys Acta *1610*, 3-10.

Duchen, M.R. (2000). Mitochondria and calcium: from cell signalling to cell death. J Physiol *529 Pt 1*, 57-68.

Dudek, J. (2017). Role of Cardiolipin in Mitochondrial Signaling Pathways. Front Cell Dev Biol *5*, 90.

Dulloo, I., Muliyil, S., and Freeman, M. (2019). The molecular, cellular and pathophysiological roles of iRhom pseudoproteases. Open Biology *9*, 190003.

Durocher, Y., Perret, S., and Kamen, A. (2002). High-level and high-throughput recombinant protein production by transient transfection of suspension-growing human 293-EBNA1 cells. Nucleic Acids Res *30*, E9.

Duvezin-Caubet, S., Koppen, M., Wagener, J., Zick, M., Israel, L., Bernacchia, A., Jagasia, R., Rugarli, E.I., Imhof, A., Neupert, W.*, et al.* (2007). OPA1 processing reconstituted in yeast depends on the subunit composition of the m-AAA protease in mitochondria. Mol Biol Cell *18*, 3582-3590.

Dyall, S.D., Brown, M.T., and Johnson, P.J. (2004). Ancient invasions: from endosymbionts to organelles. Science *304*, 253-257.

Edlich, F., Banerjee, S., Suzuki, M., Cleland, M.M., Arnoult, D., Wang, C., Neutzner, A., Tjandra, N., and Youle, R.J. (2011). Bcl-x(L) retrotranslocates Bax from the mitochondria into the cytosol. Cell *145*, 104-116.

Ehrmann, M., and Clausen, T. (2004). Proteolysis as a regulatory mechanism. Annu Rev Genet *38*, 709-724.

Ehses, S., Raschke, I., Mancuso, G., Bernacchia, A., Geimer, S., Tondera, D., Martinou, J.-C., Westermann, B., Rugarli, E.I., and Langer, T. (2009). Regulation of OPA1 processing and mitochondrial fusion by m-AAA protease isoenzymes and OMA1. The Journal of cell biology *187*, 1023-1036.

Eilers, M., Oppliger, W., and Schatz, G. (1987). Both ATP and an energized inner membrane are required to import a purified precursor protein into mitochondria. Embo j *6*, 1073-1077.

Einhauer, A., and Jungbauer, A. (2001). The FLAG peptide, a versatile fusion tag for the purification of recombinant proteins. J Biochem Biophys Methods *49*, 455-465.

Ellison, D., Hinton, J., Hubbard, S.J., and Beynon, R.J. (1995). Limited proteolysis of native proteins: the interaction between avidin and proteinase K. Protein Sci *4*, 1337-1345.

Endres, M., Neupert, W., and Brunner, M. (1999). Transport of the ADP/ATP carrier of mitochondria from the TOM complex to the TIM22.54 complex. The EMBO journal *18*, 3214-3221.

Englander, S.W., Mayne, L., Bai, Y., and Sosnick, T.R. (1997). Hydrogen exchange: the modern legacy of Linderstrøm-Lang. Protein Sci *6*, 1101-1109.

Erez, E., and Bibi, E. (2009). Cleavage of a multispanning membrane protein by an intramembrane serine protease. Biochemistry *48*, 12314-12322.

Erez, E., Fass, D., and Bibi, E. (2009). How intramembrane proteases bury hydrolytic reactions in the membrane. Nature *459*, 371-378.

Esler, W.P., and Wolfe, M.S. (2001). A portrait of Alzheimer secretases--new features and familiar faces. Science *293*, 1449-1454.

Esser, K., Tursun, B., Ingenhoven, M., Michaelis, G., and Pratje, E. (2002). A novel two-step mechanism for removal of a mitochondrial signal sequence involves the mAAA complex and the putative rhomboid protease Pcp1. J. Mol. Biol. *323*, 835-843.

Falkevall, A., Alikhani, N., Bhushan, S., Pavlov, P.F., Busch, K., Johnson, K.A., Eneqvist, T., Tjernberg, L., Ankarcrona, M., and Glaser, E. (2006). Degradation of the amyloid beta-protein by the novel mitochondrial peptidasome, PreP. J Biol Chem *281*, 29096-29104.

Feng, L., Yan, H., Wu, Z., Yan, N., Wang, Z., Jeffrey, P.D., and Shi, Y. (2007). Structure of a site-2 protease family intramembrane metalloprotease. Science *318*, 1608-1612.

Fernandez, M.A., Biette, K.M., Dolios, G., Seth, D., Wang, R., and Wolfe, M.S. (2016). Transmembrane Substrate Determinants for gamma-Secretase Processing of APP CTFbeta. Biochemistry *55*, 5675-5688.

Fiesel, F.C., James, E.D., Hudec, R., and Springer, W. (2017). Mitochondrial targeted HSP90 inhibitor Gamitrinib-TPP (G-TPP) induces PINK1/Parkin-dependent mitophagy. Oncotarget *8*, 106233-106248.

Fischer, M., and Riemer, J. (2013). The Mitochondrial Disulfide Relay System: Roles in Oxidative Protein Folding and Beyond. International Journal of Cell Biology *2013*, 742923.

Fivenson, E.M., Lautrup, S., Sun, N., Scheibye-Knudsen, M., Stevnsner, T., Nilsen, H., Bohr, V.A., and Fang, E.F. (2017). Mitophagy in neurodegeneration and aging. Neurochem Int *109*, 202-209.

Fleck, D., Voss, M., Brankatschk, B., Giudici, C., Hampel, H., Schwenk, B., Edbauer, D., Fukumori, A., Steiner, H., Kremmer, E.*, et al.* (2016). Proteolytic Processing of Neuregulin 1 Type III by Three Intramembrane-cleaving Proteases. J Biol Chem *291*, 318-333.

Fleig, L., Bergbold, N., Sahasrabudhe, P., Geiger, B., Kaltak, L., and Lemberg, M.K. (2012). Ubiquitin-Dependent Intramembrane Rhomboid Protease Promotes ERAD of Membrane Proteins. Mol Cell *47*, 558-569.

Fraint, A., Pal, D., Tam, E., Bhavsar, R., Timms, C., Metman, L.V., Hall, D., and Marder, K. (2018). Interest in Genetic Testing in Parkinson's disease patients with Deep Brain Stimulation (P4.069). Neurology *90*, P4.069.

Freeman, M. (2008). Rhomboid proteases and their biological functions. Annu Rev Genet *42*, 191-210.

Friedenauer, S., and Berlet, H.H. (1989). Sensitivity and variability of the Bradford protein assay in the presence of detergents. Analytical Biochemistry *178*, 263-268.

Friedman, J.R., Lackner, L.L., West, M., DiBenedetto, J.R., Nunnari, J., and Voeltz, G.K. (2011). ER Tubules Mark Sites of Mitochondrial Division. Science *334*, 358-362.

Friedmann, E., Lemberg, M.K., Weihofen, A., Dev, K.K., Dengler, U., Rovelli, G., and Martoglio, B. (2004). Consensus analysis of signal peptide peptidase and homologous human aspartic proteases reveals opposite topology of catalytic domains compared with presenilins. J Biol Chem *279*, 50790-50798.

Fritsch, M.J., Krehenbrink, M., Tarry, M.J., Berks, B.C., and Palmer, T. (2012). Processing by rhomboid protease is required for Providencia stuartii TatA to interact with TatC and to form functional homo-oligomeric complexes. Mol Microbiol *84*, 1108-1123.

Fu, N.Y., Sukumaran, S.K., Kerk, S.Y., and Yu, V.C. (2009). Baxbeta: a constitutively active human Bax isoform that is under tight regulatory control by the proteasomal degradation mechanism. Mol Cell *33*, 15-29.

Fujimura-Kamada, K., Nouvet, F.J., and Michaelis, S. (1997). A novel membrane-associated metalloprotease, Ste24p, is required for the first step of NH2-terminal processing of the yeast a-factor precursor. The Journal of cell biology *136*, 271-285.

Gakh, O., Cavadini, P., and Isaya, G. (2002). Mitochondrial processing peptidases. Biochim Biophys Acta *1592*, 63-77.

Gao, J., Liao, J., and Yang, G.-Y. (2009). CAAX-box protein, prenylation process and carcinogenesis. Am J Transl Res *1*, 312-325.

Gasser, S.M., Daum, G., and Schatz, G. (1982). Import of proteins into mitochondria. Energy-dependent uptake of precursors by isolated mitochondria. J Biol Chem *257*, 13034-13041.

Gasteiger, E., Gattiker, A., Hoogland, C., Ivanyi, I., Appel, R.D., and Bairoch, A. (2003). ExPASy: The proteomics server for in-depth protein knowledge and analysis. Nucleic Acids Res *31*, 3784-3788.

Gatica, D., Lahiri, V., and Klionsky, D.J. (2018). Cargo recognition and degradation by selective autophagy. Nature Cell Biology *20*, 233-242.

Gegg, M.E., Cooper, J.M., Chau, K.Y., Rojo, M., Schapira, A.H., and Taanman, J.W. (2010). Mitofusin 1 and mitofusin 2 are ubiquitinated in a PINK1/parkin-dependent manner upon induction of mitophagy. Hum Mol Genet *19*, 4861-4870.

Geisler, S., Holmstrom, K.M., Skujat, D., Fiesel, F.C., Rothfuss, O.C., Kahle, P.J., and Springer, W. (2010). PINK1/Parkin-mediated mitophagy is dependent on VDAC1 and p62/SQSTM1. Nat Cell Biol *12*, 119-131.

Gerdes, F., Tatsuta, T., and Langer, T. (2012). Mitochondrial AAA proteases--towards a molecular understanding of membrane-bound proteolytic machines. Biochim Biophys Acta *1823*, 49-55.

Ghezzi, D., Arzuffi, P., Zordan, M., Da Re, C., Lamperti, C., Benna, C., D'Adamo, P., Diodato, D., Costa, R., Mariotti, C*., et al.* (2011). Mutations in TTC19 cause mitochondrial complex III deficiency and neurological impairment in humans and flies. Nat Genet *43*, 259-263.

Gilkerson, R., De La Torre, P., and St. Vallier, S. (2021). Mitochondrial OMA1 and OPA1 as Gatekeepers of Organellar Structure/Function and Cellular Stress Response. Frontiers in Cell and Developmental Biology *9*.

Gilkerson, R.W., Selker, J.M.L., and Capaldi, R.A. (2003). The cristal membrane of mitochondria is the principal site of oxidative phosphorylation. FEBS Letters *546*, 355-358.

Glick, B.S., Brandt, A., Cunningham, K., Müller, S., Hallberg, R.L., and Schatz, G. (1992). Cytochromes c1 and b2 are sorted to the intermembrane space of yeast mitochondria by a stop-transfer mechanism. Cell *69*, 809-822.

Goblirsch, B.R., and Wiener, M.C. (2020). Ste24: An Integral Membrane Protein Zinc Metalloprotease with Provocative Structure and Emergent Biology. Journal of Molecular Biology *432*, 5079-5090.

Goldstein, J.C., Waterhouse, N.J., Juin, P., Evan, G.I., and Green, D.R. (2000). The coordinate release of cytochrome c during apoptosis is rapid, complete and kinetically invariant. Nat Cell Biol *2*, 156-162.

Götz, A., Mylonas, N., Högel, P., Silber, M., Heinel, H., Menig, S., Vogel, A., Feyrer, H., Huster, D., Luy, B*., et al.* (2019). Modulating Hinge Flexibility in the APP Transmembrane Domain Alters γ-Secretase Cleavage. Biophysical Journal *116*, 2103-2120.

Gouffi, K., Gérard, F., Santini, C.L., and Wu, L.F. (2004). Dual topology of the Escherichia coli TatA protein. J Biol Chem *279*, 11608-11615.

Goulet, B., and Nepveu, A. (2004). Complete and Limited Proteolysis in Cell Cycle Progression. Cell Cycle *3*, 984-987.

Gray, M.W., Burger, G., and Lang, B.F. (1999). Mitochondrial evolution. Science *283*, 1476-1481.

Green, D., R., and Kroemer, G. (2004). The Pathophysiology of Mitochondrial Cell Death. Science *305*, 626-629.

Greenblatt, E.J., Olzmann, J.A., and Kopito, R.R. (2011). Derlin-1 is a rhomboid pseudoprotease required for the dislocation of mutant alpha-1 antitrypsin from the endoplasmic reticulum. Nat Struct Mol Biol *18*, 1147-1152.

Greene, A.W., Grenier, K., Aguileta, M.A., Muise, S., Farazifard, R., Haque, M.E., McBride, H.M., Park, D.S., and Fon, E.A. (2012). Mitochondrial processing peptidase regulates PINK1 processing, import and Parkin recruitment. EMBO Rep *13*, 378-385.

Grieve, A.G., Yeh, Y.-C., Chang, Y.-F., Huang, H.-Y., Zarcone, L., Breuning, J., Johnson, N., Stříšovský, K., Brown, M.H., Parekh, A.B*., et al.* (2021). Conformational surveillance of Orai1 by a rhomboid intramembrane protease prevents inappropriate CRAC channel activation. Molecular Cell.

Griffiths, E.J., Ocampo, C.J., Savage, J.S., Rutter, G.A., Hansford, R.G., Stern, M.D., and Silverman, H.S. (1998). Mitochondrial calcium transporting pathways during hypoxia and reoxygenation in single rat cardiomyocytes. Cardiovasc Res *39*, 423-433.

Grigorenko, A.P., Moliaka, Y.K., Korovaitseva, G.I., and Rogaev, E.I. (2002). Novel class of polytopic proteins with domains associated with putative protease activity. Biochemistry (Mosc.) *67*, 826-835.

Griparic, L., Kanazawa, T., and van der Bliek, A.M. (2007). Regulation of the mitochondrial dynamin-like protein Opa1 by proteolytic cleavage. J Cell Biol *178*, 757-764.

Guan, Z., Yan, L., Wang, Q., Qi, L., Hong, S., Gong, Z., Yan, C., and Yin, P. (2021). Structural insights into assembly of human mitochondrial translocase TOM complex. Cell Discovery *7*, 22.

Guipponi, M., Vuagniaux, G., Wattenhofer, M., Shibuya, K., Vazquez, M., Dougherty, L., Scamuffa, N., Guida, E., Okui, M., Rossier, C.*, et al.* (2002). The transmembrane serine protease (TMPRSS3) mutated in deafness DFNB8/10 activates the epithelial sodium channel (ENaC) in vitro. Hum Mol Genet *11*, 2829-2836.

Gunter, T.E., Buntinas, L., Sparagna, G.C., and Gunter, K.K. (1998). The Ca2+ transport mechanisms of mitochondria and Ca2+ uptake from physiological-type Ca2+ transients. Biochim Biophys Acta *1366*, 5-15.

Guzman, L.M., Belin, D., Carson, M.J., and Beckwith, J. (1995). Tight regulation, modulation, and high-level expression by vectors containing the arabinose PBAD promoter. J Bacteriol *177*, 4121-4130.

Ha, Y., Akiyama, Y., and Xue, Y. (2013). Structure and mechanism of rhomboid protease. The Journal of biological chemistry *288*, 15430-15436.

Haapasalo, A., and Kovacs, D.M. (2011). The many substrates of presenilin/gamma-secretase. J Alzheimers Dis *25*, 3-28.

Haass, C., and Selkoe, D.J. (2007). Soluble protein oligomers in neurodegeneration: lessons from the Alzheimer's amyloid β-peptide. Nature Reviews Molecular Cell Biology *8*, 101-112.

Hamacher-Brady, A., Brady, N.R., Logue, S.E., Sayen, M.R., Jinno, M., Kirshenbaum, L.A., Gottlieb, R.A., and Gustafsson, Å.B. (2007). Response to myocardial ischemia/reperfusion injury involves Bnip3 and autophagy. Cell Death & Differentiation *14*, 146-157.

Hampton, S.E., Dore, T.M., and Schmidt, W.K. (2018). Rce1: mechanism and inhibition. Critical reviews in biochemistry and molecular biology *53*, 157-174.

Hansford, R.G. (1994). Physiological role of mitochondrial Ca2+ transport. J Bioenerg Biomembr *26*, 495-508.

Hao, Y.H., Zhang, J., Wang, H., Wang, H.Y., Dong, J., Xu, X.P., Yao, B.W., Wang, L.F., Zhou, H.M., Zhao, L.*, et al.* (2018). HIF-1α regulates COXIV subunits, a potential mechanism of self-protective response to microwave induced mitochondrial damages in neurons. Sci Rep *8*, 10403.

Harper, J.W., Ordureau, A., and Heo, J.-M. (2018). Building and decoding ubiquitin chains for mitophagy. Nature Reviews Molecular Cell Biology *19*, 93-108.

Hawlitschek, G., Schneider, H., Schmidt, B., Tropschug, M., Hartl, F.U., and Neupert, W. (1988). Mitochondrial protein import: identification of processing peptidase and of PEP, a processing enhancing protein. Cell *53*, 795-806.

Head, B., Griparic, L., Amiri, M., Gandre-Babbe, S., and van der Bliek, A.M. (2009). Inducible proteolytic inactivation of OPA1 mediated by the OMA1 protease in mammalian cells. The Journal of cell biology *187*, 959-966.

Hedstrom, L. (2002). Serine protease mechanism and specificity. Chem. Rev. *102*, 4501-4424.

Hell, K., Neupert, W., and Stuart, R.A. (2001). Oxa1p acts as a general membrane insertion machinery for proteins encoded by mitochondrial DNA. The EMBO journal *20*, 1281-1288.

Hemming, M.L., Elias, J.E., Gygi, S.P., and Selkoe, D.J. (2008). Proteomic profiling of gamma-secretase substrates and mapping of substrate requirements. PLoS Biol *6*, e257.

Herlan, M., Bornhovd, C., Hell, K., Neupert, W., and Reichert, A.S. (2004). Alternative topogenesis of Mgm1 and mitochondrial morphology depend on ATP and a functional import motor. J Cell Biol *165*, 167-173.

Herlan, M., Vogel, F., Bornhovd, C., Neupert, W., and Reichert, A.S. (2003). Processing of Mgm1 by the Rhomboid-type protease Pcp1 is required for maintenance of mitochondrial morphology and of mitochondrial DNA. J. Biol. Chem. *278*, 27781-27788.

Herrmann, J.M., and Riemer, J. (2014). Three approaches to one problem: protein folding in the periplasm, the endoplasmic reticulum, and the intermembrane space. Antioxid Redox Signal *21*, 438-456.

Hilgenfeld, R. (2014). From SARS to MERS: crystallographic studies on coronaviral proteases enable antiviral drug design. Febs j *281*, 4085-4096.

Hill, K., Model, K., Ryan, M.T., Dietmeier, K., Martin, F., Wagner, R., and Pfanner, N. (1998). Tom40 forms the hydrophilic channel of the mitochondrial import pore for preproteins. Nature *395*, 516-521.

Hollands, T.R., and Fruton, J.S. (1969). On the mechanism of pepsin action. Proc Natl Acad Sci U S A *62*, 1116-1120.

Hooper, N.M. (1994). Families of zinc metalloproteases. FEBS Lett *354*, 1-6.

Hoppins, S., Collins, S.R., Cassidy-Stone, A., Hummel, E., Devay, R.M., Lackner, L.L., Westermann, B., Schuldiner, M., Weissman, J.S., and Nunnari, J. (2011). A mitochondrial-focused genetic interaction map reveals a scaffold-like complex required for inner membrane organization in mitochondria. J Cell Biol *195*, 323-340.

Horibata, Y., and Sugimoto, H. (2010). StarD7 mediates the intracellular trafficking of phosphatidylcholine to mitochondria. J Biol Chem *285*, 7358-7365.

Horwich, A.L., Kalousek, F., Mellman, I., and Rosenberg, L.E. (1985). A leader peptide is sufficient to direct mitochondrial import of a chimeric protein. Embo j *4*, 1129-1135.

Houtkooper, R.H., and Vaz, F.M. (2008). Cardiolipin, the heart of mitochondrial metabolism. Cell Mol Life Sci *65*, 2493-2506.

Hsu, F.F., Chou, Y.T., Chiang, M.T., Li, F.A., Yeh, C.T., Lee, W.H., and Chau, L.Y. (2019). Signal peptide peptidase promotes tumor progression via facilitating FKBP8 degradation. Oncogene *38*, 1688-1701.

Hsu, F.F., Yeh, C.T., Sun, Y.J., Chiang, M.T., Lan, W.M., Li, F.A., Lee, W.H., and Chau, L.Y. (2015). Signal peptide peptidase-mediated nuclear localization of heme oxygenase-1 promotes cancer cell proliferation and invasion independent of its enzymatic activity. Oncogene *34*, 2360-2370.

Huang, Y., and Wang, K.K. (2001). The calpain family and human disease. Trends Mol Med *7*, 355-362.

Hulett, J.M., Lueder, F., Chan, N.C., Perry, A.J., Wolynec, P., Likić, V.A., Gooley, P.R., and Lithgow, T. (2008). The transmembrane segment of Tom20 is recognized by Mim1 for docking to the mitochondrial TOM complex. J Mol Biol *376*, 694-704.

Humphries, A.D., Streimann, I.C., Stojanovski, D., Johnston, A.J., Yano, M., Hoogenraad, N.J., and Ryan, M.T. (2005). Dissection of the mitochondrial import and assembly pathway for human Tom40. J Biol Chem *280*, 11535-11543.

Huotari, J., and Helenius, A. (2011). Endosome maturation. Embo j *30*, 3481-3500.

Hurt, E.C., Pesold-Hurt, B., and Schatz, G. (1984a). The amino-terminal region of an imported mitochondrial precursor polypeptide can direct cytoplasmic dihydrofolate reductase into the mitochondrial matrix. Embo j *3*, 3149-3156.

Hurt, E.C., Pesold-Hurt, B., and Schatz, G. (1984b). The cleavable prepiece of an imported mitochondrial protein is sufficient to direct cytosolic dihydrofolate reductase into the mitochondrial matrix. FEBS Lett *178*, 306-310.

Husnjak, K., and Dikic, I. (2012). Ubiquitin-Binding Proteins: Decoders of Ubiquitin-Mediated Cellular Functions. Annual Review of Biochemistry *81*, 291-322.

Ichimura, Y., Kumanomidou, T., Sou, Y.S., Mizushima, T., Ezaki, J., Ueno, T., Kominami, E., Yamane, T., Tanaka, K., and Komatsu, M. (2008). Structural basis for sorting mechanism of p62 in selective autophagy. J Biol Chem *283*, 22847-22857.

Ichishita, R., Tanaka, K., Sugiura, Y., Sayano, T., Mihara, K., and Oka, T. (2008). An RNAi Screen for Mitochondrial Proteins Required to Maintain the Morphology of the Organelle in Caenorhabditis elegans. The Journal of Biochemistry *143*, 449-454.

Ieva, R., Heißwolf, A.K., Gebert, M., Vögtle, F.N., Wollweber, F., Mehnert, C.S., Oeljeklaus, S., Warscheid, B., Meisinger, C., van der Laan, M.*, et al.* (2013). Mitochondrial inner membrane protease promotes assembly of presequence translocase by removing a carboxy-terminal targeting sequence. Nature communications *4*, 2853.

Isaya, G., Kalousek, F., Fenton, W.A., and Rosenberg, L.E. (1991). Cleavage of precursors by the mitochondrial processing peptidase requires a compatible mature protein or an intermediate octapeptide. Journal of Cell Biology *113*, 65-76.

Isaya, G., Kalousek, F., and Rosenberg, L.E. (1992). Amino-terminal octapeptides function as recognition signals for the mitochondrial intermediate peptidase. J Biol Chem *267*, 7904-7910.

Isaya, G., Miklos, D., and Rollins, R.A. (1994). MIP1, a new yeast gene homologous to the rat mitochondrial intermediate peptidase gene, is required for oxidative metabolism in Saccharomyces cerevisiae. Mol Cell Biol *14*, 5603-5616.

Ishida, Y., Sekine, Y., Oguchi, H., Chihara, T., Miura, M., Ichijo, H., and Takeda, K. (2012). Prevention of apoptosis by mitochondrial phosphatase PGAM5 in the mushroom body is crucial for heat shock resistance in Drosophila melanogaster. PloS one *7*, e30265.

Ishihara, N., Fujita, Y., Oka, T., and Mihara, K. (2006). Regulation of mitochondrial morphology through proteolytic cleavage of OPA1. The EMBO journal *25*, 2966-2977.

James, M.N., Hsu, I.N., and Delbaere, L.T. (1977). Mechanism of acid protease catalysis based on the crystal structure of penicillopepsin. Nature *267*, 808-813.

Jankovic, J. (2008). Parkinson's disease: clinical features and diagnosis. J Neurol Neurosurg Psychiatry *79*, 368-376.

Jarvis, D.L. (2009). Baculovirus-insect cell expression systems. Methods Enzymol *463*, 191-222.

Jeyaraju, D.V., Cisbani, G., De Brito, O.M., Koonin, E.V., and Pellegrini, L. (2009). Hax1 lacks BH modules and is peripherally associated to heavy membranes: implications for Omi/HtrA2 and PARL activity in the regulation of mitochondrial stress and apoptosis. Cell Death Differ *16*, 1622-1629.

Jeyaraju, D.V., McBride, H.M., Hill, R.B., and Pellegrini, L. (2011). Structural and mechanistic basis of Parl activity and regulation. Cell Death Differ *18*, 1531-1539.

Jeyaraju, D.V., Xu, L., Letellier, M.C., Bandaru, S., Zunino, R., Berg, E.A., McBride, H.M., and Pellegrini, L. (2006). Phosphorylation and cleavage of presenilin-associated rhomboid-like protein (PARL) promotes changes in mitochondrial morphology. Proc. Natl. Acad. Sci. USA *103*, 18562-18567.

Jin, S.M., Lazarou, M., Wang, C., Kane, L.A., Narendra, D.P., and Youle, R.J. (2010). Mitochondrial membrane potential regulates PINK1 import and proteolytic destabilization by PARL. J Cell Biol *191*, 933-942.

Jin, S.M., and Youle, R.J. (2013). The accumulation of misfolded proteins in the mitochondrial matrix is sensed by PINK1 to induce PARK2/Parkin-mediated mitophagy of polarized mitochondria. Autophagy *9*, 1750-1757.

Johnson, N., Březinová, J., Stephens, E., Burbridge, E., Freeman, M., Adrain, C., and Strisovsky, K. (2017). Quantitative proteomics screen identifies a substrate repertoire of rhomboid protease RHBDL2 in human cells and implicates it in epithelial homeostasis. Scientific Reports *7*, 7283.

Jost, P.J., Grabow, S., Gray, D., McKenzie, M.D., Nachbur, U., Huang, D.C., Bouillet, P., Thomas, H.E., Borner, C., Silke, J.*, et al.* (2009). XIAP discriminates between type I and type II FAS-induced apoptosis. Nature *460*, 1035-1039.

Jumper, J., Evans, R., Pritzel, A., Green, T., Figurnov, M., Ronneberger, O., Tunyasuvunakool, K., Bates, R., Žídek, A., Potapenko, A.*, et al.* (2021). Highly accurate protein structure prediction with AlphaFold. Nature *596*, 583-589.

Jung, J.I., Premraj, S., Cruz, P.E., Ladd, T.B., Kwak, Y., Koo, E.H., Felsenstein, K.M., Golde, T.E., and Ran, Y. (2014). Independent relationship between amyloid precursor protein (APP) dimerization and γ-secretase processivity. PloS one *9*, e111553-e111553.

Juszkiewicz, S., and Hegde, R.S. (2018). Quality Control of Orphaned Proteins. Mol Cell *71*, 443-457.

Kalkavan, H., and Green, D.R. (2018). MOMP, cell suicide as a BCL-2 family business. Cell Death Differ *25*, 46-55.

Kalousek, F., Hendrick, J.P., and Rosenberg, L.E. (1988). Two mitochondrial matrix proteases act sequentially in the processing of mammalian matrix enzymes. Proc Natl Acad Sci U S A *85*, 7536-7540.

Kalousek, F., Isaya, G., and Rosenberg, L.E. (1992). Rat liver mitochondrial intermediate peptidase (MIP): purification and initial characterization. Embo j *11*, 2803-2809.

Kanabus, M., Shahni, R., Saldanha, J.W., Murphy, E., Plagnol, V., Hoff, W.V., Heales, S., and Rahman, S. (2015). Bi-allelic CLPB mutations cause cataract, renal cysts, nephrocalcinosis and 3-methylglutaconic aciduria, a novel disorder of mitochondrial protein disaggregation. J Inherit Metab Dis *38*, 211-219.

Kanaji, S., Iwahashi, J., Kida, Y., Sakaguchi, M., and Mihara, K. (2000). Characterization of the signal that directs Tom20 to the mitochondrial outer membrane. J Cell Biol *151*, 277-288.

Kanazawa, T., Zappaterra, M.D., Hasegawa, A., Wright, A.P., Newman-Smith, E.D., Buttle, K.F., McDonald, K., Mannella, C.A., and van der Bliek, A.M. (2008). The C. elegans Opa1 homologue EAT-3 is essential for resistance to free radicals. PLoS Genet *4*, e1000022.

Kandel, R.R., and Neal, S.E. (2020). The role of rhomboid superfamily members in protein homeostasis: Mechanistic insight and physiological implications. Biochimica et Biophysica Acta (BBA) - Molecular Cell Research *1867*, 118793.

Karbowski, M., Neutzner, A., and Youle, R.J. (2007). The mitochondrial E3 ubiquitin ligase MARCH5 is required for Drp1 dependent mitochondrial division. J Cell Biol *178*, 71-84.

Karbowski, M., and Youle, R.J. (2011). Regulating mitochondrial outer membrane proteins by ubiquitination and proteasomal degradation. Curr Opin Cell Biol *23*, 476-482.

Käser, M., Kambacheld, M., Kisters-Woike, B., and Langer, T. (2003). Oma1, a novel membrane-bound metallopeptidase in mitochondria with activities overlapping with the m-AAA protease. J Biol Chem *278*, 46414-46423.

Kawano, S., Yamano, K., Naoé, M., Momose, T., Terao, K., Nishikawa, S.-i., Watanabe, N., and Endo, T. (2009). Structural basis of yeast Tim40/Mia40 as an oxidative translocator in the mitochondrial intermembrane space. Proceedings of the National Academy of Sciences *106*, 14403.

Kayatekin, C., Amasino, A., Gaglia, G., Flannick, J., Bonner, J.M., Fanning, S., Narayan, P., Barrasa, M.I., Pincus, D., Landgraf, D.*, et al.* (2018). Translocon Declogger Ste24 Protects against IAPP Oligomer-Induced Proteotoxicity. Cell *173*, 62-73 e69.

Keckesova, Z., Donaher, J.L., De Cock, J., Freinkman, E., Lingrell, S., Bachovchin, D.A., Bierie, B., Tischler, V., Noske, A., Okondo, M.C.*, et al.* (2017). LACTB is a tumour suppressor that modulates lipid metabolism and cell state. Nature *543*, 681-686.

Keil, P., and Pfanner, N. (1993). Insertion of MOM22 into the mitochondrial outer membrane strictly depends on surface receptors. FEBS Lett *321*, 197-200.

Kemper, C., Habib, S.J., Engl, G., Heckmeyer, P., Dimmer, K.S., and Rapaport, D. (2008). Integration of tail-anchored proteins into the mitochondrial outer membrane does not require any known import components. J Cell Sci *121*, 1990-1998.

Khaminets, A., Behl, C., and Dikic, I. (2016). Ubiquitin-Dependent And Independent Signals In Selective Autophagy. Trends in Cell Biology *26*, 6-16.

Kiebler, M., Pfaller, R., Söllner, T., Griffiths, G., Horstmann, H., Pfanner, N., and Neupert, W. (1990). Identification of a mitochondrial receptor complex required for recognition and membrane insertion of precursor proteins. Nature *348*, 610-616.

Kiemer, L., Lund, O., Brunak, S., and Blom, N. (2004). Coronavirus 3CLpro proteinase cleavage sites: possible relevance to SARS virus pathology. BMC bioinformatics *5*, 72-72.

Killian, J.A. (1998). Hydrophobic mismatch between proteins and lipids in membranes. Biochim Biophys Acta *1376*, 401-415.

Klein, A., Israel, L., Lackey, S.W.K., Nargang, F.E., Imhof, A., Baumeister, W., Neupert, W., and Thomas, D.R. (2012). Characterization of the insertase for β-barrel proteins of the outer mitochondrial membrane. The Journal of cell biology *199*, 599-611.

Klepsch, M.M., Persson, J.O., and de Gier, J.W. (2011). Consequences of the overexpression of a eukaryotic membrane protein, the human KDEL receptor, in Escherichia coli. J Mol Biol *407*, 532-542.

Knop, M., Finger, A., Braun, T., Hellmuth, K., and Wolf, D.H. (1996). Der1, a novel protein specifically required for endoplasmic reticulum degradation in yeast. EMBO J *15*, 753-763.

Knopf, J.D., Landscheidt, N., Pegg, C.L., Schulz, B.L., Kuhnle, N., Chao, C.W., Huck, S., and Lemberg, M.K. (2020). Intramembrane protease RHBDL4 cleaves oligosaccharyltransferase subunits to target them for ER-associated degradation. J Cell Sci.

Kolansky, D.M., Conboy, J.G., Fenton, W.A., and Rosenberg, L.E. (1982). Energy-dependent translocation of the precursor of ornithine transcarbamylase by isolated rat liver mitochondria. J Biol Chem *257*, 8467-8471.

Komatsu, M., and Ichimura, Y. (2010). Selective autophagy regulates various cellular functions. Genes Cells *15*, 923-933.

Kondadi, A.K., Wang, S., Montagner, S., Kladt, N., Korwitz, A., Martinelli, P., Herholz, D., Baker, M.J., Schauss, A.C., Langer, T.*, et al.* (2014). Loss of the m-AAA protease subunit AFG_3L_2 causes mitochondrial transport defects and tau hyperphosphorylation. Embo j *33*, 1011-1026.

König, T., Tröder, S.E., Bakka, K., Korwitz, A., Richter-Dennerlein, R., Lampe, P.A., Patron, M., Mühlmeister, M., Guerrero-Castillo, S., Brandt, U.*, et al.* (2016). The m-AAA Protease Associated with Neurodegeneration Limits MCU Activity in Mitochondria. Mol Cell *64*, 148-162.

Koonin, E.V., Makarova, K.S., Rogozin, I.B., Davidovic, L., Letellier, M.C., and Pellegrini, L. (2003). The rhomboids: a nearly ubiquitous family of intramembrane serine proteases that probably evolved by multiple ancient horizontal gene transfers. In Genome Biol., p. R19.

Kopan, R., and Goate, A. (2000). A common enzyme connects notch signaling and Alzheimer's disease. Genes Dev *14*, 2799-2806.

Kopan, R., and Ilagan, M.X. (2004). Gamma-secretase: proteasome of the membrane? Nat Rev Mol Cell Biol *5*, 499-504.

Koppen, M., Metodiev, M.D., Casari, G., Rugarli, E.I., and Langer, T. (2007). Variable and tissue-specific subunit composition of mitochondrial m-AAA protease complexes linked to hereditary spastic paraplegia. Molecular and cellular biology *27*, 758-767.

Korbel, D., Wurth, S., Käser, M., and Langer, T. (2004). Membrane protein turnover by the m-AAA protease in mitochondria depends on the transmembrane domains of its subunits. EMBO Rep *5*, 698-703.

Kornmann, B., Currie, E., Collins, S.R., Schuldiner, M., Nunnari, J., Weissman, J.S., and Walter, P. (2009). An ER-mitochondria tethering complex revealed by a synthetic biology screen. Science *325*, 477-481.

Kozjak-Pavlovic, V., Ott, C., Götz, M., and Rudel, T. (2011). Neisserial Omp85 protein is selectively recognized and assembled into functional complexes in the outer membrane of human mitochondria. The Journal of biological chemistry *286*, 27019-27026.

Kreutzberger, A.J.B., Ji, M., Aaron, J., Mihaljević, L., and Urban, S. (2019). Rhomboid distorts lipids to break the viscosity-imposed speed limit of membrane diffusion. Science (New York, N.Y.) *363*.

Kroemer, G., Galluzzi, L., and Brenner, C. (2007). Mitochondrial membrane permeabilization in cell death. Physiol Rev *87*, 99-163.

Krogh, A., Larsson, B., von Heijne, G., and Sonnhammer, E.L. (2001). Predicting transmembrane protein topology with a hidden Markov model: application to complete genomes. J. Mol. Biol. *305*, 567-580.

Krumpe, K., Frumkin, I., Herzig, Y., Rimon, N., Ozbalci, C., Brugger, B., Rapaport, D., and Schuldiner, M. (2012). Ergosterol content specifies targeting of tail-anchored proteins to mitochondrial outer membranes. Mol Biol Cell *23*, 3927-3935.

Kubli, D.A., and Gustafsson, Å.B. (2012). Mitochondria and mitophagy: the yin and yang of cell death control. Circulation Research *111*, 1208-1221.

Kühnle, N., Dederer, V., and Lemberg, M.K. (2019). Intramembrane proteolysis at a glance: from signalling to protein degradation. J Cell Sci *132*.

Kujoth, G.C., Hiona, A., Pugh, T.D., Someya, S., Panzer, K., Wohlgemuth, S.E., Hofer, T., Seo, A.Y., Sullivan, R., Jobling, W.A.*, et al.* (2005). Mitochondrial DNA Mutations, Oxidative Stress, and Apoptosis in Mammalian Aging. Science *309*, 481-484.

Kulman, J.D., and Davie, E.W. (2013). Proteases in Blood Clotting. In Encyclopedia of Biological Chemistry (Second Edition), W.J. Lennarz, and M.D. Lane, eds. (Waltham: Academic Press), pp. 585-589.

Kunitz, M. (1939). Formation of Trypsin from Crystalline Trypsinogen by Means of Enterokinase. J Gen Physiol *22*, 429-446.

Kunová, N., Ondrovičová, G., Bauer, J.A., Bellová, J., Ambro, Ľ., Martináková, L., Kotrasová, V., Kutejová, E., and Pevala, V. (2017). The role of Lon-mediated proteolysis in the dynamics of mitochondrial nucleic acid-protein complexes. Scientific Reports *7*, 631.

Kyte, J., and Doolittle, R.F. (1982). A simple method for displaying the hydropathic character of a protein. J Mol Biol *157*, 105-132.

Labrousse, A.M., Zappaterra, M.D., Rube, D.A., and van der Bliek, A.M. (1999). C. elegans Dynamin-Related Protein DRP-1 Controls Severing of the Mitochondrial Outer Membrane. Molecular Cell *4*, 815-826.

Lackner, L.L., Horner, J.S., and Nunnari, J. (2009). Mechanistic analysis of a dynamin effector. Science (New York, N.Y.) *325*, 874-877.

Laemmli, U.K. (1970). Cleavage of structural proteins during the assembly of the head of bacteriophage T4. Nature *227*, 680-685.

Langosch, D., Scharnagl, C., Steiner, H., and Lemberg, M.K. (2015). Understanding intramembrane proteolysis: from protein dynamics to reaction kinetics Trends Biochem Sci *40*, 318-327.

Langosch, D., and Steiner, H. (2017). Substrate processing in intramembrane proteolysis by γ-secretase - the role of protein dynamics. Biological chemistry *398*, 441-453.

Lastun, V.L., Grieve, A.G., and Freeman, M. (2016). Substrates and physiological functions of secretase rhomboid proteases. Semin Cell Dev Biol *60*, 10-18.

Lazareno-Saez, C., Arutyunova, E., Coquelle, N., and Lemieux, M.J. (2013). Domain swapping in the cytoplasmic domain of the Escherichia coli rhomboid protease. Journal of molecular biology *425*, 1127-1142.

Lazarou, M., Sliter, D.A., Kane, L.A., Sarraf, S.A., Wang, C., Burman, J.L., Sideris, D.P., Fogel, A.I., and Youle, R.J. (2015). The ubiquitin kinase PINK1 recruits autophagy receptors to induce mitophagy. Nature *524*, 309-314.

Leeuw, E., Porcelli, I., Sargent, F., Palmer, T., and Berks, B. (2001). Membrane interactions and self-association of the TatA and TatB components of the twin-arginine translocation pathway. FEBS letters *506*, 143-148.

Lemberg, M.K. (2011). Intramembrane Proteolysis in Regulated Protein Trafficking. Traffic *12*, 1109-1118.

Lemberg, M.K. (2013). Sampling the Membrane: Function of Rhomboid-Family Proteins. Trends Cell Biol. *23*, 210-217.

Lemberg, M.K., and Adrain, C. (2016). Inactive rhomboid proteins: New mechanisms with implications in health and disease. Semin Cell Dev Biol *60*, 29-37.

Lemberg, M.K., Bland, F.A., Weihofen, A., Braud, V.M., and Martoglio, B. (2001). Intramembrane proteolysis of signal peptides: an essential step in the generation of HLA-E epitopes. J. Immunol. *167*, 6441-6446.

Lemberg, M.K., and Freeman, M. (2007a). Cutting proteins within lipid bilayers: rhomboid structure and mechanism. Mol Cell *28*, 930-940.

Lemberg, M.K., and Freeman, M. (2007b). Functional and evolutionary implications of enhanced genomic analysis of rhomboid intramembrane proteases. Genome Res *17*, 1634-1646.

Lemberg, M.K., and Martoglio, B. (2002). Requirements for signal peptide peptidase-catalyzed intramembrane proteolysis. Mol. Cell *10*, 735-744.

Lemberg, M.K., and Martoglio, B. (2004). On the mechanism of SPP-catalysed intramembrane proteolysis; conformational control of peptide bond hydrolysis in the plane of the membrane. FEBS Lett. *564*, 213-218.

Lemberg, M.K., Menendez, J., Misik, A., Garcia, M., Koth, C.M., and Freeman, M. (2005). Mechanism of intramembrane proteolysis investigated with purified rhomboid proteases. EMBO J. *24*, 464-472.

Lemmin, T., Dimitrov, M., Fraering, P.C., and Dal Peraro, M. (2014). Perturbations of the straight transmembrane α-helical structure of the amyloid precursor protein affect its processing by γ-secretase. J Biol Chem *289*, 6763-6774.

Leonhard, K., Guiard, B., Pellecchia, G., Tzagoloff, A., Neupert, W., and Langer, T. (2000). Membrane protein degradation by AAA proteases in mitochondria: extraction of substrates from either membrane surface. Mol Cell *5*, 629-638.

Leonhard, K., Herrmann, J.M., Stuart, R.A., Mannhaupt, G., Neupert, W., and Langer, T. (1996). AAA proteases with catalytic sites on opposite membrane surfaces comprise a proteolytic system for the ATP-dependent degradation of inner membrane proteins in mitochondria. Embo j *15*, 4218-4229.

Leonhard, K., Stiegler, A., Neupert, W., and Langer, T. (1999). Chaperone-like activity of the AAA domain of the yeast Yme1 AAA protease. Nature *398*, 348-351.

Letai, A., Bassik, M.C., Walensky, L.D., Sorcinelli, M.D., Weiler, S., and Korsmeyer, S.J. (2002). Distinct BH3 domains either sensitize or activate mitochondrial apoptosis, serving as prototype cancer therapeutics. Cancer cell *2*, 183-192.

Levine, B., and Kroemer, G. (2019). Biological Functions of Autophagy Genes: A Disease Perspective. Cell *176*, 11-42.

Levitan, D., and Greenwald, I. (1995). Facilitation of lin-12-mediated signalling by sel-12, a Caenorhabditis elegans S182 Alzheimer's disease gene. Nature *377*, 351-354.

Levy-Lahad, E., Wasco, W., Poorkaj, P., Romano, D.M., Oshima, J., Pettingell, W.H., Yu, C.E., Jondro, P.D., Schmidt, S.D., Wang, K.*, et al.* (1995). Candidate gene for the chromosome 1 familial Alzheimer's disease locus. Science *269*, 973-977.

Levytskyy, R.M., Bohovych, I., and Khalimonchuk, O. (2017). Metalloproteases of the inner mitochondrial membrane. Biochemistry *56*, 4737-4746.

Lewis, A.P., and Thomas, P.J. (1999). A novel clan of zinc metallopeptidases with possible intramembrane cleavage properties. Protein Sci *8*, 439-442.

Lewis, S.C., Uchiyama, L.F., and Nunnari, J. (2016). ER-mitochondria contacts couple mtDNA synthesis with mitochondrial division in human cells. Science *353*, aaf5549.

Li, P., Nijhawan, D., Budihardjo, I., Srinivasula, S.M., Ahmad, M., Alnemri, E.S., and Wang, X. (1997). Cytochrome c and dATP-dependent formation of Apaf-1/caspase-9 complex initiates an apoptotic protease cascade. Cell *91*, 479-489.

Li, S.C., and Deber, C.M. (1994). A measure of helical propensity for amino acids in membrane environments. Nat. Struct. Biol. *1*, 368-373.

Lichtenthaler, S.F., Lemberg, M.K., and Fluhrer, R. (2018). Proteolytic ectodomain shedding of membrane proteins in mammals-hardware, concepts, and recent developments. EMBO J *37*.

Liesa, M., Palacín, M., and Zorzano, A. (2009). Mitochondrial Dynamics in Mammalian Health and Disease. Physiological Reviews *89*, 799-845.

Liesa, M., Van der Bliek, A., and Shirihai, O.S. (2019). To Fis or not to Fuse? This is the question! The EMBO Journal *38*, e101839.

Lill, R. (2009). Function and biogenesis of iron-sulphur proteins. Nature *460*, 831-838.

Lin, K., Yan, Q., Mitchell, A., Funk, N., Lu, C., and Xiao, H. (2020). A simple method for non-denaturing purification of biotin-tagged proteins through competitive elution with free biotin. Biotechniques *68*, 41-44.

Lin, W., and Kang, U.J. (2010). Structural determinants of PINK1 topology and dual subcellular distribution. BMC Cell Biol *11*, 90.

Linnane, A.W., Ozawa, T., Marzuki, S., and Tanaka, M. (1989). Mitochondrial DNA mutations as an important contributor to ageing and degenerative diseases. The Lancet *333*, 642-645.

Litman, B.J., and Mitchell, D.C. (1996). A role for phospholipid polyunsaturation in modulating membrane protein function. Lipids *31 Suppl*, S193-197.

Liu, F.-T., Agrawal, S.G., Gribben, J.G., Ye, H., Du, M.-Q., Newland, A.C., and Jia, L. (2008). Bortezomib blocks Bax degradation in malignant B cells during treatment with TRAIL. Blood *111*, 2797-2805.

Liu, G., Beaton, S.E., Grieve, A.G., Evans, R., Rogers, M., Strisovsky, K., Armstrong, F.A., Freeman, M., Exley, R.M., and Tang, C.M. (2020a). Bacterial rhomboids mediate quality control of orphan membrane proteins. EMBO J.

Liu, J., and Rost, B. (2001). Comparing function and structure between entire proteomes. Protein science : a publication of the Protein Society *10*, 1970-1979.

Liu, L., Ding, L., Rovere, M., Wolfe, M.S., and Selkoe, D.J. (2019). A cellular complex of BACE1 and γ-secretase sequentially generates Aβ from its full-length precursor. J Cell Biol *218*, 644-663.

Liu, L., Feng, D., Chen, G., Chen, M., Zheng, Q., Song, P., Ma, Q., Zhu, C., Wang, R., Qi, W.*, et al.* (2012). Mitochondrial outer-membrane protein FUNDC1 mediates hypoxia-induced mitophagy in mammalian cells. Nat Cell Biol *14*, 177-185.

Liu, L.P., and Deber, C.M. (1998). Uncoupling hydrophobicity and helicity in transmembrane segments. Alpha-helical propensities of the amino acids in non-polar environments. The Journal of biological chemistry *273*, 23645-23648.

Liu, Y.J., McIntyre, R.L., Janssens, G.E., and Houtkooper, R.H. (2020b). Mitochondrial fission and fusion: A dynamic role in aging and potential target for age-related disease. Mechanisms of Ageing and Development *186*, 111212.

Llambi, F., Moldoveanu, T., Tait, S.W., Bouchier-Hayes, L., Temirov, J., McCormick, L.L., Dillon, C.P., and Green, D.R. (2011). A unified model of mammalian BCL-2 protein family interactions at the mitochondria. Mol Cell *44*, 517-531.

Lo, S.-C., and Hannink, M. (2006). PGAM5, a Bcl-XL-interacting protein, is a novel substrate for the redox-regulated Keap1-dependent ubiquitin ligase complex. The Journal of biological chemistry *281*, 37893-37903.

Lo, S.-C., and Hannink, M. (2008). PGAM5 tethers a ternary complex containing Keap1 and Nrf2 to mitochondria. Experimental cell research *314*, 1789-1803.

Lohi, O., Urban, S., and Freeman, M. (2004). Diverse substrate recognition mechanisms for rhomboids; thrombomodulin is cleaved by Mammalian rhomboids. Curr. Biol. *14*, 236-241.

Lomize, M.A., Pogozheva, I.D., Joo, H., Mosberg, H.I., and Lomize, A.L. (2012). OPM database and PPM web server: resources for positioning of proteins in membranes. Nucleic Acids Res *40*, D370-376.

Longen, S., Woellhaf, Michael W., Petrungaro, C., Riemer, J., and Herrmann, Johannes M. (2014). The Disulfide Relay of the Intermembrane Space Oxidizes the Ribosomal Subunit Mrp10 on Its Transit into the Mitochondrial Matrix. Developmental Cell *28*, 30-42.

López-Otín, C., and Bond, J.S. (2008). Proteases. The Journal of biological chemistry *283*, 30433-30437.

López-Otín, C., and Overall, C.M. (2002). Protease degradomics: a new challenge for proteomics. Nat. Rev. Mol. Cell Biol. *3*, 509-519.

López-Pelegrín, M., Cerdà-Costa, N., Martínez-Jiménez, F., Cintas-Pedrola, A., Canals, A., Peinado, J.R., Marti-Renom, M.A., López-Otín, C., Arolas, J.L., and Gomis-Rüth, F.X. (2013). A novel family of soluble minimal scaffolds provides structural insight into the catalytic domains of integral membrane metallopeptidases. Journal of Biological Chemistry *288*, 21279-21294.

Losón, O.C., Song, Z., Chen, H., and Chan, D.C. (2013). Fis1, Mff, MiD49, and MiD51 mediate Drp1 recruitment in mitochondrial fission. Molecular Biology of the Cell *24*, 659-667.

Lu, W., Karuppagounder, S.S., Springer, D.A., Allen, M.D., Zheng, L., Chao, B., Zhang, Y., Dawson, V.L., Dawson, T.M., and Lenardo, M. (2014). Genetic deficiency of the mitochondrial protein PGAM5 causes a Parkinson's-like movement disorder. Nature communications *5*, 4930.

Lysyk, L., Brassard, R., Arutyunova, E., Siebert, V., Jiang, Z., Takyi, E., Morrison, M., Young, H.S., Lemberg, M.K., O'Donoghue, A.J.*, et al.* (2021). Insights into the catalytic properties of the mitochondrial rhomboid protease PARL. J Biol Chem *296*, 100383.

Ma, K., Zhang, Z., Chang, R., Cheng, H., Mu, C., Zhao, T., Chen, L., Zhang, C., Luo, Q., Lin, J.*, et al.* (2020). Dynamic PGAM5 multimers dephosphorylate BCL-xL or FUNDC1 to regulate mitochondrial and cellular fate. Cell Death & Differentiation *27*, 1036-1051.

MacLeod, R., Hillert, E.-K., Cameron, R.T., and Baillie, G.S. (2015). The role and therapeutic targeting of α-, β- and γ-secretase in Alzheimer's disease. Future Sci OA *1*, FSO11-FSO11.

MacVicar, T., Ohba, Y., Nolte, H., Mayer, F.C., Tatsuta, T., Sprenger, H.-G., Lindner, B., Zhao, Y., Li, J., Bruns, C.*, et al.* (2019). Lipid signalling drives proteolytic rewiring of mitochondria by YME1L. Nature *575*, 361-365.

Maechler, P., and Wollheim, C.B. (2000). Mitochondrial signals in glucose-stimulated insulin secretion in the beta cell. J Physiol *529 Pt 1*, 49-56.

Maegawa, S., Ito, K., and Akiyama, Y. (2005). Proteolytic action of GlpG, a rhomboid protease in the Escherichia coli cytoplasmic membrane. Biochemistry *44*, 13543-13552.

Maillard, Rodrigo A., Chistol, G., Sen, M., Righini, M., Tan, J., Kaiser, C.M., Hodges, C., Martin, A., and Bustamante, C. (2011). ClpX(P) Generates Mechanical Force to Unfold and Translocate Its Protein Substrates. Cell *145*, 459-469.

Mannella, C.A. (1992). The 'ins' and 'outs' of mitochondrial membrane channels. Trends Biochem Sci *17*, 315-320.

Manolaridis, I., Kulkarni, K., Dodd, R.B., Ogasawara, S., Zhang, Z., Bineva, G., O'Reilly, N., Hanrahan, S.J., Thompson, A.J., Cronin, N.*, et al.* (2013). Mechanism of farnesylated CAAX protein processing by the intramembrane protease Rce1. Nature *504*, 301-305.

Martins, L.M., Iaccarino, I., Tenev, T., Gschmeissner, S., Totty, N.F., Lemoine, N.R., Savopoulos, J., Gray, C.W., Creasy, C.L., Dingwall, C.*, et al.* (2002). The serine protease Omi/HtrA2 regulates apoptosis by binding XIAP through a reaper-like motif. J Biol Chem *277*, 439-444.

Martins, L.M., Morrison, A., Klupsch, K., Fedele, V., Moisoi, N., Teismann, P., Abuin, A., Grau, E., Geppert, M., Livi, G.P.*, et al.* (2004). Neuroprotective role of the Reaper-related serine protease HtrA2/Omi revealed by targeted deletion in mice. Mol Cell Biol *24*, 9848-9862.

Matsuda, N., Sato, S., Shiba, K., Okatsu, K., Saisho, K., Gautier, C.A., Sou, Y.S., Saiki, S., Kawajiri, S., Sato, F.*, et al.* (2010). PINK1 stabilized by mitochondrial depolarization recruits Parkin to damaged mitochondria and activates latent Parkin for mitophagy. J Cell Biol *189*, 211-221.

Matsushima, Y., Goto, Y., and Kaguni, L.S. (2010). Mitochondrial Lon protease regulates mitochondrial DNA copy number and transcription by selective degradation of mitochondrial transcription factor A (TFAM). Proc Natl Acad Sci U S A *107*, 18410-18415.

Matsushima, Y., Hirofuji, Y., Aihara, M., Yue, S., Uchiumi, T., Kaguni, L.S., and Kang, D. (2017). Drosophila protease ClpXP specifically degrades DmLRPPRC1 controlling mitochondrial mRNA and translation. Scientific Reports *7*, 8315.

Mayer, U., and Nüsslein-Volhard, C. (1988). A group of genes required for pattern formation in the ventral ectoderm of the Drosophila embryo. Genes Dev. *2*, 1496-1511.

McCormack, J.G., and Denton, R.M. (1979). The effects of calcium ions and adenine nucleotides on the activity of pig heart 2-oxoglutarate dehydrogenase complex. Biochem J *180*, 533-544.

McCormack, J.G., Halestrap, A.P., and Denton, R.M. (1990). Role of calcium ions in regulation of mammalian intramitochondrial metabolism. Physiol Rev *70*, 391-425.

McLauchlan, J., Lemberg, M.K., Hope, G., and Martoglio, B. (2002). Intramembrane proteolysis promotes trafficking of hepatitis C virus core protein to lipid droplets. EMBO J. *21*, 3980-3988.

McLelland, G.-L., Soubannier, V., Chen, C.X., McBride, H.M., and Fon, E.A. (2014). Parkin and PINK1 function in a vesicular trafficking pathway regulating mitochondrial quality control. The EMBO journal *33*, 282-295.

McQuibban, G.A., Saurya, S., and Freeman, M. (2003). Mitochondrial membrane remodelling regulated by a conserved rhomboid protease. Nature *423*, 537-541.

Meier, S., Neupert, W., and Herrmann, J.M. (2005). Proline residues of transmembrane domains determine the sorting of inner membrane proteins in mitochondria. The Journal of cell biology *170*, 881-888.

Meineke, B., Engl, G., Kemper, C., Vasiljev-Neumeyer, A., Paulitschke, H., and Rapaport, D. (2008). The outer membrane form of the mitochondrial protein Mcr1 follows a TOM-independent membrane insertion pathway. FEBS Lett *582*, 855-860.

Meissner, C., Lorenz, H., Hehn, B., and Lemberg, M.K. (2015). Intramembrane protease PARL defines a negative regulator of PINK1- and PARK2/Parkin-dependent mitophagy. Autophagy *11*, 1484-1498.

Meissner, C., Lorenz, H., Weihofen, A., Selkoe, D.J., and Lemberg, M.K. (2011). The mitochondrial intramembrane protease PARL cleaves human Pink1 to regulate Pink1 trafficking. J Neurochem *117*, 856-867.

Mentrup, T., Fluhrer, R., and Schroder, B. (2017). Latest emerging functions of SPP/SPPL intramembrane proteases. Eur J Cell Biol *96*, 372-382.

Merkwirth, C., Dargazanli, S., Tatsuta, T., Geimer, S., Löwer, B., Wunderlich, F.T., von Kleist-Retzow, J.-C., Waisman, A., Westermann, B., and Langer, T. (2008). Prohibitins control cell proliferation and apoptosis by regulating OPA1-dependent cristae morphogenesis in mitochondria. Genes & development *22*, 476-488.

Mesecke, N., Terziyska, N., Kozany, C., Baumann, F., Neupert, W., Hell, K., and Herrmann, J.M. (2005). A disulfide relay system in the intermembrane space of mitochondria that mediates protein import. Cell *121*, 1059-1069.

Milenkovic, D., Ramming, T., Müller, J.M., Wenz, L.-S., Gebert, N., Schulze-Specking, A., Stojanovski, D., Rospert, S., and Chacinska, A. (2009). Identification of the signal directing Tim9 and Tim10 into the intermembrane space of mitochondria. Molecular biology of the cell *20*, 2530-2539.

Miller, R.J. (1991). The control of neuronal Ca2+ homeostasis. Progress in Neurobiology *37*, 255-285.

Miller, R.J. (1998). Mitochondria - the Kraken wakes! Trends Neurosci *21*, 95-97.

Mitchell, P., and Moyle, J. (1967). Chemiosmotic Hypothesis of Oxidative Phosphorylation. Nature *213*, 137-139.

Mizushima, N., and Klionsky, D.J. (2007). Protein turnover via autophagy: implications for metabolism. Annu Rev Nutr *27*, 19-40.

Moin, S.M., and Urban, S. (2012). Membrane immersion allows rhomboid proteases to achieve specificity by reading transmembrane segment dynamics. elife *1*, e00173.

Mokranjac, D., and Neupert, W. (2015). Cell biology: Architecture of a protein entry gate. Nature *528*, 201-202.

Morishita, H., and Mizushima, N. (2019). Diverse Cellular Roles of Autophagy. Annu Rev Cell Dev Biol *35*, 453-475.

Mossmann, D., Meisinger, C., and Vögtle, F.N. (2012). Processing of mitochondrial presequences. Biochimica et biophysica acta *1819*, 1098-1106.

Murakawa, T., Yamaguchi, O., Hashimoto, A., Hikoso, S., Takeda, T., Oka, T., Yasui, H., Ueda, H., Akazawa, Y., Nakayama, H.*, et al.* (2015). Bcl-2-like protein 13 is a mammalian Atg32 homologue that mediates mitophagy and mitochondrial fragmentation. Nature Communications *6*, 7527.

Murata, D., Yamada, T., Tokuyama, T., Arai, K., Quirós, P.M., López-Otín, C., Iijima, M., and Sesaki, H. (2020). Mitochondrial Safeguard: a stress response that offsets extreme fusion and protects respiratory function via flickering-induced Oma1 activation. The EMBO Journal *39*, e105074.

Murphy, M.P. (2009). How mitochondria produce reactive oxygen species. The Biochemical journal *417*, 1-13.

Nakamura, N., Kimura, Y., Tokuda, M., Honda, S., and Hirose, S. (2006). MARCH-V is a novel mitofusin 2- and Drp1-binding protein able to change mitochondrial morphology. EMBO reports *7*, 1019-1022.

Nakatogawa, H., Suzuki, K., Kamada, Y., and Ohsumi, Y. (2009). Dynamics and diversity in autophagy mechanisms: lessons from yeast. Nature Reviews Molecular Cell Biology *10*, 458-467.

Naoé, M., Ohwa, Y., Ishikawa, D., Ohshima, C., Nishikawa, S., Yamamoto, H., and Endo, T. (2004). Identification of Tim40 that mediates protein sorting to the mitochondrial intermembrane space. J Biol Chem *279*, 47815-47821.

Naon, D., Zaninello, M., Giacomello, M., Varanita, T., Grespi, F., Lakshminaranayan, S., Serafini, A., Semenzato, M., Herkenne, S., Hernández-Alvarez, M.I.*, et al.* (2016). Critical reappraisal confirms that Mitofusin 2 is an endoplasmic reticulum–mitochondria tether. Proceedings of the National Academy of Sciences *113*, 11249-11254.

Narayanan, S., Sato, T., and Wolfe, M.S. (2007). A C-terminal domain of signal peptide peptidase defines a functional domain for intramembrane aspartic protease catalysis. J. Biol. Chem. *282*, 20172-20179.

Narendra, D.P., Jin, S.M., Tanaka, A., Suen, D.-F., Gautier, C.A., Shen, J., Cookson, M.R., and Youle, R.J. (2010). PINK1 is selectively stabilized on impaired mitochondria to activate Parkin. PLoS biology *8*, e1000298.

Neal, S., Jaeger, P., Duttke, S., Benner, C., Glass, T., and Hampton, R. (2018). The Dfm1 derlin is required for ERAD retrotranslocation of integral membrane proteins. Mol Cell.

Nejatfard, A., Wauer, N., Bhaduri, S., Conn, A., Gourkanti, S., Singh, N., Kuo, T., Kandel, R., Amaro, R.E., and Neal, S.E. (2021). Derlin rhomboid pseudoproteases employ substrate engagement and lipid distortion to enable the retrotranslocation of ERAD membrane substrates. Cell Rep *37*, 109840.

Neutzner, A., Benard, G., Youle, R.J., and Karbowski, M. (2008). Role of the ubiquitin conjugation system in the maintenance of mitochondrial homeostasis. Ann N Y Acad Sci *1147*, 242-253.

Neutzner, A., Youle, R.J., and Karbowski, M. (2007). Outer mitochondrial membrane protein degradation by the proteasome. Novartis Found Symp *287*, 4-14; discussion 14-20.

Ni, H.-M., Williams, J.A., and Ding, W.-X. (2015). Mitochondrial dynamics and mitochondrial quality control. Redox biology *4*, 6-13.

Niemeyer, J., Mentrup, T., Heidasch, R., Muller, S.A., Biswas, U., Meyer, R., Papadopoulou, A.A., Dederer, V., Haug-Kroper, M., Adamski, V.*, et al.* (2019). The intramembrane protease SPPL2c promotes male germ cell development by cleaving phospholamban. EMBO Rep *20*.

Nijhawan, D., Fang, M., Traer, E., Zhong, Q., Gao, W., Du, F., and Wang, X. (2003). Elimination of Mcl-1 is required for the initiation of apoptosis following ultraviolet irradiation. Genes Dev *17*, 1475-1486.

Noble, J.E., Knight, A.E., Reason, A.J., Di Matola, A., and Bailey, M.J.A. (2007). A Comparison of Protein Quantitation Assays for Biopharmaceutical Applications. Molecular Biotechnology *37*, 99-111.

Nolden, M., Ehses, S., Koppen, M., Bernacchia, A., Rugarli, E.I., and Langer, T. (2005). The m-AAA protease defective in hereditary spastic paraplegia controls ribosome assembly in mitochondria. Cell *123*, 277-289.

Nunnari, J., Fox, T.D., and Walter, P. (1993). A Mitochondrial Protease with Two Catalytic Subunits of Nonoverlapping Specificities. Science *262*, 1997-2004.

Oda, Y., Okada, T., Yoshida, H., Kaufman, R.J., Nagata, K., and Mori, K. (2006). Derlin-2 and Derlin-3 are regulated by the mammalian unfolded protein response and are required for ER-associated degradation. J Cell Biol *172*, 383-393.

Ohba, Y., MacVicar, T., and Langer, T. (2020). Regulation of mitochondrial plasticity by the i-AAA protease YME1L. Biological Chemistry *401*, 877-890.

Okamoto, H., Miyagawa, A., Shiota, T., Tamura, Y., and Endo, T. (2014). Intramolecular disulfide bond of Tim22 protein maintains integrity of the TIM22 complex in the mitochondrial inner membrane. J Biol Chem *289*, 4827-4838.

Okamura, Y., Kawanabe, A., and Kawai, T. (2018). Voltage-Sensing Phosphatases: Biophysics, Physiology, and Molecular Engineering. Physiological reviews *98*, 2097-2131.

Ong, S.E., Blagoev, B., Kratchmarova, I., Kristensen, D.B., Steen, H., Pandey, A., and Mann, M. (2002). Stable isotope labeling by amino acids in cell culture, SILAC, as a simple and accurate approach to expression proteomics. Mol Cell Proteomics *1*, 376-386.

Ong, S.E., and Mann, M. (2006). A practical recipe for stable isotope labeling by amino acids in cell culture (SILAC). Nat Protoc *1*, 2650-2660.

Ordureau, A., Sarraf, Shireen A., Duda, David M., Heo, J.-M., Jedrychowski, Mark P., Sviderskiy, Vladislav O., Olszewski, Jennifer L., Koerber, James T., Xie, T., Beausoleil, Sean A.*, et al.* (2014). Quantitative Proteomics Reveal a Feedforward Mechanism for Mitochondrial PARKIN Translocation and Ubiquitin Chain Synthesis. Molecular Cell *56*, 360-375.

Orrenius, S., Zhivotovsky, B., and Nicotera, P. (2003). Regulation of cell death: the calcium–apoptosis link. Nature Reviews Molecular Cell Biology *4*, 552-565.

Osman, C., Voelker, D.R., and Langer, T. (2011). Making heads or tails of phospholipids in mitochondria. J Cell Biol *192*, 7-16.

Osman, C., Wilmes, C., Tatsuta, T., and Langer, T. (2007). Prohibitins interact genetically with Atp23, a novel processing peptidase and chaperone for the F1Fo-ATP synthase. Mol Biol Cell *18*, 627-635.

Ott, M., and Herrmann, J.M. (2010). Co-translational membrane insertion of mitochondrially encoded proteins. Biochim Biophys Acta *1803*, 767-775.

Ott, M., Prestele, M., Bauerschmitt, H., Funes, S., Bonnefoy, N., and Herrmann, J.M. (2006). Mba1, a membrane-associated ribosome receptor in mitochondria. The EMBO journal *25*, 1603-1610.

Ou, W.J., Ito, A., Okazaki, H., and Omura, T. (1989). Purification and characterization of a processing protease from rat liver mitochondria. Embo j *8*, 2605-2612.

Oursel, D., Loutelier-Bourhis, C., Orange, N., Chevalier, S., Norris, V., and Lange, C.M. (2007). Lipid composition of membranes of Escherichia coli by liquid chromatography/tandem mass spectrometry using negative electrospray ionization. Rapid Commun Mass Spectrom *21*, 1721-1728.

Palikaras, K., Daskalaki, I., Markaki, M., and Tavernarakis, N. (2017). Mitophagy and age-related pathologies: Development of new therapeutics by targeting mitochondrial turnover. Pharmacology & Therapeutics *178*, 157-174.

Palikaras, K., Lionaki, E., and Tavernarakis, N. (2015). Coordination of mitophagy and mitochondrial biogenesis during ageing in C. elegans. Nature *521*, 525-528.

Palmer, T., and Berks, B.C. (2012). The twin-arginine translocation (Tat) protein export pathway. Nat Rev Microbiol *10*, 483-496.

Papa, L., and Germain, D. (2011). Estrogen receptor mediates a distinct mitochondrial unfolded protein response. Journal of cell science *124*, 1396-1402.

Papadopoulou, A.A., Muller, S.A., Mentrup, T., Shmueli, M.D., Niemeyer, J., Haug-Kroper, M., von Blume, J., Mayerhofer, A., Feederle, R., Schroder, B.*, et al.* (2019). Signal Peptide Peptidase-Like 2c (SPPL2c) impairs vesicular transport and cleavage of SNARE proteins. EMBO Rep *20*.

Papić, D., Elbaz-Alon, Y., Koerdt, S.N., Leopold, K., Worm, D., Jung, M., Schuldiner, M., and Rapaport, D. (2013). The role of Djp1 in import of the mitochondrial protein Mim1 demonstrates specificity between a cochaperone and its substrate protein. Mol Cell Biol *33*, 4083-4094.

Papić, D., Krumpe, K., Dukanovic, J., Dimmer, K.S., and Rapaport, D. (2011). Multispan mitochondrial outer membrane protein Ugo1 follows a unique Mim1-dependent import pathway. J Cell Biol *194*, 397-405.

Park, Y.S., Choi, S.E., and Koh, H.C. (2018). PGAM5 regulates PINK1/Parkin-mediated mitophagy via DRP1 in CCCP-induced mitochondrial dysfunction. Toxicol Lett *284*, 120-128.

Paschen, S.A., Waizenegger, T., Stan, T., Preuss, M., Cyrklaff, M., Hell, K., Rapaport, D., and Neupert, W. (2003). Evolutionary conservation of biogenesis of beta-barrel membrane proteins. Nature *426*, 862-866.

Pei, J., and Grishin, N.V. (2001). Type II CAAX prenyl endopeptidases belong to a novel superfamily of putative membrane-bound metalloproteases. Trends Biochem Sci *26*, 275-277.

Pellegrini, L., Passer, B.J., Canelles, M., Lefterov, I., Ganjei, J.K., Fowlkes, B.J., Koonin, E.V., and D'Adamio, L. (2001). PAMP and PARL, two novel putative metalloproteases interacting with the COOH-terminus of Presenilin-1 and -2. J Alzheimers Dis *3*, 181-190.

Perrin, F., Papadopoulos, N., Suelves, N., Opsomer, R., Vadukul, D.M., Vrancx, C., Smith, S.O., Vertommen, D., Kienlen-Campard, P., and Constantinescu, S.N. (2020). Dimeric Transmembrane Orientations of APP/C99 Regulate γ-Secretase Processing Line Impacting Signaling and Oligomerization. iScience *23*, 101887.

Pester, O., Barrett, P.J., Hornburg, D., Hornburg, P., Probstle, R., Widmaier, S., Kutzner, C., Durrbaum, M., Kapurniotu, A., Sanders, C.R.*, et al.* (2013a). The backbone dynamics of the amyloid precursor protein transmembrane helix provides a rationale for the sequential cleavage mechanism of gamma-secretase. J Am Chem Soc *135*, 1317-1329.

Pester, O., Gotz, A., Multhaup, G., Scharnagl, C., and Langosch, D. (2013b). The cleavage domain of the amyloid precursor protein transmembrane helix does not exhibit above-average backbone dynamics. Chembiochem *14*, 1943-1948.

Petit, D., Hitzenberger, M., Lismont, S., Zoltowska, K.M., Ryan, N.S., Mercken, M., Bischoff, F., Zacharias, M., and Chávez-Gutiérrez, L. (2019). Extracellular interface between APP and Nicastrin regulates Aβ length and response to γ-secretase modulators. Embo j *38*.

Pfanner, N., Hoeben, P., Tropschug, M., and Neupert, W. (1987a). The carboxyl-terminal two-thirds of the ADP/ATP carrier polypeptide contains sufficient information to direct translocation into mitochondria. J Biol Chem *262*, 14851-14854.

Pfanner, N., and Neupert, W. (1986). Transport of F1-ATPase subunit beta into mitochondria depends on both a membrane potential and nucleoside triphosphates. FEBS Lett *209*, 152-156.

Pfanner, N., Tropschug, M., and Neupert, W. (1987b). Mitochondrial protein import: nucleoside triphosphates are involved in conferring import-competence to precursors. Cell *49*, 815-823.

Pfeffer, S., Woellhaf, M.W., Herrmann, J.M., and Förster, F. (2015). Organization of the mitochondrial translation machinery studied in situ by cryoelectron tomography. Nature Communications *6*, 6019.

Picca, A., Guerra, F., Calvani, R., Romano, R., Coelho-Júnior, H.J., Bucci, C., and Marzetti, E. (2021). Mitochondrial Dysfunction, Protein Misfolding and Neuroinflammation in Parkinson's Disease: Roads to Biomarker Discovery. Biomolecules *11*.

Pickart, C.M., and Eddins, M.J. (2004). Ubiquitin: structures, functions, mechanisms. Biochim Biophys Acta *1695*, 55-72.

Pickles, S., Vigié, P., and Youle, R.J. (2018). Mitophagy and Quality Control Mechanisms in Mitochondrial Maintenance. Current biology : CB *28*, R170-R185.

Ponting, C.P., Hutton, M., Nyborg, A., Baker, M., Jansen, K., and Golde, T.E. (2002). Identification of a novel family of presenilin homologues. Hum. Mol. Genet. *11*, 1037-1044.

Poole, A.C., Thomas, R.E., Yu, S., Vincow, E.S., and Pallanck, L. (2010). The mitochondrial fusion-promoting factor mitofusin is a substrate of the PINK1/parkin pathway. PLoS One *5*, e10054.

Popov-Celeketić, J., Waizenegger, T., and Rapaport, D. (2008). Mim1 functions in an oligomeric form to facilitate the integration of Tom20 into the mitochondrial outer membrane. J Mol Biol *376*, 671-680.

Potting, C., Tatsuta, T., König, T., Haag, M., Wai, T., Aaltonen, M.J., and Langer, T. (2013). TRIAP1/PRELI complexes prevent apoptosis by mediating intramitochondrial transport of phosphatidic acid. Cell metabolism *18*, 287-295.

Potting, C., Wilmes, C., Engmann, T., Osman, C., and Langer, T. (2010). Regulation of mitochondrial phospholipids by Ups1/PRELI-like proteins depends on proteolysis and Mdm35. Embo j *29*, 2888-2898.

Poveda-Huertes, D., Mulica, P., and Vögtle, F.N. (2017). The versatility of the mitochondrial presequence processing machinery: cleavage, quality control and turnover. Cell and tissue research *367*, 73-81.

Powers, E.T., Morimoto, R.I., Dillin, A., Kelly, J.W., and Balch, W.E. (2009). Biological and chemical approaches to diseases of proteostasis deficiency. Annu Rev Biochem *78*, 959-991.

Pratje, E., Mannhaupt, G., Michaelis, G., and Beyreuther, K. (1983). A nuclear mutation prevents processing of a mitochondrially encoded membrane protein in Saccharomyces cerevisiae. Embo j *2*, 1049-1054.

Prestele, M., Vogel, F., Reichert, A.S., Herrmann, J.M., and Ott, M. (2009). Mrpl36 is important for generation of assembly competent proteins during mitochondrial translation. Molecular biology of the cell *20*, 2615-2625.

Preuss, M., Leonhard, K., Hell, K., Stuart, R.A., Neupert, W., and Herrmann, J.M. (2001). Mba1, a novel component of the mitochondrial protein export machinery of the yeast Saccharomyces cerevisiae. J Cell Biol *153*, 1085-1096.

Puchades, C., Ding, B., Song, A., Wiseman, R.L., Lander, G.C., and Glynn, S.E. (2019). Unique Structural Features of the Mitochondrial AAA+ Protease AFG3L2 Reveal the Molecular Basis for Activity in Health and Disease. Molecular cell *75*, 1073-1085.e1076.

Puchades, C., Rampello, A.J., Shin, M., Giuliano, C.J., Wiseman, R.L., Glynn, S.E., and Lander, G.C. (2017). Structure of the mitochondrial inner membrane AAA+ protease YME1 gives insight into substrate processing. Science *358*.

Puente, X.S., Sánchez, L.M., Overall, C.M., and López-Otín, C. (2003). Human and mouse proteases: a comparative genomic approach. Nat Rev Genet *4*, 544-558.

Python, C.P., Laban, O.P., Rossier, M.F., Vallotton, M.B., and Capponi, A.M. (1995). The site of action of Ca2+ in the activation of steroidogenesis: studies in Ca(2+)-clamped bovine adrenal zona-glomerulosa cells. Biochem J *305 (Pt 2)*, 569-576.

Qi, H., Moran, M.M., Navarro, B., Chong, J.A., Krapivinsky, G., Krapivinsky, L., Kirichok, Y., Ramsey, I.S., Quill, T.A., and Clapham, D.E. (2007). All four CatSper ion channel proteins are required for male fertility and sperm cell hyperactivated motility. Proc Natl Acad Sci U S A *104*, 1219-1223.

Qi, Y., Yan, L., Yu, C., Guo, X., Zhou, X., Hu, X., Huang, X., Rao, Z., Lou, Z., and Hu, J. (2016). Structures of human mitofusin 1 provide insight into mitochondrial tethering. Journal of Cell Biology *215*, 621-629.

Quigley, A., Dong, Y.Y., Pike, A.C., Dong, L., Shrestha, L., Berridge, G., Stansfeld, P.J., Sansom, M.S., Edwards, A.M., Bountra, C.*, et al.* (2013). The structural basis of ZMPSTE24-dependent laminopathies. Science *339*, 1604-1607.

Quinsay, M.N., Thomas, R.L., Lee, Y., and Gustafsson, Å.B. (2010). Bnip3-mediated mitochondrial autophagy is independent of the mitochondrial permeability transition pore. Autophagy *6*, 855-862.

Quirós, P.M., Langer, T., and López-Otín, C. (2015). New roles for mitochondrial proteases in health, ageing and disease. Nature reviews. Molecular cell biology *16*, 345-359.

Radke, S., Chander, H., Schäfer, P., Meiss, G., Krüger, R., Schulz, J.B., and Germain, D. (2008). Mitochondrial protein quality control by the proteasome involves ubiquitination and the protease Omi. The Journal of biological chemistry *283*, 12681-12685.

Rainbolt, T.K., Atanassova, N., Genereux, J.C., and Wiseman, R.L. (2013). Stress-regulated translational attenuation adapts mitochondrial protein import through Tim17A degradation. Cell metabolism *18*, 908-919.

Rainbolt, T.K., Lebeau, J., Puchades, C., and Wiseman, R.L. (2016). Reciprocal Degradation of YME1L and OMA1 Adapts Mitochondrial Proteolytic Activity during Stress. Cell reports *14*, 2041-2049.

Ramesh, A., Peleh, V., Martinez-Caballero, S., Wollweber, F., Sommer, F., van der Laan, M., Schroda, M., Alexander, R.T., Campo, M.L., and Herrmann, J.M. (2016). A disulfide bond in the TIM23 complex is crucial for voltage gating and mitochondrial protein import. The Journal of cell biology *214*, 417-431.

Rana, A., Oliveira, M.P., Khamoui, A.V., Aparicio, R., Rera, M., Rossiter, H.B., and Walker, D.W. (2017). Promoting Drp1-mediated mitochondrial fission in midlife prolongs healthy lifespan of Drosophila melanogaster. Nat Commun *8*, 448.

Rauschenberger, V., Bernkopf, D.B., Krenn, S., Jalal, K., Heller, J., Behrens, J., Gentzel, M., and Schambony, A. (2017). The phosphatase Pgam5 antagonizes Wnt/β-Catenin signaling in embryonic anterior-posterior axis patterning. Development (Cambridge, England) *144*, 2234-2247.

Ravanelli, S., den Brave, F., and Hoppe, T. (2020). Mitochondrial Quality Control Governed by Ubiquitin. Front Cell Dev Biol *8*, 270.

Rawlings, N.D. (2017). Using the MEROPS Database for Investigation of Lysosomal Peptidases, Their Inhibitors, and Substrates. Methods Mol Biol *1594*, 213-226.

Rawlings, N.D., and Barrett, A.J. (1995). Evolutionary families of metallopeptidases. Methods Enzymol *248*, 183-228.

Rawlings, N.D., Barrett, A.J., Thomas, P.D., Huang, X., Bateman, A., and Finn, R.D. (2018). The MEROPS database of proteolytic enzymes, their substrates and inhibitors in 2017 and a comparison with peptidases in the PANTHER database. Nucleic acids research *46*, D624-D632.

Rawlings, N.D., Tolle, D.P., and Barrett, A.J. (2004). MEROPS: the peptidase database. Nucleic Acids Res *32*, D160-164.

Rawson, R.B., Zelenski, N.G., Nijhawan, D., Ye, J., Sakai, J., Hasan, M.T., Chang, T.Y., Brown, M.S., and Goldstein, J.L. (1997). Complementation cloning of S2P, a gene encoding a putative metalloprotease required for intramembrane cleavage of SREBPs. Mol. Cell *1*, 47-57.

Reed, R.G., Feldhoff, R.C., Clute, O.L., and Peters, T., Jr. (1975). Fragments of bovine serum albumin produced by limited proteolysis. Conformation and ligand binding. Biochemistry *14*, 4578-4583.

Rehling, P., Model, K., Brandner, K., Kovermann, P., Sickmann, A., Meyer Helmut, E., Kühlbrandt, W., Wagner, R., Truscott Kaye, N., and Pfanner, N. (2003). Protein Insertion into the Mitochondrial Inner Membrane by a Twin-Pore Translocase. Science *299*, 1747-1751.

Rice, S.E., and Gelfand, V.I. (2006). Paradigm lost: milton connects kinesin heavy chain to miro on mitochondria. The Journal of cell biology *173*, 459-461.

Richter, F., Dennerlein, S., Nikolov, M., Jans, D.C., Naumenko, N., Aich, A., MacVicar, T., Linden, A., Jakobs, S., Urlaub, H.*, et al.* (2019). ROMO1 is a constituent of the human presequence translocase required for YME1L protease import. The Journal of cell biology *218*, 598-614.

Rissler, M., Wiedemann, N., Pfannschmidt, S., Gabriel, K., Guiard, B., Pfanner, N., and Chacinska, A. (2005). The essential mitochondrial protein Erv1 cooperates with Mia40 in biogenesis of intermembrane space proteins. J Mol Biol *353*, 485-492.

Rizzuto, R., Bernardi, P., and Pozzan, T. (2000). Mitochondria as all-round players of the calcium game. J Physiol *529 Pt 1*, 37-47.

Rizzuto, R., Brini, M., Murgia, M., and Pozzan, T. (1993). Microdomains with high Ca2+ close to IP3-sensitive channels that are sensed by neighboring mitochondria. Science *262*, 744-747.

Rodriguez, F., Rouse, S.L., Tait, C.E., Harmer, J., De Riso, A., Timmel, C.R., Sansom, M.S.P., Berks, B.C., and Schnell, J.R. (2013). Structural model for the protein-translocating element of the twin-arginine transport system. Proceedings of the National Academy of Sciences *110*, E1092.

Rogaev, E.I., Sherrington, R., Rogaeva, E.A., Levesque, G., Ikeda, M., Liang, Y., Chi, H., Lin, C., Holman, K., Tsuda, T.*, et al.* (1995). Familial Alzheimer's disease in kindreds with missense mutations in a gene on chromosome 1 related to the Alzheimer's disease type 3 gene. Nature *376*, 775-778.

Rogov, V.V., Suzuki, H., Marinković, M., Lang, V., Kato, R., Kawasaki, M., Buljubašić, M., Šprung, M., Rogova, N., Wakatsuki, S.*, et al.* (2017). Phosphorylation of the mitochondrial autophagy receptor Nix enhances its interaction with LC3 proteins. Scientific Reports *7*, 1131.

Roise, D., Horvath, S.J., Tomich, J.M., Richards, J.H., and Schatz, G. (1986). A chemically synthesized pre-sequence of an imported mitochondrial protein can form an amphiphilic helix and perturb natural and artificial phospholipid bilayers. Embo j *5*, 1327-1334.

Rojo, E.E., Guiard, B., Neupert, W., and Stuart, R.A. (1999). N-terminal tail export from the mitochondrial matrix. Adherence to the prokaryotic "positive-inside" rule of membrane protein topology. J Biol Chem *274*, 19617-19622.

Rojo, E.E., Stuart, R.A., and Neupert, W. (1995). Conservative sorting of F0-ATPase subunit 9: export from matrix requires delta pH across inner membrane and matrix ATP. The EMBO journal *14*, 3445-3451.

Rospert, S., Glick, B.S., Jenö, P., Schatz, G., Todd, M.J., Lorimer, G.H., and Viitanen, P.V. (1993). Identification and functional analysis of chaperonin 10, the groES homolog from yeast mitochondria. Proc Natl Acad Sci U S A *90*, 10967-10971.

Rossier, M.F. (2006). T channels and steroid biosynthesis: in search of a link with mitochondria. Cell Calcium *40*, 155-164.

Roy, A., Kucukural, A., and Zhang, Y. (2010). I-TASSER: a unified platform for automated protein structure and function prediction. Nature Protocols *5*, 725-738.

Ruiz, K., Thaker, T.M., Agnew, C., Miller-Vedam, L., Trenker, R., Herrera, C., Ingaramo, M., Toso, D., Frost, A., and Jura, N. (2019). Functional role of PGAM5 multimeric assemblies and their polymerization into filaments. Nat Commun *10*, 531.

Rujiviphat, J., Meglei, G., Rubinstein, J.L., and McQuibban, G.A. (2009). Phospholipid Association Is Essential for Dynamin-related Protein Mgm1 to Function in Mitochondrial Membrane Fusion *. Journal of Biological Chemistry *284*, 28682-28686.

Russ, W.P., and Engelman, D.M. (2000). The GxxxG motif: a framework for transmembrane helix-helix association. J Mol Biol *296*, 911-919.

Russell, C.W., Richards, A.C., Chang, A.S., and Mulvey, M.A. (2017). The Rhomboid Protease GlpG Promotes the Persistence of Extraintestinal Pathogenic Escherichia coli within the Gut. Infection and immunity *85*.

Ryan, E., Seehra, G., Sharma, P., and Sidransky, E. (2019). GBA1-associated parkinsonism: new insights and therapeutic opportunities. Curr Opin Neurol *32*, 589-596.

Rybak, J.N., Scheurer, S.B., Neri, D., and Elia, G. (2004). Purification of biotinylated proteins on streptavidin resin: a protocol for quantitative elution. Proteomics *4*, 2296-2299.

Ryu, D., Mouchiroud, L., Andreux, P.A., Katsyuba, E., Moullan, N., Nicolet-Dit-Félix, A.A., Williams, E.G., Jha, P., Lo Sasso, G., Huzard, D.*, et al.* (2016). Urolithin A induces mitophagy and prolongs lifespan in C. elegans and increases muscle function in rodents. Nat Med *22*, 879-888.

Sabouny, R., and Shutt, T.E. (2020). Reciprocal Regulation of Mitochondrial Fission and Fusion. Trends Biochem Sci *45*, 564-577.

Sai, Y., Zou, Z., Peng, K., and Dong, Z. (2012). The Parkinson's disease-related genes act in mitochondrial homeostasis. Neurosci Biobehav Rev *36*, 2034-2043.

Saita, S., Nolte, H., Fiedler, K.U., Kashkar, H., Venne, A.S., Zahedi, R.P., Kruger, M., and Langer, T. (2017). PARL mediates Smac proteolytic maturation in mitochondria to promote apoptosis. Nat Cell Biol *19*, 318-328.

Saita, S., Tatsuta, T., Lampe, P.A., Konig, T., Ohba, Y., and Langer, T. (2018). PARL partitions the lipid transfer protein STARD7 between the cytosol and mitochondria. EMBO J *37*.

Sakai, J., Duncan, E.A., Rawson, R.B., Hua, X., Brown, M.S., and Goldstein, J.L. (1996). Sterol-regulated release of SREBP-2 from cell membranes requires two sequential cleavages, one within a transmembrane segment. Cell *85*, 1037-1046.

Sakai, J., Rawson, R.B., Espenshade, P.J., Cheng, D., Seegmiller, A.C., Goldstein, J.L., and Brown, M.S. (1998). Molecular identification of the sterol-regulated luminal protease that cleaves SREBPs and controls lipid composition of animal cells. Mol Cell *2*, 505-514.

Salvesen, G.S., and Ashkenazi, A. (2011). Snapshot: caspases. Cell *147*, 476-476.e471.

Sano, T., Smith, C.L., and Cantor, C.R. (1997). Expression and purification of recombinant streptavidin-containing chimeric proteins. Methods Mol Biol *63*, 119-128.

Sato, C., Takagi, S., Tomita, T., and Iwatsubo, T. (2008). The C-terminal PAL motif and transmembrane domain 9 of presenilin 1 are involved in the formation of the catalytic pore of the gamma-secretase. J Neurosci *28*, 6264-6271.

Saunders, C., Smith, L., Wibrand, F., Ravn, K., Bross, P., Thiffault, I., Christensen, M., Atherton, A., Farrow, E., Miller, N.*, et al.* (2015). CLPB variants associated with autosomal-recessive mitochondrial disorder with cataract, neutropenia, epilepsy, and methylglutaconic aciduria. Am J Hum Genet *96*, 258-265.

Schäfer, A., Zick, M., Kief, J., Steger, M., Heide, H., Duvezin-Caubet, S., Neupert, W., and Reichert, A.S. (2010). Intramembrane proteolysis of Mgm1 by the mitochondrial rhomboid protease is highly promiscuous regarding the sequence of the cleaved hydrophobic segment. J Mol Biol *401*, 182-193.

Schagger, H., Cramer, W.A., and von Jagow, G. (1994). Analysis of molecular masses and oligomeric states of protein complexes by blue native electrophoresis and isolation of membrane protein complexes by two-dimensional native electrophoresis. Anal Biochem *217*, 220-230.

Schatz, G., and Dobberstein, B. (1996). Common principles of protein translocation across membranes. Science *271*, 1519-1526.

Schechter, I., and Berger, A. (1967). On the size of the active site in proteases. I. Papain. Biochem Biophys Res Commun *27*, 157-162.

Schendzielorz, A.B., Bragoszewski, P., Naumenko, N., Gomkale, R., Schulz, C., Guiard, B., Chacinska, A., and Rehling, P. (2018). Motor recruitment to the TIM23 channel's lateral gate restricts polypeptide release into the inner membrane. Nature Communications *9*, 4028.

Schiavi, A., Maglioni, S., Palikaras, K., Shaik, A., Strappazzon, F., Brinkmann, V., Torgovnick, A., Castelein, N., De Henau, S., Braeckman, B.P.*, et al.* (2015). Iron-Starvation-Induced Mitophagy Mediates Lifespan Extension upon Mitochondrial Stress in C. elegans. Curr Biol *25*, 1810-1822.

Schiller, J., Müller, M., Fuchs, B., Arnold, K., and Huster, D. (2007). 31P NMR Spectroscopy of Phospholipids: From Micelles to Membranes. Current Analytical Chemistry *3*, 283-301.

Schindelin, J., Arganda-Carreras, I., Frise, E., Kaynig, V., Longair, M., Pietzsch, T., Preibisch, S., Rueden, C., Saalfeld, S., Schmid, B.*, et al.* (2012). Fiji: an open-source platform for biological-image analysis. Nat Methods *9*, 676-682.

Schleyer, M., Schmidt, B., and Neupert, W. (1982). Requirement of a membrane potential for the posttranslational transfer of proteins into mitochondria. Eur J Biochem *125*, 109-116.

Schmidt, B., Wachter, E., Sebald, W., and Neupert, W. (1984). Processing peptidase of Neurospora mitochondria. Two-step cleavage of imported ATPase subunit 9. Eur J Biochem *144*, 581-588.

Schmidt, O., Pfanner, N., and Meisinger, C. (2010). Mitochondrial protein import: from proteomics to functional mechanisms. Nat Rev Mol Cell Biol *11*, 655-667.

Schmidt, P., Bender, B.J., Kaiser, A., Gulati, K., Scheidt, H.A., Hamm, H.E., Meiler, J., Beck-Sickinger, A.G., and Huster, D. (2017). Improved in Vitro Folding of the Y(2) G Protein-Coupled Receptor into Bicelles. Front Mol Biosci *4*, 100.

Schmidt, W.K., Tam, A., Fujimura-Kamada, K., and Michaelis, S. (1998). Endoplasmic reticulum membrane localization of Rce1p and Ste24p, yeast proteases involved in carboxyl-terminal CAAX protein processing and amino-terminal a-factor cleavage. Proc Natl Acad Sci U S A *95*, 11175-11180.

Schultz, B.E., and Chan, S.I. (2001). Structures and proton-pumping strategies of mitochondrial respiratory enzymes. Annu Rev Biophys Biomol Struct *30*, 23-65.

Schwager, A. (2015). Validation of PARL Interactome SILAC Data by Cell Transfection, co-IP and Western Blot Analysis. Labrotation protocol (AG Lemberg), 29.

Schwarzinger, S., Kroon, G.J., Foss, T.R., Chung, J., Wright, P.E., and Dyson, H.J. (2001). Sequence-dependent correction of random coil NMR chemical shifts. J Am Chem Soc *123*, 2970-2978.

Scorrano, L., Ashiya, M., Buttle, K., Weiler, S., Oakes, S.A., Mannella, C.A., and Korsmeyer, S.J. (2002). A distinct pathway remodels mitochondrial cristae and mobilizes cytochrome c during apoptosis. Dev Cell *2*, 55-67.

Sekine, S., Kanamaru, Y., Koike, M., Nishihara, A., Okada, M., Kinoshita, H., Kamiyama, M., Maruyama, J., Uchiyama, Y., Ishihara, N.*, et al.* (2012). Rhomboid Protease PARL Mediates the Mitochondrial Membrane Potential Loss-induced Cleavage of PGAM5. J Biol Chem *287*, 34635-34645.

Sekine, S., Wang, C., Sideris, D.P., Bunker, E., Zhang, Z., and Youle, R.J. (2019). Reciprocal Roles of Tom7 and OMA1 during Mitochondrial Import and Activation of PINK1. Molecular cell *73*, 1028-1043.

Selkoe, D.J. (2004). Cell biology of protein misfolding: the examples of Alzheimer's and Parkinson's diseases. Nat Cell Biol *6*, 1054-1061.

Selvaraj, S., and Piramanayagam, S. (2019). Impact of gene mutation in the development of Parkinson's disease. Genes & Diseases *6*, 120-128.

Serero, A., Giglione, C., Sardini, A., Martinez-Sanz, J., and Meinnel, T. (2003). An unusual peptide deformylase features in the human mitochondrial N-terminal methionine excision pathway. J Biol Chem *278*, 52953-52963.

Sesaki, H., Southard, S.M., Hobbs, A.E., and Jensen, R.E. (2003). Cells lacking Pcp1p/Ugo2p, a rhomboid-like protease required for Mgm1p processing, lose mtDNA and mitochondrial structure in a Dnm1p-dependent manner, but remain competent for mitochondrial fusion. Biochem Biophys Res Commun *308*, 276-283.

Setoguchi, K., Otera, H., and Mihara, K. (2006). Cytosolic factor- and TOM-independent import of C-tail-anchored mitochondrial outer membrane proteins. Embo j *25*, 5635-5647.

Severance, S., and Hamza, I. (2009). Trafficking of heme and porphyrins in metazoa. Chem Rev *109*, 4596-4616.

Shen, L., Gan, Q., Yang, Y., Reis, C., Zhang, Z., Xu, S., Zhang, T., and Sun, C. (2021). Mitophagy in Cerebral Ischemia and Ischemia/Reperfusion Injury. Frontiers in Aging Neuroscience *13*.

Sherrington, R., Rogaev, E.I., Liang, Y., Rogaeva, E.A., Levesque, G., Ikeda, M., Chi, H., Lin, C., Li, G., Holman, K.*, et al.* (1995). Cloning of a gene bearing missense mutations in early-onset familial Alzheimer's disease. Nature *375*, 754-760.

Shi, C., Öster, C., Bohg, C., Li, L., Lange, S., Chevelkov, V., and Lange, A. (2019). Structure and Dynamics of the Rhomboid Protease GlpG in Liposomes Studied by Solid-State NMR. Journal of the American Chemical Society *141*, 17314-17321.

Shi, G., Lee, J.R., Grimes, D.A., Racacho, L., Ye, D., Yang, H., Ross, O.A., Farrer, M., McQuibban, G.A., and Bulman, D.E. (2011). Functional alteration of PARL contributes to mitochondrial dysregulation in Parkinson's disease. Hum Mol Genet *20*, 1966-1974.

Shi, G., and McQuibban, G.A. (2017). The Mitochondrial Rhomboid Protease PARL Is Regulated by PDK2 to Integrate Mitochondrial Quality Control and Metabolism. Cell reports *18*, 1458-1472.

Shiota, T., Imai, K., Qiu, J., Hewitt, V.L., Tan, K., Shen, H.H., Sakiyama, N., Fukasawa, Y., Hayat, S., Kamiya, M.*, et al.* (2015). Molecular architecture of the active mitochondrial protein gate. Science *349*, 1544-1548.

Shore, G.C., McBride, H.M., Millar, D.G., Steenaart, N.A., and Nguyen, M. (1995). Import and insertion of proteins into the mitochondrial outer membrane. Eur J Biochem *227*, 9-18.

Shulman, J.M., De Jager, P.L., and Feany, M.B. (2011). Parkinson's disease: genetics and pathogenesis. Annu Rev Pathol *6*, 193-222.

Sideris, D.P., Petrakis, N., Katrakili, N., Mikropoulou, D., Gallo, A., Ciofi-Baffoni, S., Banci, L., Bertini, I., and Tokatlidis, K. (2009). A novel intermembrane space-targeting signal docks cysteines onto Mia40 during mitochondrial oxidative folding. The Journal of cell biology *187*, 1007-1022.

Sievers, F., Wilm, A., Dineen, D., Gibson, T.J., Karplus, K., Li, W., Lopez, R., McWilliam, H., Remmert, M., Söding, J.*, et al.* (2011). Fast, scalable generation of high-quality protein multiple sequence alignments using Clustal Omega. Molecular systems biology *7*, 539.

Sik, A., Passer, B.J., Koonin, E.V., and Pellegrini, L. (2004). Self-regulated cleavage of the mitochondrial intramembrane-cleaving protease PARL yields Pbeta, a nuclear-targeted peptide. J Biol Chem *279*, 15323-15329.

Silber, M., Hitzenberger, M., Zacharias, M., and Muhle-Goll, C. (2020). Altered Hinge Conformations in APP Transmembrane Helix Mutants May Affect Enzyme–Substrate Interactions of γ-Secretase. ACS Chemical Neuroscience *11*, 4426-4433.

Sinha, S., Anderson, J.P., Barbour, R., Basi, G.S., Caccavello, R., Davis, D., Doan, M., Dovey, H.F., Frigon, N., Hong, J.*, et al.* (1999). Purification and cloning of amyloid precursor protein beta-secretase from human brain. Nature *402*, 537-540.

Smirnova, E., Griparic, L., Shurland, D.L., and van der Bliek, A.M. (2001). Dynamin-related protein Drp1 is required for mitochondrial division in mammalian cells. Mol Biol Cell *12*, 2245-2256.

Song, Z., Chen, H., Fiket, M., Alexander, C., and Chan, D.C. (2007). OPA1 processing controls mitochondrial fusion and is regulated by mRNA splicing, membrane potential, and Yme1L. J Cell Biol *178*, 749-755.

Soubias, O., Niu, S.L., Mitchell, D.C., and Gawrisch, K. (2008). Lipid-rhodopsin hydrophobic mismatch alters rhodopsin helical content. J Am Chem Soc *130*, 12465-12471.

Soubias, O., Teague, W.E., and Gawrisch, K. (2006). Evidence for specificity in lipid-rhodopsin interactions. J Biol Chem *281*, 33233-33241.

Soubias, O., Teague, W.E., Jr., Hines, K.G., and Gawrisch, K. (2015). Rhodopsin/lipid hydrophobic matching-rhodopsin oligomerization and function. Biophys J *108*, 1125-1132.

Sparagna, G.C., Gunter, K.K., Sheu, S.S., and Gunter, T.E. (1995). Mitochondrial calcium uptake from physiological-type pulses of calcium. A description of the rapid uptake mode. J Biol Chem *270*, 27510-27515.

Spinazzi, M., and De Strooper, B. (2016). PARL: The mitochondrial rhomboid protease. Semin Cell Dev Biol *60*, 19-28.

Spinazzi, M., Radaelli, E., Horre, K., Arranz, A.M., Gounko, N.V., Agostinis, P., Maia, T.M., Impens, F., Morais, V.A., Lopez-Lluch, G.*, et al.* (2019). PARL deficiency in mouse causes Complex III defects, coenzyme Q depletion, and Leigh-like syndrome. Proc Natl Acad Sci U S A *116*, 277-286.

Stach, L., and Freemont, P.S. (2017). The AAA+ ATPase p97, a cellular multitool. Biochem J *474*, 2953-2976.

Stadtman, E.R., and Berlett, B.S. (1998). Reactive oxygen-mediated protein oxidation in aging and disease. Drug Metab Rev *30*, 225-243.

Stagg, H.R., Thomas, M., van den Boomen, D., Wiertz, E.J., Drabkin, H.A., Gemmill, R.M., and Lehner, P.J. (2009). The TRC8 E3 ligase ubiquitinates MHC class I molecules before dislocation from the ER. J Cell Biol *186*, 685-692.

Steiner, H., and Haass, C. (2000). Intramembrane proteolysis by presenilins. Nat. Rev. Mol. Cell Biol. *1*, 217-224.

Stevenson, J., Huang, E.Y., and Olzmann, J.A. (2016). Endoplasmic Reticulum-Associated Degradation and Lipid Homeostasis. Annu Rev Nutr *36*, 511-542.

Stevenson, L.G., Strisovsky, K., Clemmer, K.M., Bhatt, S., Freeman, M., and Rather, P.N. (2007). Rhomboid protease AarA mediates quorum-sensing in Providencia stuartii by activating TatA of the twin-arginine translocase. Proc. Natl. Acad. Sci. USA *104*, 1003-1008.

Stojanovski, D., Guiard, B., Kozjak-Pavlovic, V., Pfanner, N., and Meisinger, C. (2007). Alternative function for the mitochondrial SAM complex in biogenesis of alpha-helical TOM proteins. J Cell Biol *179*, 881-893.

Strasser, A., Harris, A.W., Huang, D.C., Krammer, P.H., and Cory, S. (1995). Bcl-2 and Fas/APO-1 regulate distinct pathways to lymphocyte apoptosis. Embo j *14*, 6136-6147.

Strauss, M., Hofhaus, G., Schröder, R.R., and Kühlbrandt, W. (2008). Dimer ribbons of ATP synthase shape the inner mitochondrial membrane. Embo j *27*, 1154-1160.

Strisovsky, K. (2016). Why cells need intramembrane proteases - a mechanistic perspective. FEBS J *283*, 1837-1845.

Strisovsky, K., Sharpe, H.J., and Freeman, M. (2009). Sequence-specific intramembrane proteolysis: identification of a recognition motif in rhomboid substrates. Mol Cell *36*, 1048-1059.

Stuart, R.A. (2002). Insertion of proteins into the inner membrane of mitochondria: the role of the Oxa1 complex. Biochimica et Biophysica Acta (BBA) - Molecular Cell Research *1592*, 79-87.

Sturtevant, M.A., Roark, M., and Bier, E. (1993). The Drosophila rhomboid gene mediates the localized formation of wing veins and interacts genetically with components of the EGF-R signaling pathway. Genes Dev *7*, 961-973.

Sugawara, S., Kanamaru, Y., Sekine, S., Maekawa, L., Takahashi, A., Yamamoto, T., Watanabe, K., Fujisawa, T., Hattori, K., and Ichijo, H. (2020). The mitochondrial protein PGAM5 suppresses energy consumption in brown adipocytes by repressing expression of uncoupling protein 1. J Biol Chem *295*, 5588-5601.

Sugiura, A., McLelland, G.-L., Fon, E.A., and McBride, H.M. (2014). A new pathway for mitochondrial quality control: mitochondrial-derived vesicles. The EMBO journal *33*, 2142-2156.

Sugo, M., Kimura, H., Arasaki, K., Amemiya, T., Hirota, N., Dohmae, N., Imai, Y., Inoshita, T., Shiba-Fukushima, K., Hattori, N.*, et al.* (2018). Syntaxin 17 regulates the localization and function of PGAM5 in mitochondrial division and mitophagy. Embo j *37*.

Suguna, K., Padlan, E.A., Smith, C.W., Carlson, W.D., and Davies, D.R. (1987). Binding of a reduced peptide inhibitor to the aspartic proteinase from Rhizopus chinensis: implications for a mechanism of action. Proc Natl Acad Sci U S A *84*, 7009-7013.

Sun, L., Li, X., and Shi, Y. (2016). Structural biology of intramembrane proteases: mechanistic insights from rhomboid and S2P to gamma-secretase. Curr Opin Struct Biol *37*, 97-107.

Sun, Z., and Brodsky, J.L. (2019). Protein quality control in the secretory pathway. J Cell Biol *218*, 3171-3187.

Suppanz, I.E., Wurm, C.A., Wenzel, D., and Jakobs, S. (2009). The m-AAA protease processes cytochrome c peroxidase preferentially at the inner boundary membrane of mitochondria. Mol Biol Cell *20*, 572-580.

Suzuki, H., Okazawa, Y., Komiya, T., Saeki, K., Mekada, E., Kitada, S., Ito, A., and Mihara, K. (2000). Characterization of rat TOM40, a central component of the preprotein translocase of the mitochondrial outer membrane. J Biol Chem *275*, 37930-37936.

Suzuki, Y., Imai, Y., Nakayama, H., Takahashi, K., Takio, K., and Takahashi, R. (2001). A serine protease, HtrA2, is released from the mitochondria and interacts with XIAP, inducing cell death. Mol Cell *8*, 613-621.

Svaguša, T., Martinić, M., Martinić, M., Kovačević, L., Šepac, A., Miličić, D., Bulum, J., Starčević, B., Sirotković-Skerlev, M., Seiwerth, F.*, et al.* (2020). Mitochondrial unfolded protein response, mitophagy and other mitochondrial quality control mechanisms in heart disease and aged heart. Croat Med J *61*, 126-138.

Swaisgood, H.E. (1995). H - Enzymes Indigenous to Bovine Milk. In Handbook of Milk Composition, R.G. Jensen, ed. (San Diego: Academic Press), pp. 472-476.

Szczepanowska, K., Maiti, P., Kukat, A., Hofsetz, E., Nolte, H., Senft, K., Becker, C., Ruzzenente, B., Hornig-Do, H.T., Wibom, R.*, et al.* (2016). CLPP coordinates mitoribosomal assembly through the regulation of ERAL1 levels. Embo j *35*, 2566-2583.

Taguchi, N., Ishihara, N., Jofuku, A., Oka, T., and Mihara, K. (2007). Mitotic phosphorylation of dynamin-related GTPase Drp1 participates in mitochondrial fission. J Biol Chem *282*, 11521-11529.

Tait, S.W.G., Parsons, M.J., Llambi, F., Bouchier-Hayes, L., Connell, S., Muñoz-Pinedo, C., and Green, D.R. (2010). Resistance to caspase-independent cell death requires persistence of intact mitochondria. Developmental cell *18*, 802-813.

Takeda, K., Komuro, Y., Hayakawa, T., Oguchi, H., Ishida, Y., Murakami, S., Noguchi, T., Kinoshita, H., Sekine, Y., Iemura, S.-i*., et al.* (2009). Mitochondrial phosphoglycerate mutase 5 uses alternate catalytic activity as a protein serine/threonine phosphatase to activate ASK1. Proceedings of the National Academy of Sciences of the United States of America *106*, 12301-12305.

Tanaka, A., Cleland, M.M., Xu, S., Narendra, D.P., Suen, D.F., Karbowski, M., and Youle, R.J. (2010). Proteasome and p97 mediate mitophagy and degradation of mitofusins induced by Parkin. J Cell Biol *191*, 1367-1380.

Tang, S., Beattie, A.T., Kafkova, L., Petris, G., Huguenin-Dezot, N., Fiedler, M., Freeman, M., and Chin, J.W. (2022). Mechanism-based traps enable protease and hydrolase substrate discovery. Nature *602*, 701-707.

Taskin, A.A., Kücükköse, C., Burger, N., Mossmann, D., Meisinger, C., and Vögtle, F.N. (2017). The novel mitochondrial matrix protease Ste23 is required for efficient presequence degradation and processing. Mol Biol Cell *28*, 997-1002.

Tatsuta, T., Augustin, S., Nolden, M., Friedrichs, B., and Langer, T. (2007). m-AAA protease-driven membrane dislocation allows intramembrane cleavage by rhomboid in mitochondria. EMBO J. *26*, 325-335.

Tatsuta, T., and Langer, T. (2017). Prohibitins. Curr Biol *27*, R629-r631.

Taylor, A. (1993). Aminopeptidases: structure and function. FASEB journal : official publication of the Federation of American Societies for Experimental Biology *7*, 290-298.

Teixeira, P.F., and Glaser, E. (2013). Processing peptidases in mitochondria and chloroplasts. Biochimica et Biophysica Acta (BBA) - Molecular Cell Research *1833*, 360-370.

The UniProt, C. (2021). UniProt: the universal protein knowledgebase in 2021. Nucleic acids research *49*, D480-D489.

Thevarajan, I., Zolkiewski, M., and Zolkiewska, A. (2020). Human CLPB forms ATP-dependent complexes in the mitochondrial intermembrane space. Int J Biochem Cell Biol *127*, 105841.

Thompson, C.B. (1995). Apoptosis in the pathogenesis and treatment of disease. Science *267*, 1456-1462.

Ticha, A., Collis, B., and Strisovsky, K. (2018). The Rhomboid Superfamily: Structural Mechanisms and Chemical Biology Opportunities. Trends Biochem Sci *43*, 726-739.

Ticha, A., Stanchev, S., Skerle, J., Began, J., Ingr, M., Svehlova, K.I., Polovinkin, L., Ruzicka, M., Bednarova, L., Hadravova, R*., et al.* (2017). Sensitive Versatile Fluorogenic Transmembrane Peptide Substrates for Rhomboid Intramembrane Proteases. J Biol Chem.

Tilokani, L., Nagashima, S., Paupe, V., and Prudent, J. (2018). Mitochondrial dynamics: overview of molecular mechanisms. Essays in biochemistry *62*, 341-360.

Tolia, A., Horré, K., and De Strooper, B. (2008). Transmembrane domain 9 of presenilin determines the dynamic conformation of the catalytic site of gamma-secretase. J Biol Chem *283*, 19793-19803.

Tomita, T., Watabiki, T., Takikawa, R., Morohashi, Y., Takasugi, N., Kopan, R., De Strooper, B., and Iwatsubo, T. (2001). The first proline of PALP motif at the C terminus of presenilins is obligatory for stabilization, complex formation, and gamma-secretase activities of presenilins. J Biol Chem *276*, 33273-33281.

Tondera, D., Grandemange, S., Jourdain, A., Karbowski, M., Mattenberger, Y., Herzig, S., Da Cruz, S., Clerc, P., Raschke, I., Merkwirth, C*., et al.* (2009). SLP-2 is required for stress-induced mitochondrial hyperfusion. The EMBO Journal *28*, 1589-1600.

Toomes, C., James, J., Wood, A.J., Wu, C.L., McCormick, D., Lench, N., Hewitt, C., Moynihan, L., Roberts, E., Woods, C.G*., et al.* (1999). Loss-of-function mutations in the cathepsin C gene result in periodontal disease and palmoplantar keratosis. Nature genetics *23*, 421-424.

Trifunovic, A., Wredenberg, A., Falkenberg, M., Spelbrink, J.N., Rovio, A.T., Bruder, C.E., Bohlooly-Y, M., Gidlöf, S., Oldfors, A., Wibom, R*., et al.* (2004). Premature ageing in mice expressing defective mitochondrial DNA polymerase. Nature *429*, 417-423.

Truban, D., Hou, X., Caulfield, T.R., Fiesel, F.C., and Springer, W. (2017). PINK1, Parkin, and Mitochondrial Quality Control. Journal of Parkinson's disease *7*, 13-29.

Tschantz, W.R., Pfeifer, N.D., Meade, C.L., Wang, L., Lanzetti, A., Kamath, A.V., Berlioz-Seux, F., and Hashim, M.F. (2008). Expression, purification and characterization of the human membrane transporter protein OATP2B1 from Sf9 insect cells. Protein Expr Purif *57*, 163-171.

Turk, B. (2006). Targeting proteases: successes, failures and future prospects. Nat Rev Drug Discov *5*, 785-799.

Turk, B., Turk, D., and Turk, V. (2012). Protease signalling: the cutting edge. Embo j *31*, 1630-1643.

Tyanova, S., Temu, T., Sinitcyn, P., Carlson, A., Hein, M.Y., Geiger, T., Mann, M., and Cox, J. (2016). The Perseus computational platform for comprehensive analysis of (prote)omics data. Nat Methods *13*, 731-740.

Uhlén, M., Fagerberg, L., Hallström, B.M., Lindskog, C., Oksvold, P., Mardinoglu, A., Sivertsson, Å., Kampf, C., Sjöstedt, E., Asplund, A.*, et al.* (2015). Tissue-based map of the human proteome. Science *347*, 1260419.

Ulrich, T., Oberhettinger, P., Schütz, M., Holzer, K., Ramms, A.S., Linke, D., Autenrieth, I.B., and Rapaport, D. (2014). Evolutionary conservation in biogenesis of β-barrel proteins allows mitochondria to assemble a functional bacterial trimeric autotransporter protein. J Biol Chem *289*, 29457-29470.

Urban, S. (2016). Nicastrin guards Alzheimer's gate. Proceedings of the National Academy of Sciences of the United States of America *113*, 1112-1114.

Urban, S., Lee, J.R., and Freeman, M. (2001). Drosophila rhomboid-1 defines a family of putative intramembrane serine proteases. Cell *107*, 173-182.

Urban, S., and Moin, S.M. (2014). A subset of membrane-altering agents and γ-secretase modulators provoke nonsubstrate cleavage by rhomboid proteases. Cell reports *8*, 1241-1247.

Urban, S., Schlieper, D., and Freeman, M. (2002). Conservation of intramembrane proteolytic activity and substrate specificity in prokaryotic and eukaryotic rhomboids. Curr. Biol. *12*, 1507-1512.

Urban, S., and Wolfe, M.S. (2005). Reconstitution of intramembrane proteolysis in vitro reveals that pure rhomboid is sufficient for catalysis and specificity. Proc. Natl. Acad. Sci. USA *102*, 1883-1888.

Vafai, S.B., and Mootha, V.K. (2012). Mitochondrial disorders as windows into an ancient organelle. *491*, 374-383.

van der Laan, M., Bohnert, M., Wiedemann, N., and Pfanner, N. (2012). Role of MINOS in mitochondrial membrane architecture and biogenesis. Trends Cell Biol *22*, 185-192.

Vance, J.E., and Shiao, Y.J. (1996). Intracellular trafficking of phospholipids: import of phosphatidylserine into mitochondria. Anticancer Res *16*, 1333-1339.

Vassar, R., Bennett, B.D., Babu-Khan, S., Kahn, S., Mendiaz, E.A., Denis, P., Teplow, D.B., Ross, S., Amarante, P., Loeloff, R.*, et al.* (1999). Beta-secretase cleavage of Alzheimer's amyloid precursor protein by the transmembrane aspartic protease BACE. Science *286*, 735-741.

Vaux, D.L. (2011). Apoptogenic factors released from mitochondria. Biochim Biophys Acta *1813*, 546-550.

Verhagen, A.M., Silke, J., Ekert, P.G., Pakusch, M., Kaufmann, H., Connolly, L.M., Day, C.L., Tikoo, A., Burke, R., Wrobel, C.*, et al.* (2002). HtrA2 promotes cell death through its serine protease activity and its ability to antagonize inhibitor of apoptosis proteins. J Biol Chem *277*, 445-454.

Verner, K. (1993). Co-translational protein import into mitochondria: an alternative view. Trends Biochem Sci *18*, 366-371.

Vial, S., Lu, H., Allen, S., Savory, P., Thornton, D., Sheehan, J., and Tokatlidis, K. (2002). Assembly of Tim9 and Tim10 into a functional chaperone. J Biol Chem *277*, 36100-36108.

Vinothkumar, K.R. (2011). Structure of rhomboid protease in a lipid environment. Journal of molecular biology *407*, 232-247.

Vogel, A., Scheidt, H.A., and Huster, D. (2003). The distribution of lipid attached spin probes in bilayers: application to membrane protein topology. Biophys J *85*, 1691-1701.

Vogel, F., Bornhövd, C., Neupert, W., and Reichert, A.S. (2006). Dynamic subcompartmentalization of the mitochondrial inner membrane. Journal of Cell Biology *175*, 237-247.

Vögtle, F.N., Wortelkamp, S., Zahedi, R.P., Becker, D., Leidhold, C., Gevaert, K., Kellermann, J., Voos, W., Sickmann, A., Pfanner, N.*, et al.* (2009). Global analysis of the mitochondrial N-proteome identifies a processing peptidase critical for protein stability. Cell *139*, 428-439.

von der Malsburg, K., Müller, J.M., Bohnert, M., Oeljeklaus, S., Kwiatkowska, P., Becker, T., Loniewska-Lwowska, A., Wiese, S., Rao, S., Milenkovic, D.*, et al.* (2011). Dual role of mitofilin in mitochondrial membrane organization and protein biogenesis. Dev Cell *21*, 694-707.

Voss, M., Schroder, B., and Fluhrer, R. (2013). Mechanism, specificity, and physiology of signal peptide peptidase (SPP) and SPP-like proteases. Biochim Biophys Acta *1828*, 2828-2839.

Wahlstrom, A.M., Cutts, B.A., Liu, M., Lindskog, A., Karlsson, C., Sjogren, A.-K.M., Andersson, K.M.E., Young, S.G., and Bergo, M.O. (2008). Inactivating Icmt ameliorates K-RAS-induced myeloproliferative disease. Blood *112*, 1357-1365.

Wai, T., and Langer, T. (2016). Mitochondrial Dynamics and Metabolic Regulation. Trends in Endocrinology & Metabolism *27*, 105-117.

Wai, T., Saita, S., Nolte, H., Muller, S., Konig, T., Richter-Dennerlein, R., Sprenger, H.G., Madrenas, J., Muhlmeister, M., Brandt, U.*, et al.* (2016). The membrane scaffold SLP2 anchors a proteolytic hub in mitochondria containing PARL and the i-AAA protease YME1L. EMBO Rep *17*, 1844-1856.

Waizenegger, T., Stan, T., Neupert, W., and Rapaport, D. (2003). Signal-anchor domains of proteins of the outer membrane of mitochondria: structural and functional characteristics. J Biol Chem *278*, 42064-42071.

Wales, T.E., and Engen, J.R. (2006). Hydrogen exchange mass spectrometry for the analysis of protein dynamics. Mass Spectrom Rev *25*, 158-170.

Walther, D.M., Rapaport, D., and Tommassen, J. (2009). Biogenesis of beta-barrel membrane proteins in bacteria and eukaryotes: evolutionary conservation and divergence. Cellular and molecular life sciences : CMLS *66*, 2789-2804.

Waltner, M., and Weiner, H. (1995). Conversion of a nonprocessed mitochondrial precursor protein into one that is processed by the mitochondrial processing peptidase. J Biol Chem *270*, 26311-26317.

Wang, R., Mishra, P., Garbis, S.D., Moradian, A., Sweredoski, M.J., and Chan, D.C. (2021). Identification of new OPA1 cleavage site reveals that short isoforms regulate mitochondrial fusion. Mol Biol Cell *32*, 157-168.

Wang, X., Winter, D., Ashrafi, G., Schlehe, J., Wong, Y.L., Selkoe, D., Rice, S., Steen, J., LaVoie, M.J., and Schwarz, T.L. (2011). PINK1 and Parkin target Miro for phosphorylation and degradation to arrest mitochondrial motility. Cell *147*, 893-906.

Wang, Y., and Ha, Y. (2007). Open-cap conformation of intramembrane protease GlpG. Proc. Natl. Acad. Sci. USA *104*, 2098-2102.

Wang, Y., Zhang, Y., and Ha, Y. (2006). Crystal structure of a rhomboid family intramembrane protease. Nature *444*, 179-180.

Wang, Z., Jiang, H., Chen, S., Du, F., and Wang, X. (2012). The mitochondrial phosphatase PGAM5 functions at the convergence point of multiple necrotic death pathways. Cell *148*, 228-243.

Wasiak, S., Zunino, R., and McBride, H.M. (2007). Bax/Bak promote sumoylation of DRP1 and its stable association with mitochondria during apoptotic cell death. J Cell Biol *177*, 439-450.

Waugh, D.S. (2005). Making the most of affinity tags. Trends Biotechnol *23*, 316-320.

Wei, H., Liu, L., and Chen, Q. (2015). Selective removal of mitochondria via mitophagy: distinct pathways for different mitochondrial stresses. Biochimica et Biophysica Acta (BBA) - Molecular Cell Research *1853*, 2784-2790.

Weihofen, A., Binns, K., Lemberg, M.K., Ashman, K., and Martoglio, B. (2002). Identification of signal peptide peptidase, a presenilin-type aspartic protease. Science *296*, 2215-2218.

Weihofen, A., Thomas, K.J., Ostaszewski, B.L., Cookson, M.R., and Selkoe, D.J. (2009). Pink1 forms a multiprotein complex with Miro and Milton, linking Pink1 function to mitochondrial trafficking. Biochemistry *48*, 2045-2052.

Weil, R., Laplantine, E., Curic, S., and Génin, P. (2018). Role of Optineurin in the Mitochondrial Dysfunction: Potential Implications in Neurodegenerative Diseases and Cancer. Front Immunol *9*, 1243.

Weissman, A.M., Shabek, N., and Ciechanover, A. (2011). The predator becomes the prey: regulating the ubiquitin system by ubiquitylation and degradation. Nat Rev Mol Cell Biol *12*, 605-620.

Werner, S., and Neupert, W. (1972). Functional and Biogenetical Heterogeneity of the Inner Membrane of Rat-Liver Mitochondria. European Journal of Biochemistry *25*, 379-396.

White, G.F., Schermann, S.M., Bradley, J., Roberts, A., Greene, N.P., Berks, B.C., and Thomson, A.J. (2010). Subunit organization in the TatA complex of the twin arginine protein translocase: a site-directed EPR spin labeling study. The Journal of biological chemistry *285*, 2294-2301.

Whitworth, A.J., Lee, J.R., Ho, V.M.W., Flick, R., Chowdhury, R., and McQuibban, G.A. (2008). Rhomboid-7 and HtrA2/Omi act in a common pathway with the Parkinson's disease factors Pink1 and Parkin. Dis. Model. Mech. *1*, 168-174; discussion 173.

Wiedemann, N., Kozjak, V., Chacinska, A., Schönfisch, B., Rospert, S., Ryan, M.T., Pfanner, N., and Meisinger, C. (2003). Machinery for protein sorting and assembly in the mitochondrial outer membrane. Nature *424*, 565-571.

Wiedemann, N., and Pfanner, N. (2017). Mitochondrial Machineries for Protein Import and Assembly. Annual review of biochemistry *86*, 685-714.

Wiedemann, N., Pfanner, N., and Ryan, M.T. (2001). The three modules of ADP/ATP carrier cooperate in receptor recruitment and translocation into mitochondria. The EMBO journal *20*, 951-960.

Wilkins, J.M., McConnell, C., Tipton, P.A., and Hannink, M. (2014). A conserved motif mediates both multimer formation and allosteric activation of phosphoglycerate mutase 5. The Journal of biological chemistry *289*, 25137-25148.

Willis, S.N., Fletcher, J.I., Kaufmann, T., van Delft, M.F., Chen, L., Czabotar, P.E., Ierino, H., Lee, E.F., Fairlie, W.D., Bouillet, P.*, et al.* (2007). Apoptosis initiated when BH3 ligands engage multiple Bcl-2 homologs, not Bax or Bak. Science *315*, 856-859.

Winkler, E., Julius, A., Steiner, H., and Langosch, D. (2015). Homodimerization Protects the Amyloid Precursor Protein C99 Fragment from Cleavage by γ-Secretase. Biochemistry *54*, 6149-6152.

Wishart, D.S., and Sykes, B.D. (1994). The 13C Chemical-Shift Index: A simple method for the identification of protein secondary structure using 13C chemical-shift data. Journal of Biomolecular NMR *4*, 171-180.

Wishart, D.S., Sykes, B.D., and Richards, F.M. (1992). The chemical shift index: a fast and simple method for the assignment of protein secondary structure through NMR spectroscopy. Biochemistry *31*, 1647-1651.

Wolfe, M.S. (2019). Structure and Function of the γ-Secretase Complex. Biochemistry *58*, 2953-2966.

Wolfe, M.S., Xia, W., Ostaszewski, B.L., Diehl, T.S., Kimberly, W.T., and Selkoe, D.J. (1999). Two transmembrane aspartates in presenilin-1 required for presenilin endoproteolysis and gamma-secretase activity. Nature *398*, 513-517.

Wong, Y.C., Ysselstein, D., and Krainc, D. (2018). Mitochondria–lysosome contacts regulate mitochondrial fission via RAB7 GTP hydrolysis. Nature *554*, 382-386.

Wortmann, S.B., Ziętkiewicz, S., Kousi, M., Szklarczyk, R., Haack, T.B., Gersting, S.W., Muntau, A.C., Rakovic, A., Renkema, G.H., Rodenburg, R.J.*, et al.* (2015). CLPB mutations cause 3-methylglutaconic aciduria, progressive brain atrophy, intellectual disability, congenital neutropenia, cataracts, movement disorder. Am J Hum Genet *96*, 245-257.

Wrobel, L., Sokol, A.M., Chojnacka, M., and Chacinska, A. (2016). The presence of disulfide bonds reveals an evolutionarily conserved mechanism involved in mitochondrial protein translocase assembly. Sci Rep *6*, 27484.

Wrobel, L., Trojanowska, A., Sztolsztener, M.E., and Chacinska, A. (2013). Mitochondrial protein import: Mia40 facilitates Tim22 translocation into the inner membrane of mitochondria. Molecular biology of the cell *24*, 543-554.

Wu, H., Xue, D., Chen, G., Han, Z., Huang, L., Zhu, C., Wang, X., Jin, H., Wang, J., Zhu, Y.*, et al.* (2014). The BCL2L1 and PGAM5 axis defines hypoxia-induced receptor-mediated mitophagy. Autophagy *10*, 1712-1725.

Wu, Z., Yan, N., Feng, L., Oberstein, A., Yan, H., Baker, R.P., Gu, L., Jeffrey, P.D., Urban, S., and Shi, Y. (2006). Structural analysis of a rhomboid family intramembrane protease reveals a gating mechanism for substrate entry. Nat. Struct. Mol. Biol. *13*, 1084-1091.

Wurm, C.A., and Jakobs, S. (2006). Differential protein distributions define two sub-compartments of the mitochondrial inner membrane in yeast. FEBS Lett *580*, 5628-5634.

Xu, S., Peng, G., Wang, Y., Fang, S., and Karbowski, M. (2011). The AAA-ATPase p97 is essential for outer mitochondrial membrane protein turnover. Mol Biol Cell *22*, 291-300.

Xu, W., Jing, L., Wang, Q., Lin, C.-C., Chen, X., Diao, J., Liu, Y., and Sun, X. (2015). Bax-PGAM5L-Drp1 complex is required for intrinsic apoptosis execution. Oncotarget *6*, 30017-30034.

Xue, Y., and Ha, Y. (2012). Catalytic mechanism of rhomboid protease GlpG probed by 3,4-dichloroisocoumarin and diisopropyl fluorophosphonate. J Biol Chem *287*, 3099-3107.

Xue, Y., and Ha, Y. (2013). Large lateral movement of transmembrane helix S5 is not required for substrate access to the active site of rhomboid intramembrane protease. The Journal of biological chemistry *288*, 16645-16654.

Yamaguchi, A., Ishikawa, H., Furuoka, M., Yokozeki, M., Matsuda, N., Tanimura, S., and Takeda, K. (2019). Cleaved PGAM5 is released from mitochondria depending on proteasome-mediated rupture of the outer mitochondrial membrane during mitophagy. Journal of biochemistry *165*, 19-25.

Yamano, K., and Youle, R.J. (2013). PINK1 is degraded through the N-end rule pathway. Autophagy *9*, 1758-1769.

Yan, C., Gong, L., Chen, L., Xu, M., Abou-Hamdan, H., Tang, M., Désaubry, L., and Song, Z. (2019). PHB2 (prohibitin 2) promotes PINK1-PRKN/Parkin-dependent mitophagy by the PARL-PGAM5-PINK1 axis. Autophagy *16*, 419-434.

Yan, R., Bienkowski, M.J., Shuck, M.E., Miao, H., Tory, M.C., Pauley, A.M., Brashier, J.R., Stratman, N.C., Mathews, W.R., Buhl, A.E.*, et al.* (1999). Membrane-anchored aspartyl protease with Alzheimer's disease beta-secretase activity. Nature *402*, 533-537.

Yang, G., Zhou, R., Zhou, Q., Guo, X., Yan, C., Ke, M., Lei, J., and Shi, Y. (2019). Structural basis of Notch recognition by human γ-secretase. Nature *565*, 192-197.

Yang, L., Lewkowich, I., Apsley, K., Fritz, J.M., Wills-Karp, M., and Weaver, T.E. (2015). Haploinsufficiency for Stard7 is associated with enhanced allergic responses in lung and skin. J Immunol *194*, 5635-5643.

Yang, Z., and Klionsky, D.J. (2010). Mammalian autophagy: core molecular machinery and signaling regulation. Curr Opin Cell Biol *22*, 124-131.

Yates, A.D., Achuthan, P., Akanni, W., Allen, J., Allen, J., Alvarez-Jarreta, J., Amode, M.R., Armean, I.M., Azov, A.G., Bennett, R.*, et al.* (2020). Ensembl 2020. Nucleic acids research *48*, D682-D688.

Ye, J., Rawson, R.B., Komuro, R., Chen, X., Dave, U.P., Prywes, R., Brown, M.S., and Goldstein, J.L. (2000). ER stress induces cleavage of membrane-bound ATF6 by the same proteases that process SREBPs. Mol. Cell *6*, 1355-1364.

Ye, Y., Shibata, Y., Yun, C., Ron, D., and Rapoport, T.A. (2004). A membrane protein complex mediates retro-translocation from the ER lumen into the cytosol. Nature *429*, 841-847.

Yogev, O., and Pines, O. (2011). Dual targeting of mitochondrial proteins: Mechanism, regulation and function. Biochim Biophys Acta *1808*, 1012-1020.

Yonashiro, R., Ishido, S., Kyo, S., Fukuda, T., Goto, E., Matsuki, Y., Ohmura-Hoshino, M., Sada, K., Hotta, H., Yamamura, H.*, et al.* (2006). A novel mitochondrial ubiquitin ligase plays a critical role in mitochondrial dynamics. Embo j *25*, 3618-3626.

Yoon, Y., Krueger, E.W., Oswald, B.J., and McNiven, M.A. (2003). The mitochondrial protein hFis1 regulates mitochondrial fission in mammalian cells through an interaction with the dynamin-like protein DLP1. Mol Cell Biol *23*, 5409-5420.

York, J.L., McCoy, S., Taylor, D.N., and Caughey, W.S. (1967). Heme A of cytochrome c oxidase. I. Isolation from bovine heart. The Journal of biological chemistry *242*, 908-911.

Yoshii, S.R., Kishi, C., Ishihara, N., and Mizushima, N. (2011). Parkin mediates proteasome-dependent protein degradation and rupture of the outer mitochondrial membrane. J Biol Chem *286*, 19630-19640.

Yoshioka, H., Katsu, M., Sakata, H., Okami, N., Wakai, T., Kinouchi, H., and Chan, P.H. (2013). The role of PARL and HtrA2 in striatal neuronal injury after transient global cerebral ischemia. Journal of

cerebral blood flow and metabolism : official journal of the International Society of Cerebral Blood Flow and Metabolism *33*, 1658-1665.

Youle, R.J. (2007). Cell biology. Cellular demolition and the rules of engagement. Science *315*, 776-777.

Youle, R.J., and Narendra, D.P. (2011). Mechanisms of mitophagy. Nat Rev Mol Cell Biol *12*, 9-14.

Youle, R.J., and Strasser, A. (2008). The BCL-2 protein family: opposing activities that mediate cell death. Nat Rev Mol Cell Biol *9*, 47-59.

Youle, R.J., and van der Bliek, A.M. (2012). Mitochondrial fission, fusion, and stress. Science *337*, 1062-1065.

Young, J.C., Hoogenraad, N.J., and Hartl, F.U. (2003). Molecular chaperones Hsp90 and Hsp70 deliver preproteins to the mitochondrial import receptor Tom70. Cell *112*, 41-50.

Young, L., Leonhard, K., Tatsuta, T., Trowsdale, J., and Langer, T. (2001). Role of the ABC transporter Mdl1 in peptide export from mitochondria. Science *291*, 2135-2138.

Yu, B., Ma, J., Li, J., Wang, D., Wang, Z., and Wang, S. (2020). Mitochondrial phosphatase PGAM5 modulates cellular senescence by regulating mitochondrial dynamics. Nature Communications *11*, 2549.

Yu, M., Liu, F.T., Newland, A.C., and Jia, L. (2008). The alpha-5 helix of Bax is sensitive to ubiquitin-dependent degradation. Biochem Biophys Res Commun *371*, 10-15.

Yu, R., Jin, S.-B., Lendahl, U., Nistér, M., and Zhao, J. (2019). Human Fis1 regulates mitochondrial dynamics through inhibition of the fusion machinery. The EMBO Journal *38*, e99748.

Yuan, L., Zhai, L., Qian, L., Huang, D., Ding, Y., Xiang, H., Liu, X., Thompson, J.W., Liu, J., He, Y.H.*, et al.* (2018). Switching off IMMP2L signaling drives senescence via simultaneous metabolic alteration and blockage of cell death. Cell Res *28*, 625-643.

Yücel, S.S., Stelzer, W., Lorenzoni, A., Wozny, M., Langosch, D., and Lemberg, M.K. (2019). The Metastable XBP1u Transmembrane Domain Defines Determinants for Intramembrane Proteolysis by Signal Peptide Peptidase. Cell Rep *26*, 3087-3099 e3011.

Zeb, A., Choubey, V., Gupta, R., Kuum, M., Safiulina, D., Vaarmann, A., Gogichaishvili, N., Liiv, M., Ilves, I., Tämm, K.*, et al.* (2021). A novel role of KEAP1/PGAM5 complex: ROS sensor for inducing mitophagy. Redox Biology, 102186.

Zeng, X., Neupert, W., and Tzagoloff, A. (2007). The metalloprotease encoded by ATP23 has a dual function in processing and assembly of subunit 6 of mitochondrial ATPase. Mol Biol Cell *18*, 617-626.

Zettl, M., Adrain, C., Strisovsky, K., Lastun, V., and Freeman, M. (2011). Rhomboid family pseudoproteases use the ER quality control machinery to regulate intercellular signaling. Cell *145*, 79-91.

Zhang, J., Liem, D.A., Mueller, M., Wang, Y., Zong, C., Deng, N., Vondriska, T.M., Korge, P., Drews, O., Maclellan, W.R.*, et al.* (2008). Altered proteome biology of cardiac mitochondria under stress conditions. J Proteome Res *7*, 2204-2214.

Zhang, K., Li, H., and Song, Z. (2014). Membrane depolarization activates the mitochondrial protease OMA1 by stimulating self-cleavage. EMBO reports *15*, 576-585.

Zhang, L., Lin, D., Kusov, Y., Nian, Y., Ma, Q., Wang, J., von Brunn, A., Leyssen, P., Lanko, K., Neyts, J.*, et al.* (2020a). α-Ketoamides as Broad-Spectrum Inhibitors of Coronavirus and Enterovirus Replication: Structure-Based Design, Synthesis, and Activity Assessment. J Med Chem *63*, 4562-4578.

Zhang, L., Lin, D., Sun, X., Curth, U., Drosten, C., Sauerhering, L., Becker, S., Rox, K., and Hilgenfeld, R. (2020b). Crystal structure of SARS-CoV-2 main protease provides a basis for design of improved α-ketoamide inhibitors. Science *368*, 409-412.

Zhang, S.L., Tang, H.B., Hu, J.T., Zang, Z.L., Ding, X., Li, S., and Yang, H. (2019). PGAM5-CypD pathway is involved in bromocriptine-induced RIP3/MLKL-dependent necroptosis of prolactinoma cells. Biomed Pharmacother *111*, 638-648.

Zhang, Y., Lee, K.M., Kinch, L.N., Clark, L., Grishin, N.V., Rosenbaum, D.M., Brown, M.S., Goldstein, J.L., and Radhakrishnan, A. (2016). Direct Demonstration That Loop1 of Scap Binds to Loop7: A CRUCIAL EVENT IN CHOLESTEROL HOMEOSTASIS. J Biol Chem *291*, 12888-12896.

Zhao, Q. (2002). A mitochondrial specific stress response in mammalian cells. The EMBO journal *21*, 4411-4419.

Zhou, R., Yang, G., Guo, X., Zhou, Q., Lei, J., and Shi, Y. (2019). Recognition of the amyloid precursor protein by human gamma-secretase. Science *363*.

Zhuang, M., Guan, S., Wang, H., Burlingame, A.L., and Wells, J.A. (2013). Substrates of IAP ubiquitin ligases identified with a designed orthogonal E3 ligase, the NEDDylator. Molecular cell *49*, 273-282.

Ziviani, E., Tao, R.N., and Whitworth, A.J. (2010). Drosophila Parkin requires PINK1 for mitochondrial translocation and ubiquitinates Mitofusin. Proceedings of the National Academy of Sciences *107*, 5018.

Zoll, S., Stanchev, S., Began, J., Skerle, J., Lepsik, M., Peclinovska, L., Majer, P., and Strisovsky, K. (2014). Substrate binding and specificity of rhomboid intramembrane protease revealed by substrate-peptide complex structures. EMBO J.

6. Appendix

6.1. Supplementary Figures

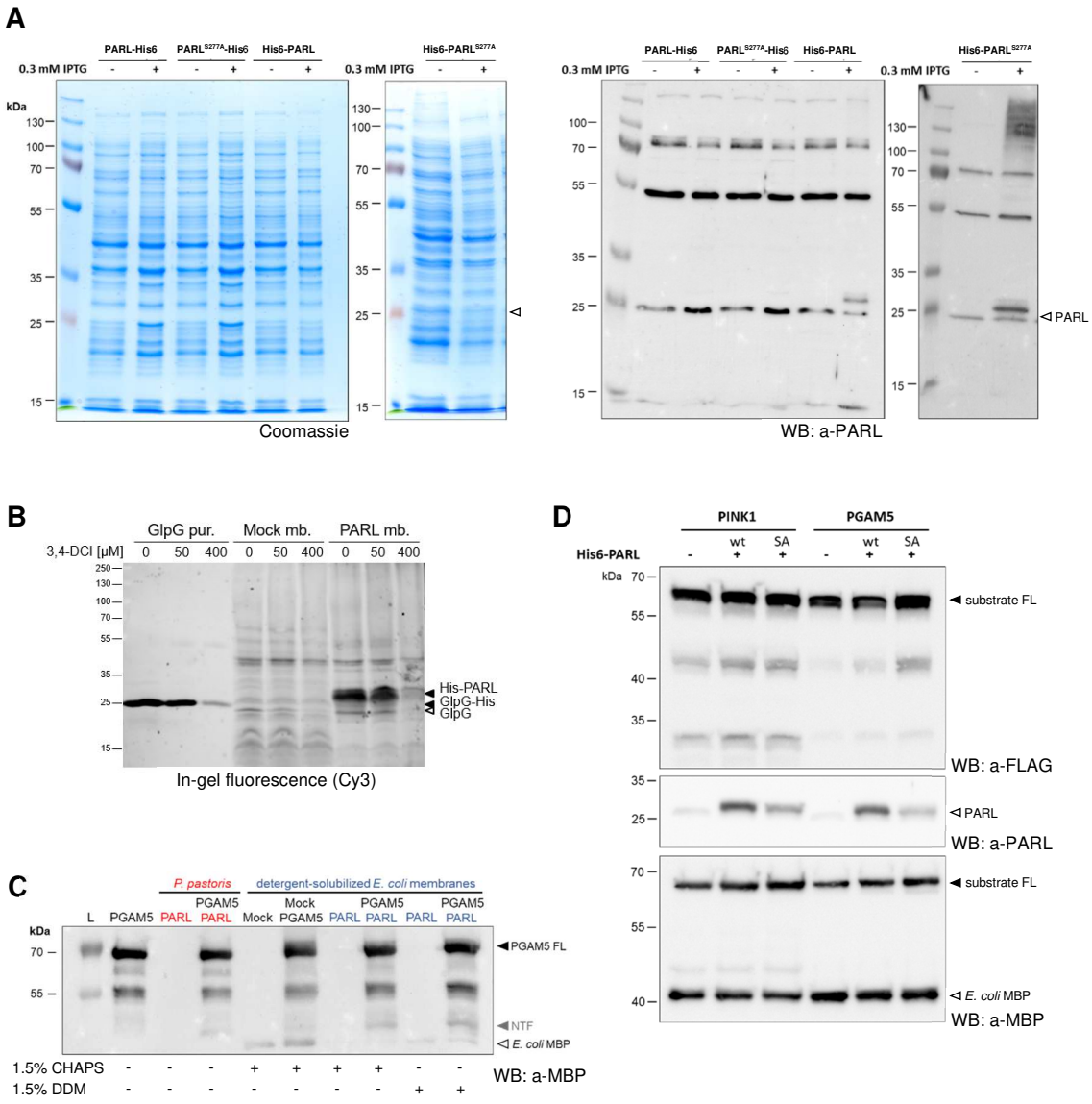

Figure S1 | Expression and purification of human PARL in *E. coli*, (related to Figure 7).
(A) N-terminally and C-terminally His6-tagged PARL was expressed in *E. coli*. Aliquots were resolved by SDS-PAGE and stained by Coomassie (left panel) or analyzed in western blotting with an antibody against PARL (right panel). **(B)** PARL activity measured by labelling of *E. coli* membranes with the TAMRA-FP serine hydrolase probe in presence of 3,4-dichloroisocoumarin (DCI) followed by SDS-PAGE and fluorescent imaging. Purified *E. coli* GlpG rhomboid and *E. coli* membranes lacking PARL (mock) were used as controls. Image by Baptiste Cordier. **(C)** His6-PARL activity detected by cleavage of MBP-PGAM5 after solubilization from *E. coli* membranes with the detergents CHAPS or DDM, resolved by SDS-PAGE and visualized by western blotting with an antibody against MBP. Yeast *P. pastoris*-purified human PARL and *E. coli* membranes lacking PARL (mock) were used as controls. L: protein ladder, PGAM5 FL: MBP-PGAM5 full length, NTF: N-terminal cleavage fragment of MBP-PGAM5. **(D)** Co-expression of human His6-PARL wt and catalytic inactive His6-PARL^{S277A} (SA) with the chimeric substrates MBP-PINK1 (amino acids 70-134) and MBP-PGAM5 (amino acids 1-46) to test substrate cleavage *in vivo*. MBP-substrates were visualized by western blotting with antibodies against FLAG and MBP. Equal sample loading was confirmed by the ubiquitous expression levels of endogenous MBP. Substrate FL: MBP-substrates full length; no *in vivo* cleavage could be detected.

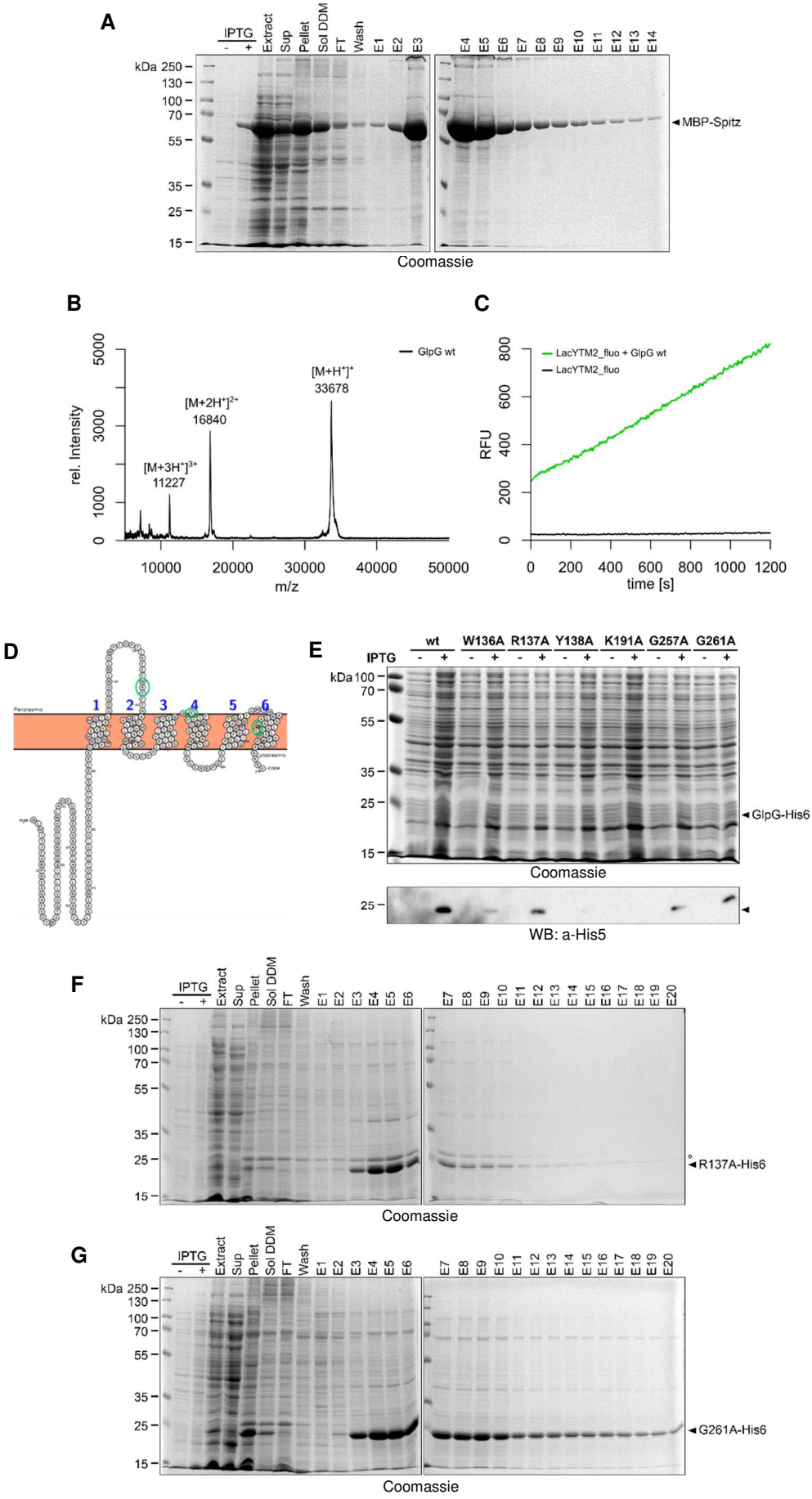

Figure S2 (Caption overleaf)

Figure S2 | Purified GlpG is active and cleaves the model substrates MBP-Spitz and LacYTM2, (related to Figure 8-9). **(A)** Coomassie-stained gel of each purification step using nickel-nitrilotriacetic acid (Ni-NTA) affinity purification. Chimeric MBP-Spitz was expressed in *E. coli* with 0.3 mM IPTG and solubilized from the membranes with 1.5% DDM. Aliquots were resolved by SDS-PAGE in gels containing 12% acrylamide. Sup: supernatant, Sol DDM: DDM-solubilized fraction, FT: flow through, E1-E14: elution fraction 1-14. **(B+C)** Data recorded by Huster laboratory. **(B)** MALDI-TOF-MS spectrum of purified GlpG in DDM micelles. The spectrum shows signals for GlpG species with one, two and three proton adducts with clear signal to noise ratios, indicating an intact primary sequence of GlpG-His6. **(C)** GlpG protease activity of purified GlpG-His6 was determined in DDM micelles using the fluorogenic kinetic substrate LacYTM2 (LacYTM2_fluo). 10 µM of the substrate were incubated with (green) or without (black) 0.4 µM GlpG-His6 at 37°C for 120 sec and EDANS fluorescence was monitored. **(D)** Snakeplot of GlpG with its loops and TM domains and showing the individual amino acids. Green circles indicate the mutation sites. The TM domains are numbered 1-6; Protter.ch (ETH Zürich). **(E)** Test expression of GlpG-His6 wt and the six mutants. Coomassie-stained gel (upper panel) shows the uninduced and induced samples; western blot analysis with anti-His5 is depicted in the lower panel. **(F+G)** Representative Coomassie-stained gel of each purification step using Ni-NTA affinity purification of the GlpG-His6 mutants R137A and G261A. Aliquots were resolved by SDS-PAGE in gels containing 12% acrylamide. Circle: minor contamination with OmpA (outer membrane protein A) from GlpG preparation, Sup: supernatant, Sol DDM: DDM-solubilized fraction, FT: flow through, E1-E20: elution fraction 1-20

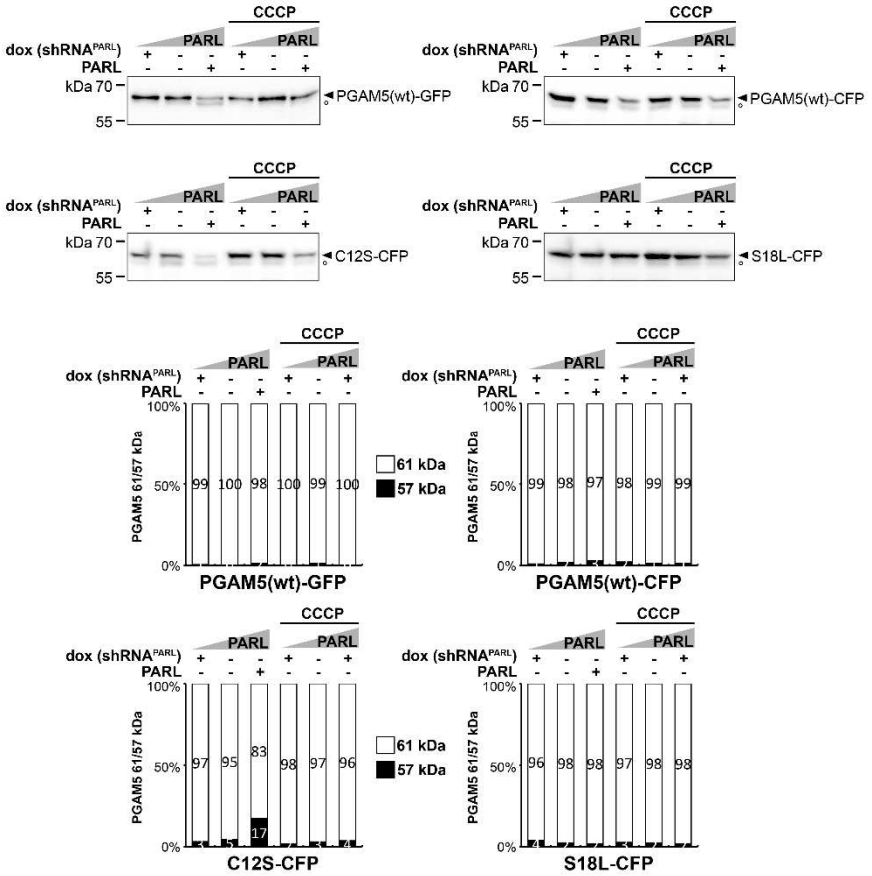

Figure S3 | A fluorescent protein tag abolishes PARL-catalyzed cleavage, (related to chapter 2.3.1).
wt and mutant PGAM5 was C-terminally tagged with GFP or CFP and processing was analyzed in a corresponding cell-based PARL gain- and loss-of-function assay. Endogenous PARL was knocked down by doxycyclin (dox)-induced expression of a PARL-specific shRNA. Ectopic expression of PARL and treatment with CCCP did not increase cleavage when using a bulky GFP or CFP tag. Lower panels show quantification of PGAM5 61/57 kDa distribution upon PARL knockdown, endogenous levels or PARL over-expression without or with CCCP treatment. Circle: PARL-independent band, most likely due to degradational processes of the GFP/CFP constructs.

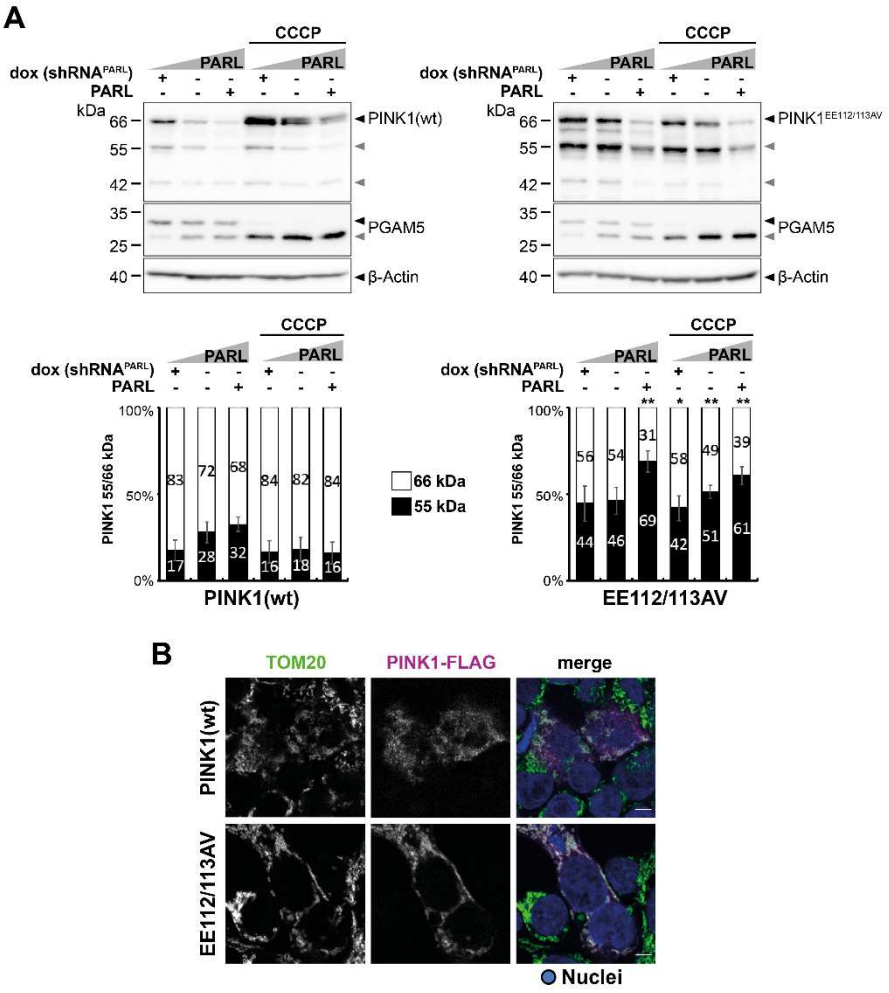

Figure S4 | Negative charges in the substrate's juxtamembrane region influence cleavage efficiency (part I), (related to Figure 18).

(A) wt and mutant PINK1 processing was analyzed in a corresponding cell-based PARL gain- and loss-of-function assay. Endogenous PARL was knocked down by doxycyclin (dox)-induced expression of a PARL-specific shRNA. Ectopic expression of PARL leads to decreased processing. PINK1 cleavage was inhibited by treating cells with the mitochondrial uncoupling agent CCCP. Lower panels show quantification of PINK1 66/55 kDa distribution upon PARL knockdown, endogenous levels or PARL over-expression without or with CCCP treatment (n = 3, means ± SEM. Significant changes versus wt PINK1-FLAG are indicated with blue stars (*p ≤ 0.05, **p ≤ 0.01; unpaired two-tailed t-test). Grey arrowheads: PNK1 and PGAM5 cleavage fragments. **(B)** IF analysis examines mitochondrial targeting of ectopically expressed PINK1-FLAG constructs (purple) co-stained with endogenous TOM20 (green); cell nuclei are stained with Hoechst (blue). Scale bar, 5 µm; immunofluorescence performed by Elena Heuten (Lemberg lab).

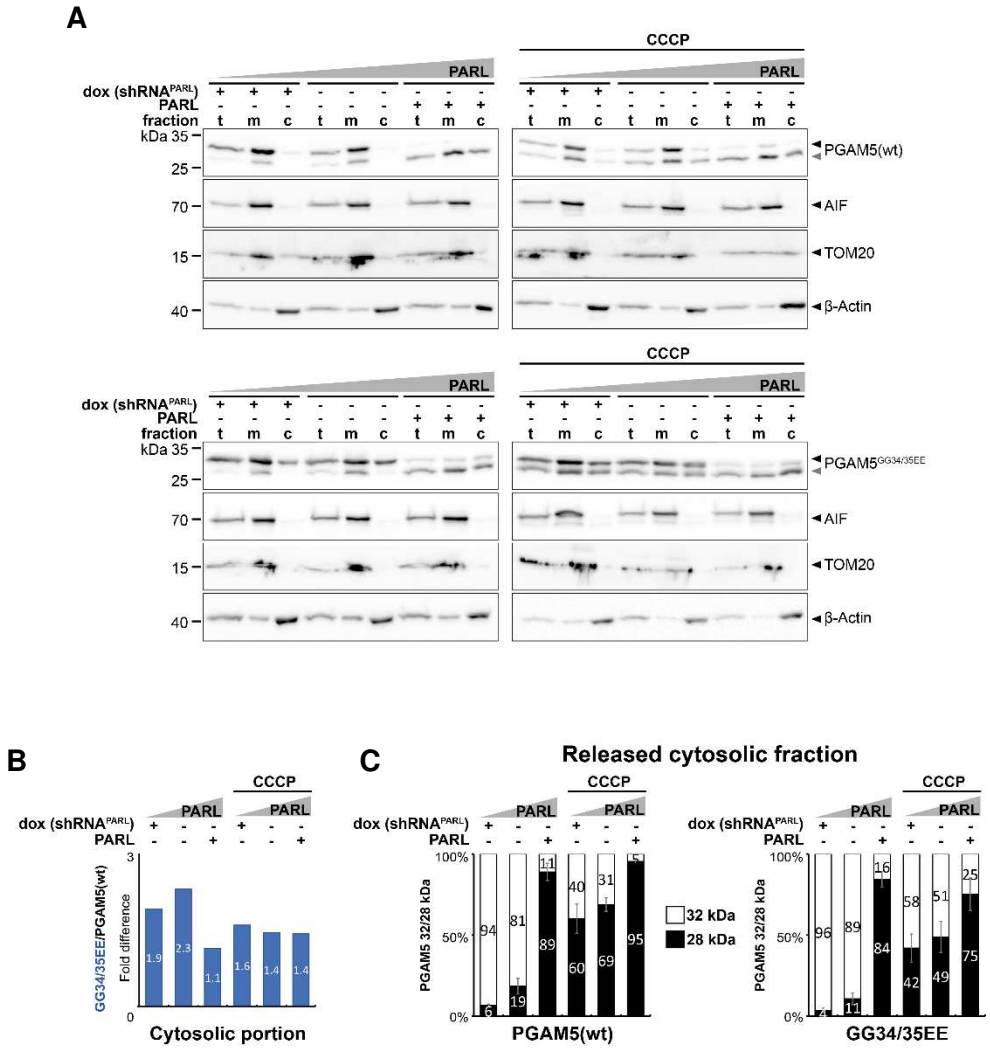

Figure S5 | Negative charges in the substrate's juxtamembrane region influence cleavage efficiency (part II), (related to Figure 18).

(A) Subcellular fractionation of wt and mutant PGAM5 cleavage depicted in total cell extract (t) 10% loaded, mitochondrial (m) and soluble fraction (c) 4% loaded, each. The cellular markers AIF (apoptosis-inducing factor), TOM20 (translocase of the outer membrane) for mitochondria, and β-actin were used as transfection and loading controls. Grey arrowhead: 28 kDa cleavage fragment. **(B)** Quantification of total PGAM5-FLAG released to the cytosol upon PARL knockdown, endogenous levels or PARL over-expression without or with CCCP treatment, comparing PGAM5 wt and GG34/35EE (GG34/35EE/PGAM5(wt) ratio). **(C)** Quantification of PGAM5 32/28 kDa distribution in the cytoplasmic fraction upon the same conditions (n = 3, means ± SEM).

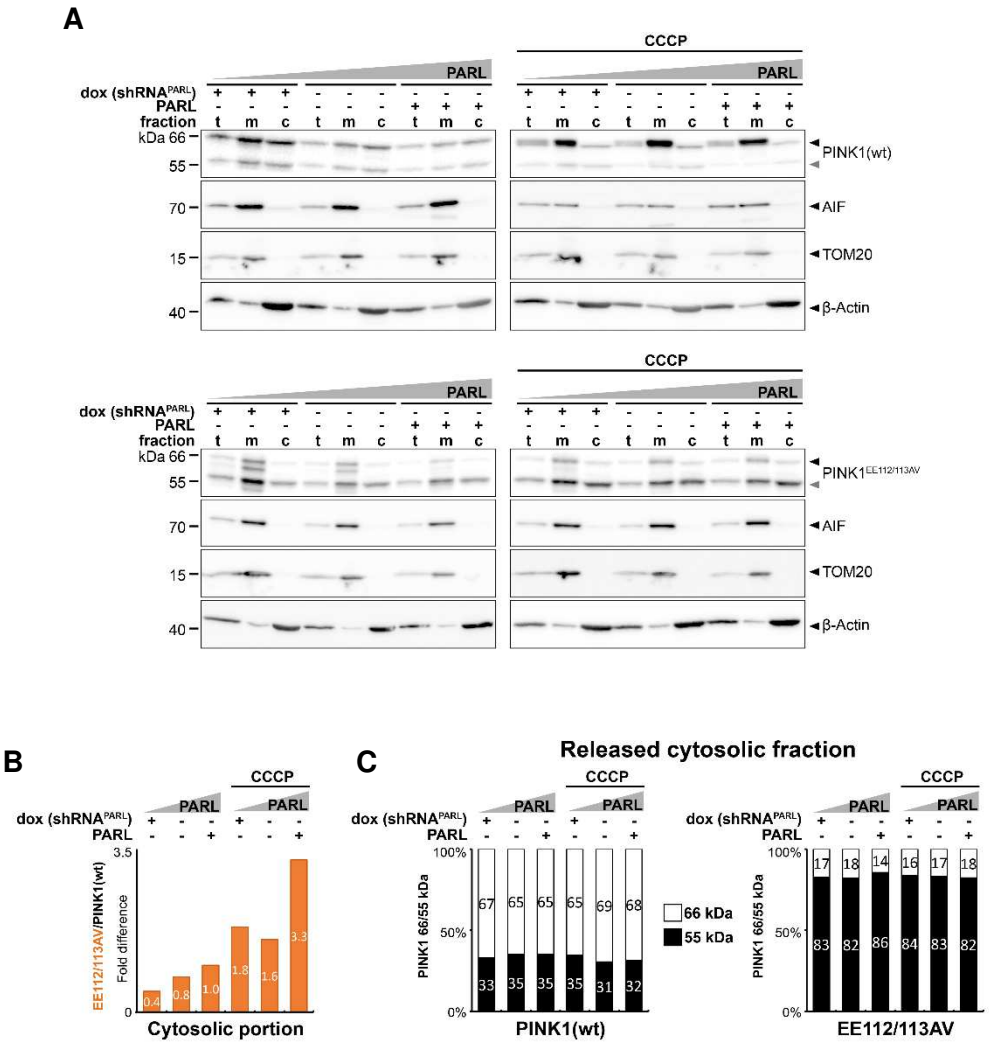

Figure S6 | Negative charges in the substrate's juxtamembrane region influence cleavage efficiency (part III), (related to Figure 18).

(A) Corresponding subcellular fractionation of wt PINK1 and PINK1$^{EE112/113AV}$ depicted in total cell extract (t) 10% loaded, mitochondria (m) and soluble fraction (c) 4% loaded, each. The cellular markers AIF (apoptosis-inducing factor), TOM20 (translocase of the outer membrane) for mitochondria, and β-actin were used as transfection and loading controls. Grey arrowhead: 55 kDa cleavage fragment. **(B)** Quantification of total PINK1-FLAG released to the cytosol upon PARL knockdown, endogenous levels or PARL over-expression without or with CCCP treatment, comparing wt PINK1 and EE112/113AV (EE112/113AV/PINK1(wt) ratio). **(C)** Quantification of PINK1 66/55 kDa distribution of the cytoplasmic fraction upon the same conditions (n = 1).

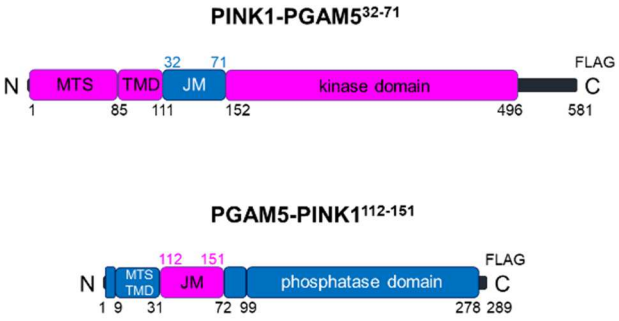

Figure S7 | PINK1-PGAM5 JM domain swap constructs, (related to chapter 2.3.4).
Schematic representation of PINK1-PGAM5$^{32-71}$-FLAG and PGAM5-PINK1$^{112-151}$-FLAG domain structure. MTS: matrix targeting signal, TMD: transmembrane domain, JM: juxtamembrane region.

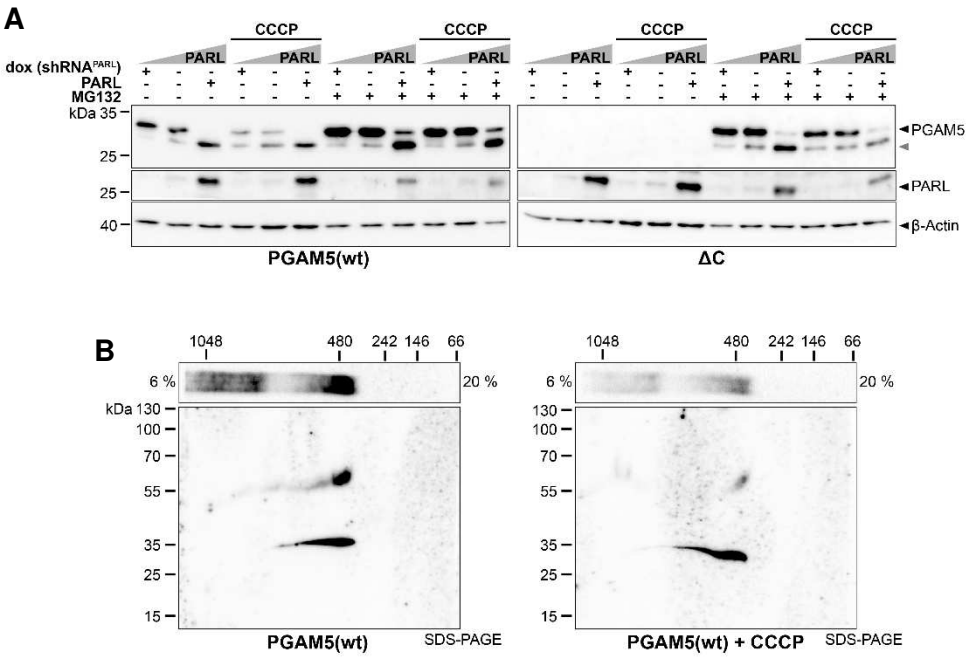

Figure S8 | Detection limit of PGAM5$^{\Delta C}$ due to rapid cleavage in steady-state analysis, (related to Figure 20-21).
(A) To demonstrate the detection limit of PGAM5$^{\Delta C}$ due to rapid cleavage in steady-state analysis, samples of PGAM5 wt and monomeric PGAM5$^{\Delta C}$ were incubated for longer than 36 h before harvesting and were treated without or with proteasome inhibitor MG132 (2 µM, 24 h). Only PGAM5$^{\Delta C}$ samples treated with MG132 could be detected when loading next to the untreated samples, whereas PGAM5 wt could be detected in both scenarios. Grey arrowhead: 28 kDa cleavage fragment. **(B)** A second dimension added to PGAM5 wt samples run in BN-PAGE by two-dimensional PAGE (2D-PAGE) could resolve PGAM5 higher molecular assemblies into signals around 60 kDa and 35 kDa.

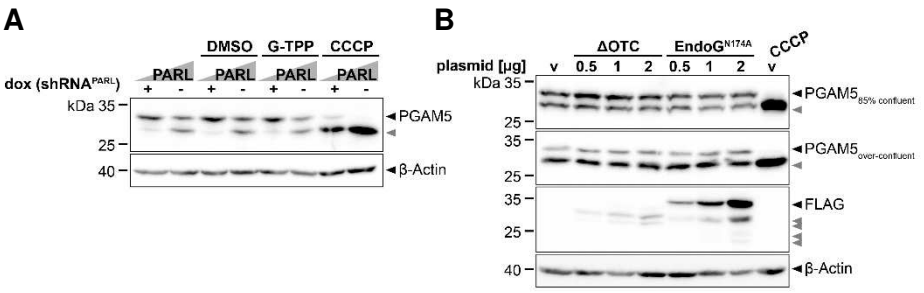

Figure S9 | Different mitochondrial stressors, (related to Discussion chapter 3.6.1).
(A) Endogenous PGAM5 levels were analyzed in a cell-based PARL loss-of-function assay, comparable to the PARL gain- and loss-of-function assay just lacking PARL overexpression. Cells were treated with vehicle DMSO, 5 µM G-TPP for 16 h or 10 µM CCCP for 3 h before harvesting. **(B)** Endogenous PGAM5 levels analyzed in Hek293T cells transiently transfected with either 2 µg empty vector (v), 0.5 µg - 2 µg plasmid expressing ΔOTC-3xFLAG or 0.5 µg - 2 µg plasmid expressing EndoG^{N174A}-3xFLAG to induce proteotoxic stress in mitochondria. Outcome was compared to control sample treated with 10 µM CCCP between cells that were harvested with 85% confluency (first panel) and cells harvested in an overconfluent state (second panel). Grey arrowheads: cleavage fragments.

6.2. Supplementary Tables

Table S1 | List of intrinsic mitoproteases and their associated functions.
Adapted from (Deshwal *et al.*, 2020). M: matrix, IMS: intermembrane space, IMM: inner mitochondrial membrane, MCU: mitochondrial Ca^{2+} uniporter, ND: no data, PE: phosphatidylethanolamine.

Name	Location	Regulatory functions	Reference
Processing peptidases			
ATP23	IMS	Protein maturation F_1F_O-ATP synthase assembly	(Osman *et al.*, 2007; Zeng *et al.*, 2007)
IMMP	IMS, IMM	Protein maturation Apoptosis/senescence	(Ieva *et al.*, 2013; Yuan *et al.*, 2018)
METAP1D	Matrix	Protein maturation	(Serero *et al.*, 2003)
MIP	Matrix	Protein maturation Coenzyme Q biosynthesis Complex III and IV activity	(Allan *et al.*, 2015; Branda and Isaya, 1995; Isaya *et al.*, 1994)
OMA1	IMS, IMM	Mitochondrial dynamics	(Anand *et al.*, 2014)
PARL	IMM	Apoptosis Coenzyme Q biosynthesis Complex III assembly Lipid trafficking Mitophagy	(Meissner *et al.*, 2015; Saita *et al.*, 2017; Saita *et al.*, 2018; Shi and McQuibban, 2017; Spinazzi *et al.*, 2019)
PMPCB, MPP	Matrix	Protein maturation	(Gakh *et al.*, 2002)
XPNPEP3	Matrix	Protein maturation and stability	(Vögtle *et al.*, 2009)

ATP-dependent proteases			
AFG3L2 AFG3L2/SPG7 (Paraplegin) AFG3L1	Matrix, IMM (*m*-AAA)	Ribosome assembly MCU assembly	(Kondadi *et al.*, 2014; König *et al.*, 2016) (Koppen *et al.*, 2007)
CLPXP (CLPP, CLPX)	Matrix	Transcription/translation Ribosome assembly	(Matsushima *et al.*, 2017; Szczepanowska *et al.*, 2016)
LONP1	Matrix	mtDNA maintainence mtDNA replication Adaptation to hypoxia	(Hao *et al.*, 2018; Kunová *et al.*, 2017; Matsushima *et al.*, 2010)
YME1L	IMS, IMM (*i*-AAA)	Protein import Lipid trafficking Mitochondrial dynamics	(Anand *et al.*, 2014; Potting *et al.*, 2013; Richter *et al.*, 2019)
Oligopeptidases			
MEP (Neurolysin)	IMS	Peptide degradation	(Mossmann *et al.*, 2012; Teixeira and Glaser, 2013)
PITRM1, PreP	Matrix	Aβ degradation	(Falkevall *et al.*, 2006; Taskin *et al.*, 2017)
Other mitochondrial proteases			
HTRA2	IMS	Stress signaling Apoptosis	(Papa and Germain, 2011; Radke *et al.*, 2008)
LACTB	IMS	PE metabolism	(Keckesova *et al.*, 2017)

Table S2 | List of putative PARL substrates identified in the gain-of-function PARL-trapping approach using SILAC.

Shown are the average values of medium-over-light (M/L), heavy-over-light (H/L) and heavy-over-medium (H/M) ratios from at least two biological replicates out of four. Only proteins, whose log2-transformed H/M ratio of the normalized values exceed 0.1 were presented in this table. Known substrates are highlighted in green, non-substrates (also still under debate) in orange and complex partners in blue. GHITM (Spinazzi *et al.*, 2019); OPA1 (Anand *et al.*, 2014; Duvezin-Caubet *et al.*, 2007; Song *et al.*, 2007); CLPB (Cupo and Shorter, 2020; Saita *et al.*, 2017), STOML2 (Wai *et al.*, 2016).

Average values			**Gene names**	**Protein names**	**Protein ID**
Ratio M/L	Ratio H/L	**Ratio H/M**			
-3.8045	-1.9623	**2.2147**	**HSD17B8**	Estradiol 17-beta-dehydrogenase 8	Q92506
-1.8242	-0.1669	**1.8507**	**HAX1**	HCLS1-associated protein X-1	O00165
-1.0851	0.2216	**1.5944**	**GHITM**	Growth hormone-inducible transmembrane protein	Q9H3K2
-0.8612	0.4994	**1.4975**	**CLPB**	Caseinolytic peptidase B protein homolog; Suppressor of potassium transport defect 3	Q9H078

-1.7506	-0.3259	**1.1863**	**STOML2**	Stomatin-like protein 2, mitochondrial	Q9UJZ1
-0.3133	0.3140	**0.9303**	**CSDE1**	Cold shock domain-containing protein E1	O75534
-1.2584	-0.8582	**0.5962**	**COMT**	Catechol O-methyltransferase	P21964
-3.7311	-1.4779	**0.5432**	**SPRYD4**	SPRY domain-containing protein 4	Q8WW59
-0.9746	-1.0123	**0.4473**	**YME1L1**	ATP-dependent zinc metalloprotease YME1L1	Q96TA2
-1.2857	-1.1996	**0.4445**	**OPA1**	Dynamin-like 120 kDa protein, form S1;Dynamin-like 120 kDa protein, mitochondrial	O60313
-0.2566	0.0438	**0.4196**	**CAT**	Catalase	P04040
-0.9906	-0.8765	**0.4152**	**SLC27A2**	Very long-chain acyl-CoA synthetase	O14975
-1.5320	-0.9640	**0.4144**	**CECR5**	Cat eye syndrome critical region protein 5	Q9BXW7
-0.4450	-0.2357	**0.3707**	**DHTKD1**	Probable 2-oxoglutarate dehydrogenase E1 component DHKTD1, mitochondrial	Q96HY7
-0.8180	-0.7035	**0.3624**	**SLC25A6**	ADP/ATP translocase 3;ADP/ATP translocase 3, N-terminally processed	P12236
-0.3692	-0.2383	**0.3583**	**RHOT2**	Mitochondrial Rho GTPase 2	Q8IXI1
-0.1726	-0.1218	**0.3536**	**D2HGDH**	D-2-hydroxyglutarate dehydrogenase, mitochondrial	Q8N465
-1.3153	-1.2273	**0.3486**	**HK1**	Hexokinase;Hexokinase-1	P19367
-0.7076	-0.6008	**0.3384**	**KARS**	Lysine-tRNA ligase	Q15046
-1.2043	-1.0770	**0.3356**	**TXN**	Thioredoxin	P10599
-0.8707	-0.6467	**0.2982**	**TBRG4**	Protein TBRG4	Q969Z0
0.0670	-0.2194	**0.2923**	**CPOX**	Oxygen-dependent coproporphyrinogen-III oxidase, mitochondrial	P36551
-0.7845	-0.5790	**0.2771**	**HIGD1A**	HIG1 domain family member 1A, mitochondrial	Q9Y241
-0.3974	-0.3056	**0.2768**	**MCCC1**	Methylcrotonoyl-CoA carboxylase subunit alpha, mitochondrial	Q96RQ3
-0.6898	-0.5963	**0.2648**	**RPL10A**	60S ribosomal protein L10a	P62906
-0.6966	-0.6029	**0.2509**	**HCFC1**	HCF C-terminal chain 1,2,3,4,5,6;Host cell factor 1	P51610
0.0237	-0.6021	**0.2473**	**PPP2CA**	Serine/threonine-protein phosphatase;Serine/threonine-protein phosphatase 2A catalytic subunit alpha isoform	P67775;P62714;P60510
-1.2124	-1.2420	**0.2139**	**MTCH2**	Mitochondrial carrier homolog 2	Q9Y6C9
-0.3448	-0.2765	**0.2118**	**DLAT**	Acetyltransferase component of pyruvate dehydrogenase complex;Dihydrolipoyllysine-residue acetyltransferase component of pyruvate dehydrogenase complex, mitochondrial	P10515
-1.1270	-1.4633	**0.2061**	**SARS2**	Serine-tRNA ligase, mitochondrial	Q9NP81
-0.3810	-0.3139	**0.2013**	**TIMM23**	Mitochondrial import inner membrane translocase subunit Tim23	O14925; Q5SRD1
-0.3945	-0.4960	**0.1985**	**TIMM21**	Mitochondrial import inner membrane translocase subunit Tim21	Q9BVV7
-0.5225	-0.5013	**0.1710**	**TIMM23B**	Putative mitochondrial import inner membrane translocase subunit Tim23B	O14925; Q5SRD1
-0.5225	-0.5013	**0.1710**	**GLRX5**	Glutaredoxin-related protein 5, mitochondrial	Q86SX6
-0.0544	-0.1966	**0.1655**	**PDHA1**	Pyruvate dehydrogenase E1 component subunit alpha, somatic form, mitochondrial	P08559
-0.4020	-0.4325	**0.1618**	**TOMM40**	Mitochondrial import receptor subunit TOM40 homolog	O96008
-0.3237	-0.2602	**0.1611**	**ATP6V1A**	V-type proton ATPase catalytic subunit A	P38606

-0.1767	-0.1089	**0.1463**	**PPIF**	Peptidyl-prolyl cis-trans isomerase;Peptidyl-prolyl cis-trans isomerase F, mitochondrial	P30405
-0.4400	-0.5090	**0.1454**	**ACOX1**	Peroxisomal acyl-coenzyme A oxidase 1	Q15067
-1.0125	-1.1725	**0.1400**	**PPP2R1A**	Serine/threonine-protein phosphatase 2A 65 kDa regulatory subunit A alpha isoform	P30153;P30154
-0.2627	-0.4563	**0.1328**	**L2HGDH**	L-2-hydroxyglutarate dehydrogenase, mitochondrial	Q9H9P8
-0.7283	-0.6394	**0.1252**	**CNP**	2',3'-cyclic-nucleotide 3'-phosphodiesterase	P09543
-0.7087	-1.1270	**0.1222**	**WASF1**	Wiskott-Aldrich syndrome protein family member 1	Q92558
-0.8180	-0.7791	**0.1177**	**PABPC5**	Polyadenylate-binding protein 5	P11940;Q9H361;Q4VXU2;Q96DU9
-0.4479	-0.4207	**0.1175**	**SLC25A4**	ADP/ATP translocase 1	P12235
-0.1230	-0.4290	**0.1100**	**FKBP8**	Peptidyl-prolyl cis-trans isomerase;Peptidyl-prolyl cis-trans isomerase FKBP8	Q14318
-0.6544	-0.6949	**0.1090**	**CAMK2A**	Calcium/calmodulin-dependent protein kinase type II subunit alpha	Q13554; Q9UQM7; Q13555
-0.2348	-0.4915	**0.1080**	**C2orf47**	Uncharacterized protein C2orf47, mitochondrial	Q8WWC4

Table S3 | List of putative PARL interactors identified in the gain-of-function PARL-trapping approach using SILAC.

Shown are the average values of medium-over-light (M/L), heavy-over-light (H/L) and heavy-over-medium (H/M) ratios from at least two biological replicates out of four. Only proteins, whose log2-transformed M/L ratio of the normalized values exceed 0.4 were presented in this table.

Average values			**Gene names**	**Protein names**	**Protein ID**
Ratio M/L	Ratio H/L	Ratio H/M			
4.6290	3.0392	-0.1669	**KRT5**	Keratin, type II cytoskeletal 5	CON_P13647;P13647
4.3247	4.2996	0.1845	**GPT2**	Alanine aminotransferase 2	Q8TD30; P24298
3.9962	3.2864	0.1830	**ATP5O**	ATP synthase subunit O, mitochondrial	P48047
3.0977	1.7102	0.2593	**ATP5L**	ATP synthase subunit g, mitochondrial	O75964
2.4346	1.5872	0.0534	**PARS2**	Probable proline-tRNA ligase, mitochondrial	Q7L3T8
0.6112	0.1609	-0.4512	**HADHB**	3-ketoacyl-CoA thiolase;Trifunctional enzyme subunit beta, mitochondrial	P55084
0.6061	0.1332	-0.2579	**HMGCL**	Hydroxymethylglutaryl-CoA lyase, mitochondrial	P35914
0.4934	-0.4629	-0.5312	**PTCD3**	Pentatricopeptide repeat domain-containing protein 3, mitochondrial	Q96EY7

6.3. List of Amino Acids

Table S4 | List of amino acids.

Given is the full name of the amino acid, the three-letter code, the one-letter code and the corresponding DNA codons.

Amino acid	Three letter code	One letter code	DNA codons
Alanine	Ala	A	GCT, GCC, GCA, GCG
Arginine	Arg	R	CGT, CGC, CGA, CGG, AGA, AGG
Asparagine	Asn	N	AAT, AAC
Aspartic acid	Asp	D	GAT, GAC
Cysteine	Cys	C	TGT, TGC
Glutamine	Gln	Q	CAA, CAG
Glutamic acid	Glu	E	GAA, GAG
Glycine	Gly	G	GGT, GGC, GGA, GGG
Histidine	His	H	CAT, CAC
Isoleucine	Ile	I	ATT, ATC, ATA
Leucine	Leu	L	CTT, CTC, CTA, CTG, TTA, TTG
Lysine	Lys	K	AAA, AAG
Methionine	Met	M	ATG
Phenylalanine	Phe	F	TTT, TTC
Proline	Pro	P	CCT, CCC, CCA, CCG
Serine	Ser	S	TCT, TCC, TCA, TCG, AGT, AGC
Threonine	Thr	T	ACT, ACC, ACA, ACG
Tryptophan	Trp	W	TGG
Tyrosine	Tyr	Y	TAT, TAC
Valine	Val	V	GTT, GTC, GTA, GTG

7. Acknowledgements

I would like to thank everyone from the bottom of my heart without whom this work would not have been possible.

First of all, I would like to thank my supervisor **Prof. Marius Lemberg**, for giving me the opportunity to do my PhD research in his laboratory and for providing the exciting research topic surrounding the rhomboid proteases PARL and GlpG. Thank you for making three fruitful collaborations possible and for all your support beyond that. I wish you and your family all the best in Cologne!

I am grateful to my TAC committee and examination commission members **Prof. Michael Brunner** and **Prof. Irmgard Sinning** for their helpful suggestions and discussions, bringing new perspectives and inspirations to the project and for evaluating my thesis. Furthermore, I would like to thank **Dr. Wilhelm Palm** for joining my dissertation committee and his time to evaluate my PhD work.

Special thanks to **Dr. Claudia Muhle-Goll**, **Prof. Joanne Lemieux** and **Prof. Daniel Huster** for our productive collaborations. Thanks to **Mara**, all master students, PhD students and postdocs who were involved in these collaborations throughout the years. I also had three wonderful weeks in Leipzig, thank you **David** and **Oskar**.

The biggest thank goes to my dear current and past peers of the **Lemberg lab**: Adrian, Alessandra, Ali, Andrea, Baptiste, Birte, Camille, Dönem, Elena, Friederike, Jan, Josephine, Julia F., Julia K., Laura, Martina, Nathalie, Ronny, Susanne, Verena D. (…) and especially **Suna** for not being only a colleague but also a friend.

Thank you all for enduring the daily chaos and also fun time with me. PhD projects do not necessarily come in bright and joyful colors only. I will never forget the 4 years at our home institute ZMBH, the **SARS-CoV-2 shutdown** (March-May 2020), the breath-taking **water-pipe burst** (July 2020) leaving us unoccupied again, with the final resumption of lab work for nearly 1 year at a **replacement building** (October 2020-July 2021). For those of you who moved away with the lab, all the best in Cologne!

I would in particular like to thank our secretaries **Konny** and **Karin**, for always being “schnelle Mädels”. Thank you for all your support and the warm working atmosphere!

Thanks also go to the **women in the central scullery** of the ZMBH, without whom a lot of things wouldn’t run at all!

Special thanks go to my **family**, my **friends** and **Alex**, who protect, support and encourage me in all situations.

*Ganz besonderer Dank gilt meinem verstorbenen **Opa**, der mir beigebracht hat den Zauber und die unzähligen auch noch so kleinsten Naturwunder zu erkennen. Opa, ohne dich hätte ich nicht schon als Kind mehr über die einheimischen Tiere und Pflanzen in unserem Wald gewusst, als viele andere Kinder und so manch ein Erwachsener. Auch hast du mir, wie kein anderer, beigebracht niemals aufzugeben, egal wie eklig meine Mitmenschen zu mir sind und hast mir bewusst gemacht, wie wichtig es ist mich von Personen und Dingen zu befreien, die mir nicht guttun. Du wirst schmerzlichst vermisst und niemals vergessen.*

Eidesstattliche Erklärung

Eidesstattliche Versicherung gemäß § 8 Abs. 3 der Promotionsordnung in der aktuellen Fassung vom 29. Juli 2015 für die Naturwissenschaftlich-Mathematische Gesamtfakultät der Universität Heidelberg

Hiermit erkläre ich, Verena Siebert, dass es sich bei der vorliegenden Dissertation zum Thema **„Substrate recognition and cleavage by the mitochondrial rhomboid protease PARL“** um eine eigenständig erbrachte Leistung handelt.

Ich habe nur die angegebenen Quellen und Hilfsmittel benutzt und mich keiner unzulässigen Hilfe Dritter bedient. Insbesondere habe ich wörtlich oder sinngemäß aus anderen Werken übernommene Inhalte als solche kenntlich gemacht.

Die Arbeit oder Teile davon habe ich bislang nicht an einer anderen Hochschule des In- oder Auslands als Bestandteil einer Prüfungs- oder Qualifikationsleistung vorgelegt. Die Richtigkeit der vorstehenden Erklärungen bestätige ich.

Die Bedeutung der eidesstattlichen Versicherung und die strafrechtlichen Folgen einer unrichtigen oder unvollständigen eidesstattlichen Versicherung sind mir bekannt.

_____ _____

Ort, Datum Verena Siebert